Density Functional-based Tight Binding for novel Nanomaterials: Development of Parameters for Boron and Application of DFTB to Adsorbates on Graphene

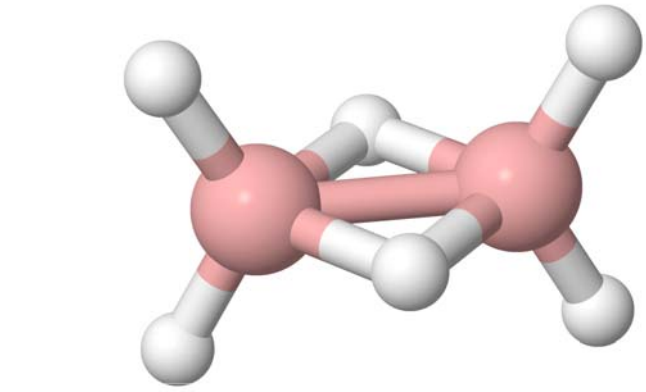

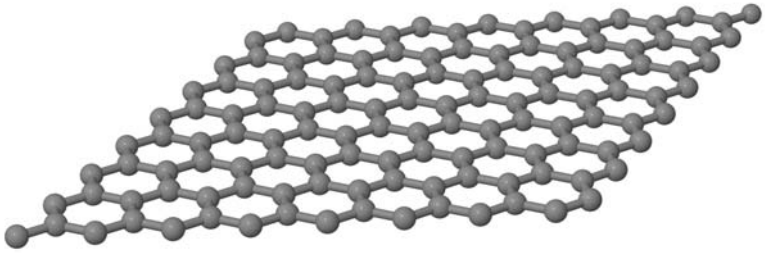

Dissertation zur Erlangung des Grades

Doktor der Naturwissenschaften, Dr. rer. nat.

dem Fachbereich Physik

an der Universität Bremen

vorgelegt durch
Bernhard Grundkötter-Stock, geb. Grundkötter

Bremen, September 2013

Erster Gutachter: Prof. Dr. Thomas Frauenheim

Zweiter Gutachter: Prof. Dr. Tim Wehling

Meinem Vater,
ich wünschte du wärst hier

Contents

Abbreviations and Nomenclature

2e3c	two electron three centered bonds; two electrons from a bond between three atoms, thus leading to bonding situations barely describable by lewis structure formulas
HF	Hartree Fock Theory; wave function based method of electronic structure calculations
B-H-B	2e3c bond between two boron atoms with a hydrogen as a bridge
BNT	boron nanotubes
BOA	Born-Oppenheimer approximation, separation of motion of nuclei and electrons.
CNT	carbon nanotubes
DFTB	density functional-based tight-binding, approximative scheme to DFT
edl	electron doping level, value of additional electrons per carbon atom
DFT	Densuty Functional Theory, method for the approximation of the electron-electron interaction based on the electron density
HOMO	Highest Occupied Molecular Orbital
IP	(vertical) ionization potential, total energy difference between relaxed molecule and ionized molecule in same geometry
LCAO	Linear Combination of Atomic Orbitals
RMS	root mean squares
SCC	self-consistent charge; extension to the DFTB method in order to retain second-order corrections to the Harris functional

Part I.

The Basis

1. Motivation and Aim

"There is plenty of room at the bottom" - Richard Feynman (1959)

With this the physicist and (later) noble prize winner stated his believe that scientists would be able to work with materials at the atomic scale - once the necessary instruments are developed. The development of such instruments started in the 1980's, when scientists at the ETH Zurich at first observed and manipulate atoms with atomic microscopy. Since then the availability of tools has increased, which allow the work at (or near) the atomic scale, and thus has the interest of other disciplines in the so-called nanoscience and/or nanotechnology. The prefix *nano* has found its way into many new word creations like nanoparticle, nanomachines, nanoelectronics, nanochemistry, and nanobiotechnology. The approaches behind these are considered revolutionary in their fields of application.

The aim behind the use of nanomaterials is an ascent in technology. This ascent is considered to be the key to solve the problems, which our society is facing in the near future because of the increase in the world's population and the accompanying higher resource demand. Therefore, new developments must not only satisfy demands of economy but also of ecology. This is necessary in order to obtain an efficient acquaintance with the finite resources of the world, which we all call our home. The development of new fabrication processes and the recycling of products, which are no longer in use, are substantial steps to achieve that goal. The computational material science reaches in the same direction. As the computational power improves, the possibility of predicting the properties of materials and outcome of chemical reactions becomes feasible for more complex and larger systems with rising accuracy. Already when I started my chemistry study 10 years ago, some of my professors were convinced of the possibilities of computational methods. They stated that in the near future, we would not do the experiments in the lab hoping that they work. But that we would use computational methods to determine if and how the reaction can work beforehand. And that by doing this, we could save time, money and resources since experiments would result in far less failures. Thus, the computational material science provides a very valuable tool to obtain the goals described above.

Although the last years have led to a remarkable increase in the computational power available, most methods, which can achieve the so-called chemical accuracy, still require to high for practical usage in nanoscience or even computational biochemistry. For example, the computational demand of methods like DFT is too high to tackle systems with more than 100 atoms using a reasonable large basis set outside of a high-performance computer cluster within a satisfying amount of time. Therefore for such systems, more approximate methods have be to used like semi-empirical PM3 (and further advancements) or force-field methods. These methods rely on the generalization of parameters for the investigation at hand.

A method similar to this procedure is Density Functional-basd Tight-Binding (DFTB), which combines computational speed of the semi-empirical methods with the accuracy of more sophisticated methods like DFT. The preparation of parameters for DFTB requires good testing in order to ensure that the desired quality of the method is attained. But with such parameters the ability to study larger systems on the atomic scale is gained. An area of great interest are the electronic properties of nanomaterials, which can be investigated by DFTB. Many new nanomaterials are considered to be of relevance in the future, if their electronic properties can be customized to the specific needs of the application.

One of the top materials here is graphene, which is famous for its geometric as well as for its electronic structure. Also boron is becoming more and more interesting, especially since pure boron nanomaterials have been discovered. But even before that the structural characteristic of boron in molecular and bulk systems was known and studied in the hope to gain insight into the nature of the chemical bond. The feature of electron-poor, so-called two-electron-three-centered bonds, which form especially within boranes, are also a challenge for a method, which relies on the decomposition of the system into the pair interactions. Furthermore the fact, that the element boron is missing in the otherwise well developed, tested and approved *mio*-SKF-set, makes it a even more desirable intent to get a parametrization, which complements the existing parameters and works for the description of boranes and pure boron systems like nanotubes.

Therefore, the aim of this work is two-fold: In part II an extension to the application range of the DFTB method (reviewed in chapter 3) is presented with a new parametrization of boron, which supplements existing and well accepted parametrization for other elements. While in part III existing parameters of DFTB are applied to one of the most interesting new materials, graphene, in order to answer the question whether the sublattice symmetry of that system can be broken if atoms adsorb on its surface (part III). Further introductions to the systems under study are given in their respective parts of this thesis.

2. Density Functional Theory

On the following pages will be given a brief narration of density functional theory (DFT) [1–6] and in the next following chapter of the further approximate method of density functional-based tight-binding (DFTB) up to the self-consistent charge level[6–9]. Additional developments and tests of the DFTB method are discussed in [10–26].

2.1. Quantum Mechanic Basics

The ultimate goal of quantum mechanical calculations is the determination of the many-electron wave function for N interacting electrons, moving in the potential of M moving atomic nuclei of a molecule or solid. This function contains all possible information of the system under investigation. In general the wave function is assigned by parameters x_i, which consist of the spatial and spin coordinates, r_i and s_i respectively[27].

$$\Psi = \Psi\left(\{x_i\}\right) = \Psi\left(\{r_i, s_i\}\right) \tag{2.1}$$

For most quantum mechanical problems, the mathematical equation, which is used to ascertain the wave function, is the non-relativistic, stationary Schrödinger equation (eq. 2.2) [28]. In this equation, the operator $\hat{\mathrm{H}}$ is the so-called Hamiltonian, which defines the interactions within the system under study, Ψ is the wave function, the state function of the system, and E is the energy eigenvalue of this state.

$$\hat{\mathrm{H}}\Psi = E\Psi \tag{2.2}$$

The Hamilton Operator is usually build up from the kinetic energies of nuclei and electrons, $\hat{\mathrm{T}}_{nuc}$ and $\hat{\mathrm{T}}_{el}$, respectively, and their electrostatic interaction with each other, $\hat{V}_{nuc-el}$, and among themselves, $\hat{\mathrm{V}}_{nuc-nuc}$ and $\hat{\mathrm{V}}_{el-el}$, respectively. Using atomic units the respective equations read:

$$\hat{\mathrm{H}} = \hat{\mathrm{T}}_{nuc} + \hat{\mathrm{T}}_{el} + \hat{\mathrm{V}}_{nuc-el} + \hat{\mathrm{V}}_{nuc-nuc} + \hat{\mathrm{V}}_{el-el} \tag{2.3}$$

$$\hat{\mathrm{T}}_{nuc} = \sum_{A=1}^{M} \frac{1}{2m_A} \triangle_A \tag{2.4}$$

$$\hat{\mathrm{T}}_{el} = \sum_{i=1}^{N} \frac{1}{2} \triangle_i \tag{2.5}$$

$$\hat{\mathrm{V}}_{nuc-el} = -\sum_{i=1}^{N} \sum_{A=1}^{M} \frac{Z_A}{\left|\overrightarrow{R_A} - \overrightarrow{r_j}\right|} \tag{2.6}$$

$$\hat{\mathrm{V}}_{nuc-nuc} = \sum_{A=1}^{M} \sum_{B<A}^{M} \frac{Z_A Z_B}{\left|\overrightarrow{R_A} - \overrightarrow{R_B}\right|} \tag{2.7}$$

$$\hat{\mathrm{V}}_{el-el} = \sum_{i=1}^{N} \sum_{j<i}^{N} \frac{1}{|\overrightarrow{r_i} - \overrightarrow{r_j}|} \tag{2.8}$$

Δ is the Laplace operator with respect to the coordinates of the electron i or the nucleus A, which has the nuclear mass m_A and the nuclear charge Z_A. $\overrightarrow{r_i}$ and $\overrightarrow{R_A}$ are the positions of electron i and nucleus A, respectively.

In order to solve this many particle problem the Born-Oppenheimer approximation (BOA) or adiabatic approximation is often applied. According to the BOA the motion of the nuclei and electrons can be separated justified by the large mass difference of the nuclei and electrons. Thus, assuming that the electrons react instantaneously to any motion of the nuclei. With such separation it is valid to split the Schrödinger equation into a nuclear and an electronic part, eq. 2.12 and 2.11, and to use a product ansatz for the wave function Ψ (eq. 2.9).

$$\Psi = \Psi_{elec}\Phi_{nuc} \tag{2.9}$$

$$\hat{\mathrm{H}}\Psi_{elec}\Phi_{nuc} = E\Psi_{elec}\Phi_{nuc} \tag{2.10}$$

$$\hat{\mathrm{H}}_{elec}\Psi_{elec} = E_{elec}\left(\overline{R}\right)\Psi_{elec} \tag{2.11}$$

$$\hat{\mathrm{H}}_{nuc}\Phi_{nuc} = E\Phi_{nuc} \tag{2.12}$$

$$\hat{\mathrm{H}}_{elec} = \hat{\mathrm{T}}_{el} + \hat{\mathrm{V}}_{el-el} + \hat{\mathrm{V}}_{nuc-el}\left(\overline{R}\right) \tag{2.13}$$

$$\hat{\mathrm{H}}_{nuc} = \hat{\mathrm{T}}_{nuc} + \hat{\mathrm{V}}_{nuc-nuc} + E_{elec}\left(\overline{R}\right) \tag{2.14}$$

In this way, the electronic Hamilton operator and thus the electronic energy depend on the positions of the nuclei only parametrically as is indicated by$\hat{\mathrm{V}}_{nuc-el}\left(\overline{R}\right)$ and $E_{elec}\left(\overline{R}\right)$. The nuclear Hamiltonian meanwhile contains the electronic energy, $E_{elec}\left(\overline{R}\right)$.

Most properties of a stable compound are derived from the electronic Schrödinger equation, eq. 2.11, why the further focus is on this equation. But still this equation cannot be solved analytically due to $\hat{\mathrm{V}}_{el-el}$, which couples the motion of the different electrons to

each other. Hence, additional approximations have to be utilized. Examples for these approximations are the Hartree- and Hartree-Fock theory (HF) and their extensions[29–31]. In their application the many-electron wave function Ψ is expressed as a simple product of one-electron wave functions in Hartree theory and as a Slater determinant of one-electron spin orbitals in Hartree-Fock theory.

The form of the Slater determinant ensures that the solution of eq. 2.11 is antisymmetric with respect to the exchange of two electrons. That this has to be the case is dictated by the Fermi statistics and is also known as the Pauli principle. Thus, the exchange interaction of electrons is treated correctly by HF. Further many-electron effects, so-called electron correlation effects, are not covered by HF due to the restriction to a single Slater determinant. Beyond HF methods like configuration interaction (CI), which use a linear combination of multiple determinants, embrace the electron-electron interaction by considering different electronic states.

2.2. The Basis of DFT

The density functional theory (DFT) is another method for the calculation of molecular properties. It is not based on the HF method, but uses the charge or electron density $\rho(r)$ directly instead of the wave function Ψ[1, 32–35].

$$\rho(r) = \sum_{s_1 \ldots s_N} \int \Psi^*(r_1 s_1, r_2 s_2, \ldots r_N s_N)\, \Psi(r_1 s_1, r_2 s_2, \ldots r_N s_N)\, \mathrm{d}r_2 \ldots r_N \tag{2.15}$$

The basis of DFT are the statements/theorems of Hohenberg and Kohn[32]. These are that

1. "the ground state density of a bound system of a fixed number of interacting electrons in an external potential determines this potential uniquely to within an additive constant"[6] and
2. a universal functional exists, which describes ground state energy of a systems of N electrons within an external potential $\mathrm{V}_{ext}(r)$.

The external potential in atomic systems is the potential of the nuclei, in which the electrons move.

$$\mathrm{V}_{ext}(r) = \hat{\mathrm{V}}_{nuc-el} = -\sum_{i=1}^{N} \sum_{A=1}^{M} \frac{Z_A}{\left|\overrightarrow{R_A} - \overrightarrow{r_j}\right|} \tag{2.16}$$

That these two statements are true and mathematically exact for any density, was proven for non-degenerate and degenerate systems[2, 36, 37]. As a result of these theorems, the density defines completely the Hamiltonian $\hat{\mathrm{H}}$ of the system and thus determines all properties derived from $\hat{\mathrm{H}}$ including the eigenstates Ψ of the Schrödinger equation. Their total energy values are essential for the appraisal of the atomic arrangement and stability of the

compound as the lowest value defines the ground state of said molecule or solid. Given that the Schrödinger equation is an eigenvalue problem of normalized wave functions, the variational principle or Rayleigh-Ritz principle[37] may be applied to find that ground state and its energy eigenvalue E_0. The transition from wave functions to densities was done by Hohenberg and Kohn [32] and refined by Levy and Lieb [38, 39]. Hence, the self-consistency circle "density ρ determines the potential, which defines the Hamiltonian $\hat{\mathrm{H}}$ and thus the wave function Ψ, which itself is a functional of the density ρ" is formed.

2.3. Universal Functional and Variational Principle

Although the density functional of the wave function is nontrivial, in [38, 39] the wave function Ψ was defined as the minimum of a universal functional of a trial density as

$$F\left[\tilde{\rho}\left(r\right)\right] = \min_{\tilde{\Psi}\to\tilde{\rho}} \left(\tilde{\Psi}\left|\hat{\mathrm{T}}_{el} + \hat{\mathrm{V}}_{el-el}\right|\tilde{\Psi}\right) \tag{2.17}$$

where $\tilde{\Psi}$ is the test wave function that yields the density $\tilde{\rho}\left(r\right)$. The universal character of this functional refers to its independence of any external potential $\mathrm{V}_{ext}\left(r\right)$, which is fixed for a given density according to the first basic statement of DFT (see above). Thus, eq. 2.17 minimizes the total energy in the context of the test wave functions producing the argument density $\tilde{\rho}\left(r\right)$, following the equation

$$E\left[\tilde{\rho}\left(r\right)\right] = F\left[\tilde{\rho}\left(r\right)\right] + \int \mathrm{V}_{ext}\left(r\right)\tilde{\rho}\left(r\right)\mathrm{d}r \tag{2.18}$$

Now, this energy functional has to be minimized with respect to all densities $\tilde{\rho}\left(r\right)$, for which $F\left[\tilde{\rho}\left(r\right)\right]$ is defined, in order to obtain the ground state density $\rho_{\mathrm{GS}}\left(r\right)$. This is known as the Hohenberg-Kohn variational principle, which states that the minimum of the energy functional (eq. 2.18) is only assumed at the ground state density $\rho_{\mathrm{GS}}\left(r\right)$.

$$E\left[\tilde{\rho}\left(r\right)\right] \geq E_{\mathrm{GS}} \tag{2.19}$$

$$E_{\mathrm{GS}} = \min_{\tilde{\rho}(r)\to N} E\left[\tilde{\rho}\left(r\right)\right] = E\left[\rho_{\mathrm{GS}}\left(r\right)\right] \tag{2.20}$$

Therefore, the expression of the electronic ground state energy has been shifted from the usage of the many-particle wave function to terms of spatial charge density. But still this does not solve all the difficulties, especially since the universal functional (eq. 2.17) is unknown although it contains the most important electron-electron interaction.

2.4. Kohn-Sham Equations

Kohn and Sham suggested a beneficial splitting of the functional[40]:

$$F[\rho(r)] = T_0[\rho(r)] + E_H[\rho(r)] + E_{xc}[\rho(r)] \tag{2.21}$$

Here, $T_0[\rho(r)]$ is the kinetic energy functional of non-interacting electrons, $E_H[\rho(r)]$ is the Hartree energy, from the collective Coulomb repulsion of the electrons,

$$\begin{aligned} E_H[\rho(r)] &= \frac{1}{2}\int\int \frac{\rho(r)\,\rho(r')}{|\overrightarrow{r} - \overrightarrow{r}'|}\mathrm{d}\overrightarrow{r}\,\mathrm{d}\overrightarrow{r}' && (2.22)\\ &= \frac{1}{2}\int \mathrm{V}_H([\rho(r)], r)\,\rho(r)\,\mathrm{d}r && (2.23)\\ \mathrm{V}_H([\rho(r)], r) &= \frac{\delta E_H[\rho(r)]}{\delta\rho(r)} && (2.24) \end{aligned}$$

and $E_{xc}[\rho(r)]$ is the so-called exchange-correlation functional, which acts as a correction term and holds all the many-body effects.

With this, equation 2.18 takes the form:

$$E_{\mathrm{KS}}[\rho(r)] = T_0[\rho(r)] + \int \mathrm{V}_{ext}(r)\,\rho(r)\,\mathrm{d}r + \frac{1}{2}\int \mathrm{V}_H([\rho(r)], r)\,\mathrm{d}r + E_{xc}[\rho(r)] \tag{2.25}$$

All of these terms except the exchange-correlation functional can be derived analytically, while the $E_{xc}[\rho(r)]$ must be approximated and the implementation of $E_{xc}[\rho(r)]$ classifies the practical application of DFT (LDA, GGA, Hybrid).

Kohn and Sham expressed the kinetic energy functional $T_0[\rho(r)]$ as normalized, single quasi-particle orbitals $\Phi_i(r)$, which represent the density according to normalized occupation numbers n_i[41].

$$\begin{aligned} \langle\Phi_i|\Phi_i\rangle &= \int |\Phi_i(r)|^2\,\mathrm{d}r = 1 && (2.26)\\ \rho(r) &= \sum_{i=1}^{occ.} n_i\,|\Phi_i(r)|^2 && (2.27)\\ N &= \sum_{i=1}^{occ.} n_i && (2.28) \end{aligned}$$

Hence, the kinetic energy functional follows as:

$$\begin{aligned} T_0[\rho(r)] &\approx T[\{\Phi_i\}] && (2.29)\\ T[\{\Phi_i\}] &= \sum_{i=1}^{occ.} n_i \left\langle \Phi_i \left| -\frac{\triangle}{2} \right| \Phi_i \right\rangle && (2.30)\\ &= \sum_{i=1}^{occ.} n_i \int \Phi_i^*(r) \left[-\frac{\triangle}{2}\right] \Phi_i(r)\,\mathrm{d}r && (2.31) \end{aligned}$$

With this, the ground state energy can be derived from the energy functional (eq. 2.25) with the constraint of eq. 2.26 using the Euler-Lagrange formalism with Lagrange parameters ϵ_i. Finally, an eigenvalue equation is obtained in the form of a single-particle Hartree equation (eq. 2.33), but it includes the many-body effects of the interacting electrons by the exchange-correlation potential, $\mathrm{V}_{xc}\left(\left[\rho\left(r\right)\right], r\right)$, and thus is (formally) exact.

$$\frac{\delta}{\delta\Phi_i^*\left(r\right)}\left\{E\left[\rho\left(r\right)\right] + \sum_{i=1}^{occ.} n_i\epsilon_i\left[1 - \int\left|\Phi_i\left(r\right)\right|^2 \mathrm{d}r\right]\right\} = 0 \quad \forall i \tag{2.32}$$

$$\left[-\frac{\triangle}{2} + \mathrm{V}_{ext}\left(r\right) + \mathrm{V}_H\left(\left[\rho\left(r\right)\right], r\right) + \mathrm{V}_{xc}\left(\left[\rho\left(r\right)\right], r\right)\right]\Phi_i\left(r\right) = \epsilon_i\Phi_i\left(r\right) \quad \forall i \tag{2.33}$$

$$\mathrm{V}_{xc}\left(\left[\rho\left(r\right)\right], r\right) = \frac{\delta E_{xc}\left[\rho\left(r\right)\right]}{\delta\rho\left(r\right)} \tag{2.34}$$

2.5. Basis Set Expression and Matrix Equations

Although the Kohn-Sham equation (eq. 2.33) is an advancement, it is still not analytically solvable and the Kohn-Sham orbitals $\Phi_i\left(r\right)$ have to be sought out numerically. For this, two approaches can generally be utilized: basis function expansion and real-space grid methods. In both approaches the differential equation for the unknown $\Phi_i\left(r\right)$ is converted into a set of equations for unknown, but easier determinable expansion coefficients or grid values. The more common is the basis function method, where $|\Phi_i\rangle$ are represented in a known basis $\{|\varphi_v\rangle\}$.

$$|\Phi_i\rangle = \sum_{v=1}^{N} C_{iv}\,|\varphi_v\rangle \quad \forall i \tag{2.35}$$

As a matter of principle, the basis $\{|\varphi_v\rangle\}$ ought to be complete, but in practice a basis as small as possible is employed in order to reduce the computational effort in the determination process of the expansion- or Fourier-coefficients, C_{iv}. The choice of the basis set is influenced by the problem investigated: For systems with periodic boundary conditions, such as crystals, plane waves are often used, because their mathematical handling is easy and linked to the Bloch paradigm. For spatially restricted systems, such as clusters and molecules, atomic-like basis functions (LCAO) are the method of choice, since the localized density distribution requires a larger number of plane waves for a reasonable representation. On top, the definition of plane waves requires the application of periodic boundary conditions, which results in a consideration of artifacts due to the periodicity versus the large basis extension due to the vacuum zone between the molecule images.

In either case the Hamilton operator must be written as a matrix in such basis. Thus, the combination of equations 2.33 and 2.35 leads to:

$$\hat{\mathrm{H}}\,|\Phi_i\rangle = \sum_{v=1}^{N}\hat{\mathrm{H}}C_{iv}\,|\varphi_v\rangle = \sum_{v=1}^{N}\epsilon_i C_{iv}\,|\varphi_v\rangle = \epsilon_i\,|\Phi_i\rangle \quad \forall i \tag{2.36}$$

The multiplication with $\langle\varphi_\mu|$ from the left and the linearity of the operator results in the generalized, hermitian eigenvalue equation:

$$\sum_{v=1}^{N} C_{iv}\left(h_{v\mu} - \epsilon_i s_{v\mu}\right) = 0 \quad \forall i,\mu \tag{2.37}$$

$$h_{v\mu} = \left\langle \varphi_\mu \left| \hat{\mathrm{H}} \right| \varphi_v \right\rangle = \int \varphi_\mu^*(r)\,\hat{\mathrm{H}}\varphi_v(r)\,\mathrm{d}r \tag{2.38}$$

$$\hat{\mathrm{H}} = -\frac{\triangle}{2} + \mathrm{V}_{ext}(r) + \mathrm{V}_H\left([\rho(r)], r\right) + \mathrm{V}_{xc}\left([\rho(r)], r\right) \tag{2.39}$$

$$s_{v\mu} = \langle \varphi_\mu | \varphi_v \rangle = \int \varphi_\mu^*(r)\,\varphi_v(r)\,\mathrm{d}r \tag{2.40}$$

The matrices h and s are the so-called Hamilton- and overlap-matrix, respectively, and depend on the atomic positions and the density $\rho(r)$. Due to this, a self-consistency loop with equations 2.27 and 2.37 can be constructed. There an initial density $\rho_{in}(r)$ constructs the potentials in Hamiltonian $\hat{\mathrm{H}}$, which then is used to solve eq. 2.37 to achieve $\Phi_i(r)$, which construct a new density $\rho_{out}(r)$. This new density (or a weighted mixture with the former densities) may then be taken as the new initial density $\rho_{in}(r)$ and thus starting a new iteration circle. At the end of the procedure stand densities as in- and output, which are identical (theoretical goal) or agree to each other within a predefined precision (practical approximation). With this density, the electronic problem is then finally solved and all the physical properties may be extracted.

An example for a physical property might be given by the ionization potential derived from the formula for the electronic energy. The energy functional (eq. 2.25) expressed with the kinetic functional (eq. 2.31) reads as

$$\begin{aligned} E_{\mathrm{KS}}[\rho(r)] = & \sum_{i=1}^{occ.} n_i \int \Phi_i^*(r)\left[-\frac{\triangle}{2}\right]\Phi_i(r)\,\mathrm{d}r + \int \mathrm{V}_{ext}(r)\,\rho(r)\,\mathrm{d}r \\ & + \frac{1}{2}\int \mathrm{V}_H\left([\rho(r)], r\right)\mathrm{d}r + E_{xc}[\rho(r)] \end{aligned} \tag{2.41}$$

and can then be rewritten according to the Kohn-Sham equation (eq. 2.33) and the normalization of the orbitals (eq. 2.26), while correcting for double counting with $-\frac{1}{2}\int \mathrm{V}_H(r)\,\rho(r)\,\mathrm{d}r$ and $-\int \mathrm{V}_{xc}(r)\,\rho(r)\,\mathrm{d}r$ as

$$\begin{aligned} E_{\mathrm{KS}}[\rho(r)] = & \sum_{i=1}^{occ.} n_i \int \Phi_i^*(r)\left[-\frac{\triangle}{2} + \mathrm{V}_{ext}(r) + \mathrm{V}_H(r) + \mathrm{V}_{xc}(r)\right]\Phi_i(r)\,\mathrm{d}r \\ & - \frac{1}{2}\int \mathrm{V}_H(r)\,\rho(r)\,\mathrm{d}r - \int \mathrm{V}_{xc}(r)\,\rho(r)\,\mathrm{d}r + E_{xc}[\rho(r)] \end{aligned} \tag{2.42}$$

$$= \sum_{i=1}^{occ.} n_i\epsilon_i - \frac{1}{2}\int \mathrm{V}_H(r)\,\rho(r)\,\mathrm{d}r - \int \mathrm{V}_{xc}(r)\,\rho(r)\,\mathrm{d}r + E_{xc}[\rho(r)] \tag{2.43}$$

With this the energy is given in terms of the Lagrange parameters or single-particle Hartree-type energies ϵ_i, which include the majority of electronic shell structure effects due to the exact treatment of the kinetic energy[42]. A physical meaning of the parameters ϵ_i is assigned by the interpretation through the so-called Janak's Theorem[41] or DFT-Koopmans' Theorem[43, 44] for

$$\frac{\delta E}{\delta n_i} = \epsilon_i \tag{2.44}$$

which is accepted to be an approximation to the ionization energies for the highest occupied electronic levels (HOMO). Although the relation originates from a fictitious one-electron system, proof was given that the highest occupied eigenvalue is equal to the first ionization potential[45].

3. Density Functional-based Tight Binding

Now follows a short summary of the further approximate method of density functional-based tight-binding (DFTB) up to the self-consistent charge level[6–9]. Additional developments and tests of the DFTB method are discussed in [10–26].

3.1. Stationary principle approach

The total energy of an atomic systems in DFT consists of the electronic energy and the nucleus-nucleus repulsion:

$$E_{\mathrm{tot}}^{\mathrm{DFT}} = E_{\mathrm{KS}}\left[\rho\left(r\right)\right] + \hat{\mathrm{V}}_{nuc-nuc} \tag{3.1}$$

While determination of the the latter is trivial, the whole section 2 and at last equation 2.43 are devoted to achieving the first term. The density $\rho\left(r\right)$ was obtained as the self-consistent iterative solution of equation 2.33. This involved the formation of the potential $\mathrm{V}\left(\rho_{\mathrm{in}}\left(r\right), r\right)$ from a guessed input density $\rho_{\mathrm{in}}\left(r\right)$ to calculate the Kohn-Sham orbitals $\Phi_i\left(r\right)$, which together with the occupation numbers n_i form the output density $\rho_{\mathrm{out}}\left(r\right)$, that serves as input density for the next iteration. Meanwhile, the energy expression (eq. 2.43) usually depends on the input and output densities due to the potential terms $\int \mathrm{V}\left(\rho_{\mathrm{in}}\left(r\right), r\right)\rho_{\mathrm{out}}\left(r\right)\mathrm{d}r$. Although, this equation is only evaluated as a last step of the process, the iteration cycle can be cut short by the formulation of a non-self-consistent energy functional[46]. This results in an functional $\varepsilon\left[\rho_{\mathrm{in}}\left(r\right)\right]$, that is regulated by the input density only and called Harris-functional. Thus, this functional is not strictly variational but it is equal to the Kohn-Sham functional at the ground state and stationary. This means that deviations of the input from the ground state density affect the energy only in second or higher order. The influence of those quadratic terms was analyzed by Foulkes and Haydock[47]. They rewrote the Kohn-Sham functional as

$$E_{\mathrm{KS}}\left[\rho\left(r\right)\right] = T_0\left[\rho\left(r\right)\right] + \upsilon\left[\rho\left(r\right)\right] \tag{3.2}$$

$$\upsilon\left[\rho\left(r\right)\right] = \int \mathrm{V}_{ext}\left(r\right)\rho\left(r\right)\mathrm{d}r + \frac{1}{2}\int \mathrm{V}_H\left(\left[\rho\left(r\right)\right], r\right)\mathrm{d}r + E_{xc}\left[\rho\left(r\right)\right] \tag{3.3}$$

$$\frac{\delta\upsilon\left[\rho\left(r\right)\right]}{\delta\rho\left(r\right)} = \mathrm{V}_{ext}\left(r\right) + \mathrm{V}_H\left(\left[\rho\left(r\right)\right], r\right) + \mathrm{V}_{xc}\left(\left[\rho\left(r\right)\right], r\right) = \mathrm{V}_{\mathrm{eff}}\left(\left[\rho\left(r\right)\right], r\right) \tag{3.4}$$

Therefore, the non-self-consistent Kohn-Sham equation for a given input density $\rho_{\text{in}}(r)$ was written as

$$\left[-\frac{\triangle}{2} + \mathrm{V}_{\text{eff}}\left(\left[\rho_{\text{in}}(r)\right], r\right)\right]\Phi_i(r) = \epsilon_i \Phi_i(r) \quad \forall i \tag{3.5}$$

and leading to one-electron eigenvalues ϵ_i and orbitals $\Phi_i(r)$, which form the output density

$$\rho_{\text{out}}(r) = \sum_{i=1}^{occ.} n_i \int \left|\Phi_i(r)\right|^2 \mathrm{d}r \tag{3.6}$$

But this density is neglected to obtain the non-self-consistent Harris functional $\varepsilon\left[\rho_{\text{in}}(r)\right]$ and just the eigenvalues ϵ_i enter the equation:

$$\varepsilon\left[\rho_{\text{in}}(r)\right] = \sum_{i=1}^{occ.} n_i \epsilon_i - E_H\left[\rho_{\text{in}}(r)\right] - E_{xc}\left[\rho_{\text{in}}(r)\right] - \int \mathrm{V}_{xc}\left(\left[\rho_{\text{in}}\right], r\right)\rho_{\text{in}}(r)\,\mathrm{d}r \tag{3.7}$$

The deviation from the Kohn-Sham energy functional at the ground state (eq. 2.43), which equation 3.7 resembles, was concluded from a Taylor-expansion of $\upsilon\left[\rho(r)\right]$ to be of second order in the charge density difference.

$$\begin{aligned}
\Delta\rho(r) &= \rho_{\text{out}}(r) - \rho_{\text{in}}(r) && (3.8)\\
E_{\text{KS}}\left[\rho_{\text{out}}\right] &= \varepsilon\left[\rho_{\text{in}}\right] + \varepsilon^{(2)}\left[\rho_{\text{in}}, \Delta\rho\right] && (3.9)\\
&= \varepsilon\left[\rho_{\text{in}}\right] + \frac{1}{2}\int\int \left.\frac{\delta^2\upsilon\left[\rho\right]}{\delta\rho^2}\right|_{\rho_{in}} \Delta\rho(r)\,\Delta\rho\left(r'\right)\mathrm{d}r\mathrm{d}r' && (3.10)\\
\frac{\delta^2\upsilon\left[\rho\right]}{\delta\rho^2} &= \frac{\delta \mathrm{V}_{\text{eff}}\left(\left[\rho(r')\right], r\right)}{\delta\rho(r')} = \frac{1}{|r-r'|} + \frac{\delta \mathrm{V}_{xc}\left(\left[\rho(r')\right], r\right)}{\delta\rho(r')} && (3.11)
\end{aligned}$$

The basis for the DFTB method is the functional $\varepsilon\left[\rho_{\text{in}}(r)\right]$ of equation 3.7. The self-consistent charge (SCC) formalism of the method comprises the $\varepsilon^{(2)}\left[\rho_{\text{in}}, \Delta\rho\right]$ correction term by iterative refinement of the charge fluctuations $\Delta\rho(r)$. Nevertheless, a good initial guess of the input density is essential for the method.

3.2. Approximations

The DFTB method relies on the stationary principle while adopting a number of additional approximations. The goal of these approximations is the separation of global quantities like potentials, densities and wave functions into their atomic and pairwise contributions, which allow the advance calculation of Hamilton matrix elements and double-counting terms based on isolated atomic systems and atom pairs. The main approximations are

1. superposition of pseudo-atomic densities as starting density
2. minimal-basis, valence-only LCAO wave functions

3. neglection of three-centre and crystal-field terms in the Hamiltonian (two-centre Hamiltonian)
4. repulsive pair potential for the double-counting and inter-nuclear energies
5. Mulliken charges, monopole approximation and extrapolation of $\frac{\delta \mathrm{V}_{xc}([\rho],r)}{\delta\rho}$

The total energy expression of DFTB based on equations 3.7 and 3.10 is:

$$E_{\mathrm{tot}}\left[\rho_{\mathrm{in}}+\Delta\rho\right] = \sum_{i=1}^{occ.} n_i \left\langle \Phi_i \left| \hat{\mathrm{H}}^0 \right| \Phi_i \right\rangle + E_{\mathrm{rep}}\left[\rho_{\mathrm{in}}\right] + \varepsilon^{(2)}\left[\rho_{\mathrm{in}},\Delta\rho\right] \tag{3.12}$$

$$= E_{\mathrm{BS}} + E_{\mathrm{rep}} + E_{\mathrm{G}} \tag{3.13}$$

$$\hat{\mathrm{H}}^0 = -\frac{\triangle}{2} + \mathrm{V}_{\mathrm{eff}}\left(\left[\rho_{\mathrm{in}}\right],r\right) \tag{3.14}$$

The term E_{BS} is the so-called band structure energy and is the trace of the reference Hamitonian $\hat{\mathrm{H}}^0$. The E_{rep} is the repulsive potential, which is similar to standard tight-binding theory and concentrates the double-counting terms and inter-nuclear repulsion. The last term, E_{G}, subsumes the charge fluctuations $\Delta\rho\left(r\right)$ and is achieved by the SCC treatment.

3.3. Pseudo-atomic densities

The starting density of DFTB is chosen as superposition of compressed densities of neutral atoms.

$$\rho_{\mathrm{in}}\left(r\right) = \sum_A \rho_0^A\left(r-R_A\right) \tag{3.15}$$

Due to the fact that the densities of free atoms are too spread to represent the density in poly-atomic systems, employing them would not provide a good initial guess. Hence, the compression anticipates such modification of the density in condensed systems. Furthermore, the operating experience has shown that the spatially confined densities are beneficial for a number of the applied approximations[6]. Therefore, the densities are obtained from DFT calculations of single, isolated atoms placed in an additional parabolic constriction potential. Therefore, the modified Kohn-Sham equation has to be solved:

$$\left[-\frac{\triangle}{2} + \mathrm{V}_{\mathrm{eff}}^{\mathrm{atom}}\left[\rho_0^A\right] + \left(\frac{r}{r_0}\right)^m\right]\varphi_v^{ps-at}\left(r\right) = \epsilon_v^{ps-at}\varphi_v^{ps-at} \tag{3.16}$$

The confinement potential is defined by the exponent m and the range r_0. The exponent is usually chosen to be 2, since it was shown to be of small influence on the results[12]. The range parameter is more difficult to pinpoint. Typically, it is connected to the covalent radius, r_{cov}, of an element and for covalent bond systems with the exception to $3d$ transition metals chosen to be $r_0 \approx 1.85 \times r_{\mathrm{cov}}$[12].

The slightly empirical nature of the determination of the compression radius leads to a certain degree of capriciousness in the chosen density and potential, of which the Hamilton matrix elements are calculated. This is reflected by the fact that different schemes for the pseudo-atomic calculations are at hand[10, 12, 14]. In the scheme employed here, the compression or confinement radii for the density (r_{dc}) and the wave function (r_{wfc}) are chosen separately in accordance with the scheme of [13, 14, 17]

Nevertheless, the pseudo-atomic wave functions are given as Slater type-orbitals (STO) characterized by coefficients a_{ij} and exponents α_i.

$$\varphi_v^{ps-at}(r) = \varphi_{nlm}(r) = \sum_{i=1}^{5}\sum_{j=0}^{3} a_{ij} r^{l+j} e^{-\alpha_i r} Y_{lm}\left(\frac{\vec{r}}{r}\right) \tag{3.17}$$

An in depth discussion of the basis set optimization can be found in [12] for the first- and second-row elements.

3.4. Two-Centre Approximation

The pseudo-atomic basis set is used for a LCAO expansion of the eigenfunctions $\Phi_i(r)$:

$$\Phi_i(r) = \sum_A \sum_{v[A]} C_{iv}\varphi_v(r) \tag{3.18}$$

$$h^0_{\mu v} = \left\langle \varphi_\mu \left| \hat{\mathrm{H}}^0 \right| \varphi_v \right\rangle = \int \varphi^*_\mu(r)\, \hat{\mathrm{H}}^0 \varphi_v(r)\, \mathrm{d}r \tag{3.19}$$

$$s_{\mu v} = \langle \varphi_\mu | \varphi_v \rangle = \int \varphi^*_\mu(r)\, \varphi_v(r)\, \mathrm{d}r \tag{3.20}$$

$h^0_{\mu v}$ and $s_{\mu v}$ denote the hamilton- and non-orthogonal overlap matrix elements in this basis. The elements can be calculated as soon as the pseudo-atomic calculations are complete and then tabulated as function of the distance between two centers. To get to this two-centre representation, the effective Kohn-Sham potential has to be decomposed into atomic-like contributions. Given that the exchange-correlation potential is non-linear, there are two possibilities to achieve said decomposition: potential and density superposition. The potential superposition was applied by [10, 12] and density superposition by [14].

$$\mathrm{V}_{\mathrm{eff}}([\rho_{\mathrm{in}}], r) \approx \begin{cases} \sum_c \mathrm{V}^0_c([\rho^c_0], r_c) \\ \mathrm{V}_{\mathrm{eff}}\left(\sum_c \rho^c_0(r_c)\right) \end{cases} \tag{3.21}$$

Besides, applying a valence-only basis, a number of the possible integrals are neglected (see table 3.1). The largest simplification is performed by disregarding the three-centre integrals, both because of the complexity of the integrals as well as the sheer number of combinations. Although, the crystal-field terms are relatively easy to achieve and could be used

Table 3.1.: DFTB Hamilton integrals

integral type	involved centers	DFTB status
onsite	$a = b = c$	used
two-centres	$a \neq b$, $c = a$ or $c = b$	used
three-centres	$a \neq b$, $b \neq c$ and $a \neq c$	neglected
crystal-field	$a = b \neq c$	neglected

Integrals in the DFTB Hamiltonian $h^0_{\mu v}$ (eq. 3.19). Centers a and b are orbital centers with basis functions $\mu \in a$, $v \in b$, and center c is the potential center (eq. 3.21).

for improvements, the neglection of both types results in considerable error-cancellation[6]. The discussion of the whole, complex process can be found in [10] and [7]. The remaining terms are the onsite integrals, which result from the atom calculations, and two-centre integrals, for which potentials and densities of two distinct atoms are needed.

$$h^0_{vv} = \epsilon_v \tag{3.22}$$

$$h^0_{\mu v} = \left\langle \varphi_\mu \left| -\frac{\triangle}{2} + \left\{ \begin{array}{c} \mathrm{V}^0_a\left(r_a\right) + \mathrm{V}^0_b\left(r_b\right) \\ \mathrm{V}_{\mathrm{eff}}\left(\left[\rho^a_{\mathrm{in}} + \rho^b_{\mathrm{in}}\right], r\right) \end{array} \right\} \right| \varphi_v \right\rangle \quad \mu \in a,\, v \in b \tag{3.23}$$

3.5. Repulsive Potential

The repulsive potential, which contains the double-counting terms appraised at the input density, and the inter-nuclear interaction, is approximated as a sum of pair potentials.

$$E_{\mathrm{rep}}\left(\rho_{\mathrm{in}}, \left\{\overrightarrow{R_A}\right\}\right) \approx \frac{1}{2}\sum_A \sum_{B \neq A} \mathrm{V}^{AB}_{\mathrm{rep}}\left(\left|\overrightarrow{R_A} - \overrightarrow{R_B}\right|\right) \tag{3.24}$$

The justification is given by:

- Neutral atomic fragments form the density ρ_{in} and this results in no unscreened long-range Coulomb contributions being present in the Hartree and nuclear interaction terms.
- The Hartree integrals for atom pairs depend on the internuclear distance only, since the atomic starting densities are spherical.
- Although the exchange-correlation interactions are in general not separable into pair potentials, a cluster expansion [7, 47] enables the extraction of two-body components. While higher-order terms involve density overlap between three centers, which are neglected due to the compressed starting densities, the two-body terms can be expressed by pair-potentials.

Given that all monomer contributions are summed up in the atomic orbital energies ϵ_v, the repulsive potential becomes zero in the dissociation limit. The practical approach for the determination of E_{rep} is as the distance-dependent difference between the DFTB band structure energy and the DFT total energy.

$$E_{\mathrm{rep}}(R) = E_{\mathrm{tot}}^{\mathrm{DFT}}(R) - E_{\mathrm{BS}}^{\mathrm{DFTB}}(R) \tag{3.25}$$

Hence, calculations have to be performed for one or more reference systems. These systems may be solids, dimers or simple molecules like ethane. According to the concepts and approximations thus far, the repulsive potential has some notable properties:

- For small interatomic distances, the repulsive potential has a steep slope owing to the Pauli repulsion of the electron shells.
- Between the first- and second-neighbour distance it rapidly assumes zero. This should be the case with respect to the valid pair-potential representation embodied within E_{rep}.
- The repulsive potentials calculated for different reference systems are close to each other. This is evidence for the transferability of the potential between different systems and therefore for the transferability of the method. A known exception are the potentials for highly coordinated structures such as fcc and bcc crystals[6].

The repulsive potential is practically stored in the form of a polynom or spline. These are cut at a certain distance, the cutoff radius r_{cutoff}. Beyond this radius, which is typically between the first and second neighbor distance of the atom pair, the potential should have vanished or is taken as such.

3.6. Self-Consistent Charge Corrections

The last term of the DFTB energy expressions (E_{G} in eq. 3.13) consists of the second-order corrections to the Harris functional in comparison to the Kohn-Sham functional (eq. 3.9). It becomes important when different elements are in a system and thus charge transfer and long-range Coulomb effects have a considerable influence. As before, the change in the charge $\Delta\rho$ is split into the atomic parts $\Delta\rho_a$.

$$E_{\mathrm{G}} = \varepsilon^{(2)}[\rho_{\mathrm{in}}, \Delta\rho] \tag{3.26}$$

$$= \frac{1}{2}\sum_{a,b}\int\int\left[\frac{1}{|r-r'|} + \frac{\delta \mathrm{V}_{xc}([\rho(r')], r)}{\delta\rho(r')}\right]_{\rho_{in}} \Delta\rho_a(r)\,\Delta\rho_b(r')\,\mathrm{d}r\mathrm{d}r' \tag{3.27}$$

$$\Delta\rho_a(r) = \sum_{lm} c_{lm}^a F_{lm}^a(r_a)\, Y_{lm}\left(\frac{\overrightarrow{r_a}}{r_a}\right) \approx \Delta q_a F_{00}^a(r_a)\, Y_{00} \tag{3.28}$$

$$r_a = r - R_a \tag{3.29}$$

Therefore, the correction term can be rewritten in the rather simple form:

$$E_{\mathrm{G}} = \frac{1}{2}\sum_{a,b}^{M}\gamma_{ab}\Delta q_a \Delta q_b \tag{3.30}$$

$$\gamma_{ab} = \int\int\left[\frac{1}{|r-r'|}+\frac{\delta \mathrm{V}_{xc}\left([\rho\left(r'\right)],r\right)}{\delta\rho\left(r'\right)}\right]_{\rho_{in}} F_{00}^{a}\left(r_a\right)F_{00}^{b}\left(r'_b\right)\frac{1}{4\pi}\mathrm{d}r\mathrm{d}r' \tag{3.31}$$

Hence, the γ_{ab} embodies the distance dependence of E_{G} on the ionic positions. If the entering pseudo-atomic densities and the orbital relaxations functions $F_{00}^{a}\left(r_a\right)$ are taken to be fixed and only weighted by Δq_a, then γ_{ab} depends geometrically only on the interatomic distance $R = \left|\overrightarrow{R_A} - \overrightarrow{R_B}\right|$.

In the limit of $R \to 0$, which is the case for coinciding atoms A and B, γ_{ab} or rather γ_{aa} equals the Hubbard-like parameter U_a of the atom. The Hubbard parameter is related to the chemical hardness, which is a scale for the electron affinity and the ionization potential. If the influence of the environment is disregarded and Janak's Theorem[41] is used, then U_a can be determined from the DFT calculations of the pseudo-atom as the second derivative of the HOMO of the free atom considering its occupation number.

$$\gamma_{aa} = U_a = \left.\frac{\partial^2 E_{\mathrm{atom}}}{\partial q_{\mathrm{atom}}^2}\right|_{q=q_0} = \frac{\partial \epsilon_{\mathrm{HOMO}}^{a}}{\partial n_{\mathrm{HOMO}}} \tag{3.32}$$

In the other limit, that is the for large interatomic distance, γ_{ab} scales as $\frac{1}{R}$ due to the vanishing exchange-correlation interaction. There are a number of ways to reach a continuous transition between these two limits[48–50].

Finally, the atomic charge deviations Δq_a are needed for the evaluation of equation 3.30. These are achieved from Mulliken charges as the difference from charge of the respective neutral atom q_a^0.

$$q_a = \sum_{i}^{occ} n_i \sum_{\mu[a]}\sum_{v} C_{i\mu}C_{iv}s_{\mu v} = \sum_{\mu[a]}\sum_{v} q_{\mu v} \tag{3.33}$$

$$\Delta q_a = q_a - q_a^0 \tag{3.34}$$

3.7. DFTB Secular Equation

With all the former approximations, the DFTB total energy reads as:

$$E_{\mathrm{tot}}^{\mathrm{DFTB}} = \sum_{i}^{occ} n_i \sum_{\mu[a]}\sum_{v} C_{i\mu}C_{iv}h_{\mu v}^{0} + \frac{1}{2}\sum_{a,b}^{M}\gamma_{ab}\Delta q_a \Delta q_b + E_{\mathrm{rep}}\left(\left\{\overrightarrow{R_A}\right\}\right) \tag{3.35}$$

The LCAO coefficients are found by the variational principle for a given set of atomic coordinates, which determine the matrices $h_{\mu v}$, $s_{\mu v}$ and γ_{ab}.

$$\frac{\partial}{\partial C_{i\mu}}\left[E_{\mathrm{tot}}^{\mathrm{DFTB}}+\sum_{i}^{occ} n_i\widetilde{\epsilon}_i\left(1-\sum_{\mu}\sum_{v} C_{i\mu}C_{iv}s_{\mu v}\right)\right]=0 \tag{3.36}$$

As a result the secular equation (eq. 3.37) is obtained, with the augmented Hamilton matrix elements due to the minimization of E_{G} and E_{BS}.

$$\sum_{v=1}^{N} C_{iv}\left(h_{\mu v}-\widetilde{\epsilon}_i s_{\mu v}\right) = 0 \quad \forall i,\mu \tag{3.37}$$

$$h_{\mu v} = h^0_{\mu v}+\frac{1}{2}s_{\mu v}\sum_{c}^{M}\left(\gamma_{ac}+\gamma_{bc}\right)\left(q_c-q_c^0\right) \tag{3.38}$$

As for DFT at the Kohn-Sham level (eq. 2.37), equation 3.37 is an eigenvalue problem, which has to be solved self-consistently. The result gives the eigenvectors $C_{i\mu}$ and the one-electron energies $\widetilde{\epsilon}_i$ and with these the dependent properties like charge distribution and density of states.

In the same fashion as done for the DFT energy (eq. 2.43), the DFTB total energy can be written in terms of the one-electron energies $\widetilde{\epsilon}_i$ to simplify the calculation of equation 3.35. A detailed explanation of the necessary steps is given in [7, 12–14].

$$\sum_{i}^{occ} n_i\widetilde{\epsilon}_i = \sum_{i}^{occ} n_i\left\langle\Phi_i\left|\hat{\mathrm{H}}\right|\Phi_i\right\rangle \tag{3.39}$$

$$= \sum_{i}^{occ} n_i\sum_{\mu}\sum_{v} C_{i\mu}C_{iv}h^0_{\mu v}+\sum_{i}^{occ} n_i\sum_{\mu}\sum_{v} C_{i\mu}C_{iv}\frac{s_{\mu v}}{2}\sum_{c}\left(\gamma_{ac}+\gamma_{bc}\right)\Delta q_c \quad a\,[\mu],\ b\,[v] \tag{3.40}$$

$$= E_{\mathrm{BS}}+\frac{1}{2}\sum_{c}\Delta q_c\left(\sum_{a} q_a\gamma_{ac}+\sum_{b} q_b\gamma_{bc}\right) \tag{3.41}$$

$$= E_{\mathrm{BS}}+\frac{1}{2}\sum_{c}\Delta q_c\sum_{b} 2q_b\gamma_{bc} \tag{3.42}$$

$$= E_{\mathrm{BS}}+E_{\mathrm{G}}+\frac{1}{2}\sum_{bc}\gamma_{bc}\Delta q_c\left(q_b+q_b^0\right) \tag{3.43}$$

$$E_{\mathrm{tot}}^{\mathrm{DFTB}} = \sum_{i}^{occ} n_i\widetilde{\epsilon}_i-\frac{1}{2}\sum_{ab}^{M}\gamma_{ab}\left(q_a+q_a^0\right)\left(q_b+q_b^0\right)+E_{\mathrm{rep}}\left(\left\{\overrightarrow{R_A}\right\}\right) \tag{3.44}$$

3.8. The Parametrization Recipe

According to all the above, to parametrize an element for the SCC-DFTB method the following steps have to be taken:

1. Perform DFT calculations on the neutral atom to determine the LCAO basis functions φ_v and the reference density n^a_{in}.

2. Determine suitable confinement radii for the density (r_{dc}) and wave function (r_{wfc}).
3. Numerically integrate Hamiltonian ($h_{\mu\nu}$) and overlap ($s_{\mu\nu}$) matrix elements and tabulate the values as a function of interatomic distance (R_{AB})
4. Obtain E_{rep} for every element combination under interest using suitable reference systems.

The transferability of the achieved parameters has to be subject to further testing. For this, full DFT calculations or experimental results might be used as the reference. Although, the parametrization requires a lot of thorough preparatory work, its success yields a calculation method, which is significantly less computationally demanding than but as accurate as DFT. Thus, it is faster and can handle much larger systems.[6, 51]

Part II.

SCC-DFTB Parametrization of Boron

4. Introduction to Boron

4.1. Element and Bonding Situation

The element boron was discovered in 1808 at the same time by L.-J. Gay-Lussac and L. J. Thenard in France as well as by Sir H. Davy in England. The name is reminiscent of the boron containing mineral borax, which is known since the antiquity, and the chemical resemblance to carbon[52]. Boron is the fifth element in the periodic table right before carbon and the first in group 13. It has (by default) three valence shell electrons distributed over four valence shell orbitals. Due to the larger number of valence shell orbitals compared to the valence shell electrons, boron is characterized as an electron deficient element/system. This electron "poorness" gives rise to special bonding behaviors like 2-electrons-3-centered bonds (2e3c)[53–55]. In contrast to its heavier homologues, boron forms monomers of the type BR_3 in the gas phase, which are of planar triangular geometry with bond angles of about 120° and a sp^2 hybridization of the boron atom[56]. In these compounds boron has only an electron sextet instead of an octet. Thus, the boron atom is still undercoordinated or unsaturated. The electron octet can be generated depending on the substituent through three mechanisms:

1. Adduct formation with an electron pair donor as a Lewis base[57, 58]; the intermolecular formation of so-called dative bonds[59].
2. Intramolecular, $p_\pi - p_\pi$ interaction, if the substituents R in BR_3 have free electron pairs like for example halogenides do. In this case, the free electron pairs partially occupy the empty p_z-orbital of the boron[57, 58].
3. Formation of 2e3c; in these bonds one electron pair is shared by three atoms. For example in B_2H_6, the dimer of the monomer BH_3, two hydrogens share their electron each not only with one but two boron atoms and thus act like a bridge between the two boron atoms. The formation of 2e3c is known to happen in boranes or boron hydrides and boride clusters. Hence, 2e3c also occur between three boron atoms.

4.2. Solids

The electron poorness of boron results in the exhibition of a remarkable complexity in its bulk phases: "situated between metals and insulators in the periodic table, boron has only three valence electrons, which would favor metallicity, but they are sufficiently localized that insulating states emerge"[60]. Of elemental boron at least 16 polymorphs are known

[61] and at ambient conditions the most stable phase of boron is still not experimentally determined[62]. All known elemental bulk modifications are described on the basis of a three-dimensional framework of slightly distorted B_{12} icosahedra. The currently established pure bulk phases are α-rhombohedral (α-B12)[63, 64], β-rhombohedral (β-B106)[65], β-tetragonal (T-192)[66], and γ -orthorhombic (γ- B28)[60, 67]. The static energies of α-B12 and β-B106 are nearly equal at ambient conditions, while disordered β-B106 is slightly favored when zero-point energies are considered[68, 69]. At higher pressures of several gigapascals, the α-B12 phase is expected to be more stable at all temperatures, since it is much denser. But there are opposing effects at high pressure: favoritism of metallic states and stabilization of metallic-like icosahedral clusters[70] versus the low space filling in icosahedral packed structures (34% for α-B12). These effects result in the formation of even denser phases with less icosahedra, as for example the α-Ga-type phase[71]. It was found that boron is extremely hard and semiconducting in all of these phases, but boron phases with impurities/doping atoms are often found to be metallic[60]. Experiments with β-B106 at room-temperature revealed even metastable amorphization at 100GPa[70] and onset of superconductivity at 160 GP[72].

4.3. Nanostructures

In addition to the various solid phases, the prospect of nanostructures similar to graphene and carbon nanotubes (CNT) was nourished by the prediction [73, 74] and experimental confirmation [75, 76] of stable quasi-planar and tubular clusters of elemental boron. Coming from these clusters, different models of stable boron nanostructures have been considered like fullerene-type macromolecules, nanotubes, and two-dimensional sheets.[77–84]. Even, first successes in the synthesis and characterization of boron nanotubes (BNT) [85, 86] and hints on their atomic structure and electronic properties [87, 88] have been reported. But, the exact atomic structure of these BNTs is still under research, since the quasi two-dimensional boron sheet(s), which is/are rolled up to form the BNTs, is/are yet not experimentally achieved. The so far proposed sheet models can be divided into three structural classes: triangular, hexagonal, and mixed triangular-hexagonal. One favorable representative of each class[89] are the so-called buckled triangular (BT) sheet[84], distorted hexagonal (DH) sheet[81], and α-sheet[82]. Due to the pronounced polymorphism of boron, it might be that one or more of these and other sheet structures are feasible in experiment. Nevertheless, BNTs of all classes are preestimated to have a metallic character independent of their diameter and chiral angles [79, 81, 84, 90]. Only for an α-sheet BNT of small diameter ($<$1.7 nm), semiconducting properties emerged from DFT calculations due to curvature-induced slight out-of-plane buckling[80, 83, 91]. But MP2 calculations indicate that the buckling and so the semiconducting character is a product of DFT deficiency[90]. Conductivity measurements reported by Liu et al. [87] on large-diameter (10 to 40 nm) multi-walled BNTs confirmed the prediction of metallic properties. Theoretical investigations of electronic structure and transport properties are published for fullerene-like[92] and flat[93, 94] boron clusters as well as small-radius boron nanotubes[95, 96] and BNTs

with diameters of approximately 10 nm [88]. The last allows for a comparison with the experiments of Liu et al.[87].

4.4. Boron-Hydrogen systems / Boranes

Boron hydrogen compounds are counted to the family/class of electron deficient systems, since their number of covalent interactions surpasses the number of electron pairs available. Given that these compounds do not have the possibility of comprehension by $p_\pi - p_\pi$ interaction, the covalent interactions are accompanied by 2e3c. W. N. Lipscomb was the first to publish a description of the bonding situation in these compounds by using 2e3c[53–55]. The consideration of the bonding within the molecular orbital theory has shown that the 2e3c bonds are interactions of the hydrogen 1s orbital with two sp^3 hybrid orbitals of two boron atoms (B-H-B bond) or of three sp^3 hybrid orbitals of three boron atoms (B-B-B bond). The smallest borane with 2e3c is the diborane B_2H_6, the dimer of BH_3. Longuet-Higgens and Bell have described its structure already 1943 with hydrogen bridges and not as an ethane (C_2H_6) analogue structure[97]. A more recent work on the charge density of B_2H_6 has confirmed the absence of a direct B-B bond[98] and thus ended a long discussion decisively[99].

Of great interest is also the bonding nature of the polyhedral *closo*-boranes and their isoelectronic carbaboranes and azaboranes. This is because of the electron deficiency, which results in special bonding situations and geometric arrangements[100]. The bonds existing in these substances cannot be described by the same means as organic compounds, that are Lewis structures. Hence, new concepts for these structures have been developed by W. N. Lipscomb[101], K. Wade[102, 103], and R. E. Williams[104]. Their rules allowed the prediction of structure, stability and existence of isomers. The special stability of *closo*-borane clusters was described by Morrison[105], who used a "magic number" $2n + 2$, which is also known as "inorganic Hückel's rule". Additional works were done using tensor surface harmonics[106, 107], six-electron-rule[108], Graph-theory[109], and three dimensional aromaticity[110, 111].

Overall one can say that due to the electron deficit in boranes, additional electron pairs can stabilize a structure instead of leading to its decomposition as known for organic compounds. Therefore, the variety of boranes with unorthodox geometries is quite large.

4.5. Wade's Rule

In the following the rule of Wade (other names are "Wade/Mingos rule" and "polyhedral skeletal electron pair theory") shall be explained a bit more, since it allows for the easy classification of boranes.

According to Wade's rule, there is a relation between the number of valence electrons and the structure of the *closo*-borane clusters (B_nH_{n+2}, $B_nH_{n+1}^{1-}$, $B_nH_n^{2-}$). For a polyhedron

Figure 4.1.: Classes of Boranes

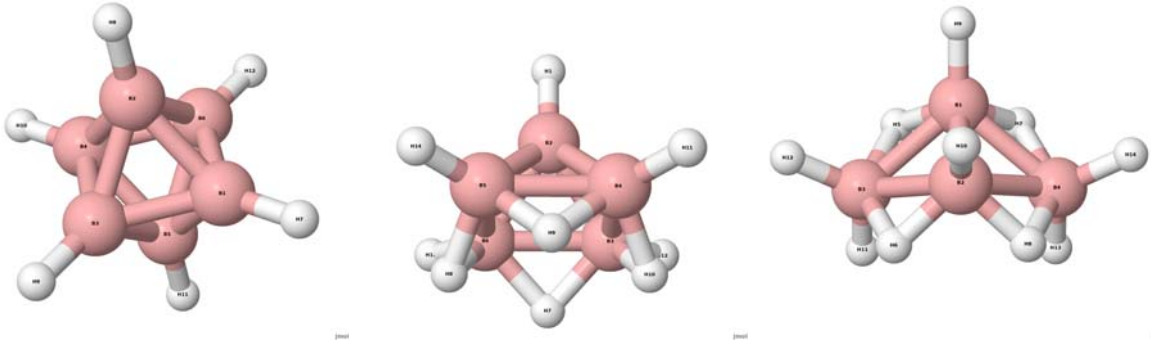

Closo-, *nido*- and *arachno*-clusters are shown for $n = 6$ from left to right, respectively. The left molecule is $B_6H_6^{2-}$, the middle one is B_5H_9, while the molecule on the right is B_4H_{10}. The labeling of the atoms is not according to the positional convention.

Table 4.1.: Types of Borane Clusters according to Wade's Rules

name	number of vertices of the polyhedron	chemical formula neutral	anion	dianion	backbone electrons
closo	n	B_nH_{n+2}	$B_nH_{n+1}^{1-}$	$B_nH_n^{2-}$	$2n+2$
nido	$n+1$	B_nH_{n+4}	$B_nH_{n+3}^{1-}$	$B_nH_{n+2}^{2-}$	$2n+4$
arachno	$n+2$	B_nH_{n+6}	$B_nH_{n+5}^{1-}$	$B_nH_{n+4}^{2-}$	$2n+6$
hypho	$n+3$	B_nH_{n+8}	$B_nH_{n+7}^{1-}$	$B_nH_{n+6}^{2-}$	$2n+8$

with n vertices, $2n + 2$ electrons are needed as backbone. This number of electrons is less than for directed, normal covalent bonds or 2e3c bonds. As backbone electrons are counted those valence electrons, which are not spent on the formation of terminal covalent bonds. For example, $B_{12}H_{12}^{2-}$ forms an icosahedron (bicapped pentagonal antiprism, $n = 12$) and has 50 valence electrons (48 from the atoms, 2 from charge). 24 of these electrons are needed for the terminal B-H bonds, which leaves 26 electrons for the cluster stabilization. Therefore, $B_{12}H_{12}^{2-}$ is an experimentally known molecule, while $B_{12}H_{12}^{1-}$ (25 backbone electrons) and $B_{12}H_{12}$ (24 backbone electrons) are unstable.

The rule of Wade has been extended to describe also non-*closo* clusters, where the boron atoms do not form a closed polyhedron. In these clusters, some of the corner of the polyhedron are unoccupied and additional hydrogens and/or electrons are added. Therefore, the number of backbone electrons changes, too. For clusters, which have one vertex unoccupied, the number of backbone electrons is $2n + 4$ and the name has the supplement "*nido*". With two missing vertices, the number changes to $2n + 6$ and the name add-on is "*arachno*". Furthermore, the unoccupied positions are nearest to each other, thus explaining the origin of the names: *closo* and *nido* stem from Latin, *clausus* and *nidus* meaning closed and nest, respectively. *Arachno* originates from Greek and stands for web. For a better understanding figure 4.1 shows *closo*-, *nido*- and *arachno*-clusters for an equal $n = 6$. A small overview over possible chemical formulas with the number of corners of the polyhedral structure basis, backbone electrons and name extensions is given in table 4.1.

Figure 4.2.: Diastereomeres of Carbaheptaborane (7) Anion

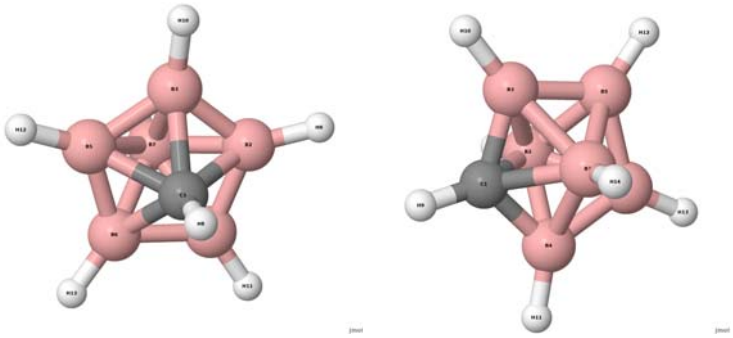

The left molecule is $1-\mathrm{CB_6H_7^{1-}}$ or $o-\mathrm{CB_6H_7^{1-}}$, while the molecule on the right is $2-\mathrm{CB_6H_7^{1-}}$ or $p-\mathrm{CB_6H_7^{1-}}$. The labeling of the atoms is not according to the positional convention.

4.6. Heteroatom Structures / Carba- and Azaboranes

The variety of clusters is further enlarged by the possibility of incorporation of one or more non-boron atoms in the boron framework. Especially for the double charged *closo*-clusters, the exchange of a boron atom by a carbon or nitrogen results in stable compounds.[110] The isoelectronic relation is given in equation 4.1.

$$\mathrm{B}_n\mathrm{H}_n^{2-} \longleftrightarrow \mathrm{CB}_{n-1}\mathrm{H}_n^{1-} \longleftrightarrow \mathrm{C_2B}_{n-2}\mathrm{H}_n \longleftrightarrow \mathrm{NB}_{n-1}\mathrm{H}_n \tag{4.1}$$

Moreover, this leads to the distinction of diastereomers, because the heteroatom breaks the symmetry of the molecule. Hence, there is a rule for the precise nomenclature of these systems. The atom positions are distinguished according to the highest priority axis, this is the axis of highest symmetry. The vertex atom on this axis has the position 1 and is the origin for the further numbering. The atoms are numbered in the the sequence: atom on the axis, atoms in the surrounding ring, atoms in the next ring(s), atom on the opposite side of the ring(s). The resulting numbers for the heteroatom position shall by definition be as small as possible. For clarification, an example for the carba- and dicarbaboranes each is given in the following.

The carbaheptaborane (7) anion has the geometry of a pentagonal bipyramide. Thus, the incorporation of the C-atom can happen on the top of a pyramid (position 1) or in the five-membered ring (position 2). This results in two non-equivalent molecules $1-\mathrm{CB_6H_7^{1-}}$ and $2-\mathrm{CB_6H_7^{1-}}$ or $o(rtho)-\mathrm{CB_6H_7^{1-}}$ and $p(ara)-\mathrm{CB_6H_7^{1-}}$, respectively. Ball-stick representations of these structures are given in figure 4.2.

In the case of the dicarbaboranes, there are two carbon atoms, whose positions relative to each other allow the distinction of diastereomeres. Assuming as example $\mathrm{C_2B_{10}H_{12}}$, which is of icosahedral shape, the positions for the first carbon are all equivalent (position 1). The second carbon atom can be in direct neighborhood, that is in the subsequent five-membered ring, (position 2), in the next-neighborhood, which is in the second five-membered ring, (position 7), or on the opposite side (position 12). The yielded molecules

Figure 4.3.: Diastereomeres of Dicarbadodecaborane (12)

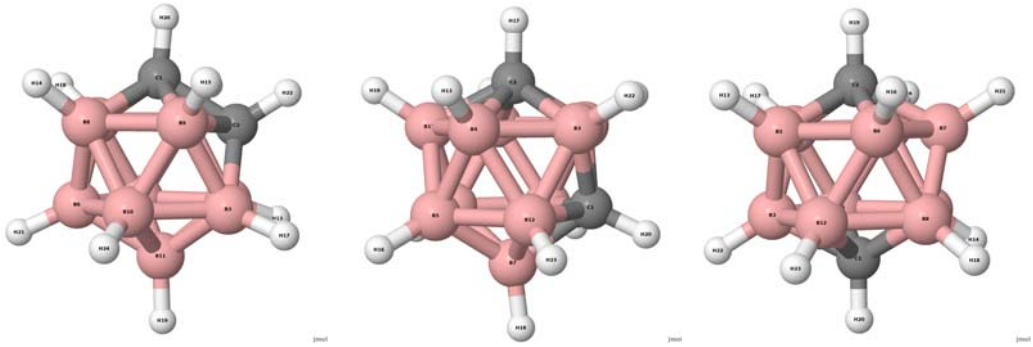

The left molecule is $1,2-C_2B_{10}H_{12}$ or $o-C_2B_{10}H_{12}$, the middle one is $1,7-C_2B_{10}H_{12}$ or $m-C_2B_{10}H_{12}$, while the molecule on the right is $1,12-C_2B_{10}H_{12}$ or $p-C_2B_{10}H_{12}$. The labeling of the atoms is not according to the positional convention.

are named accordingly $1,2-C_2B_{10}H_{12}$ or $o-C_2B_{10}H_{12}$, $1,7-C_2B_{10}H_{12}$ or $m-C_2B_{10}H_{12}$, and $1,12-C_2B_{10}H_{12}$ or $p-C_2B_{10}H_{12}$, respectively. They are shown in figure 4.3.

4.7. Dative Bonds and Isoelectronic Structures

Chemical bonds are usually defined as covalent, electrostatic or metallic[112]. But molecules like aminoborane (H_3B-NH_3), where the finding of high experimental dipole moment suggests a ionic description, are better characterized as electron-donor-acceptor-adducts.[113–115] Electron-donor-acceptor-adducts comprise all molecules, which are bonded by electrostatic, covalent and/or van-der-Waals interactions. The concepts is based on the work of Lewis[116] and the qualitative model of "Hard and Soft Acids and Bases" (HSAB) by Pearson[114, 117, 118]. The main difference of such adducts compared to "classic" covalent compounds is the dissociation. The former decompose into two closed shell fragments, while the latter form two open shell fragments.[119] Thus, this can be used as the definition of a dative bond, where the bond breaking results in an electron donor and an acceptor part or a cation-anion-pair[120]. Another difference is that the bond length in such complexes varies much more owing to the aggregate state[121–127]. Although over 40 years have been spent on these bonds by experimentalists and theoreticians, a final characterization of such bonds is still missing[59]. A common class of donor-acceptor-compounds are adducts of "electron-poor" boranes with "electron-rich" amines, acting as Lewis acids and bases respectively. Thus, the B-N bond is a classical example for the description of an electron transfer from the free electron pair of the nitrogen to the empty orbital of the boron in order to form a bond[119].

However, more complex structures than aminoborane are also known. The aminoborane is isoelectronic to ethane (C_2H_6), meaning that the two systems have the same number of valence electrons and the same type of valence orbitals. Therefore, their ground state structures are also almost the same. As a consequence of the relationship between the C_2 module to BN, many systems of organic chemistry origin can be thought of and realized,

Figure 4.4.: Structure of Borazine, the inorganic Benzene

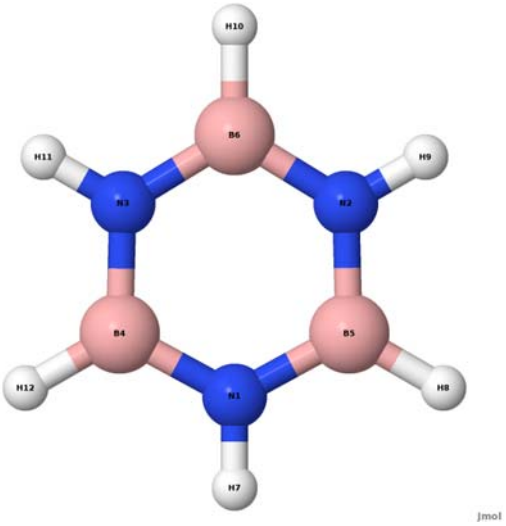

which contain the isoelectronic, inorganic BN moiety instead. A famous example is the inorganic benzene analogue borazine $B_3N_3H_6$. Its structure is shown in figure 4.4.

4.8. Application Fields of Boron

In addition to the above mentioned hope of utilizing boron nanostructures for electronic nanoscale devices, boron already has a wide area of applications. With its two natural isotopes ^{10}B and ^{11}B in 20% and 80% abundance, it is a good neutron capture agent, which is used for reactor shielding[128]. Boron is also a dopant for semiconductors as silicon and silicon carbide, where it donates a hole for p-type conductivity. The implementation is typically done via atomic diffusion at high temperatures or ion implantation from BF_3[129]. Many boron compounds have extreme hardness and toughness. Boron carbide and cubic boron nitride powders are used as abrasives, while metal borides coat tools to increase the surface resistance[130]. Borosilicate glasses usually have a low coefficient of thermal expansion, making it resistant to thermal shock and ideal for the usage in the laboratory interior (brand names Duran and Pyrex) or in consumer cook- and bakeware[131]. Furthermore, in the (organic) synthesis boron has many uses. For example, in hydroboration-oxidation reactions it is applied in order to introduce alcohols or carbonyls as functional groups[132]. Other reactions are asymmetric ally boration[132], transmetallation with organopalladium compounds or the Suzuki reaction[133]. Due to the polarization of the B-H bond, compounds of boron nitride are also under research for hydrogen storage materials[134, 135]. In general, hydrogen atoms connected to boron have a slight hydridic character, while hydrogen bonded to carbon, nitrogen or oxygen has a protonic character. Therefore, molecular hydrogen can be formed from the negative and positive polarized hydrogens in the system.

5. Simulation Results of the Boron Parametrization

5.1. Boron and boranes

The results presented in this part have been published in reference [136] and the parameters for boron have been applied in reference [88]. The calculations of the molecular systems (5.1.1 and 5.1.2) have been performed by the author of this thesis. The presented results for periodic systems shown in 5.1.3 are based on calculations, which were conducted by the co-authors of the publication [136]. They are given here for the purpose of completeness.

5.1.1. Confinement Radii and Repulsive Potential

In previous DFTB parametrizations for other elements the used confinement radii were connected to the covalent radius of the atom. It was found that five times and approximately two times the covalent radius are reasonable values as confinement radii for the atomic density (r_{dc}) and wave function (r_{wfc}), respectively[6]. For boron the covalent radius, r_{cov}, is 82 pm[52].

These findings of former parametrizations were used as a starting point to find suitable confinement radii for boron. Hence, confinement radii were tested in the range of 3 to 10 and 1.5 to 3.5 times r_{cov} for the density and the wave function, respectively. This resulted in a total number of 3150 tested combinations. For each combination of confinement radii, the repulsive potential had been determined in order to perform geometry optimizations on the whole transferability test set. The transferability test set consisted only of the molecular systems, which are described in detail later. The best confinement radii were identified as the combination leading to the smallest deviations from DFT calculations with respect to interatomic distances and angles. This led to values of $4.65 \cdot r_{cov}$ and $3.23 \cdot r_{cov}$ for the density and wave function radii, respectively.

The repulsive potentials (E_{rep}) necessary for the optimizations were created as described above in chapter 3. DFT calculations were performed using the exchange-correlation functional B3LYP[137, 138] and basis set 6-31G(d) with the program Gaussian 2003[139]. As reference system diborane(4), B_2H_4, in D_{2d} symmetry was chosen. This is the stable configuration compared to D_{2h} symmetry according to frequency calculations. The same reference system was used for both pairwise interactions, H-B and B-B. For the H-B interaction, all four hydrogens were set to equal distances R_{AB} , conserving the symmetry of

the system. The resulting energies were divided by four, the number of extended distances, to get the interaction of one H-B pair.

Since the new parameters are intended to complement the *mio*-set[13, 17, 19, 140], they should reproduce the known overbinding error of roughly 10 kcal/mol per bond. This overbinding is observable in atomization energies, but does not have any effect in isodesmic reactions. In order to achieve a balanced description of reactions, that conserve the number of shared electron pairs, the repulsive potentials for H-B and B-B were shifted to obtain a consistent overbinding with respect to atomization energies. Therefore, at a certain cutoff distance, r_{cut}, the repulsive potential was then smoothly brought back to zero to ensure correct dissociation energies. For the present parametrization, the cutoff values were chosen to minimize the errors in bonding distances, angles and vibrations, which lead to the values $r_{\mathrm{cut}}^{\mathrm{H\text{-}B}} = 1.36$Å and $r_{\mathrm{cut}}^{\mathrm{B\text{-}B}} = 1.99$Å. The shifting process has usually only marginal influence on geometries and frequencies, since the cutoff radius is chosen to be larger than any typical bonding distance. Nevertheless, a high sensitivity on the cutoff values was found especially for compounds with 2e3c bonds like tetraborane(10), B_4H_{10} . This is probably due to the bigger range of bonding distances in such molecules.

5.1.2. Molecular Systems

The former mentioned transferability test set for the new parameters included structures of *closo*-, *nido*- and *archano*-borane type as well as charged and uncharged molecules. To evaluate whether the B-B interaction is described correctly, also systems were added, which are formally forming solely covalent two electron bonds. These molecules could be referred to as "carbon-like" and are hypothetical and unsaturated. Examples of such molecules are triborane(5), B_3H_5, and tetraborane(6), B_4H_6. The complete test of transferability consisted of 16 molecules (B_2H_2, B_2H_4, B_2H_6, B_3H_5, B_4H_6, B_4H_{10}, B_5H_9, $B_{12}(D_{3h})$, $B_nH_n^{2-}$ with $n = 5 - 12$), for which the interatomic distances and angles were calculated and examined. DFT calculations with B3LYP and the 6-31G(d) basis set serve as reference, while calculations with the gradient corrected PBE[141] functional, the semi-empirical wave function based methods AM1[142] and MNDO[143] as with the existing DFTB-MatSci parametrization[140, 144] were used for a better placement of the new parametrization. Overviews of the findings for the distances and angles are given in table 5.1 and table 5.2, respectively.

The decision to use B3LYP calculations as reference instead of experimental results was based on the preference of a uniform reference. While B3LYP calculations could be performed for every structure, experimental data for the hypothetical "carbon-like" systems is not at hand, since these have not been synthesized up to now. Moreover, experimental information available on bond distances is mostly obtained by single crystal X-ray diffraction, which can not be directly compared to the calculated gas phase structures under discussion.

The root mean square (RMS) deviation error for the new SCC-DFTB parametrization is with about 1% comparable to the one of PBE, while the values of AM1 and MNDO

Table 5.1.: Molecular Boron and Borane Systems: Selected Atomic Distances

molecule	bond	B3LYP	PBE	AM1	MNDO	MatSci	DFTB (new)
B_{12}	B-B	1.643	1.643	1.659	1.657	1.645	1.669
B_2H_2	B-B	1.525	1.545	1.584	1.603	1.519	1.508
	H-B	1.176	1.171	1.199	1.160	1.204	1.185
B_2H_4	B-B	1.641	1.632	1.513	1.572	1.625	1.639
	H-B	1.201	1.212	1.190	1.159	1.214	1.201
B_2H_6	B-B	1.770	1.767	1.752	1.754	1.797	1.796
	H-B	1.191	1.201	1.192	1.164	1.211	1.197
	B-H-B	1.317	1.325	1.329	1.350	1.363	1.308
B_3H_5	B-B	1.638	1.626	1.509	1.567	1.622	1.642
	H-B	1.200	1.200	1.190	1.160	1.214	1.201
B_4H_6	B-B	1.639	1.633	1.513	1.571	1.623	1.645
	H-B	1.200	1.211	1.191	1.160	1.214	1.201
B_4H_{10}	B-B	1.724	1.721	1.660	1.752	1.663	1.696
	H-B	1.191	1.202	1.193	1.166	1.212	1.198
	B-H-B	1.257	1.272	1.268	1.257	1.337	1.266
	B-**H-B**	1.417	1.420	1.413	1.515	1.381	1.366
B_5H_9	B-B	1.695	1.700	1.668	1.759	1.721	1.718
	H-B	1.186	1.197	1.185	1.149	1.210	1.194
	B-H-B	1.348	1.357	1.348	1.292	1.373	1.321
$B_5H_5^{2-}$	B-B	1.676	1.686	1.518	1.592	1.665	1.679
	H-B	1.220	1.228	1.190	1.160	1.253	1.223
$B_6H_6^{2-}$	B-B	1.735	1.743	1.726	1.734	1.736	1.744
	H-B	1.223	1.232	1.187	1.158	1.244	1.227
$B_7H_7^{2-}$	B-B	1.829	1.831	1.783	1.836	1.869	1.831
	H-B	1.221	1.230	1.189	1.163	1.240	1.225
$B_8H_8^{2-}$	B-B	1.821	1.819	1.780	1.843	1.884	1.824
	H-B	1.217	1.225	1.190	1.166	1.237	1.221
$B_9H_9^{2-}$	B-B	1.712	1.719	1.580	1.846	1.726	1.725
	H-B	1.215	1.225	1.192	1.166	1.233	1.226
$B_{10}H_{10}^{2-}$	B-B	1.821	1.820	1.760	1.831	1.822	1.798
	H-B	1.211	1.221	1.189	1.166	1.231	1.222
$B_{11}H_{11}^{2-}$	B-B	2.026	2.011	1.910	2.061	2.029	1.956
	H-B	1.210	1.221	1.194	1.170	1.231	1.229
$B_{12}H_{12}^{2-}$	B-B	1.787	1.791	1.758	1.817	1.825	1.793
	H-B	1.208	1.217	1.188	1.166	1.227	1.217
RMS error in %		–	0.59	3.48	4.69	2.47	1.02

The values are given in Å. The root mean square (RMS) error with respect to B3LYP is given for the full set in the last row. Bold printing indicates the respective part of a 2e3c bond.

Table 5.2.: Molecular Boron and Borane Systems: Selected Atomic Angles

molecule	angle	B3LYP	PBE	AM1	MNDO	MatSci	DFTB (new)
B_{12}	B-B-B	179.4	179.4	141.1	178.7	179.9	179.8
B_2H_4	H-B-B	122.3	122.3	120.5	121.8	122.1	123.1
	H-B-H	115.4	114.8	118.9	116.4	115.8	113.7
B_2H_6	H-B-B	119.0	119.0	118.1	119.5	119.5	120.0
	B-H-B	84.4	83.7	82.5	81.0	82.5	86.7
	H-B-H	122.1	122.0	123.9	121.0	121.0	119.9
B_3H_5	B-B-B	129.4	130.8	129.5	127.5	122.2	129.1
	H-B-B	121.7	121.5	120.2	121.5	121.7	122.5
	H-B-H	116.4	116.4	119.5	117.0	116.6	115.0
B_4H_6	B-B-B	128.3	128.3	127.9	127.3	121.8	128.4
	H-B-B	114.9	114.4	115.9	116.2	118.3	114.9
	H-B-H	116.3	116.2	119.6	117.0	116.5	115.1
B_4H_{10}	B-B-B	98.6	98.1	102.0	103.7	97.3	99.2
	H-B-B	115.7	115.7	112.2	111.5	126.3	121.5
	B-H-B	88.1	86.5	86.3	84.8	95.2	92.3
	H-B-H	119.0	118.4	126.3	122.9	120.4	117.3
B_5H_9	B-B-B	64.1	63.8	66.1	64.9	65.8	64.5
	H-B-B	131.4	131.7	129.7	118.1	129.8	131.0
	B-H-B	83.7	82.9	85.0	86.4	85.8	87.9
	H-B-H	90.8	90.3	93.8	102.7	90.4	92.1
$B_5H_5^{2-}$	B-B-B	56.9	57.2	49.9	52.1	53.4	55.8
	H-B-B	129.2	128.7	140.7	137.9	133.5	130.4
$B_6H_6^{2-}$	B-B-B	60.0	60.0	60.1	60.1	60.0	60.0
	H-B-B	135.0	135.0	136.9	135.1	135.00	135.0
$B_7H_7^{2-}$	B-B-B	63.1	63.0	63.4	63.5	63.6	63.0
	H-B-B	140.4	140.7	139.5	139.8	139.3	140.7
$B_8H_8^{2-}$	B-B-B	60.2	60.1	60.4	59.8	61.0	60.6
	H-B-B	122.4	122.6	119.5	120.6	121.2	121.3
$B_9H_9^{2-}$	B-B-B	58.6	58.5	62.1	52.7	56.9	57.8
	H-B-B	127.2	127.2	131.0	130.9	127.2	127.0
$B_{10}H_{10}^{2-}$	B-B-B	90.0	90.0	89.9	90.0	90.0	90.0
	H-B-B	131.8	131.8	131.3	131.2	130.8	131.6
$B_{11}H_{11}^{2-}$	B-B-B	60.9	60.8	61.5	62.0	61.2	61.0
	H-B-B	107.2	106.3	108.0	110.2	109.6	105.4
$B_{12}H_{12}^{2-}$	B-B-B	60.0	60.0	59.9	59.8	60.0	60.0
	H-B-B	121.7	121.7	121.7	121.5	121.7	121.7
RMS error in %		–	0.44	3.40	3.36	2.57	1.17

The values are given in degree. The root mean square (RMS) error with respect to B3LYP is given for the full set in the last row.

show larger deviations (errors of about 3% and 4% , respectively). The average result for DFTB-MatSci is somewhere in between. It can be seen that all methods perform quite well for small, uncharged molecules and even for the hypothetical molecules the semi-empirical methods yield satisfactory results. This is worth mentioning since these molecules are probably not part of their parametrization. An exception for MNDO are the *arachno*-structure tetraborane(10), B_4H_{10}, and the *nido*-structure pentaborane(9), B_5H_9, where the 2e3c-bonds are broken and therefore the molecules are deformed. In the case of B_5H_9, this deformation is so drastic that the *nido*-character of the molecule is changed to an *arachno*-like character, meaning that the basic structural polyhedron is changed. The errors of AM1 for B_{12} are fortified by buckling of the originally planar structure. The limitations of AM1 and MNDO are identifiable for the charged molecules, when compared to PBE and SCC-DFTB. DFTB-MatSci seems to be less exact for 2e3c-bonds, where deviations of up to 8% were found, while the descriptions of terminal H-B bonds and B-B interactions are reasonable even for charged molecules. In the molecules $B_5H_5^{2-}$, $B_9H_9^{2-}$ and $B_{11}H_{11}^{2-}$, notable bond elongations of about 4% at most are observed for SCC-DFTB. Those are mainly leading to enlarging the closed polyhedral cluster on one side and therefore "clustering" of atoms on the other side. But still the symmetry of the molecules is conserved. While the clustering of atoms is observable for AM1 and MNDO, too, these methods also tend to break the symmetry, which lead to errors of up to 12% and 24% , respectively.

A full normal mode analysis was performed for five, uncharged molecules. This yielded 108 vibrational frequencies in total for comparison. In table 5.3 the SCC-DFTB results are compared to PBE/6-31G(d), AM1 and MNDO, while B3LYP/6-31G(d) is again the reference. This is due to the fact that experimental values are not available for all molecules and/or have an unresolved symmetry of the vibrational modes, which might lead to assignment problems. The RMS errors show that the agreement of SCC-DFTB and PBE with the reference is significantly better than the one of AM1 and MNDO. As examples the complete list of individual vibrational modes of B_2H_6 and B_4H_{10} are compared in table 5.4 and table 5.5. The close analysis reveals that the largest errors of SCC-DFTB occur for bending modes. The stretching modes on the other hand are more accurately described. The mean of the absolute discrepancy of SCC-DFTB from DFT/B3LYP is approximately 53 cm^{-1}. This is nearly the same as for PBE with 41 cm^{-1}. Whereas the deviations for AM1 and MNDO are more than twice as large. The symmetry ordering of the modes is quite the same for B3LYP and PBE. The other methods (AM1, MNDO and SCC-DFTB) show all the same difficulties in matching the symmetry ordering.

As further test for the new parametrization atomization energies were calculated. As mentioned, shifts were applied to the repulsive potentials of H-B and B-B in order to match the overbinding of the *mio*-set. The shifts were determined for the B-B and H-B interaction on B_{12} and BH_3, respectively. Therefore, the overbinding for each combination could be isolated. In table 5.6 and table 5.7 the results of the atomization energy and overbinding are listed for DFT using B3LYP, PBE and LDA exchange-correlation functionals together with SCC-DFTB. As expected, LDA strongly overbinds while the gradient corrected PBE and

Table 5.3.: RMS Error of Harmonic Vibrational Frequencies of Boranes

molecule	PBE	AM1	MNDO	DFTB
B_2H_4	6.47	13.68	16.78	8.36
B_2H_6	4.84	10.67	10.76	7.37
B_3H_5	6.36	17.01	19.15	8.98
B_4H_6	5.59	18.93	20.09	6.59
B_4H_{10}	4.60	9.99	10.33	4.57
full test set	5.57	14.05	15.42	7.17

RMS errors are given in % with respect to the B3LYP/6-31G(d) reference for each molecule and the full test. Prior to the normal mode analysis, the geometries of the molecules have been optimized at the respective level of theory.

Table 5.4.: Harmonic Vibrational Frequencies of B_2H_6

symmetry	B3LYP	PBE	AM1	MNDO	DFTB
B_{2u}	356	305	320	402	357
A_g	797	792	787	819	749
A_u	852	832	871	853	747
B_{2g}	888	878	710	823	767
B_{1g}	947	917	966	972	813
B_{2u}	978	897	1128	1192	952
B_{1u}	1000	963	1169	1144	873
B_{3g}	1055	980	1228	1239	1055
B_{3u}	1205	1159	1113	1223	1083
A_g	1210	1161	1301	1308	1098
B_{3u}	1730	1688	1377	1530	1809
B_{2g}	1862	1851	1694	1815	1833
B_{1u}	2019	2020	2117	2303	2162
A_g	2203	2167	2252	2430	2230
B_{3u}	2638	2578	2814	2908	2650
A_g	2651	2590	2807	2905	2661
B_{1g}	2731	2670	2825	2972	2755
B_{2u}	2744	2683	2838	2981	2762
RMS error in %	–	4.84	10.67	10.76	7.37

The modes are given in cm^{-1}. Prior to the normal mode analysis, the geometries of the molecules have been optimized at the respective level of theory.

Table 5.5.: Harmonic Vibrational Frequencies of B_4H_{10}

symmetry	B3LYP	PBE	AM1	MNDO	DFTB
A_1	212	196	196	243	204
B_2	357	342	356	261	397
A_2	416	402	274	409	384
B_2	466	552	474	494	522
A_1	561	586	540	479	452
B_1	571	580	522	512	553
A_2	678	693	535	549	638
A_1	683	660	823	768	627
B_1	770	723	756	801	748
A_1	807	794	892	889	758
A_1	865	844	1036	1016	957
B_2	888	865	897	918	833
A_2	911	898	790	811	801
B_1	921	892	929	908	837
B_2	954	909	927	968	907
A_1	1021	965	1184	1187	1014
B_1	1027	986	1076	1084	929
A_2	1044	1002	1021	1017	930
A_2	1102	1059	1203	1212	1035
B_1	1120	1067	1211	1226	1081
B_2	1171	1125	1235	1249	1101
A_1	1187	1138	1242	1260	1110
B_2	1332	1309	1347	1400	1374
A_2	1462	1439	1410	1441	1461
B_1	1536	1493	1429	1460	1543
A_1	1579	1550	1546	1596	1582
A_1	2258	2187	2357	2489	2298
B_1	2260	2203	2373	2504	2282
B_2	2274	2212	2289	2476	2304
A_2	2284	2231	2291	2480	2296
B_2	2615	2545	2782	2871	2642
A_1	2620	2549	2781	2871	2646
A_1	2706	2638	2803	2916	2730
B_2	2708	2640	2829	2954	2740
B_1	2713	2659	2792	2912	2726
A_1	2722	2665	2831	2955	2743
RMS error in %	–	4.60	9.99	10.33	4.57

The modes are given in cm^{-1}. Prior to the normal mode analysis, the geometries of the molecules have been optimized at the respective level of theory.

Table 5.6.: Atomization Energies of Molecular Boron and Borane Systems

molecule	B3LYP	LDA	PBE	DFTB
B_{12}	1323.85	1662.03	1453.80	1563.95
BH_3	286.74	309.39	295.03	316.84
B_2H_2	266.20	302.65	337.10	300.43
B_2H_4	460.12	509.04	459.31	512.23
B_2H_6	622.64	685.83	614.26	732.58
B_3H_5	603.66	712.13	640.29	709.76
B_4H_6	812.05	914.12	820.47	906.67
B_4H_{10}	1107.73	1273.90	1128.64	1370.55
B_5H_9	1182.77	1377.93	1219.35	1464.34

The spin polarization energy of isolated atoms was taken into account.
No correction for zero point motion was performed.

Table 5.7.: Overbinding of Molecular Boron and Borane Systems

molecule	LDA	PBE	DFTB
B_{12}	14.00	5.34	10.00
BH_3	7.42	2.64	10.03
B_2H_2	12.03	23.49	11.41
B_2H_4	9.66	-0.28	10.42
B_2H_6	6.93	-1.02	12.21
B_3H_5	15.37	5.12	15.16
B_4H_6	11.21	0.82	10.51
B_4H_{10}	8.66	1.03	13.83
B_5H_9	11.38	2.06	16.56
Average	10.74	4.36	12.24

The values are given in kcal/mol per bond with respect to B3LYP/6-31G(d).
The spin polarization energy of isolated atoms was taken into account.
No correction for zero point motion was performed.

the hybrid functional B3LYP both give more similar results. SCC-DFTB yields results of the level of LDA. Although the resulting average overbinding is close to the desired 10 kcal/mol per bond with 12.24 kcal/mol per bond, results for some bonds exceed 16 kcal/mol. Since this is the case for the molecule with the most B-H-B bonds in the test set (B_5H_9), this suggests that 2e3c bonds are energetically not well enough described. However, the errors for B_2H_6 and B_4H_{10}, which also comprise B-H-B bonds to a large extent, are smaller than for B_3H_5, a carbon-like borane.

Due to the molecules in the test set, the (vertical) ionization potentials (IP) of the double charged *closo*-clusters are of interest. McKee and co-workers[145] performed calculations on these systems. They found that in the series of clusters, which are covered in the test set, only $B_{12}H_{12}^{2-}$ should overcome the Coulomb repulsion. Therefore, it should be the only cluster with a positive vertical IP. The values of the IP are given in table 5.8 and visualized in figure 5.1. The same trend of the IP is achieved for DFT and SCC-DFTB, although SCC-DFTB gives a slightly negative IP for $B_{12}H_{12}^{2-}$. Any influence of spin polarization for DFTB[19] has also been examined, but was found to be of only marginal effect. Given the fact that the SCC-DFTB basis set has roughly the same size as the STO-3G one, the

Table 5.8.: Ionization Potentials for Boron Hydride Dianions $(B_nH_n^{2-})$

n	McKee et. al.	LDA 6-311++G**	PBE 6-311++G**	B3LYP 6-311++G**	B3LYP STO-3G	DFTB
5	-2.60	-2.29	-2.12	-2.21	-6.27	-2.97
6	-1.50	-1.14	-0.78	-0.96	-4.29	-2.24
7	-1.00	-0.93	-0.58	-0.68	-3.68	-1.77
8	-1.69	-1.62	-1.73	-1.70	-4.57	-2.06
9	-1.20	-1.03	-1.22	-1.18	-3.98	-2.03
10	-0.27	-0.04	0.22	0.08	-2.28	-1.17
11	-0.54	-0.47	-0.54	-0.54	-2.88	-1.25
12	1.64	1.20	1.97	1.63	-0.03	-0.21

The values are given in eV. The structure of the ionized anion was not relaxed; i.e., vertical ionization potentials are computed. Reference data by McKee[145] are included for comparison.

Figure 5.1.: Ionization Potentials for Boron Hydride Dianions $(B_nH_n^{2-})$

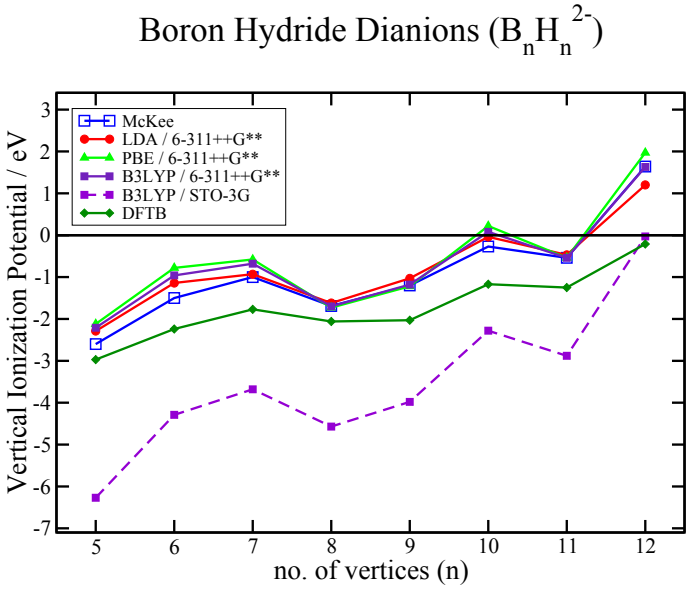

The structure of the ionized anion was not relaxed; i.e., vertical ionization potentials are computed. Reference data by McKee[145] are included for comparison.

proximity of the SCC-DFTB results to DFT with larger basis sets is remarkable.

5.1.3. Periodic Systems

To check the reliability of the new SCC-DFTB parametrization for boron in periodic systems, geometry relaxations and electronic structure calculations of bulk elemental boron, three models of stable two-dimensional boron sheets, and three boron nanotubes obtained by rolling up each of the three sheets were performed. To speed up the convergence of the self-consistent loop during geometry relaxations, the molecular orbital occupations were determined according to a Fermi distribution function corresponding to an electronic temperature of 100 K. For the subsequent single point calculations at the converged geometries the temperature was kept equal to zero. In order to validate the SCC-DFTB results, full DFT calculations with the generalized gradient approximation[141] (called

Figure 5.2.: Structure of *alpha*-Boron

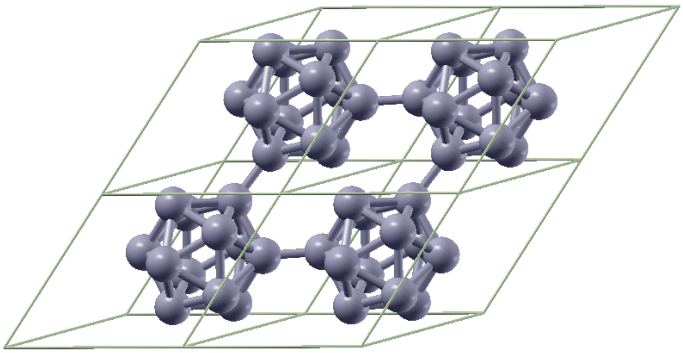

Schematic view of four neighboring unit cells of α-rhombohedral boron.
One unit cell comprises a B_{12} icosahedron.

here DFT/PBE) were performed for the same systems. For the DFT/PBE calculations the projector augmented wave method[146] as implemented in the VASP package[147] was used. The decision for the PBE exchange-correlation functional as the reference here instead of the B3LYP is justified as the former provides more reliable geometries and atomization energies of metallic and small-gap semiconducting systems than the latter[148]. Full geometry optimizations (optimization of lattice vectors and the atomic coordinates within a unit cell) have been carried out, and the atomic forces were reduced to be below 1 meV/Å. For all these calculations the energy convergence over the number of k points was reached, and the tetrahedron method for k-integration was used.

As a test system for bulk boron, the α-rhombohedral boron crystal[63, 64] is chosen. Its rhombohedral unit cell comprises one B_{12} icosahedron. Figure 5.2 shows four neighboring unit cells of α-rhombohedral boron. The three models of boron sheets studied here are the so-called α-sheet[82], the buckled triangular sheet[84] (BT-sheet), and the distorted hexagonal sheet[81] (DH-sheet). The lattice structures of these sheets with the corresponding lattice vectors are shown in figure 5.3. Boron nanotubes can be obtained by rolling up the corresponding boron sheet along the direction of the so-called chiral vector. This chiral vector ($\vec{C}$) is expressed in terms of the sheet's lattice vectors (a_1 and a_2) as

$$\vec{C} = n\vec{a_1} + m\vec{a_2} \tag{5.1}$$

Knowing the lattice vectors of the original sheet, the structure of a particular nanotube is defined by the pair of numbers (n, m). Here the results of calculations are presented for a (4,0) α-BNT, a (0,12) BT-BNT and a (4,4) DH-BNT, which originate from the α-sheet, the BT-sheet and the DH-sheet, respectively (see figure 5.4).

The results of geometry optimizations (bond lengths and angles) for each system are compared, and the RMS of deviations in percent are summarized in table 5.9. The overall agreement of the structures obtained with the two different methods is discernible. For several systems (bulk boron, DH-sheet and the DH-BNT) the average deviation of the geometric parameters is close to 2%. The other systems show larger deviations, however,

Figure 5.3.: Schematic View of three Models of two-dimensional Boron Sheets

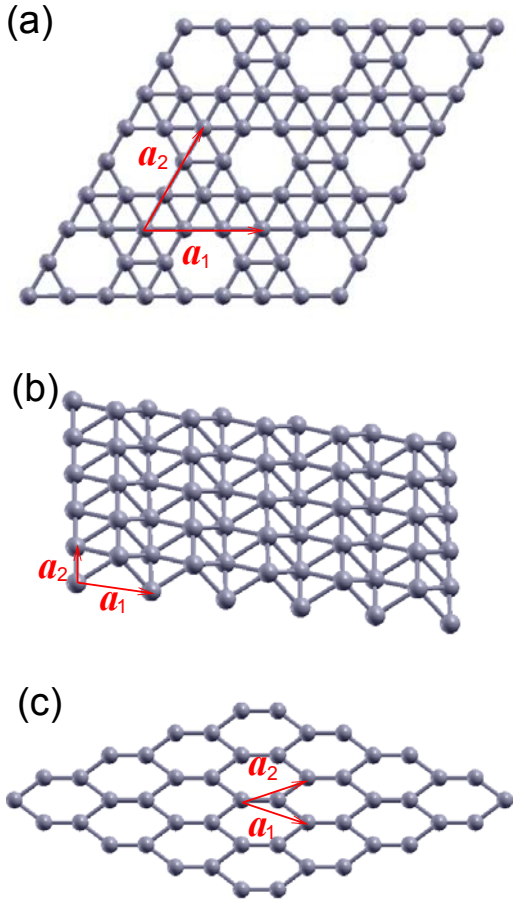

Presented are the three considered models of two-dimensional boron sheets: (a) α-sheet, (b) buckled triangular sheet, and (c) distorted hexagonal sheet; a_1 and a_2 are the lattice vectors.

Figure 5.4.: Schematic View of three Boron Nanotubes

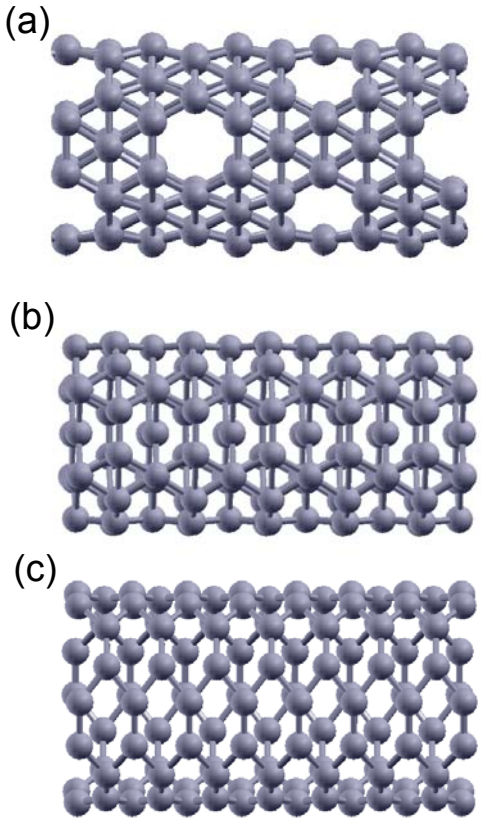

Structures are obtained by rolling up the three different boron sheets:
(a) (4,0) α-BNT, (b) (0,12) BT-BNT, and (c) (4,4) DH-BNT.

Table 5.9.: Overview of Deviation of the Geometric Parameters for Periodic Boron Systems Calculations

system	bond lengths	angles
α-rhombohedral	1.7	1.0
α-sheet	5.0	1.9
BT-sheet	3.8	1.6
DH-sheet	1.3	1.4
α-BNT (4,0)	4.3	4.2
BT-BNT (0,12)	3.4	3.4
DH-BNT (4,4)	1.4	2.9

The deviation between DFT/PBE and DFTB is given as RMS in %.

Figure 5.5.: Comparison of Band Structures of α-rhombohedral Boron

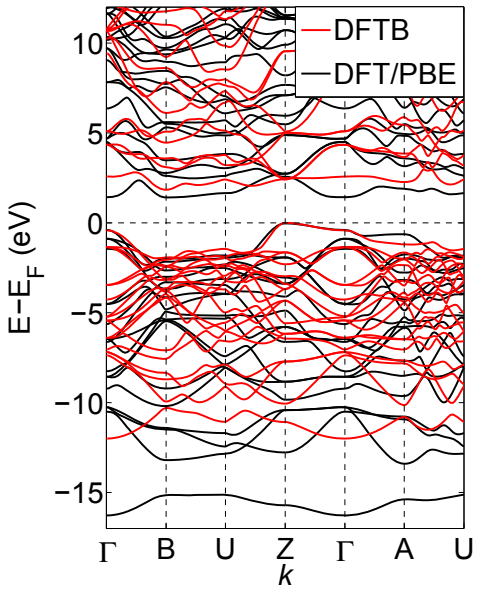

Data obtained at the DFTB (red lines) and DFT/PBE (black lines) levels of approximation for the same geometry (taken from the DFT/PBE calculation).

they do not exceed 5%. Interestingly, comparing the RMS deviations of a boron sheet and the corresponding nanotube, it is found that average deviations of lengths are almost similar, while those of angles are roughly twice as high for the nanotubes than for the sheets. Compared to the results for molecular systems (see table 5.1 and table 5.2), the deviations of the geometric parameters in case of periodic systems are larger. However, it has to emphasize here that the DFTB parametrization for boron was done in finite molecular systems using i) local basis set and ii) B3LYP exchange-correlation functional. Despite of this, it can be concluded that the standard geometry optimization procedures using the new boron SK files is able to deliver reliable results not only for finite molecules but also for periodic structures.

The next point is the comparison of band structures calculated with the DFTB and the DFT/PBE methods for each of the chosen periodic systems. To allow for an unbiased comparison, both types of electronic structure calculations are performed for a fixed geom-

etry, namely the relaxed DFT/PBE geometry. The results for the α-rhombohedral boron are presented in figure 5.5. In general, the valence bands qualitatively agree. For energies close to the Fermi level (E_F) the bands almost coincide, however for energies far from E_F the two sets of bands deviate quite strongly: namely, the DFTB valence bands are shifted towards higher values with respect to the DFT/PBE bands. The deviation of conduction bands is also quite noticeable: the lowest DFTB conduction band lies higher compared to the corresponding DFT/PBE one. Both calculation methods show that α-rhombohedral boron has an indirect band gap, which is defined between the top of the valence band at Z point and the bottom of the conduction band at B point. The calculated band gap is equal to 1.840 eV for DFTB and 1.446eV for DFT/PBE. The experimentally obtained values of the band gap for this system range from 1.9 to 2.055eV[149–152]. Thus, both theoretical approaches underestimate the band gap of α-rhombohedral boron, however the DFTB result is closer to the experimental value. The DFT/PBE values for the energy of the lowest conduction band at the points B and Γ are almost equal to one another (1.446 and 1.460eV, respectively). Earlier calculations[64] (with different exchange-correlation functional) gave similar results, however the bottom of the conduction band (1.427 eV) was found to be at the Γ point, and the indirect band gap was defined between Z and Γ. In contrast, the DFTB value of the lowest conduction band at Γ is noticeably higher (by 0.736 eV) than at Z.

In the case of two-dimensional boron sheets (see figure 5.6) the DFTB calculation reproduces the DFT band structures close to Fermi energy quite well (both valence and conduction bands). The deviations become larger for energies 2 eV and further away from E_F. However, the qualitative agreement for all valence bands is apparent, and the main difference between the two sets of bands is seen as a shift of DFTB valence bands upwards. In the region of unoccupied states the number of DFTB conduction bands is lower than that of DFT because of smaller DFTB basis set. Similar conclusions as for boron sheets can be drawn for band structures of BNTs (in figure 5.7 the bands are shown for the energy range from -3 to 3 eV). It is seen that even for such complicated structures like nanotubes with up to 64 atoms per unit cell (case of (4,0) α-BNT) the agreement between bands, obtained within DFTB and DFT/PBE approaches, is good.

Therefore, the comparison of the electronic structures of different periodic systems shows that the DFTB parametrization is able to reproduce the band structures quite well for energies close to Fermi energy (within 2 eV). Again, it has to be emphasized that the DFTB parametrization used here for the electronic structure calculation of periodic systems was constructed for finite molecules using a different basis set and exchange-correlation functional than those used in our benchmark periodic calculations. Therefore, these small deviations of the two sets of bands are to be expected. The energy bands start to noticeably deviate for energies far from E_F, that is seen as a "compression" of the DFTB set of the valence bands. This result indicates that in the tight binding approach the so-called hopping integrals are underestimated. However, overall qualitative agreement of valence bands is obtained. Especially well reproduced are the bands of metallic systems (like boron sheets and tubes tested here), while the band structure near the band gap of non-metallic

Figure 5.6.: Comparison of Band Structures of three two-dimensional boron sheets

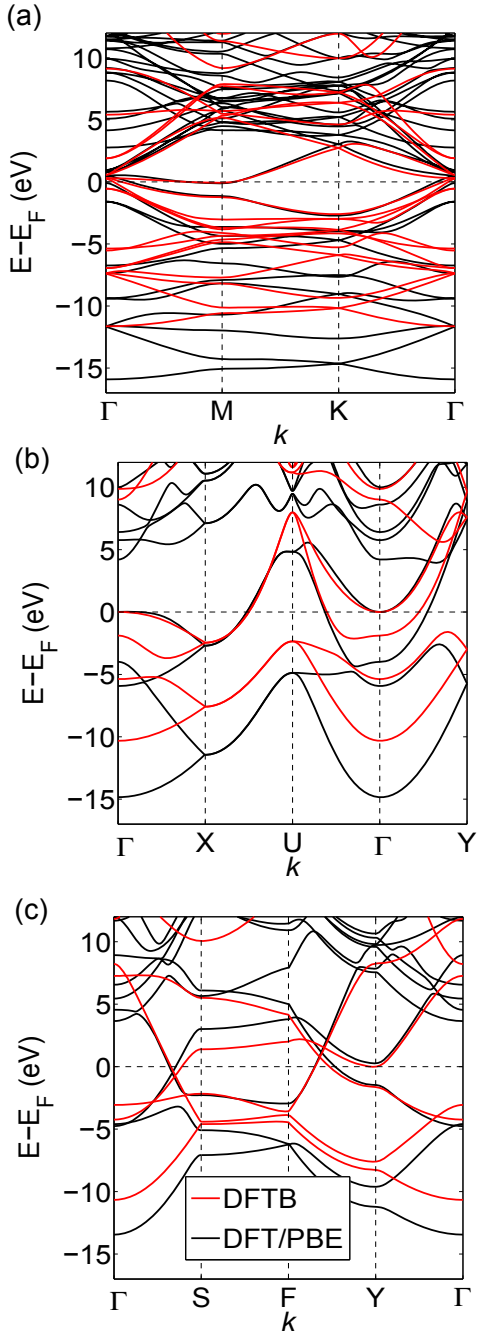

Data obtained at the DFTB (red lines) and DFT/PBE (black lines) levels of approximation for the same geometry (taken from the DFT/PBE calculation): (a) α-sheet, (b) buckled triangular sheet, and (c) distorted hexagonal sheet. Valence bands qualitatively agree. Due to a relatively small basis set, DFTB shows fewer conduction bands than DFT/PBE. Close to the Fermi energy, DFTB accurately reproduces all bands.

Figure 5.7.: Comparison of Band Structures of three Boron Armchair Nanotubes

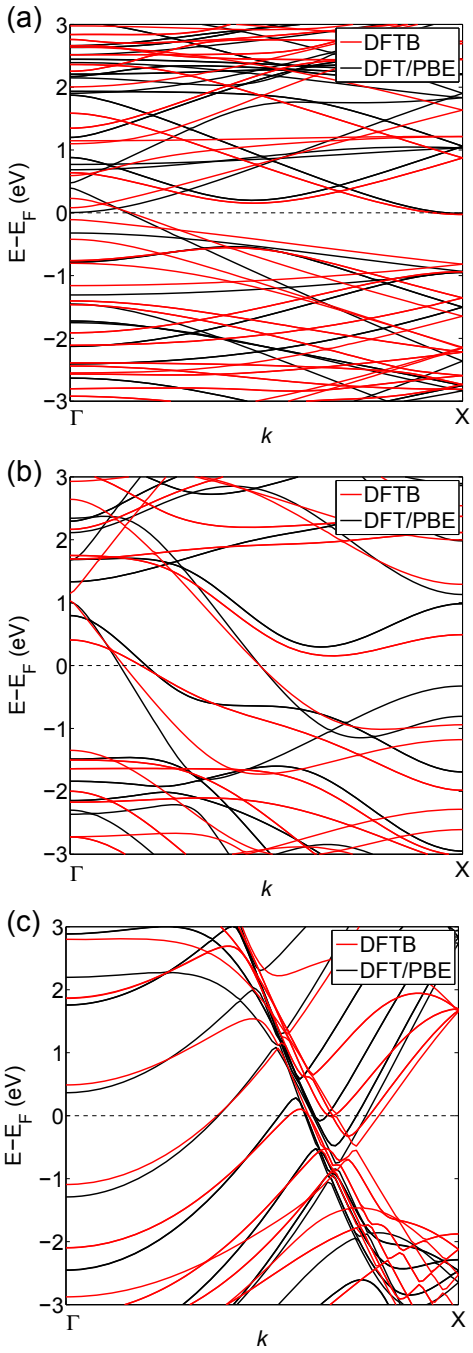

Data obtained at the DFTB (red lines) and DFT/PBE (black lines) levels of approximation for the same geometry (taken from the DFT/PBE calculation): (a) (4,0) α-BNT, (b) (0,12) BT-BNT, and (c) (4,4) DH-BNT.

Table 5.10.: Cohesive (Atomization) Energies of Periodic Systems and DFTB Overbinding Per Bond

System	E^{coh} (DFT/PBE)	E^{coh} (DFTB)	overbinding per bond
α-rhombohedral	6.669	7.418	5.74
α-sheet	6.265	6.523	2.26
BT-sheet	6.178	8.038	14.25
DH-sheet	6.025	7.506	13.61
α-BNT (4,0)	6.175	6.517	2.99
BT-BNT (0,12)	5.912	6.780	6.14
DH-BNT (4,4)	5.924	7.428	13.82

The values for the cohesive energies are given in eV/atom, while the overbinding per bond is in kcal/mol. The spin polarization energy of isolated atoms was taken into account. No correction for zero point motion was performed.

systems cannot be accurately reproduced by DFTB. The problem here is a relatively small basis set for a proper calculation of unoccupied states, which results also in smaller number of DFTB conduction bands.

In addition to energy bands, the cohesive (atomization) energies E^{coh} of periodic systems obtained with DFTB and DFT/PBE are compared for the optimized geometries. The cohesive energy is defined as

$$E^{\mathrm{coh}} = E^{\mathrm{at}} - {}^{E^{\mathrm{tot}}}\!/_{N} \tag{5.2}$$

There E^{at} and E^{tot} are the ground-state energies of a spin-polarized isolated boron atom and the whole system, respectively, and N is the number of atoms in the system. From this definition it follows that positive values of E^{coh} correspond to bound (stable) structures. For periodic systems E^{tot} is calculated for one unit cell, and N is equal to the number of atoms per unit cell. The cohesive energies of the periodic test systems obtained with the two methods and the DFTB overbinding per bond are summarized in table 5.10. The comparison shows that DFTB overestimates E^{coh} on the average by ca. 1.0 eV/atom. Normalized to a single bond, we obtain an average overbinding of 0.366 eV = 8.4 kcal/mol. Such an overestimation is in agreement with the mentioned overbinding of approximately 10 kcal/mol per bond.

5.2. Carbaboranes

Although it is fine to have a parametrization that works for an element in homonuclear molecules and periodic systems, the application of the SCC-DFTB method needs all elemental combinations in the system of interest. Therefore, the next step for a diversified parametrization is the creation of the boron-carbon Slater-Koster-File. Carbon is the natural choice for the strutted extension to the *mio*-set[13, 17, 19, 140], since carbon is the central element of the set. The test set for this combination consisted of boron containing alkanes (H_2C-BH, H_3C-BH_2, $H_5C_2-BH_2$, $(H_3C)_2-BH$, $H_2C-(BH_2)_2$, $H_3C-B_2H_3$) as well as *closo*-carbaborane anions ($CB_{n-1}H_n^{1-}$) and -dicarbaboranes ($C_2B_{n-2}H_n$), which are derived from the *closo*-borane dianions ($B_nH_n^{2-}$ with $n = 5-12$). As reference system for the repulsive potential H_3C-BH_2 was used. Its structure is shown in figure 5.8. Different diastereomeres of *closo*-carbaboranes have to be considered, since the inclusion of one carbon atom breaks the initial symmetry of the boranes.

Figure 5.8.: Reference System E_{rep}(B-C)

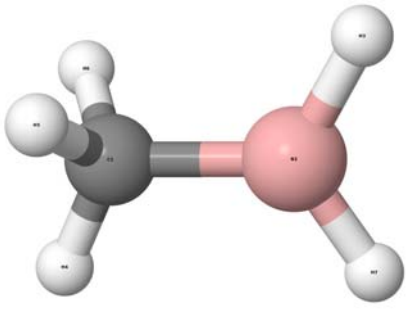

To determine the performance of the parameters for B-C, the results of SCC-DFTB were compared to full DFT calculations using NWChem program[153] with LDA, PBE and B3LYP as exchange-correlation functional with 6-311++G**[154, 155] as basis set taken from [156]. As for the parameters for B-B and B-H (5.1.2) and for the same reasons B3LYP had been chosen as reference for the comparison. Table 5.12 and table 5.16 show the RMS errors for LDA, PBE and SCC-DFTB with respect to B3LYP from the atomic distances and angles, respectively. Examples for the examined distances are given in table 5.11, and for angles in tables 5.13, 5.14 and 5.15.

Figure 5.9.: Structure of $CH_3-B_2H_3$

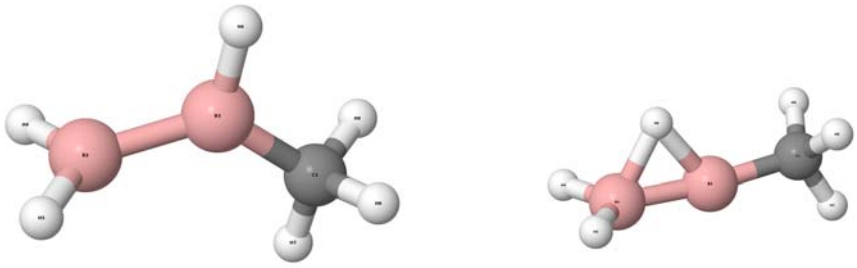

a) b)

The structure of methyldiborane as it resulted from B3LYP (a) and LDA (b) calculation.

Table 5.11.: Carbaborane Systems: Selected C-B Distances

molecule	B3LYP	LDA	PBE	DFTB
H_2C-BH	1.376	1.372	1.376	1.368
H_3C-BH_2	1.557	1.536	1.553	1.554
$H_5C_2-BH_2$	1.556	1.535	1.553	1.516
$H_2C-(BH_2)_2$	1.562	1.544	1.558	1.569
$H_3C-B_2H_3$	1.570	1.516	1.566	1.569
$(H_3C)_2-BH$	1.564	1.545	1.560	1.567
$2-CB_4H_5^{1-}$	1.716	1.680	1.705	1.761
$CB_5H_6^{1-}$	1.627	1.615	1.624	1.609
$1-CB_6H_7^{1-}$	1.739	1.718	1.731	1.723
$2-CB_6H_7^{1-}$	1.740	1.714	1.729	1.626
$1-CB_7H_8^{1-}$	1.521	1.512	1.518	1.496
$3-CB_7H_8^{1-}$	1.990	1.821	1.844	1.708
$1-CB_8H_9^{1-}$	1.701	1.677	1.693	1.658
$4-CB_8H_9^{1-}$	1.613	1.599	1.609	1.615
$1-CB_9H_{10}^{1-}$	1.604	1.594	1.601	1.616
$1-CB_{10}H_{11}^{1-}$	2.030	1.959	1.977	2.063
$CB_{11}H_{12}^{1-}$	1.708	1.687	1.699	1.709
$1,2-C_2B_4H_6$	1.628	1.616	1.624	1.576
$1,6-C_2B_4H_6$	1.624	1.613	1.620	1.644
$1,2-C_2B_5H_7$	1.757	1.734	1.745	1.853
$1,7-C_2B_5H_7$	1.739	1.722	1.731	1.762
$1,2-C_2B_8H_{10}$	1.712	1.688	1.706	1.577
$1,6-C_2B_8H_{10}$	1.760	1.730	1.745	1.720
$1,10-C_2B_8H_{10}$	1.600	1.568	1.596	1.614
$1,2-C_2B_{10}H_{12}$	1.719	1.698	1.709	1.719
$1,7-C_2B_{10}H_{12}$	1.692	1.676	1.687	1.698
$1,12-C_2B_{10}H_{12}$	1.706	1.686	1.698	1.710
RMS error in %	–	1.59	0.76	2.16

The distances are given in Å. RMS errors are given in % with respect to the B3LYP/6-311++G** reference for all C-B distances.

For the LDA calculation of methyldiborane (4) ($H_3C-B_2H_3$) the resulting errors are exceptionally high. This is due to distortion of the structure, which is visualized in figure 5.9. Nevertheless, the agreement between the different exchange-correlation functionals is quite good. The average errors are smaller than 2% for atomic distances and angles. The discrepancy for the new DFTB parameters is a little larger than for the DFT methods, but still acceptable. The average errors are less than 3% for atomic distances and less than 4% for the angles. The comparison of the average errors for C-B distances (LDA 1.59 / PBE 0.76 / DFTB 2.16) and all distances (LDA 1.49 / PBE 0.54 / DFTB 1.76) shows that the C-B parameters work well together with the pre-existing parameters. A look at the errors for the angles also reflects this (LDA 1.31 / 1.47 , PBE 0.60 / 0.48 , and DFTB 3.31 / 2.69 for C-B containing and all angles, respectively). The distances of the small molecules, which only have the common, two-electron bonds (first part of table 5.12), seem to be very well described. The DFTB errors for these molecules are close to the ones of the DFT. For $H_5C_2-BH_2$ the difference is a bit large, due to the fact that the C-C bond is shortened

Table 5.12.: Carbaborane Systems: Overview Distances RMS Errors

molecule	LDA	PBE	DFTB
H_2C-BH	0.97	0.24	0.62
H_3C-BH_2	1.06	0.25	0.47
$H_5C_2-BH_2$	1.10	0.29	1.65
$H_2C-(BH_2)_2$	1.07	0.33	0.73
$H_3C-B_2H_3$	6.28	0.25	0.44
$(H_3C)_2-BH$	1.00	0.18	0.30
$2-CB_4H_5^{1-}$	1.12	0.35	1.66
$CB_5H_6^{1-}$	0.81	0.25	1.13
$1-CB_6H_7^{1-}$	0.96	0.33	0.92
$2-CB_6H_7^{1-}$	0.98	0.35	3.02
$1-CB_7H_8^{1-}$	1.19	0.53	1.90
$3-CB_7H_8^{1-}$	2.91	2.47	4.07
$1-CB_8H_9^{1-}$	3.28	2.85	6.43
$4-CB_8H_9^{1-}$	1.24	0.56	2.04
$1-CB_9H_{10}^{1-}$	1.10	0.36	1.13
$1-CB_{10}H_{11}^{1-}$	1.60	0.99	1.47
$CB_{11}H_{12}^{1-}$	1.07	0.34	0.80
$1,2-C_2B_4H_6$	0.87	0.30	1.61
$1,6-C_2B_4H_6$	0.84	0.28	1.11
$1,2-C_2B_5H_7$	1.07	0.51	3.77
$1,7-C_2B_5H_7$	0.95	0.35	1.13
$1,2-C_2B_8H_{10}$	1.22	0.47	4.54
$1,6-C_2B_8H_{10}$	1.18	0.43	1.55
$1,10-C_2B_8H_{10}$	3.30	0.42	1.16
$1,2-C_2B_{10}H_{12}$	1.13	0.39	0.80
$1,7-C_2B_{10}H_{12}$	1.12	0.38	0.82
$1,12-C_2B_{10}H_{12}$	1.12	0.39	0.84
test set average	1.49	0.54	1.76

RMS errors are given in % with respect to the B3LYP/6-311++G** reference for each complete molecule and the full test set.

by 3.8%. The C-B bond in this molecule is as well shortened in DFTB by 2.6%. Given that also the non-bonding C-B distance is shortened, the corresponding angle B-C-C has an error of 16%. This causes the average error for the angles of nearly 5% in this molecule. Otherwise, the error would be less than 3%. The obvious reason for such behavior would be a general shortening of C-B bonds by the DFTB parameters, but this is not the case, hence bond elongations are observed in the larger monocarbaborane anions and dicarbaboranes. Another possibility might be that the cutoff for the repulsive potential could be too long and also next-neighboring atoms are covered by the C-B interaction. But if this would be true, similar findings of ones in $H_5C_2-BH_2$ should result for $H_3C-B_2H_3$, which is described fine. Taking a look at the monocarbaborane anions, second part of tables 5.12 and 5.16, it can be noticed that the deviation rises considerably for medium clusters depending on the diastereomere. For example, $1-CB_6H_7^{1-}$ does rather well agree with the reference, although closer examination reveals that the cone tops of the bipyramide are pulled to the ring plane, while the ring is slightly enlarged. In the other diastereomere,

Table 5.13.: Carbaborane Systems: Selected C-B Angles

molecule	angle	B3LYP	LDA	PBE	DFTB
H_2C-BH	B-C-H	180.0	180.0	180.0	180.0
	C-B-H	122.6	122.7	122.5	124.3
H_3C-BH_2	B-C-H	116.0	117.1	116.1	115.5
	C-B-H	119.5	119.2	119.4	119.8
$H_5C_2-BH_2$	C-C-B	118.4	119.0	118.4	100.3
	B-C-H	106.7	106.0	106.5	114.4
	C-B-H	119.5	119.5	119.5	122.1
$H_2C-(BH_2)_2$	B-C-B	108.0	105.3	106.8	113.7
	H-C-B	109.1	109.1	109.2	108.9
	C-B-H	120.6	120.4	120.6	120.5
$H_3C-B_2H_3$	C-B-B	128.4	173.3	128.4	127.4
	H-C-B	116.4	113.1	116.4	115.6
	C-B-H	116.0	117.4	116.0	114.5
$(H_3C)_2-BH$	C-B-C	125.1	124.8	125.1	123.0
	B-C-H	110.0	110.0	109.9	111.9
	C-B-H	117.5	117.6	117.5	118.5
RMS error in %		–	1.31	0.60	3.31

The angles are given in degree. RMS errors are given in % with respect to the B3LYP/6-311++G** reference for all C-B containing angles.

Table 5.14.: Closo Carbaborane Anions: Selected C-B Angles

molecule	angle	B3LYP	LDA	PBE	DFTB
$2-CB_4H_5^{1-}$	C-B-B	64.3	63.2	63.9	66.2
	B-C-B	60.8	61.4	61.1	60.3
	H-C-B	125.0	124.4	124.8	125.9
	C-B-H	143.6	143.2	143.4	142.3
$CB_5H_6^{1-}$	C-B-B	58.1	58.1	58.1	57.1
	B-C-B	96.8	96.8	96.8	100.3
	H-C-B	131.6	131.6	131.6	129.9
	C-B-H	130.7	130.6	130.6	129.7
$1-CB_6H_7^{1-}$	C-B-B	61.9	61.7	61.8	61.3
	B-C-B	56.2	56.6	56.5	57.3
	H-C-B	126.7	126.2	126.4	125.3
	C-B-H	134.3	134.7	134.4	132.9
$2-CB_6H_7^{1-}$	C-B-B	90.9	91.7	91.4	84.6
	B-C-B	84.3	83.9	84.1	93.2
	H-C-B	137.9	138.1	138.0	133.4
	C-B-H	125.4	125.0	125.1	127.1
$1-CB_7H_8^{1-}$	C-B-B	106.9	107.9	107.7	106.2
	B-C-B	69.7	69.1	69.2	70.9
	H-C-B	131.4	131.8	131.7	128.7
	C-B-H	120.1	120.3	120.2	119.0
$3-CB_7H_8^{1-}$	C-B-B	62.0	62.2	62.3	62.0
	B-C-B	53.6	57.0	56.7	59.3
	H-C-B	117.7	118.4	118.2	110.9
	C-B-H	128.4	130.4	130.2	130.6
$1-CB_8H_9^{1-}$	C-B-B	61.5	61.2	61.4	58.4
	B-C-B	122.7	121.4	121.4	126.2
	H-C-B	116.8	115.7	115.8	106.7
	C-B-H	124.7	125.6	125.4	123.4
$4-CB_8H_9^{1-}$	C-B-B	108.4	109.1	108.8	108.2
	B-C-B	67.2	67.3	67.4	69.5
	H-C-B	123.8	124.4	124.2	124.5
	C-B-H	123.8	124.4	124.2	124.5
$1-CB_9H_{10}^{1-}$	C-B-B	108.2	108.5	108.5	107.6
	B-C-B	70.3	69.8	70.0	70.4
	H-C-B	125.5	126.0	125.8	125.4
	C-B-H	119.3	119.3	119.3	116.7
$1-CB_{10}H_{11}^{1-}$	C-B-B	75.7	73.2	73.5	77.2
	B-C-B	55.6	55.7	56.1	52.9
	H-C-B	104.6	103.0	103.2	106.2
	C-B-H	123.0	123.9	123.4	121.0
$CB_{11}H_{12}^{1-}$	C-B-B	104.5	104.5	104.5	104.6
	B-C-B	62.9	62.9	62.9	62.9
	H-C-B	117.5	117.5	117.4	117.4
	C-B-H	119.3	119.1	119.1	117.9
RMS error in %		–	1.31	0.60	3.31

The angles are given in degree. RMS errors are given in % with respect to the B3LYP/6-311++G** reference for all C-B containing angles.

Table 5.15.: Dicarbaboranes: Selected C-B Angles

molecule	angle	B3LYP	LDA	PBE	DFTB
$1,2-C_2B_4H_6$	C-C-B	61.5	61.6	61.6	62.8
	C-B-B	58.0	58.0	58.0	55.8
	C-B-C	57.0	56.8	56.8	54.5
	B-C-B	64.6	64.4	64.5	65.8
$1,6-C_2B_4H_6$	C-B-B	58.2	58.2	58.2	58.4
	C-B-C	83.6	83.7	83.6	84.5
	B-C-B	63.6	63.6	63.6	63.1
$1,2-C_2B_5H_7$	C-C-B	66.8	66.6	66.8	75.0
	C-B-B	60.5	60.6	60.7	56.2
	C-B-C	59.4	59.0	58.9	51.0
	B-C-B	97.6	98.7	98.5	101.1
$1,7-C_2B_5H_7$	C-B-B	62.1	62.0	62.0	62.3
	C-B-C	74.6	74.1	74.2	75.7
	B-C-B	55.8	56.0	55.9	55.3
$1,2-C_2B_8H_{10}$	C-C-B	115.2	115.2	115.5	123.8
	C-B-B	106.9	107.3	107.2	97.1
	B-C-B	109.2	108.9	109.2	131.0
$1,6-C_2B_8H_{10}$	C-B-B	108.2	108.4	108.4	106.2
	C-B-C	104.4	104.9	104.8	103.0
	B-C-B	95.6	95.7	95.8	101.0
$1,10-C_2B_8H_{10}$	C-B-B	107.6	109.2	108.0	106.9
	B-C-B	70.9	70.5	70.5	71.0
$1,2-C_2B_{10}H_{12}$	C-C-B	111.7	111.7	111.8	112.1
	C-B-B	104.0	104.0	104.0	103.6
	C-B-C	56.4	56.5	56.4	56.0
	B-C-B	115.7	115.7	115.8	116.1
$1,7-C_2B_{10}H_{12}$	C-B-B	105.0	104.9	105.0	105.1
	C-B-C	100.6	100.6	100.6	100.8
	B-C-B	114.7	114.8	114.8	114.6
$1,12-C_2B_{10}H_{12}$	C-B-B	103.9	104.0	103.9	103.6
	B-C-B	115.6	115.5	115.7	116.2
RMS error in %		–	1.31	0.60	3.31

The angles are given in degree. RMS errors are given in % with respect to the B3LYP/6-311++G** reference for all C-B containing angles.

Table 5.16.: Carbaborane Systems: Overview RMS Angles

molecule	LDA	PBE	DFTB
H_2C-BH	0.07	0.06	1.15
H_3C-BH_2	0.50	0.13	1.26
$H_5C_2-BH_2$	0.65	0.15	4.89
$H_2C-(BH_2)_2$	0.93	0.36	2.00
$H_3C-B_2H_3$	21.60	0.09	1.35
$(H_3C)_2-BH$	0.43	0.10	1.38
$2-CB_4H_5^{1-}$	0.95	0.35	1.66
$CB_5H_6^{1-}$	0.04	0.04	1.89
$1-CB_6H_7^{1-}$	0.41	0.26	1.52
$2-CB_6H_7^{1-}$	0.48	0.29	5.75
$1-CB_7H_8^{1-}$	0.70	0.54	3.20
$3-CB_7H_8^{1-}$	3.32	3.08	6.44
$1-CB_8H_9^{1-}$	3.20	2.97	8.69
$4-CB_8H_9^{1-}$	0.66	0.45	1.74
$1-CB_9H_{10}^{1-}$	0.35	0.24	1.00
$1-CB_{10}H_{11}^{1-}$	1.03	0.95	1.45
$CB_{11}H_{12}^{1-}$	0.12	0.11	0.38
$1,2-C_2B_4H_6$	0.18	0.11	2.36
$1,6-C_2B_4H_6$	0.04	0.03	0.53
$1,2-C_2B_5H_7$	0.54	0.44	6.77
$1,7-C_2B_5H_7$	0.29	0.20	0.66
$1,2-C_2B_8H_{10}$	0.46	0.31	8.12
$1,6-C_2B_8H_{10}$	0.44	0.26	2.42
$1,10-C_2B_8H_{10}$	2.73	1.49	1.35
$1,2-C_2B_{10}H_{12}$	0.13	0.10	0.52
$1,7-C_2B_{10}H_{12}$	0.14	0.09	0.49
$1,12-C_2B_{10}H_{12}$	0.17	0.11	0.67
test set average	1.47	0.48	2.69

RMS errors are given in % with respect to the B3LYP/6-311++G** reference for each complete molecule and the full test set.

$2-CB_6H_7^{1-}$, the tips are also pulled towards the C atom, which is now part of the central five-membered ring. Thus, the distortion could be delineated as a symmetry conserving squeeze of the ring between the cone atoms. In case of $3-CB_7H_8^{1-}$ and $1-CB_8H_9^{1-}$, the question arises if the structure predicted by B3LYP is suitable as reference. For these two B3LYP opens the structure to an extent that the carbon has a smaller coordination than the boron in the initial borane dianions, $B_8H_8^{2-}$ and $B_9H_9^{2-}$, respectively. Thus, the structure of a threefold capped trigonal prism is scarcely cognizable in case of $1-CB_8H_9^{1-}$. In contrast, $4-CB_8H_9^{1-}$ resembles its borane basis structure much more. Since the results for LDA and PBE tend to deviate in the same direction as the DFTB results, the larger errors for these structures seem tolerable. In the third part of tables 5.12 and 5.17, there are the dicarbaboranes, of which two structures seem worth a closer examination. These are $1,2-C_2B_5H_7$ and $1,2-C_2B_8H_{10}$. For $1,2-C_2B_5H_7$, it is like a combination of the effects seen in $1-CB_5H_7^{1-}$ and $2-CB_5H_7^{1-}$. The carbon tip of the pyramid is pulled towards the ring carbon atom. The same is true in $1,2-C_2B_8H_{10}$, but to a much larger extent. The carbon atom in the upper four-membered ring is pulled nearly over the lower four-membered ring. The non-bonding distance from the ring-carbon to the second ring-borons is shortened from 2.7 Å to 2.2 Å. Hence, the B-C-B angles dilate by approximately 10%.

Overall, the similarity of all results shows that the present SCC-DFTB parameters are capable of describing the geometry on a level with usual DFT methods, which use a much larger basis set.

For the smaller, uncharged molecules the vibrational modes have been computed. The summary of the results is given in table 5.17. The performance of the B-C DFTB parameters is not as good as for the B-B and B-H parameters. The average error here is with about 10% quite large. The largest single error is found for $H_2B-C_2H_5$, where a mode in the range of $400\,cm^{-1}$ suffers a deviation of $250\,cm^{-1}$ or 80%. The LDA result for $H_3C-B_2H_3$ is not worth mentioning, since already the structure is not consistent with the other methods. Nevertheless, it is given for completeness.

Since the B-C parameters shall be an extension to the *mio*-set, the atomization energies and the overbinding per bond have been derived. The values are given in tables 5.18 and 5.19, respectively. The achieved average overbinding for DFTB with 14.04 kcal/mol is reasonable close to the desired value of 10 kcal/mol. In addition to that the fact that there is no correlation between the number of B-C bonds and the molecule size leads to the assumption that the parameters and their overbinding is well balanced.

On the basis of the tests for the boranes and carbaboranes, reactions can be formulated, which conserve the number of bonds in the involved molecules and where therefore the overbinding of the DFTB method should not have much impact. As examples for such reactions, the exchange of one or two boron atoms in the *closo*-dianion clusters against carbon shall be considered. The possible reactions are given in equations 5.3, 5.4 and 5.5. In these reactions the inclusion of carbon is performed in steps (equations 5.3 and 5.4) and as sum of these steps (equation 5.5).

Table 5.17.: Carbaborane Systems: Overview RMS Modes

molecule	LDA	PBE	DFTB
H_2C-BH	7.95	1.80	10.32
H_3C-BH_2	4.58	1.00	4.30
$H_3C-B_2H_3$	(16.52)	6.73	4.48
$H_2C-(BH_2)_2$	4.24	1.22	5.86
$H_5C_2-BH_2$	4.38	0.94	19.91
$1,2-C_2B_4H_6$	4.53	3.14	9.67
$1,6-C_2B_4H_6$	4.88	1.26	9.65
$1,2-C_2B_5H_7$	4.38	3.41	11.48
$1,7-C_2B_5H_7$	5.34	3.51	15.57
test set	5.03 (6.31)	2.56	10.14

RMS errors are given in % with respect to the B3LYP/6-311++G** reference for each molecule and the full test. For the values within brackets the structure differs significantly from the reference. Hence, the test set sum is given excluding and including this value, with and without brackets, respectively.

$$B_nH_n^{2-} + CH_4 \longrightarrow CB_{n-1}H_n^{1-} + BH_4^{1-} \tag{5.3}$$

$$CB_{n-1}H_n^{1-} + CH_4 \longrightarrow C_2B_{n-2}H_n + BH_4^{1-} \tag{5.4}$$

$$B_nH_n^{2-} + 2 \times CH_4 \longrightarrow C_2B_{n-2}H_n + 2 \times BH_4^{1-} \tag{5.5}$$

$$\Delta E_{\text{reac}} = \sum E_{\text{products}} - \sum E_{\text{educts}} \tag{5.6}$$

The reaction energies are derived as the difference of the total energies according to equation 5.6. The tables 5.20 and 5.21 present the deliverables for *closo*-carbaborane anions and *closo*-dicarbaboranes as products, respectively. The energies for the incorporation of a single carbon atom (eq. 5.3) in the cluster are all negative. With respect to the definition (eq. 5.6), this means that the up-take is energetically favored. This is not surprising if it is considered that that the *closo*-borane cluster are dianions and the Coulomb repulsion therefore is quite large. But the difference in the reaction energies is surprisingly large. While the values of the DFT methods are in proximity of 10 kcal/mol, the DFTB data favors the *closo*-carbaboranes even stronger by 95-120 kcal/mol compared to DFT. Furthermore the energetic ordering of the diastereomers is not retained in all cases. The energies for the second carbon up-take (eq. 5.4) suffer a similar fate, meaning that the reaction energies of DFTB are again consistently lower than for DFT. This time, the difference is about 60-100 kcal/mol. As a result the direct reaction from boranes to dicarbaboranes (eq. 5.5) is also badly described in the DFTB energies (deviation of 150-200 kcal/mol).

While the preference for the first incorporation seems reasonable, this second result is quite disturbing. The error for the first may be attributed to the strength of the Coulomb

Table 5.18.: Carbaborane Systems: Atomization Energies

molecule	B3LYP	B3LYP	LDA	PBE	DFTB
	6-31G(d)	6-311++G**			
H_2C-BH	427.34	468.76	524.43	473.05	483.36
H_3C-BH_2	591.52	627.71	692.95	630.90	654.25
$H_5C_2-BH_2$	882.40	956.75	1066.49	968.42	967.34
$H_2C-(BH_2)_2$	767.59	800.29	887.72	805.56	873.22
$H_3C-B_2H_3$	762.79	796.35	891.57	801.74	846.45
$(H_3C)_2-BH$	895.77	971.79	1082.87	983.76	990.53
$1,2-C_2B_4H_6$	1202.20	1267.25	1469.28	1316.85	1507.02
$1,6-C_2B_4H_6$	1210.73	1275.90	1478.57	1325.14	1516.21
$1,2-C_2B_5H_7$	1377.42	1438.51	1674.79	1496.54	1756.89
$1,7-C_2B_5H_7$	1352.22	1413.91	1653.51	1472.23	1723.99
$1,2-C_2B_8H_{10}$	1995.51	2043.35	2391.94	2132.89	2512.23
$1,6-C_2B_8H_{10}$	2013.98	2061.82	2409.05	2150.81	2541.64
$1,10-C_2B_8H_{10}$	2035.55	2082.79	2430.02	2170.72	2544.60
$1,2-C_2B_{10}H_{12}$	2420.72	2459.76	2881.09	2570.88	2995.25
$1,7-C_2B_{10}H_{12}$	2436.92	2475.91	2896.56	2586.63	3050.16
$1,12-C_2B_{10}H_{12}$	2439.79	2478.80	2899.48	2589.43	3051.56

The values are given in kcal/mol. The spin polarization energy of isolated atoms was taken into account. No correction for zero point motion was performed.

repulsion in DFTB with its minimal basis. Here, the electrons cannot be distributed over as many and spatially spread orbitals as in DFT with the 6-311++G** basis. Hence, the DFTB method drastically favors the single charged *closo*-carbaborane anions. Another explanation is needed for the reaction to the *closo*-dicarbaboranes. The former reasoning should tend to the charge on the larger molecule, where it can be smeared over more orbitals and space. Such thinking is backed up by the DFT results, which are all positive for the second carbon incorporation. But the calculations within DFTB show else and favor the localization of the charge on the small borohydride. For most of the whole reactions (eq. 5.5) the DFT energies are even positive, which means, that the Coulomb repulsion is not as "bad" as the localization of the charge on small molecules. A deviation from this is only observed for the smallest of the clusters. The question has to be posed why DFTB favors the charge on the borohydride. An answer could be the size of the basis set. The minimal basis of DFTB does not distinguish as much as DFT between the clusters and the methane/borohydride structure.

Table 5.19.: Carbaborane Systems: Overbinding Energies

molecule	B3LYP	LDA	PBE	DFTB
	6-311++G**			
H_2C-BH	10.36	24.27	11.43	14.00
H_3C-BH_2	6.03	16.90	6.56	10.45
$H_5C_2-BH_2$	8.26	20.45	9.56	9.44
$H_2C-(BH_2)_2$	4.09	15.02	4.75	13.20
$H_3C-B_2H_3$	4.19	16.10	4.87	10.46
$(H_3C)_2-BH$	8.45	20.79	9.78	10.53
$1,2-C_2B_4H_6$	3.61	14.84	6.37	16.93
$1,6-C_2B_4H_6$	3.62	14.88	6.36	16.97
$1,2-C_2B_5H_7$	2.78	13.52	5.41	17.25
$1,7-C_2B_5H_7$	2.80	13.70	5.46	16.90
$1,2-C_2B_8H_{10}$	1.41	11.66	4.04	15.20
$1,6-C_2B_8H_{10}$	1.41	11.62	4.02	15.52
$1,10-C_2B_8H_{10}$	1.39	11.60	3.98	14.97
$1,2-C_2B_{10}H_{12}$	0.93	10.96	3.58	13.68
$1,7-C_2B_{10}H_{12}$	0.93	10.94	3.56	14.60
$1,12-C_2B_{10}H_{12}$	0.93	10.94	3.56	14.57
Average	3.82	14.89	5.83	14.04

The values are given in kcal/mol per bond with respect to B3LYP/6-31G(d). The spin polarization energy of isolated atoms was taken into account. No correction for zero point motion was performed.

Table 5.20.: Reaction Energies *closo*-Carbaborane Systems

product molecule	B3LYP	LDA	PBE	DFTB
	6-311++G**			
$2-CB_4H_5^{1-}$	-73.29	-69.64	-69.68	-166.55
$CB_5H_6^{1-}$	-73.92	-69.29	-69.97	-185.92
$1-CB_6H_7^{1-}$	-41.26	-38.04	-37.23	-162.57
$2-CB_6H_7^{1-}$	-71.05	-65.85	-66.68	-187.14
$1-CB_7H_8^{1-}$	-64.07	-58.76	-59.42	-168.97
$3-CB_7H_8^{1-}$	-40.97	-36.69	-36.04	-168.04
$1-CB_8H_9^{1-}$	-38.07	-34.12	-33.04	-164.36
$4-CB_8H_9^{1-}$	-58.36	-53.03	-53.64	-152.35
$1-CB_9H_{10}^{1-}$	-52.62	-46.99	-47.78	-146.09
$1-CB_{10}H_{11}^{1-}$	-7.93	-4.81	-2.24	-114.21
$CB_{11}H_{12}^{1-}$	-22.40	-19.47	-18.33	-122.96

The values are given in kcal/mol. No correction for zero point motion was performed.

Table 5.21.: Reaction Energies *closo*-Dicarbaborane Systems

educt molecule	product molecule	B3LYP	LDA	PBE	DFTB
		6-311++G**			
$CB_5H_6^{1-}$	$1,2-C_2B_4H_6$	55.50	58.62	58.71	-9.27
	$1,6-C_2B_4H_6$	46.85	49.33	50.43	-18.46
$1-CB_6H_7^{1-}$	$1,2-C_2B_5H_7$	53.68	57.61	57.44	-21.31
	$1,7-C_2B_5H_7$	78.28	78.88	81.75	11.60
$2-CB_6H_7^{1-}$	$1,2-C_2B_5H_7$	83.46	85.43	86.90	3.25
	$1,7-C_2B_5H_7$	108.07	106.70	111.20	36.16
$1-CB_9H_{10}^{1-}$	$1,2-C_2B_8H_{10}$	91.08	92.10	94.49	-4.90
	$1,6-C_2B_8H_{10}$	72.62	74.99	76.58	-34.32
	$1,10-C_2B_8H_{10}$	51.65	54.02	56.67	-37.28
$CB_{11}H_{12}^{1-}$	$1,2-C_2B_{10}H_{12}$	95.21	97.01	98.81	36.35
	$1,7-C_2B_{10}H_{12}$	79.06	81.53	83.07	-18.57
	$1,12-C_2B_{10}H_{12}$	76.17	78.62	80.26	-19.97
$B_6H_6^{2-}$	$1,2-C_2B_4H_6$	-18.41	-10.67	-11.25	-195.19
	$1,6-C_2B_4H_6$	-27.06	-19.96	-19.54	-204.38
$B_7H_7^{2-}$	$1,2-C_2B_5H_7$	12.42	19.57	20.21	-183.88
	$1,7-C_2B_5H_7$	37.02	40.84	44.52	-150.98
$B_{10}H_{10}^{2-}$	$1,2-C_2B_8H_{10}$	38.46	45.11	46.72	-150.99
	$1,6-C_2B_8H_{10}$	19.99	28.00	28.80	-180.40
	$1,10-C_2B_8H_{10}$	-0.97	7.03	8.89	-183.36
$B_{12}H_{12}^{2-}$	$1,2-C_2B_{10}H_{12}$	72.81	77.54	80.48	-86.61
	$1,7-C_2B_{10}H_{12}$	56.66	62.06	64.74	-141.53
	$1,12-C_2B_{10}H_{12}$	53.77	59.15	61.93	-142.93

The values are given in kcal/mol. No correction for zero point motion was performed.

Figure 5.10.: Reference System E_{rep}(B-N)

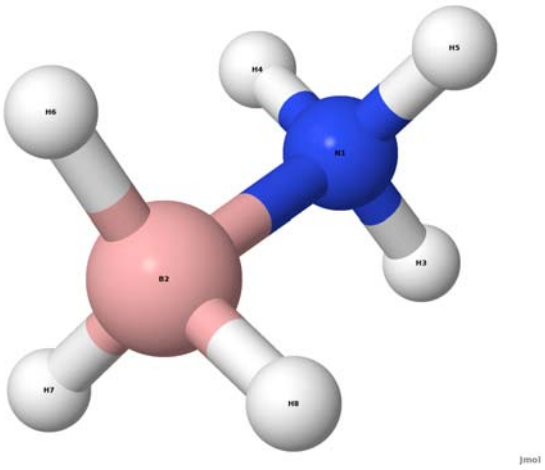

5.3. Azaboranes and Boron Nitride

As further extension to the application range of boron in SCC-DFTB, the parameters for the combination boron-nitrogen have been determined. As for the parameters so far, the main focus is on molecular systems, but since there are well defined and important bulk systems these will also be investigated.

5.3.1. Molecular Systems

For this combination molecular systems are chosen in the same fashion as for the boron-boron and boron-carbon interaction. Included in the test set were $HN-BH$, H_2N-BH_2 and H_3N-BH_3. These are isoelectronic to ethyne, ethene, and ethane, respectively. Of these three, H_3N-BH_3 (figure 5.10) has been used for the creation of the repulsive potential. A well-known boron nitride molecule is borazine, $B_3N_3H_6$, which is similar to benzene and often called "inorganic benzene". Hence, the test set contained structures, which are isoelectronic to benzene or larger planar aromatic systems. The structures are $B_3N_3H_6$, $B_5N_5H_8$, $B_7N_6H_9$, $B_7N_7H_{10}$, $B_8N_8H_{10}$, $B_9N_9H_{12}$, $B_{11}N_{11}H_{12}$. Furthermore the *closo*-azaboranes ($NB_{n-1}H_n$) are entrained, which are derived from the *closo*-borane dianions ($B_nH_n^{2-}$ with $n = 5-12$). As for the carbaboranes, different diastereomeres of these systems are accounted for. And at last additional molecules are enclosed in the test set, which are build up by conventional two electron bonds. These molecules are $H_2N-B_2H_3$, $(H_2N)_2-BH$, $(H_2B)_2-NH$ and $H_2B-N_2H_3$.

For all of these, the structures were optimized using the NWChem program[153] with LDA, PBE and B3LYP and 6-311++G** basis[156] to compare with the results of DFTB. As for the other parameters presented thus far, B3LYP was used as the reference for the comparison. An overview and examples of the analyzed distances are given in tables 5.23 and 5.22, respectively. The summary of the angles is shown in table 5.27, while selected angles are displayed in tables 5.24, 5.25 and 5.26 grouped with respect to the different

Table 5.22.: Azaborane Systems: Selected N-B Distances

molecule	B3LYP	LDA	PBE	DFTB
$HN-BH$	1.236	1.239	1.236	1.2164
H_2N-BH_2	1.391	1.382	1.388	1.3674
H_3N-BH_3	1.665	1.613	1.643	1.6558
$H_2N-B_2H_3$	1.397	1.397	1.397	1.3756
$(H_2N)_2-BH$	1.415	1.406	1.412	1.4210
$HN-(BH_2)_2$	1.456	1.444	1.452	1.4746
$H_3N_2-BH_2$	1.386	1.377	1.384	1.3729
$B_3N_3H_6$	1.431	1.422	1.427	1.4409
$B_5N_5H_8$	1.439	1.430	1.435	1.4592
$B_7N_6H_9$	1.445	1.436	1.441	1.4696
$B_7N_7H_{10}$	1.439	1.430	1.436	1.4606
$B_8N_8H_{10}$	1.457	1.446	1.452	1.4823
$B_9N_9H_{12}$	1.439	1.430	1.435	1.4605
$B_{11}N_{11}H_{12}$	1.446	1.436	1.441	1.4676
$1-NB_4H_5$	1.510	1.501	1.508	1.5408
$2-NB_4H_5$	1.709	1.663	1.689	1.9690
NB_5H_6	1.608	1.591	1.600	1.6649
$1-NB_6H_7$	1.758	1.728	1.741	1.8551
$2-NB_6H_7$	1.984	1.768	1.800	2.3707
$1-NB_7H_8$	1.728	1.679	1.698	2.3741
$3-NB_7H_8$	2.315	2.234	2.270	2.3775
$1-NB_8H_9$	1.505	1.499	1.503	1.4911
$4-NB_8H_9$	1.599	1.578	1.588	1.6319
$1-NB_9H_{10}$	1.588	1.572	1.580	1.6361
$1-NB_{10}H_{11}$	1.512	1.510	1.520	1.5000
$NB_{11}H_{12}$	1.717	1.689	1.702	1.7880
RMS error in %	–	1.37	0.80	3.75

The distances are given in Å. RMS errors are given in % with respect to the B3LYP/6-311++G** reference for all N-B distances.

Table 5.23.: Azaborane Systems: Overview RMS Distances

molecule	LDA	PBE	DFTB
$HN - BH$	0.94	0.24	1.13
$H_2N - BH_2$	0.96	0.28	1.18
$H_3N - BH_3$	1.49	0.57	0.55
$H_2N - B_2H_3$	0.00	0.00	1.02
$(H_2N)_2 - BH$	0.90	0.23	0.91
$HN - (BH_2)_2$	1.14	0.34	1.65
$H_3N_2 - BH_2$	1.18	0.46	1.72
$B_3N_3H_6$	0.84	0.28	0.92
$B_5N_5H_8$	0.83	0.29	1.17
$B_7N_6H_9$	0.83	0.32	1.31
$B_7N_7H_{10}$	0.83	0.30	1.25
$B_8N_8H_{10}$	0.81	0.29	1.31
$B_9N_9H_{12}$	0.82	0.29	1.30
$B_{11}N_{11}H_{12}$	0.79	0.30	1.37
$1 - NB_4H_5$	1.18	0.42	1.79
$2 - NB_4H_5$	1.35	0.52	6.13
NB_5H_6	0.95	0.36	2.27
$1 - NB_6H_7$	1.16	0.54	3.13
$2 - NB_6H_7$	4.06	3.40	6.50
$1 - NB_7H_8$	1.47	0.75	11.30
$3 - NB_7H_8$	1.75	0.87	2.18
$1 - NB_8H_9$	1.33	0.52	3.54
$4 - NB_8H_9$	1.38	0.66	2.46
$1 - NB_9H_{10}$	1.22	0.44	1.52
$1 - NB_{10}H_{11}$	2.05	1.49	2.26
$NB_{11}H_{12}$	1.23	0.49	1.71
test set average	1.20	0.55	2.31

RMS errors are given in % with respect to the B3LYP/6-311++G** reference for each complete molecule and the full test set.

Table 5.24.: Azaborane Systems: Selected N-B Angles

molecule	angle	B3LYP	LDA	PBE	DFTB
$HN-BH$	H-B-N	180.0	180.0	180.0	180.0
	B-N-H	180.0	180.0	180.0	180.0
H_2N-BH_2	H-B-N	104.9	105.8	105.2	105.8
	B-N-H	111.1	111.1	111.1	111.4
H_3N-BH_3	H-B-N	119.0	118.7	118.9	119.2
	B-N-H	123.3	123.2	123.2	124.2
$H_2N-B_2H_3$	N-B-B	128.9	128.9	128.9	126.4
	H-B-N	116.0	116.0	116.0	115.0
	B-N-H	124.1	124.1	124.1	124.4
$(H_2N)_2-BH$	N-B-N	122.9	122.8	122.9	120.3
	H-B-N	118.5	118.6	118.5	119.9
	B-N-H	122.0	121.8	121.8	123.5
$HN-(BH_2)_2$	B-N-B	130.4	130.1	130.2	130.0
	H-B-N	121.2	121.1	121.2	121.6
	B-N-H	114.8	115.0	114.9	115.0
$H_3N_2-BH_2$	N-N-B	127.5	126.8	127.5	126.0
	H-B-N	117.8	117.9	117.8	118.3
	B-N-H	122.3	121.6	122.0	121.9
RMS error in %		–	0.77	0.54	3.78

The distances are given in degree. RMS errors are given in % with respect to the B3LYP/6-311++G** reference for all N-B containing angles.

types of molecules considered. The overall RMS errors of all methods are quite small and even for DFTB less than 3% in both distances and angles. The deviations for interactions, which must include B-N, are a bit higher at all levels of theory. For the DFTB results (ca. 4% RMS error) this is mainly due to the bad description of $2-NB_6H_7$ and $1-NB_7H_8$, where the latter also contains the largest single error with up to 38% or 0.7 Å deviation. Without those two molecules the average errors for the whole molecules as well as for the B-N containing interactions would be about 2%, which would be more than satisfactory. The errors in these molecules can be attributed to the DFTB tendency to push boron atoms away, which are in the larger coordination sphere of nitrogen. Meaning that the closest boron atoms are bound well and in a reasonable distance, whereas boron atoms with a slightly larger distance are the ones pushed. Although this tendency can be found in all the azaborane clusters, there is no specific distance, at which this behavior sets in. The bonds in $2-NB_6H_7$ and $1-NB_7H_8$ under discussion are in the range of $1.7-1.9$ Å with respect to the B3LYP calculations. For the bonds in H_3N-BH_3, NB_5H_6, $3-NB_7H_8$ and $NB_{11}H_{12}$, which are also in this realm, the DFTB parameters work fine. Therefore, the reason is seen to be a competitive issue. In the clusters, where different bond length and geometric strain coincide, the description with DFTB has to be treated with care. On the other hand, one should state that DFTB works in principle fine for all the different bonding situations in the tested molecules. For the triple bond in $HN-BH$, the dative bond in H_3N-BH_3 and the conjugated π-system in the molecules of $B_3N_3H_6$ to $B_{11}N_{11}H_{12}$ the results are all good.

Table 5.25.: Aromatic Azaborane Systems: Selected N-B Angles

molecule	angle	B3LYP	LDA	PBE	DFTB
$B_3N_3H_6$	B-N-B	122.9	123.1	122.9	123.6
	N-B-N	117.1	116.9	117.1	116.4
	H-B-N	121.5	121.5	121.4	121.8
	B-N-H	118.5	118.5	118.6	118.2
$B_5N_5H_8$	B-N-B	122.8	122.7	122.6	123.0
	N-B-N	122.9	123.0	122.9	122.0
	H-B-N	121.6	121.6	121.5	121.7
	B-N-H	119.2	119.3	119.3	117.8
$B_7N_6H_9$	B-N-B	120.3	120.1	120.2	120.8
	N-B-N	118.5	118.3	118.5	118.0
	H-B-N	120.8	120.5	120.7	121.2
	B-N-H	118.3	118.3	118.3	117.6
$B_7N_7H_{10}$	B-N-B	122.8	122.7	122.6	123.1
	N-B-N	123.0	123.1	123.0	122.2
	H-B-N	120.5	121.1	120.7	120.6
	B-N-H	119.3	119.4	119.4	117.7
$B_8N_8H_{10}$	B-N-B	122.7	122.7	122.6	123.2
	N-B-N	120.0	119.9	119.9	120.7
	H-B-N	121.3	121.3	121.2	121.6
	B-N-H	119.2	119.2	119.3	117.7
$B_9N_9H_{12}$	B-N-B	119.9	120.1	120.0	119.6
	N-B-N	118.5	118.4	118.5	119.0
	H-B-N	119.7	119.8	119.8	119.8
	B-N-H	119.3	119.4	119.4	117.8
$B_{11}N_{11}H_{12}$	B-N-B	119.8	120.0	119.9	119.1
	N-B-N	119.7	119.8	119.8	119.3
	H-B-N	120.9	120.5	120.7	121.3
	B-N-H	118.3	118.3	118.4	117.5
RMS error in %		–	0.77	0.54	3.78

The distances are given in degree. RMS errors are given in % with respect to the B3LYP/6-311++G** reference for all N-B containing angles.

Table 5.26.: *Closo*-Azaboranes: Selected N-B Angles

molecule	angle	B3LYP	LDA	PBE	DFTB
$1-NB_4H_5$	B-N-B	75.5	74.4	75.0	75.7
	N-B-B	94.9	96.2	95.4	94.7
	H-B-N	124.9	125.3	124.9	120.1
	B-N-H	134.9	135.6	135.2	134.9
$2-NB_4H_5$	B-N-B	61.5	62.1	61.8	57.0
	N-B-B	64.6	63.1	63.9	75.0
	H-B-N	129.1	129.0	128.9	126.0
	B-N-H	124.1	123.5	123.8	128.2
NB_5H_6	B-N-B	65.1	65.3	65.2	63.2
	N-B-B	57.5	57.4	57.4	58.4
	H-B-N	125.0	124.8	124.8	121.3
	B-N-H	130.5	130.3	130.3	132.2
$1-NB_6H_7$	B-N-B	56.2	56.7	56.6	53.8
	N-B-B	75.6	75.1	75.2	79.6
	H-B-N	127.3	127.5	127.1	122.7
	B-N-H	126.8	126.1	126.2	129.7
$2-NB_6H_7$	B-N-B	76.5	83.1	82.6	63.3
	N-B-B	51.8	48.5	48.7	58.4
	H-B-N	114.3	117.6	117.3	103.2
	B-N-H	141.8	138.5	138.7	148.4
$1-NB_7H_8$	B-N-B	71.9	71.1	71.4	56.9
	N-B-B	103.3	105.0	104.5	101.2
	H-B-N	114.1	114.7	114.5	97.8
	B-N-H	130.0	130.0	130.0	143.5
$3-NB_7H_8$	B-N-B	61.1	60.8	60.9	63.1
	N-B-B	85.0	82.6	83.5	87.7
	H-B-N	120.9	121.1	120.8	117.3
	B-N-H	118.4	118.3	118.1	122.1
$1-NB_8H_9$	B-N-B	68.4	68.1	68.2	65.9
	N-B-B	98.4	94.8	96.0	104.5
	H-B-N	119.8	120.0	119.9	116.2
	B-N-H	116.4	116.1	116.0	119.4
$4-NB_8H_9$	B-N-B	117.5	116.2	116.7	112.4
	N-B-B	50.2	50.8	50.6	53.4
	H-B-N	115.0	114.8	114.7	111.9
	B-N-H	121.3	121.9	121.6	123.8
$1-NB_9H_{10}$	B-N-B	72.5	72.2	72.3	71.2
	N-B-B	53.7	53.9	53.8	54.4
	H-B-N	115.4	115.5	115.4	111.9
	B-N-H	123.2	123.6	123.4	124.5
$1-NB_{10}H_{11}$	B-N-B	142.4	144.6	145.5	131.2
	N-B-B	87.9	85.1	84.9	91.7
	H-B-N	118.2	118.3	118.1	115.5
	B-N-H	108.8	107.7	107.2	114.4
$NB_{11}H_{12}$	B-N-B	118.0	118.2	118.4	113.2
	N-B-B	101.8	101.9	101.8	104.0
	H-B-N	114.0	114.1	113.9	111.3
	B-N-H	115.7	115.6	115.5	118.6
RMS error in %		–	0.77	0.54	3.78

The distances are given in degree. RMS errors are given in % with respect to the B3LYP/6-311++G** reference for all N-B containing angles.

Table 5.27.: Azaborane Systems: Overview RMS Angles

molecule	LDA	PBE	DFTB
$HN - BH$	0.00	0.00	0.00
$H_2N - BH_2$	0.17	0.06	0.55
$H_3N - BH_3$	0.66	0.24	0.67
$H_2N - B_2H_3$	0.00	0.00	1.47
$(H_2N)_2 - BH$	0.17	0.06	2.38
$HN - (BH_2)_2$	0.14	0.08	0.28
$H_3N_2 - BH_2$	0.72	0.18	1.34
$B_3N_3H_6$	0.08	0.04	0.39
$B_5N_5H_8$	0.18	0.09	0.70
$B_7N_6H_9$	0.22	0.07	0.46
$B_7N_7H_{10}$	0.19	0.09	0.68
$B_8N_8H_{10}$	0.16	0.07	0.56
$B_9N_9H_{12}$	0.19	0.09	0.57
$B_{11}N_{11}H_{12}$	0.16	0.07	0.51
$1 - NB_4H_5$	0.97	0.42	1.32
$2 - NB_4H_5$	1.35	0.52	6.13
NB_5H_6	0.21	0.20	2.09
$1 - NB_6H_7$	0.56	0.48	2.78
$2 - NB_6H_7$	4.88	4.28	10.23
$1 - NB_7H_8$	1.09	0.77	22.84
$3 - NB_7H_8$	1.43	0.91	3.19
$1 - NB_8H_9$	1.23	0.75	4.11
$4 - NB_8H_9$	0.77	0.52	2.56
$1 - NB_9H_{10}$	0.42	0.25	1.18
$1 - NB_{10}H_{11}$	1.56	1.56	3.41
$NB_{11}H_{12}$	0.24	0.19	1.31
test set average	0.67	0.45	2.73

RMS errors are given in % with respect to the B3LYP/6-311++G** reference for each complete molecule and the full test.

Table 5.28.: Azaborane Systems: Overview RMS Modes

molecule	LDA	PBE	DFTB
$HN-BH$	3.89	4.61	19.62
H_2N-BH_2	3.54	3.58	9.03
H_3N-BH_3	5.08	4.32	6.53
$H_2N-B_2H_3$	9.46	11.75	7.47
$H_3N_2-BH_2$	33.09	15.63	14.92
$(H_2N)_2-BH$	3.40	3.75	16.51
test set	9.74	7.27	12.35

RMS errors are given in % with respect to the B3LYP/6-311++G** reference for each molecule and the full test.

The next common test are the vibrational modes. Hence, a normal mode analysis for some of the smaller molecules has been performed. The results are shown in table 5.28. As for the carbaboranes, the average error of 12% is quite large, but also the agreement between the different DFT implementations is not as good as before. The largest deviation is found for a LDA result with 33% average and 139% or $120\,\mathrm{cm}^{-1}$ for a single mode. In general most of the large deviations between the methods are found in the range of $500\,\mathrm{cm}^{-1}$ and less.

Further, the calculated atomization energies and overbinding are given in tables 5.29 and 5.30. The achieved average overbinding for DFTB in comparison to B3LYP/6-31G(d) is with 8.1 kcal/mol close to the target value of 10 kcal/mol. But the range of overbinding is quite large. For the boron nitride nanoflake $B_{11}N_{11}H_{12}$ the "overbinding" is -3.22 kcal/mol, whereas for $HN-BH$ emerged a value of 30.90 kcal/mol. Even the values for the azaborane *closo*-clusters spread from 1.71 kcal/mol to 10.49 kcal/mol. Since the smaller overbinding is observed for the smaller clusters, where more B-N interactions are present, one might assume that the B-N overbinding is not as high as for the other parameters. But the overbinding was determined for H_3N-BH_3 to be 15 kcal/mol. As a result also the "carbon-like" molecules have a overbinding in the range of 7.77 kcal/mol to 26.38 kcal/mol. The compounds with the conjugated π-systems on the contrary show nearly no overbinding with values between -3.32 kcal/mol and 4.90 kcal/mol.

5.3.2. Bulk Boron Nitride

As test for the transferability of the B-N parameters to periodic systems calculations for hexagonal alpha-boron nitride, cubic beta-boron nitride, and wurzite gamma-boron nitride are performed. The structures are shown in figures 5.11, 5.12 and 5.13, respectively. The performance of the new parameters for the geometry optimization as comparison to the literature values [157, 158] are given in table 5.31. The results show the trend observed already for the molecular systems. The structure of the cubic β-boron nitride can be described as a face-centered cubic alignment of the nitrogens and the occupation of half of the tetrahedral cavities by boron. In this system all boron-nitrogen bonds have the same length and the deviation of DFTB from the reference is with less than 4% acceptable. In the hexagonal α-boron nitride, which is a stacking of graphene-like BN-sheets, there are two

Table 5.29.: Azaborane Systems: Atomization Energies

molecule	B3LYP 6-31G(d)	B3LYP	LDA	PBE	DFTB
		6-311++G**			
$HN-BH$	341.37	388.78	402.81	350.82	434.06
H_2N-BH_2	490.10	536.02	561.04	497.25	575.85
H_3N-BH_3	598.67	643.32	682.80	603.92	703.61
$H_2N-B_2H_3$	656.56	699.71	746.78	663.14	764.14
$H_3N_2-BH_2$	621.70	712.00	740.22	639.79	806.38
$(H_2N)_2-BH$	676.62	773.23	801.65	701.19	809.88
$HN-(BH_2)_2$	635.30	675.52	717.25	637.25	689.66
$B_3N_3H_6$	1190.88	1319.57	1393.71	1222.59	1249.72
$B_5N_5H_8$	1884.77	2095.96	2219.46	1941.14	1913.89
$B_7N_6H_9$	2388.55	2632.13	2801.26	2452.73	2333.91
$B_7N_7H_{10}$	2578.26	2872.02	3044.87	2659.40	2577.48
$B_8N_8H_{10}$	2878.54	3211.91	3408.97	2973.72	2830.18
$B_9N_9H_{12}$	3271.78	3648.11	3870.33	3377.68	3241.13
$B_{11}N_{11}H_{12}$	3871.61	4327.26	4597.78	4005.69	3745.84
$1-NB_4H_5$	915.07	948.47	1063.59	935.86	998.78
$2-NB_4H_5$	863.45	897.52	1017.92	885.12	887.36
NB_5H_6	1111.19	1140.12	1293.40	1139.22	1167.65
$1-NB_6H_7$	1261.36	1286.69	1473.24	1292.96	1314.21
$2-NB_6H_7$	1312.90	1337.89	1522.36	1343.87	1538.38
$1-NB_7H_8$	1498.00	1518.40	1739.85	1534.79	1757.94
$3-NB_7H_8$	1475.64	1496.77	1713.31	1508.22	1684.44
$1-NB_8H_9$	1684.54	1701.45	1956.01	1722.62	1919.81
$4-NB_8H_9$	1700.70	1716.80	1976.17	1743.56	1915.04
$1-NB_9H_{10}$	1919.82	1931.33	2229.70	1970.24	2181.22
$1-NB_{10}H_{11}$	2056.62	2065.47	2396.04	2105.03	2455.19
$NB_{11}H_{12}$	2323.75	2326.60	2698.18	2386.16	2614.82

The values are given in kcal/mol. The spin polarization energy of isolated atoms was taken into account. No correction for zero point motion was performed.

Table 5.30.: Azaborane Systems: Overbinding Energies

molecule	B3LYP	LDA	PBE	DFTB
	6-311++G**			
$HN-BH$	15.80	20.48	3.15	30.90
H_2N-BH_2	9.18	14.19	1.43	17.15
H_3N-BH_3	6.38	12.02	0.75	14.99
$H_2N-B_2H_3$	6.16	12.89	0.94	15.37
$H_3N_2-BH_2$	12.90	16.93	2.58	26.38
$(H_2N)_2-BH$	13.80	17.86	3.51	19.04
$HN-(BH_2)_2$	5.75	11.71	0.28	7.77
$B_3N_3H_6$	10.72	16.90	2.64	4.90
$B_5N_5H_8$	11.12	17.62	2.97	1.53
$B_7N_6H_9$	10.15	17.20	2.67	-2.28
$B_7N_7H_{10}$	11.30	17.95	3.12	-0.03
$B_8N_8H_{10}$	11.50	18.29	3.28	-1.67
$B_9N_9H_{12}$	11.40	18.14	3.21	-0.93
$B_{11}N_{11}H_{12}$	11.68	18.62	3.44	-3.22
$1-NB_4H_5$	2.39	10.61	1.48	5.98
$2-NB_4H_5$	2.43	11.03	1.55	1.71
NB_5H_6	1.61	10.12	1.56	3.14
$1-NB_6H_7$	1.15	9.63	1.44	2.40
$2-NB_6H_7$	1.14	9.52	1.41	10.25
$1-NB_7H_8$	0.78	9.30	1.41	10.00
$3-NB_7H_8$	0.81	9.14	1.25	8.03
$1-NB_8H_9$	0.56	9.05	1.27	7.84
$4-NB_8H_9$	0.54	9.18	1.43	7.14
$1-NB_9H_{10}$	0.34	9.11	1.48	7.69
$1-NB_{10}H_{11}$	0.23	8.93	1.27	10.49
$NB_{11}H_{12}$	0.07	8.91	1.49	6.93
Average	6.13	13.24	1.89	8.10

The values are given in kcal/mol per bond with respect to B3LYP/6-31G(d). The spin polarization energy of isolated atoms was taken into account. No correction for zero point motion was performed.

Figure 5.11.: Structure of α-Boron Nitride

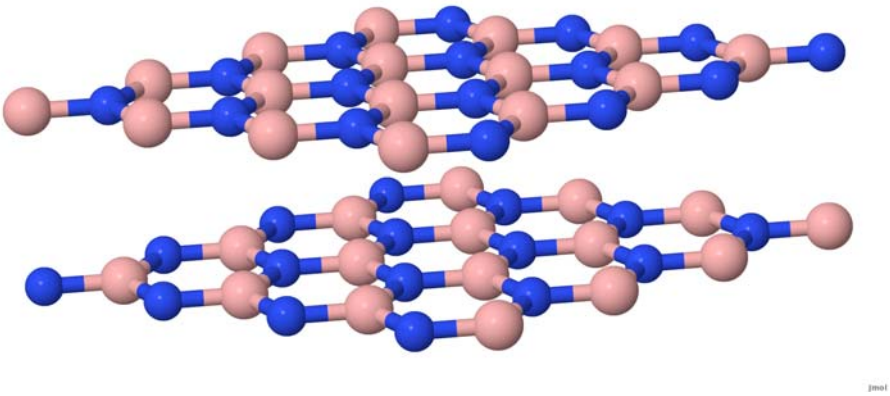

Figure 5.12.: Structure of β-Boron Nitride

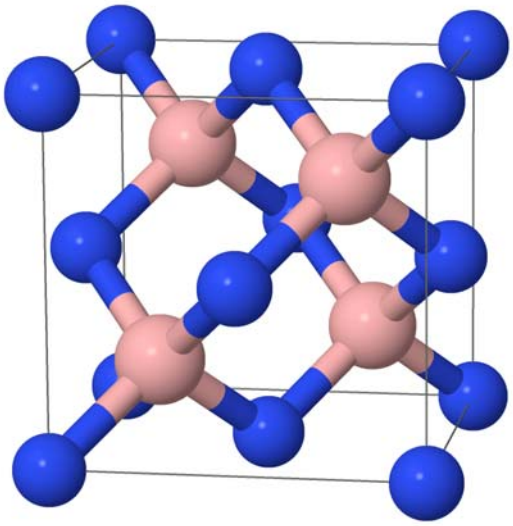

interesting distances B-N: within the sheet (in plane) and between the sheets (trans plane). The deviation for the in-plane distance is quite low ($< 2\%$), whereas the sheet distance (lattice constant c) and thus the trans-sheet B-N distance are off by 10%. For the γ-boron nitride the results are even worse. The results achieved with DFTB are very similar to the ones for α-boron nitride. Indeed the examination of the relaxed structure is a sheet stacking like α-boron nitride. Although γ-boron nitride is a meta-stable modification of boron nitride [52], this result is a bit unsatisfying. Nevertheless, the overall performance for the periodic structures is reasonable, especially since the main focus of the parametrization of boron were molecular systems.

Furthermore for all three systems, the band structure was calculated in the literature geometry [157, 158] and compared to DFT/PBE calculations with the program ELK[159]. The results of these calculations are shown in figures 5.14, 5.15, and 5.16 for α-BN, β-BN, and γ-BN respectively.

While the valence bands of the all systems analyzed are in reasonable agreement with

Figure 5.13.: Structure of γ-Boron Nitride

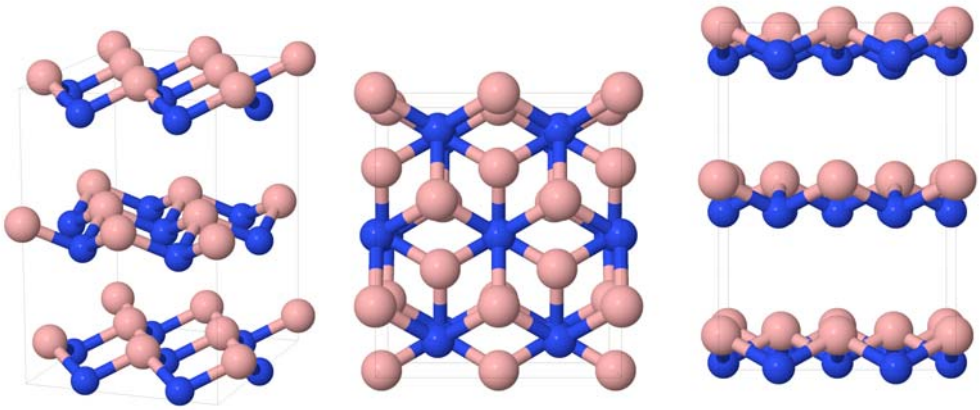

Table 5.31.: Overview of Deviation of the Geometric Parameters for Bulk Boron Nitride Systems

system	property	Literature	DFTB	deviation
α-BN	B-N (in plane)	1.45	1.47	1.87
	B-N (trans plane)	3.33	3.67	10.24
	lattice constant a	2.50	2.55	2.00
	lattice constant c	6.66	7.34	10.26
β-BN	B-N	1.57	1.63	3.82
	lattice constant a	3.62	3.75	3.65
γ-BN	B-N (in plane)	1.60	1.47	-7.76
	B-N (trans plane)	3.05	3.71	21.60
	lattice constant a	2.55	2.55	0.00
	lattice constant c	4.20	7.41	76.38

The values are given in Å, while deviation of DFTB is given in %. The literature values of the geometry are taken from [157, 158].

Figure 5.14.: Comparison of Band Structures of α-Boron Nitride

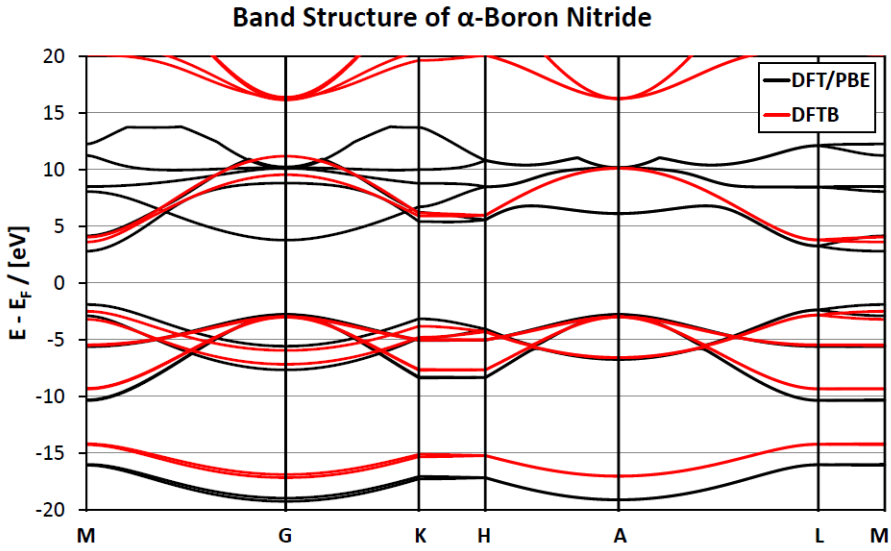

Data obtained at the DFTB (red lines) and DFT/PBE (black lines) levels of approximation for the same geometry (taken from literature [157, 158]).

Figure 5.15.: Comparison of Band Structures of β-Boron Nitride

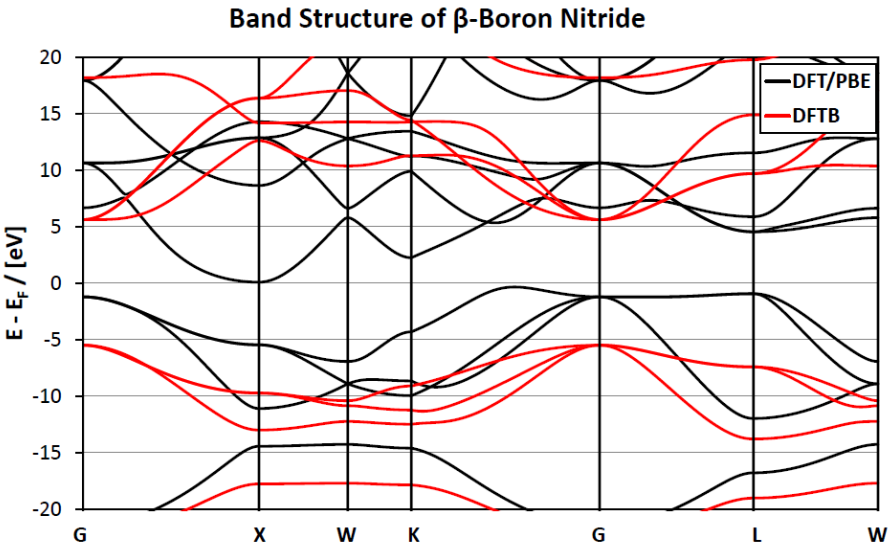

Data obtained at the DFTB (red lines) and DFT/PBE (black lines) levels of approximation for the same geometry (taken from literature [157, 158]).

Figure 5.16.: Comparison of Band Structures of γ-Boron Nitride

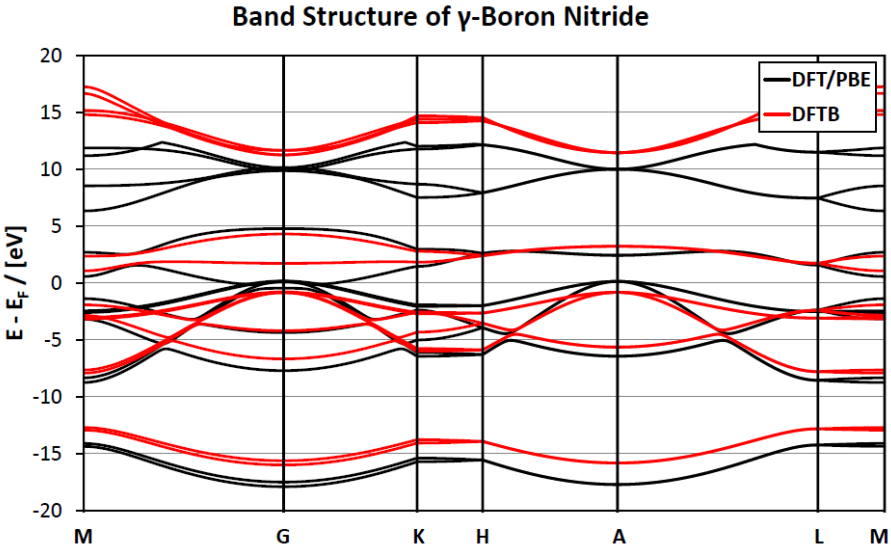

Data obtained at the DFTB (red lines) and DFT/PBE (black lines) levels of approximation for the same geometry (taken from literature [157, 158]).

the results from DFT/PBE, the description of the conduction bands is not as good. For example, for α-BN SCC-DFTB completely misses the band, which produces the conduction band minimum at the Γ-point. Furthermore the band, which gives the conduction band minimum at the A-point, has an apparently different progression. For β-BN there is not even any resemblance of the conduction bands to the ones obtained with DFT/PBE. In this case also the valence bands are down-shifted in energy compared to the DFT/PBE bands by nearly 4.3 eV at the Γ-point. While the trend of the valence bands between the points Γ and L, L and W, and Γ and X is qualitatively correct, level crossings between X and W, W and K, and K and Γ could not be reproduced with DFTB. The situation for γ-BN again is similar to α-BN, where the agreement for the valence bands is good but the conduction bands are off. In the case of the wurzite structure the deviations are considerably larger than for the hexagonal. So the level touching at the Γ-point found by DFT/PBE is not observed for the DFTB results.

Part III.

Graphene with Adatoms

6. Introduction to Graphene

6.1. Discovery

The ability of carbon to form complex networks is unmatched by any other element of the periodic system. The complete organic chemistry is based on carbon and its bonds in molecules[160]. Furthermore pure carbon systems are also of large variety. The bulk carbon modifications diamond and graphite are known for ages, but the rather recently discovered fullerenes and nanotubes are of great interest to chemists and physicists[161–164]. The research in carbon based materials increased further with the successful synthesis of the first two-dimensional crystal, graphene[165, 166]. Graphene is probably the best theoretically studied carbon allotrope since its structure of planar, hexagonal arranged carbon atoms is part of many other carbon systems as graphite, nanotubes and fullerenes. The first successful synthesis of graphene was performed by extraction of a monolayer from graphite by micromechanical cleavage[167, 168]. This technique could be used considering that graphite can be viewed as a stacking of two-dimensional graphene crystals weakly coupled together[169]. The message of the synthesis and its application to other materials[168] is that truly "two-dimensional crystals do exist and are stable under ambient conditions"[169], although this was against the common belief[170–173]. Nevertheless for an industrial production and real application, the micromechanical cleavage or scotch tape method is not suited and other techniques have to be developed like the exfoliation of intercalated graphitic compounds[174–178] or the Si sublimation from SiC substrates[179]. But for "prove of principle", the samples of graphene are of so high quality that quantum Hall effect[165, 166] and ballistic transport[167] could be observed.

6.2. Geometry and Band Structure

The structure of graphene is that of a planar honeycomb, hexagonal lattice of carbon atoms. The primitive unit cell contains two symmetry equivalent carbon atoms and thus can be described as using two symmetry equivalent sublattices A and B (see figure 6.1). In this planar structure both carbon atoms are sp^2-hybridized and form directed σ-bonds to their direct neighbors. The fourth electron of each carbon atom is added via the p_z-orbital to the system-wide, conjugated π-system. The bond distance in graphene is 1.42Å, which is just between the single bond distance (1.54Å in ethane) and the double bond distance (1.33Å in ethane) as typical for aromatic, organic systems (1.39Å in benzene). Therefore, graphene is related to (polycyclic) aromatic hydrocarbons benzene, naphthalene, anthracene and/or coronene and can be considered as the infinite extension of such systems.

Figure 6.1.: Structure of Graphene

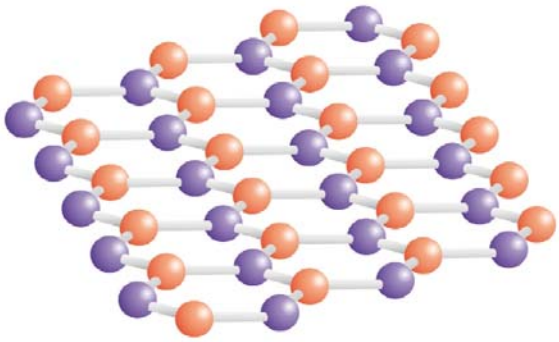

Structure of graphene. Different colors for the carbon atoms mark their affiliation to the different sublattices.

Figure 6.2.: Band Structure of Graphene

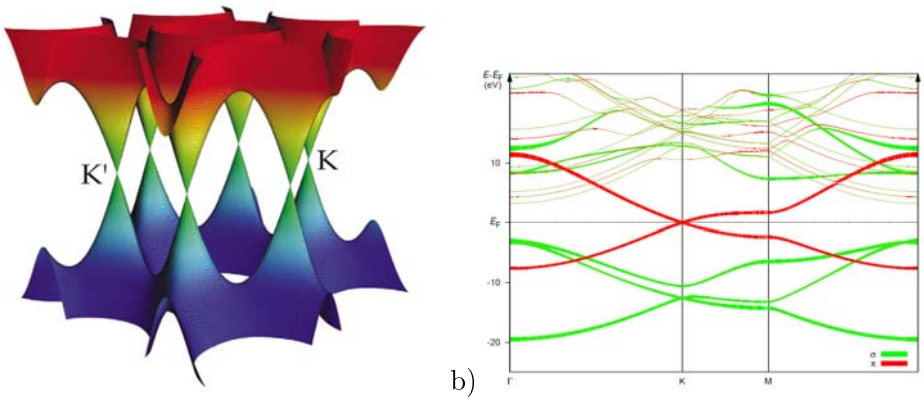

a) b)

a) Bandstructure of graphene with touching bands at the conical points K and K' taken from ref. [169].

b) Bandstructure of graphene with the assignment of the basis character of the bands. Taken from ref. [184].

The bandstructure of graphene is one of the most interesting aspects of the material. The band structure can be described by the simple nearest-neighbor, tight-binding approximation [180]. It is shown in figure 6.2. Pristine graphene has no bandgap. The symmetry of the atoms in the unit cell results in two conical points (K and K') in the Brillouin zone, where the conduction and valence band cross each other. Near these crossing points, the relation of electron energy and wave vector is linear, which closely resembles the Dirac spectrum for massless fermions [181, 182]. Because of this linearity, the quasiparticles in graphene are expected to behave different from those in conventional metals and semiconductors [169]. The mobilities of charge carriers within graphene already are found to exceed those of modern Si transistors by a magnitude and are hoped to further increase as "graphene technology" improves [169, 183].

Figure 6.3.: Band Structure of Graphene for varying Sublattice Occupations

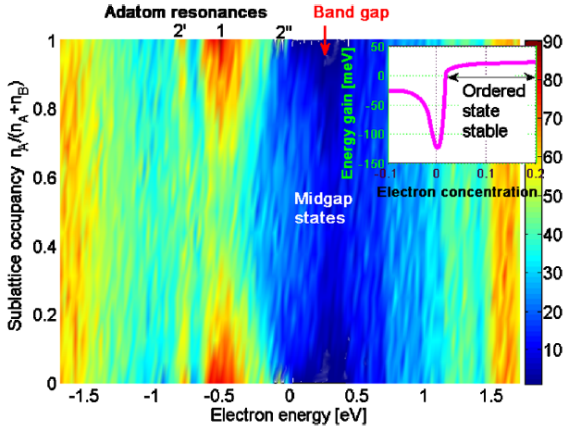

The density of electronic states as a function of energy for different sublattice occupancy ratios. The band gap, which opens at $n_A \gg n_B$ and $n_B \gg n_A$, is immune to disorder: no electronic states are found inside the gap. The picture is taken from ref. [186].

6.3. Electronic Structure Manipulation

In the search for new materials for molecular electronic devices, graphene strikes many scientists as a promising candidate due to its high electron mobility. But in order to be suitable for applications the engineering of a band gap in a controlled fashion is needed. For this, the low dimensional material provides unique opportunities for the manipulation of its properties by chemical means. For example, graphene can be transformed from a zero band gap Dirac material into a wide band gap insulator by hydrogenation. The material gained is the so-called graphane, where all carbons are sp^3-hybridized and bond to a hydrogen each. Partially functionalized graphene offers the chance to tune the optical and electronic transport properties between disordered Dirac material and insulating characteristics. This could be done by variation of the adsorbate concentration and the real space arrangement of the adsorbates. Shytov et. al. [185, 186] and Cheianov et. al. [187] have shown with their calculations that the opening of a band gap in graphene occurs due to adatom adsorption, if the adsorbates break the sublattice symmetry (see figure 6.3).

The means of control for this tuning are the formation of chemical bonds between the carbon and the adsorbate as these bonds alter the covalent bonds between carbons in the graphene framework. The mechanisms, which contribute to the interaction of carbon and its bonding partners, can be illustrated as follows: First, covalent adsorbates like hydrogen or fluorine lead to a rehybrizidation of their carbon bonding partner in the graphene plane from sp^2 to sp^3. Thereby the adsorbates induce a change in the inter carbon bond angles and local strains in the lattice. These lattice deformations mediate an effective adsorbate-adsorbate interaction on the length scale of a few interatomic spacings, which can be as large as 0.5eV per adsorbate pair.[188] Second, adsorbates effectively remove their bonding partners from the conjugated π-system of the carbons and thus locally break the aromaticity. The preference to restore aromaticity globally leads to inter adsorbate coupling. On the atomic scale, aromaticity induced adsorbate coupling has been

Figure 6.4.: Structure of 25% hydrogenated Graphene

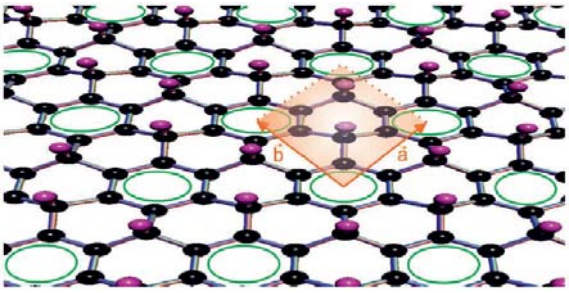

Model of the ordered adsorption of hydrogen on graphene in the stoichiometry C_4H.
Isolated aromatic rings are indicated.
The vectors $\vec{a}$ and $\vec{b}$ define the unit cell of C_4H and connect the aromatic rings.
They define a 2x2 super structure with respect to pristine graphene.
The picture is taken from ref. [189].

demonstrated to stabilize para-type H-adsorption patterns in 25% hydrogenated graphene, i.e. C_4H by means of experiments and first-principles calculations.[189] This long range coupling is the sublattice pseudo-spin analog of RKKY interaction between real spins in metals.[186, 187] Similar to RKKY, this electronically mediated interaction depends strongly on the location of the Fermi level. Starting from impurity coverages of a few percent both strain and electronically mediated inter impurity coupling can be expected to interfere and thus determine the phase diagram of covalently functionalized graphene systems.

Therefore, if the interplay of electronic and deformational coupling can be largely manipulated either by adsorbate concentration and/or charge doping, an ordering transition of the adsorbates could be observed, where the sublattice symmetry is spontaneously broken. Thus, the controlled engineering of a band gap should be possible.

7. Simulation Results for Adatoms on Graphene

7.1. Hydrogen on Graphene

7.1.1. Comparison of DFT and DFTB for the Adsorption of atomic Hydrogen on Graphene

To validate, if the SCC-DFTB method is appropriate to study the adsorption of hydrogen on graphene and the possibility of sublattice symmetry breaking, geometry optimizations with one and two hydrogen atoms on pristine graphene using SCC-DFTB with the DFTB+ code[51] and DFT/PBE[141] within the VASP package[147] have been performed.

Figure 7.1 shows the optimized structure of one hydrogen atom adsorbed on graphene. Due to the adatom the structure is no longer perfectly planar, but the connected carbon is pulled out of the plane by 0.52Å and even the neighboring C-atoms are displaced by 0.17Å in the direction of the hydrogen. This results significantly differs from the results of Boukhvalov and co-workers [188], who found that the neighboring carbon atoms are pushed to the other side of the graphene plane enabling the sp^3-hybridization of the substrate C-atom while the planeness of graphene is conserved to the greatest extend. Nevertheless, those results could not be reproduced within VASP or SCC-DFTB, which both give the buckle around the adsorbed hydrogen. The findings with VASP and SCC-DFTB are independent of constriction of the lattice parameters to the ones of perfect graphene.

For the adsorption of two hydrogen atoms three different patterns have been considered, namely the directly neighboring positions on the two sublattices ($A_0 - B_1$), the directly neighboring positions on one sublattices ($A_0 - A_2$), and the next-neighboring positions on the two sublattices ($A_0 - B_3$). For each of these, also the positioning of the atoms on both sides of the graphene plane ($A_0 - B_1'$, $A_0 - A_2'$, and $A_0 - B_3'$) have been taken

Figure 7.1.: Optimized Structure of one Hydrogen on Graphene

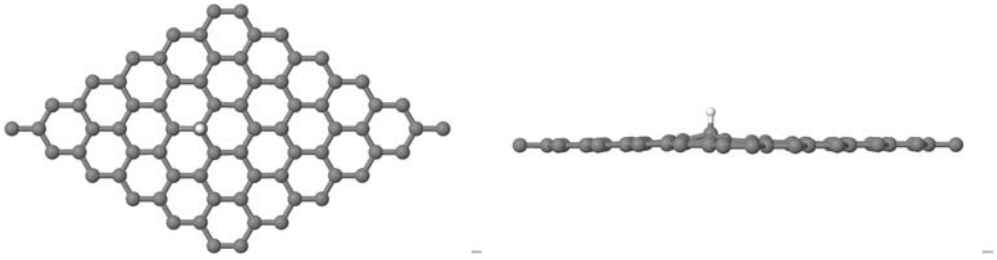

Figure 7.2.: Optimized Structure of two Hydrogens on one Side of Graphene

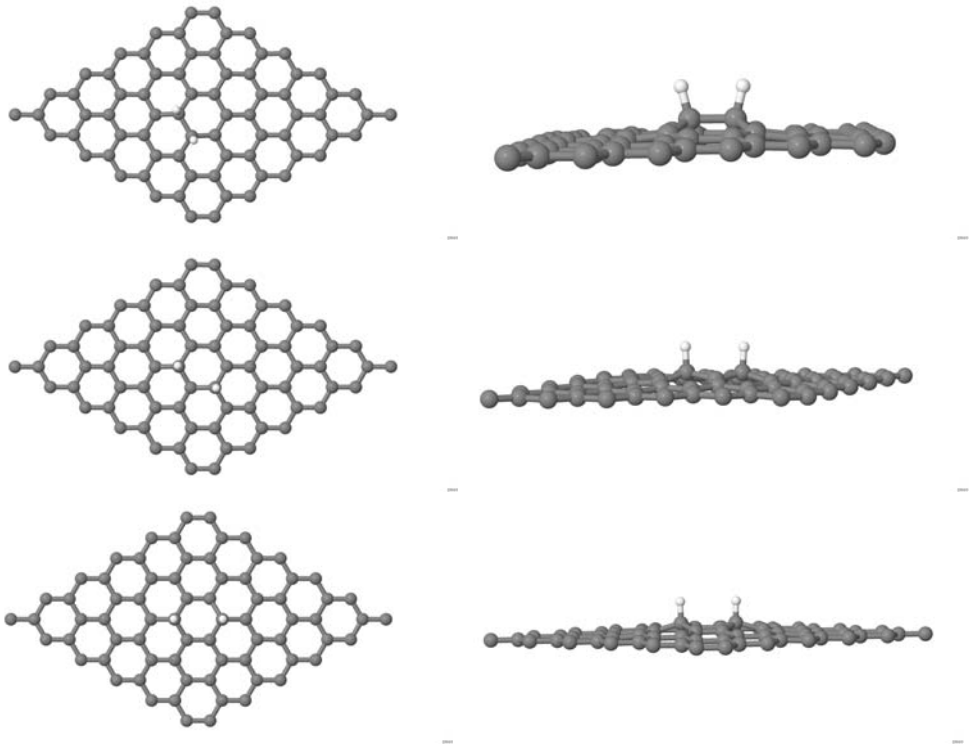

Table 7.1.: Relative Energies of two Hydrogens on Graphene

structure	DFT/PBE	DFTB
$A_0 - B_1$	0.00	0.00
$A_0 - A_2$	1.32	1.18
$A_0 - B_3$	0.05	0.03
$A_0 - B_1'$	-0.43	-0.51
$A_0 - A_2'$	1.32	1.20
$A_0 - B_3'$	0.24	0.23

Energies are given in eV. The configuration with the closest hydrogen positions was taken as zero point.

into account. The structures were relaxed within the optimized lattice constants of pure graphene. Representations of the optimized systems are given in figures 7.2 and 7.3, while table 7.1 shows the energies of the calculated patterns relative to the structure with the smallest hydrogen-hydrogen distance. It can be seen that SCC-DFTB correctly reproduces the energetic differences between the structures compared to DFT.

These results indicate that the SCC-DFTB method can be used to investigate the sublattice depended adsorption of hydrogen on graphene and the possibility of sublattice symmetry breaking.

Figure 7.3.: Optimized Structure of two Hydrogens on both Sides of Graphene

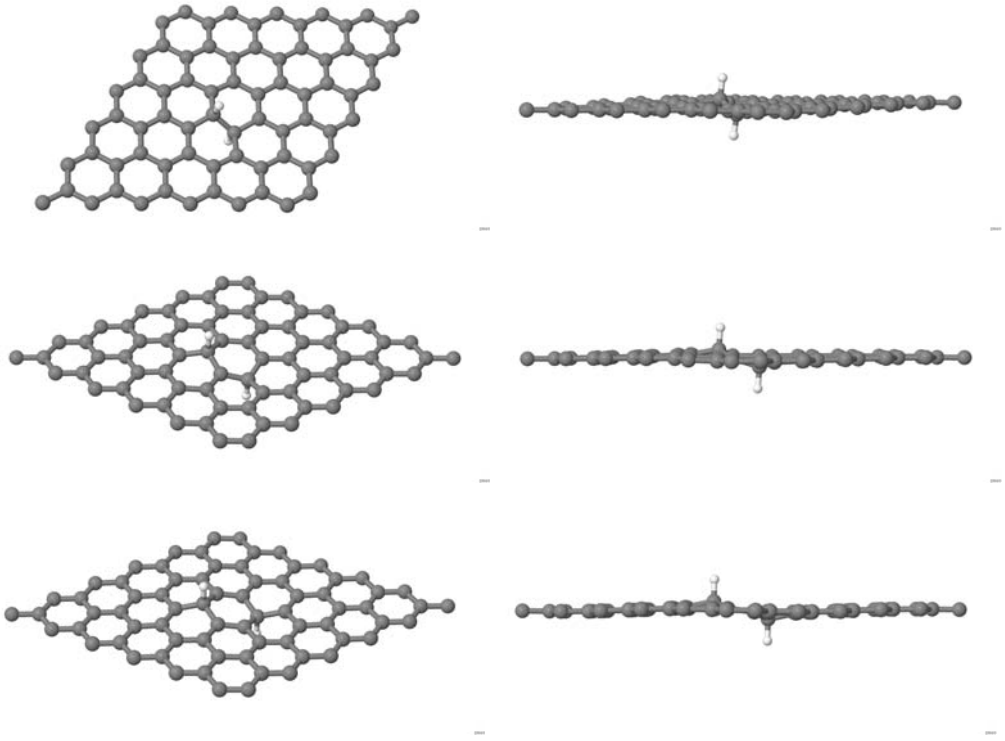

7.1.2. Adsorption Energy for different Hydrogen Concentrations

Since SCC-DFTB provides results comparable to DFT (see section 7.1.1), SCC-DFTB calculations were performed for different concentrations of hydrogen on graphene. To compare the different concentrations the total energies calculated must be normalized by the number of hydrogens in the system. Hence, the interaction energy per carbon-hydrogen bond, E_{int}, is defined as:

$$E_{\text{int}}\,(\text{C-H}) = \frac{E_{\text{System}} - E_{\text{Graphene}}}{n_{\text{H}}} - \frac{1}{2}E_{\text{H}_2} \tag{7.1}$$

where E_{System} is the total energy of the hydrogenated graphene, E_{Graphene} is the total energy of a pure graphene sheet of the same size as the hydrogenated system, n_{H} is the number of hydrogens on the graphene system, and E_{H_2} is the total energy of the hydrogen dimere. This energy expression should also enable the direct comparison with the data of Shytov and co-workers [185]. There, the energy is calculated for low adatom concentrations (2-20% hydrogen on graphene) and a monotonous increase or decrease of the energy is found for sublattice broken or equal population, respectively.

Calculations are performed for one-sided adsorption of hydrogen on sublattice A only ("A only"), one-sided adsorption with equal distribution of the adatoms on the sublattices A and B ("AB one-sided"), and for adsorption on sublattice A from one side and on sublattice B from the other side with equal distribution of the adatoms on the sublattices ("A top, B bottom"). For each these adsorption patterns hydrogen concentrations in the range of

Figure 7.4.: Graphene with different Hydrogen Concentrations

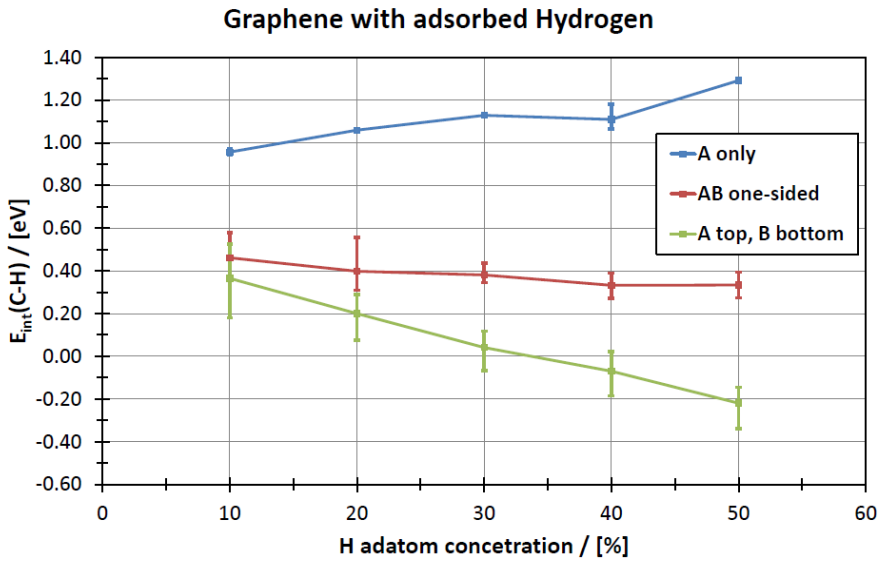

Each data point gives the average over approximately 10 different adsorption configurations of hydrogen atoms on a (10x10) graphene cell (200 carbon atoms). The error bars indicate the full (maximum to minimum) energy distribution of calculated configurations.

Table 7.2.: Interaction Energy per C-H bond of Graphene with Hydrogen Adatom Concentrations

concentration	A only			AB one-sided			A top, B bottom		
[H-%]	average	max	min	average	max	min	average	max	min
10	0.9570	0.9706	0.9438	0.4618	0.5785	0.3583	0.3650	0.5269	0.1800
20	1.0595	1.0644	1.0513	0.3986	0.5567	0.3092	0.2000	0.2894	0.0762
30	1.1287	1.1338	1.1230	0.3812	0.4371	0.3448	0.0411	0.1173	-0.0682
40	1.1098	1.1802	1.0660	0.3327	0.3891	0.2715	-0.0698	0.0228	-0.1858
50	1.2923	-	-	0.3341	0.3946	0.2738	-0.2194	-0.1445	-0.3378

Energies are given in eV. Approximately 10 different adsorption configurations of hydrogen atoms on a (10x10) graphene cell (200 carbon atoms) are averaged and the maximum and minimum energies of calculated configurations are presented as well.

10 to 50% adatom concentration have been considered. The results of the calculations are presented in table 7.2 and graphically in figure 7.4. One should note that in case of 50% hydrogens for "A only" this concentration equals the adsorption of hydrogen on every carbon atom of sublattice A.

The figure shows that sublattice symmetry breaking even for high hydrogen concentrations is not favorable compared to the equal distribution of the hydrogens over both sublattices. The "A top, B bottom" pattern would lead to graphane at an adsorbate concentration of 100% coverage and thus gets more preferred with the rise in adsorbate concentration. The "A only" pattern is the energetically least favorable adsorption pattern and this increases with the adsorbate concentration as more and more "radical traps" on the graphene are formed. By "radical traps" are meant the adsorptions of three hydrogens around one carbon atom of the other sublattice, which prevent the electron in the p_z-orbital of that

Figure 7.5.: Delocalization and Radical Trap in Partially Hydrogenated Graphene

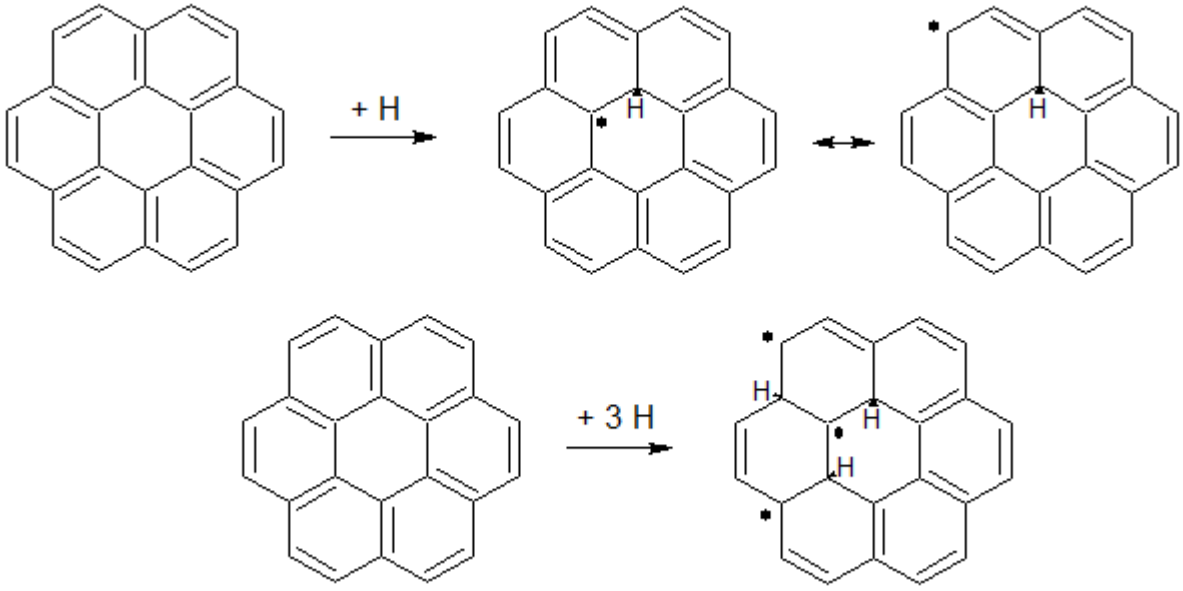

Top: Examples for the delocalization of an unpaired electron in graphene due to hydrogen adsorption.
Bottom: Formation of a "hydrogen cage" or "radical trap", which prevents the delocalization of the caged unpaired electron in graphene.

carbon atom from forming a π-bond to another carbon atom and thus delocalization of the unpaired electron through the conjugated π-system of the graphene. A schematic sketch of the delocalization and trapping is given in figure 7.5. The third pattern, the "AB one-sided", reveals the influence of the hydrogen-hydrogen repulsion and the π-bond reformation, which are absent in the "A top, B bottom" and "A only" pattern, respectively. For low concentrations (10-20%) the hydrogen-hydrogen repulsion is nearly neglectable and the π-bond reformation makes the difference. For larger concentrations the hydrogen-hydrogen repulsion and the according deformation of the graphene sheet become more prominent and nearly no additional energy is gained from the adsorption. Therefore, the data strengthens Cheianov and co-workers [187], who claimed that the hydrogen-hydrogen repulsion must be considered and the observation of Haberer and co-workers [189], who found a maximum concentration of 25% hydrogen adsorption in their experiments.

Nevertheless, the results definitely state that the pure adsorption of hydrogen on graphene at any concentration is not enough to induce sublattice symmetry breaking.

7.1.3. Adsorption Energy for different Electron Doping Values

Because of the inability of sublattice symmetry breaking by the adatom concentration (section 7.1.2), the influence of electron doping on the sublattices ordering of hydrogen adsorbed on graphene shall be considered. In order to investigate this doping effect, the virtual crystal approach (VCA) [190, 191] was chosen. In this approach the number of protons in the core and the number of electrons in the shell of an atom sort are modified to

Figure 7.6.: Band Structure for Electron-doped Pristine Graphene

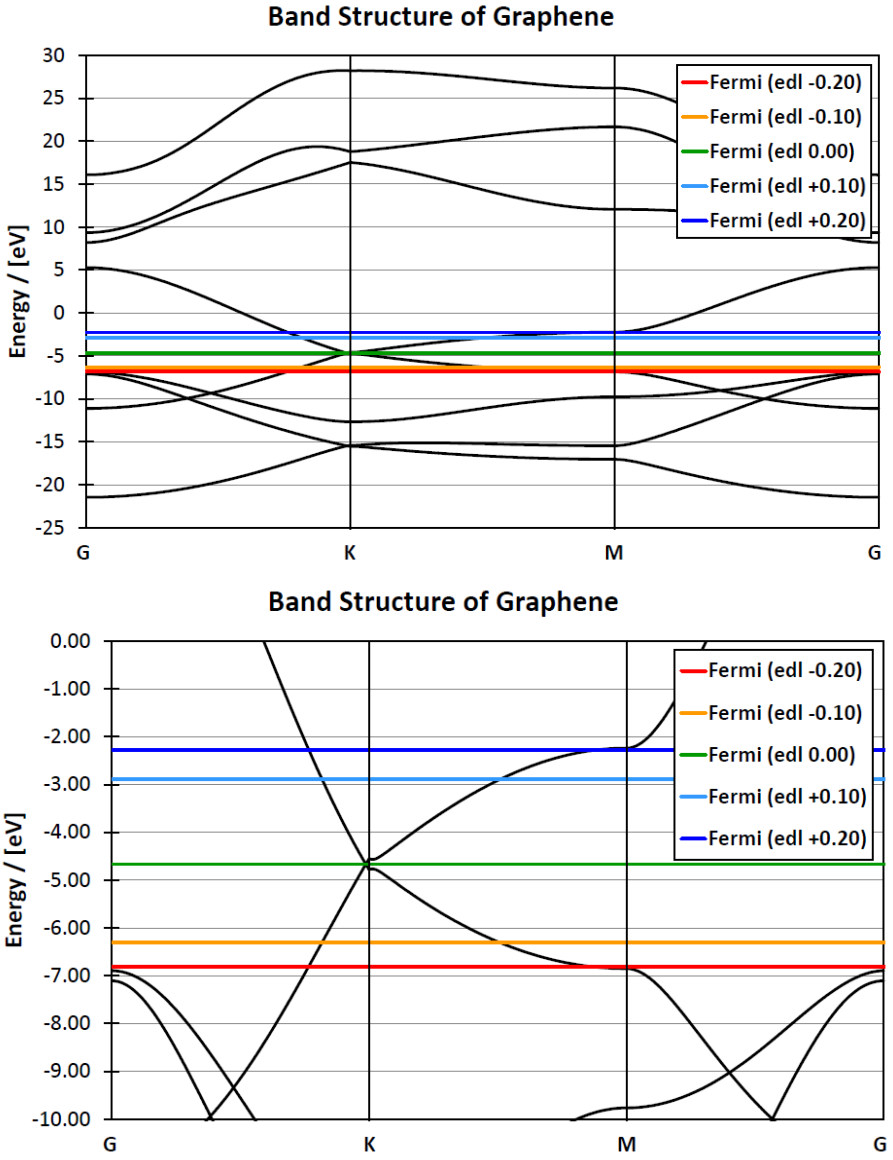

Band Structure with Fermi energy at different electron doping levels (edl).

simulate the effect of doping without ionic contributions. For the present application the doping was done by editing of the SKF for carbon and adjusting the number of 2p-electrons in the range of -0.20 to +0.20 electrons. By this, not only electron but also hole doping of the graphene has been considered. The usage of the VCA allows this without the necessity to balance any charges in the unit cell by a jellium, which is still under debate how to do correctly.

The range of doping is visualized in figures 7.6 and 7.7, where the bandstructure and density of states computed with SCC-DFTB is shown with the Fermi energies of different electron doping levels (edl).

The doping was performed for graphene with 10% adsorbed hydrogen atoms on one side of the graphene and for three different ratios of sublattice coverage. Tested sublattice occu-

Figure 7.7.: Density of States for Electron-doped Pristine Graphene

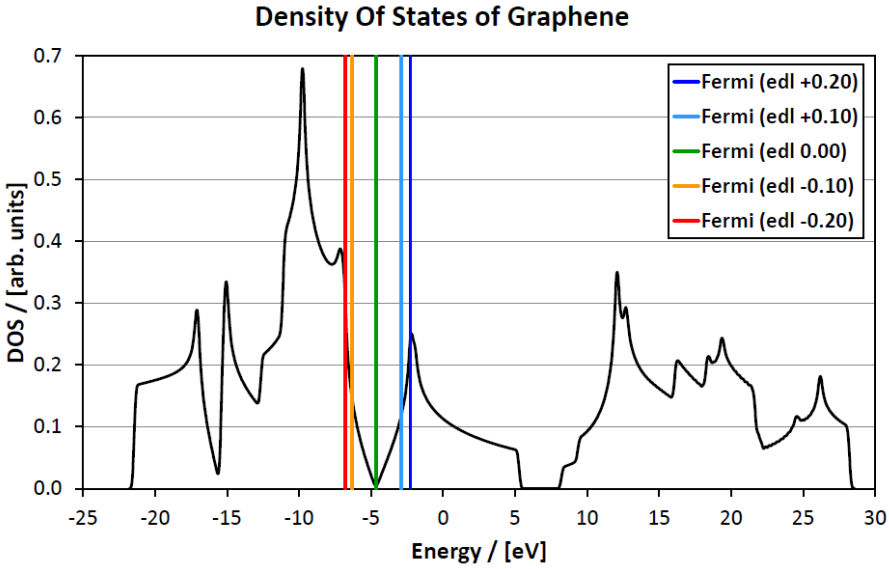

Density of states with Fermi energy at different electron doping levels (edl).

pations were total sublattice symmetry breaking ($^{A}/_{B} = {}^{1}/_{0}$), equal sublattice population ($^{A}/_{B} = {}^{1}/_{1}$), and intermediate ($^{A}/_{B} = {}^{3}/_{1}$). In figures 7.8, 7.9, and 7.10, the results are presented graphically while table 7.3 shows the average over the tested configurations with the maximum and minimum values of the interaction energies as used in section 7.1.2 and defined in equation 7.1.

The figures 7.8, 7.9, 7.10 and 7.11, all show that the effect of hole- and electron-doping on the C-H interaction energy is not symmetric. The present overlap of the energy distribution ranges at zero doping (see figure 7.8) reflects the findings of Haberer and co-workers [189], who stated that the adsorption of hydrogen at concentrations below 25% is not ordered at room temperature. The maxima and minima of the distributions are achieved by configurations created due to chemical intuition. Therefore, the assumption appears warrantable that although the configurational space is considerably larger than the small group of tested configurations, the tested configurations compasses the whole energy distribution range. Hence, the discussion of the energetic minima (figures 7.10 and 7.11) is sensible. Figure 7.10 reveals that a change of sublattice population preference occurs for hole-doping of -0.10 electrons per carbon atom. For electron-doping this preference change is observed only at the edge of the tested doping levels, for a value of +0.20 electrons per carbon atom. The alternation in the trends for ($^{A}/_{B} = {}^{1}/_{1}$) and ($^{A}/_{B} = {}^{1}/_{0}$) at -0.10 and +0.10 electrons, respectively, are attributed to a change of the respective energy minimum configurations. For a better awareness of the symmetry breaking possibility due to the doping the relative energy of the minimun configurations as defined by equation 7.2 is plotted in figure 7.11. There, the difference of total and partial sublattice symmetry breaking of the adatoms to the equal occupation of the sublattices is shown.

Table 7.3.: Interaction Energy per C-H bond of doped Graphene with 10% Hydrogen Adatoms

doping	A/B = 1/0			A/B = 3/1			A/B = 1/1		
	average	max	min	average	max	min	average	max	min
-0.20	-0.7476	-0.1875	-0.8347	-0.7134	-0.4225	-0.8034	-0.6674	-0.2949	-0.7690
-0.16	-0.5892	0.0374	-0.7113	-0.5751	-0.4021	-0.6906	-0.5377	-0.2855	-0.6609
-0.12	-0.3711	0.1156	-0.5190	-0.3782	0.0383	-0.4920	-0.3583	-0.1212	-0.4663
-0.10	-0.2171	0.0942	-0.3949	-0.2745	-0.1161	-0.3639	-0.2509	0.0072	-0.3628
-0.06	0.3135	0.4827	0.2445	0.0483	0.1334	-0.0425	0.0266	0.5657	-0.2685
-0.02	0.8044	0.9129	0.7783	0.4684	0.5786	0.3242	0.3313	0.8562	-0.0680
0.00	0.9594	1.0356	0.9433	0.6069	0.7446	0.4673	0.4556	0.9650	0.0291
0.002	0.9611	1.0345	0.9435	0.6180	0.7469	0.4684	0.4580	0.9663	0.0282
0.02	0.9087	0.9697	0.8723	0.5708	0.7062	0.4143	0.4293	0.9199	-0.0259
0.04	0.7810	0.8795	0.7301	0.4667	0.5935	0.3079	0.3614	0.8386	-0.1152
0.06	0.6126	0.8006	0.5458	0.3528	0.4803	0.2172	0.2875	0.7373	-0.1735
0.08	0.4185	0.7010	0.3328	0.2455	0.4803	0.2172	0.2115	0.6234	-0.2195
0.10	0.2400	0.5936	0.1064	0.1552	0.3327	0.0827	0.1416	0.5202	-0.2341
0.12	0.1108	0.4953	0.0395	0.0827	0.2496	0.0217	0.0761	0.4138	-0.2460
0.16	-0.0734	0.2961	-0.1202	-0.0492	0.0966	-0.0922	-0.0459	0.1844	-0.2530
0.20	-0.2267	0.0730	-0.2610	-0.1766	-0.0781	-0.2210	-0.1644	0.0074	-0.2515

Energies are given in eV. Different adsorption configurations of 20 hydrogen atoms on a (10x10) graphene cell (200 carbon atoms) are averaged and the maximum and minimum energies of calculated configurations are presented as well.

Figure 7.8.: Doped Graphene with Hydrogen Adatoms - Energy Distributions

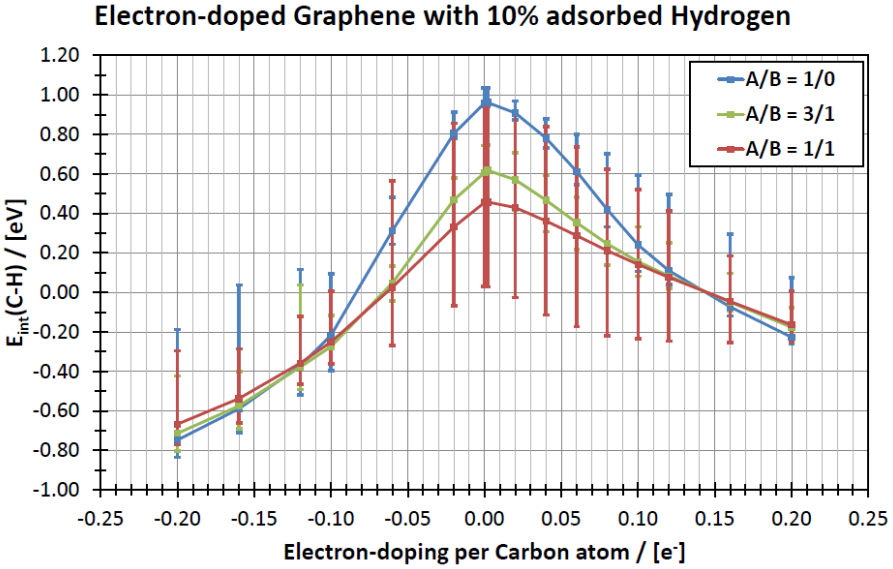

Each data point gives the average of different adsorption configurations of 20 hydrogen atoms on a (10x10) graphene cell (200 carbon atoms). The error bars indicate the full (maximum to minimum) energy distribution of calculated configurations.

Figure 7.9.: Doped Graphene with Hydrogen Adatoms - Energy Averages

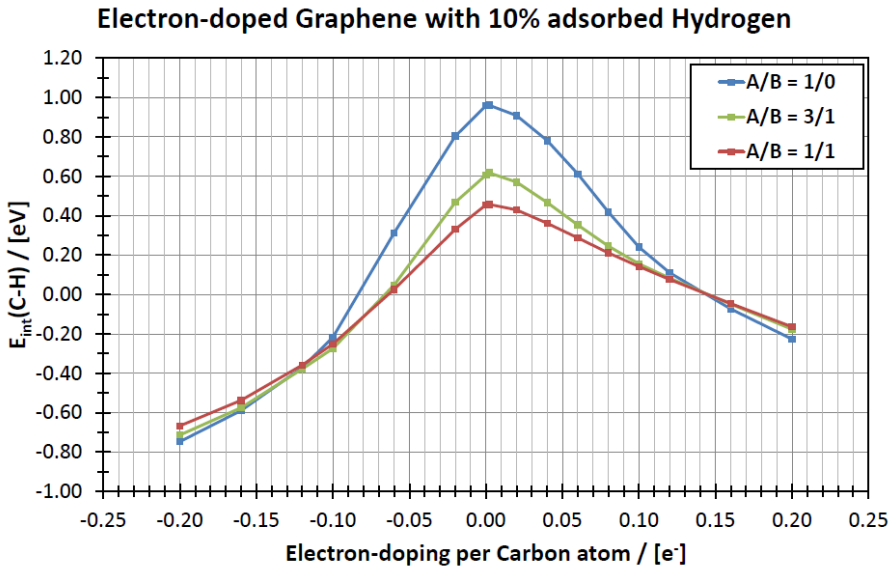

Each data point gives the average of the different adsorption configurations of 20 hydrogen atoms on a (10x10) graphene cell (200 carbon atoms).

Figure 7.10.: Doped Graphene with Hydrogen Adatoms - Energy Minima

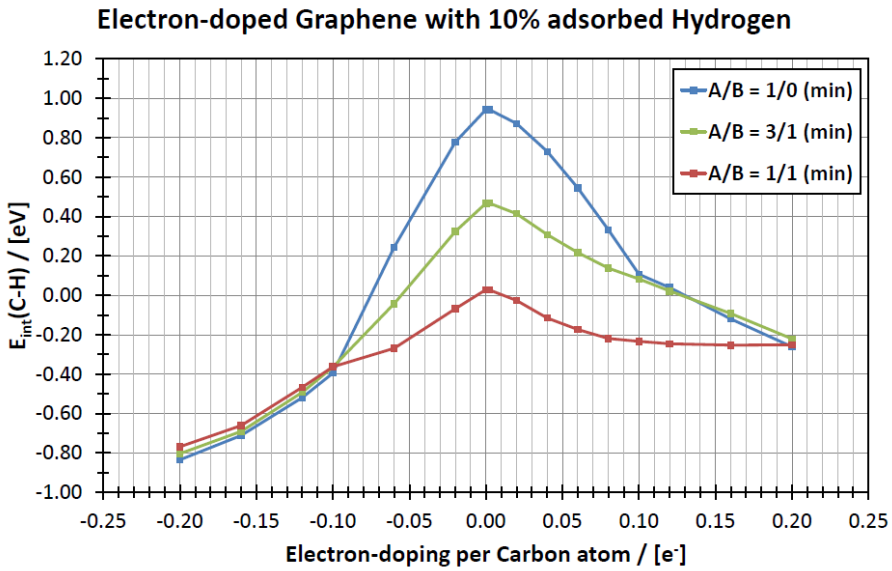

Each data point gives the energy minimum of the different adsorption configurations of 20 hydrogen atoms on a (10x10) graphene cell (200 carbon atoms).

Figure 7.11.: Doped Graphene with Hydrogen Adatoms - Energy Differences

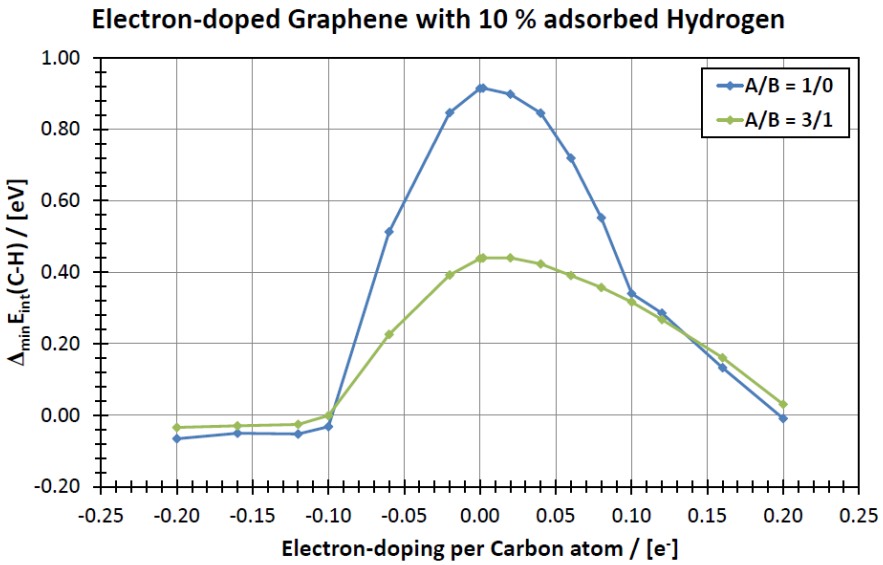

Each data point shows the difference of the energy minima of the sublattice symmetry broken adsorption patterns ($^{A}/_{B} = {}^{1}/_{0}$ and $^{A}/_{B} = {}^{3}/_{1}$) to the sublattice equally occupied pattern ($^{A}/_{B} = {}^{1}/_{1}$) for the tested electron doping levels.

$$\Delta_{\min}E_{\text{int}} \quad = \quad \min\left[E_{\text{int}}\left(^{A}/_{B} = {}^{x}/_{y}\right)\right] - \min\left[E_{\text{int}}\left(^{A}/_{B} = {}^{1}/_{1}\right)\right] \tag{7.2}$$

It can be concluded that within the limits of calculated doping levels and tested configurations, total sublattice breaking should be possible beyond 0.10 hole- and 0.20 electron-doping. Hence, the adsorption of hydrogen atoms on graphene introduces non-symmetric impurities. Furthermore, the results clearly show that total sublattice symmetry breaking is more likely to achieve than partial symmetry breaking.

Table 7.4.: Relative Energies of two Fluorine Atoms on Graphene

structure	DFT/PBE	DFTB
$A_0 - B_1$	0.00	0.00
$A_0 - A_2$	0.47	1.32
$A_0 - B_3$	-0.17	0.04
$A_0 - B_1'$	-0.64	-0.54
$A_0 - A_2'$	0.37	1.21
$A_0 - B_3'$	-0.13	0.10

Energies are given in eV. The configuration with the closest fluorine positions was taken as zero point.

7.2. Fluorine on Graphene

In section 7.1.3 is shown that the sublattice symmetry breaking of hydrogen atoms adsorbed on graphene is possible for certain levels of electron- and hole-doping. Since the calculations revealed a preference for the hole-doping, the question whether this preference can be shifted to electron doping by the adsorption of a different atom type. The fluorine atom seems to be a good candidate for such modification because the C-F bond has a opposite polarization than the C-H bond.

7.2.1. Comparison of DFT and DFTB for the Adsorption of atomic Hydrogen on Graphene

As for the case of the hydrogen adsorption (see section 7.1.1), at first a comparison of the results from DFT and DFTB calculations is done. For this, the same test as for hydrogen is performed, namely the comparison of energy differences for neighboring adsorption sites. As before the three different patterns are the directly neighboring positions on the two sublattices ($A_0 - B_1$), the directly neighboring positions on one sublattices ($A_0 - A_2$), and the next-neighboring positions on the two sublattices ($A_0 - B_3$). For each of these, also the positioning of the atoms on both sides of the graphene plane ($A_0 - B_1'$, $A_0 - A_2'$, and $A_0 - B_3'$) have been taken into account. The structures were relaxed within the optimized lattice constants of pure graphene. The calculations are performed for SCC-DFTB with the DFTB+ code[51] and the *pbc*-SKF-set[140] and DFT/PBE[141] with the VASP package[147]. The summary of the results are presented in table 7.4 as the relative energies of the tested configurations.

As for hydrogen the systems with positioning of the fluorine atoms on different sublattices are energetically favored. For the directly neighboring adatoms ($A_0 - B_1$ and $A_0 - B_1'$) the effect of adatom repulsion can be noticed the best as the difference between the one-sided and two-sided adsorption is with both methods about 0.5eV. The adsorption of the adatoms on one sublattice is the least favored configuration in both methods, but the relative energy difference is higher in DFTB by about 0.9eV compared to DFT. This relative difference is consistent for the one-sided and both-sided adsorption and nearly the same as for the hydrogen adatoms (see section 7.1.1). Although the discrepancy between DFT and DFTB

Table 7.5.: Interaction Energy per C-F bond of doped Graphene with 10% Fluorine Adatoms

doping	$^{A}/_{B} = {}^{1}/_{0}$			$^{A}/_{B} = {}^{3}/_{1}$			$^{A}/_{B} = {}^{1}/_{1}$		
	average	max	min	average	max	min	average	max	min
-0.20	-0.8812	-0.8459	-0.9408	-0.8608	-0.8170	-0.8987			
-0.16	-0.7590	-0.7056	-0.8400	-0.7597	-0.7008	-0.8056	-0.7657	-0.7192	-0.8181
-0.12	-0.5853	-0.5011	-0.6984	-0.6504	-0.5702	-0.7964	-0.6391	-0.5768	-0.6908
-0.10	-0.4576	-0.3714	-0.6004	-0.5732	-0.4885	-0.7547	-0.5599	-0.4867	-0.6253
-0.06	-0.0583	0.1325	-0.1111	-0.3824	-0.0633	-0.4684	-0.3445	-0.2570	-0.4346
-0.02	0.2795	0.3087	0.2453	-0.2053	0.1016	-0.3147	-0.0773	0.0185	-0.1588
0.00	0.3628	0.4023	0.3228	-0.1526	0.1410	-0.2653	0.0028	0.0939	-0.0764
0.02	0.2391	0.2841	0.1906	-0.2511	0.0142	-0.3478	-0.1148	-0.0327	-0.1939
0.06	-0.2185	-0.1725	-0.2851	-0.5219	-0.3138	-0.5831	-0.4916	-0.4064	-0.5818
0.10	-0.7604	-0.6893	-0.9100	-0.7659	-0.6243	-0.8393	-0.7880	-0.7313	-0.8599
0.12	-0.9209	-0.8585	-1.0252	-0.8542	-0.4406	-0.9351	-0.8944	-0.8555	-0.9765
0.16	-1.1431	-1.0673	-1.2018	-1.0359	-0.7161	-1.1311	-1.0719	-1.0044	-1.1801
0.20	-1.3167	-1.2399	-1.3331	-1.2007	-1.0179	-1.2717	-1.2333	-1.1471	-1.3095

Energies are given in eV. Different adsorption configurations of 20 fluorine atoms on a (10x10) graphene cell (200 carbon atoms) are averaged and the maximum and minimum energies of calculated configurations are presented as well.

is much higher than for hydrogen and much larger than one would like, it should mean that any sublattice symmetry breaking determined with DFTB should be even more favored within DFT calculations.

7.2.2. Adsorption Energy for different Electron Doping Values

The influence of electron doping on the sublattices ordering of fluorine adsorbed graphene shall be considered. In order to investigate this the virtual crystal approach [190, 191] was chosen again. As before (see section 7.1.3) the following sublattice occupations were tested: total sublattice symmetry breaking ($^{A}/_{B} = {}^{1}/_{0}$), equal sublattice population ($^{A}/_{B} = {}^{1}/_{1}$), and intermediate ($^{A}/_{B} = {}^{3}/_{1}$). The results are presented in figures 7.12, 7.13 and 7.14 graphically while table 7.5 shows the average over the considered configurations with the maximum and minimum values of the interaction energies. For it, equation 7.1 has to modified and results in equation 7.3.

$$E_{\text{int}} = \frac{E_{\text{System}} - E_{\text{Graphene}}}{n_{\text{F}}} - \frac{1}{2}E_{F_2} \tag{7.3}$$

The first notable difference for fluorine adatoms is that already for no doping the adsorption energy minima for the intermediate and equal sublattice adsorption pattern is below zero. Therefore, the adsorption of fluorine on graphene should be favored. For the symmetry broken adsorption pattern the configuration is the lowest in energy, which has the largest distance between the adsorbed fluorines. The results for the equal and intermediate adsorption pattern show the same favoritism for an edl of +0.10 and beyond. The comparison of the graphs for hydrogen (see section 7.1.3) and fluorine also reflect the difference

Figure 7.12.: Doped Graphene with Fluorine Adatoms - Energy Distributions

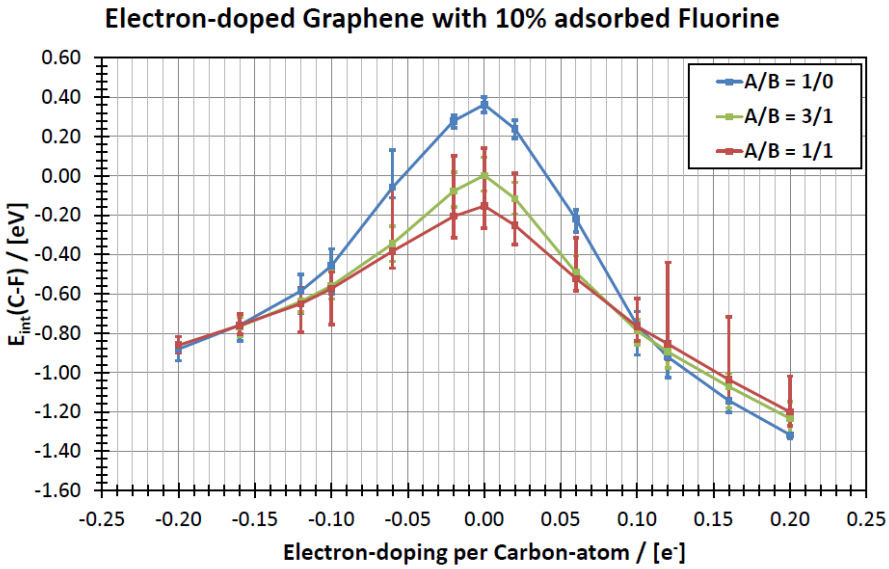

Each data point gives the average of different adsorption configurations of 20 fluorine atoms on a (10x10) graphene cell (200 carbon atoms). The error bars indicate the full (maximum to minimum) energy distribution of calculated configurations.

Figure 7.13.: Doped Graphene with Fluorine Adatoms - Energy Averages

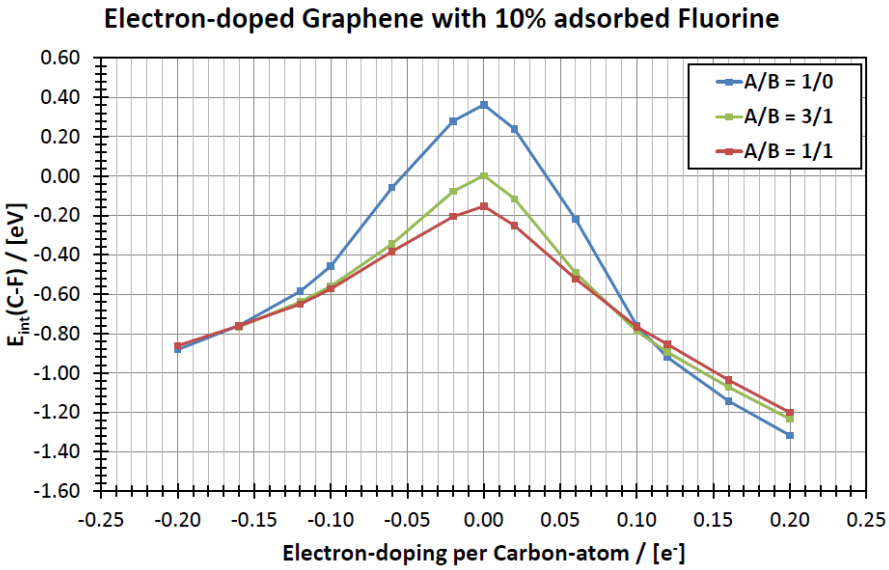

Each data point gives the average of the different adsorption configurations of 20 fluorine atoms on a (10x10) graphene cell (200 carbon atoms).

Figure 7.14.: Doped Graphene with Fluorine Adatoms - Energy Minima

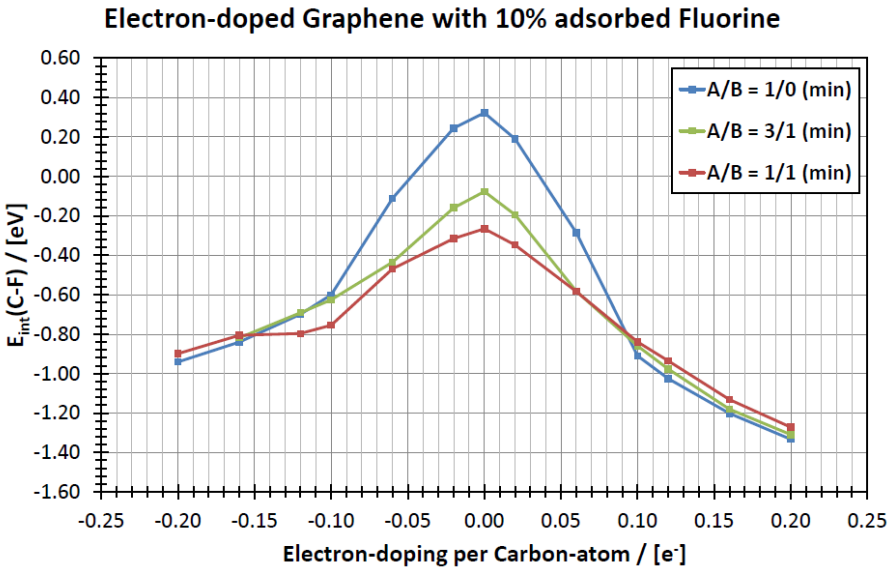

Each data point gives the energy minimum of the different adsorption configurations of 20 fluorine atoms on a (10x10) graphene cell (200 carbon atoms).

Figure 7.15.: Doped Graphene with Fluorine Adatoms - Energy Differences

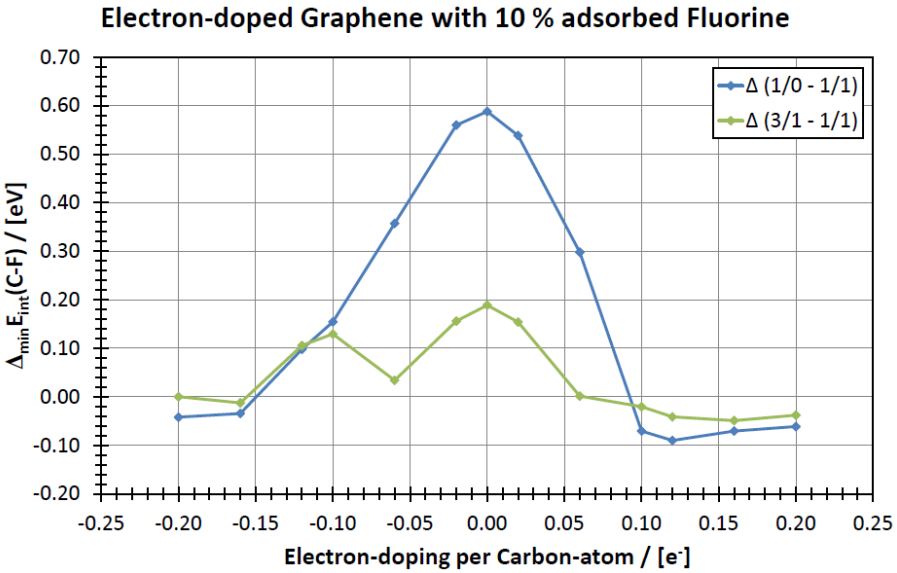

Each data point shows the difference of the energy minima of the sublattice symmetry broken adsorption patterns ($^{A}/_{B} = {}^{1}/_{0}$ and $^{A}/_{B} = {}^{3}/_{1}$) to the sublattice equally occupied pattern ($^{A}/_{B} = {}^{1}/_{1}$) for the tested electron doping levels.

in the polarization of the C-X bond (X = H or F). The fluorine prefers electron doping while hydrogen favors hole doping. Similar to the results for the hole doping with hydrogen, for fluorine with electron doping the switch between the energetic favored adsorption pattern occurs at 0.10 doping level. And as for hydrogen the present calculations do not reliably reveal a doping range, where the adsorption pattern with partial symmetry breaking is energetically favored compared to the pattern with the total symmetry breaking. For the hole doping, the tipping point lies with -0.16 edl well within the tested doping level range. Hence, the doping level dependence of the interaction is stronger for fluorine, which is represented in the higher and narrower graph for fluorine compared to the one for hydrogen.

Part IV.

Summary and Outlook

8. Boron Parametrization

Boron and its special structural behavior has been of great interest since its discovery.[53–55] Not only do several bulk phases exist and the most stable modification at ambient conditions still evades the experiment confirmation, but also nanomaterials like nanotubes and nanowires have been synthesized.[85, 86] While their exact structure is still a matter of research, their estimated electronic properties rise the hope, that they could be useful in future electronic devices as they supplement the semi-conducting carbon nanotubes by their metallic character. But also besides the pure boron structures, compounds contain boron have a wide application range: in catalytic chemistry [132], neutron capture for reactor shielding [128] or hydrogen storage materials [134, 135].

Therefore, in order to enlarge the application range of DFTB towards these kind of materials, parameters of boron for the SCC-DFTB method have been successfully developed in this thesis. These new parameters supplement the existing existing *mio*-parameters [13, 17, 19, 140] and include the B-B, B-H, B-C and B-N interactions. The range of tested compression radii for the element boron, on which DFTB relies (see chapter 3), consisted of 3150 tested combinations for the confinement radii for the density and the wave function. The radii were determined from the range of 3 to 10 and 1.5 to 3.5 times the covalent radius of boron for the density and the wave function, respectively. The compressions for the other element were taken as determined for the *mio*-parameters.

For the evaluation of the new DFTB parameters full DFT calculations have been performed on molecular and periodic systems, although the reference for the determination of the parameters were only molecules. The properties, which are taken into account, are geometries (bond/atomic distances and angles), vibrational modes, reaction energies and bandstructures. Since the parameters are constructed to supplement the existing *mio*-parameters, they are adjusted to reproduce the known overbinding of that set.

The comparison of the new parametrization to the DFT calculations displays overall a good agreement for the geometries. The deviations from the DFT reference for molecular systems are in average about 4% in terms of root mean square errors (RMS). The errors for the vibrational modes tested in these systems are higher but still acceptable when compared to the differences between various DFT functionals. The average RMS error here is about 10%. The reaction energies determined between the molecules in the test set for these parameters reveal quite a difference to the DFT calculations, when boranes are converted into carba- and dicarbaboranes. This is although the overbinding of the parameters is successfully adjusted to the target value of 10 kcal/mol.

For the periodic systems of bulk boron, pure boron sheets and nanotubes, and two out

of three boron nitride phases the geometric parameters are also in reasonable agreement with DFT results and/or literature values. The RMS here is about 5%. For the third BN phase a transition into one of the other phases occurred. The reason for this could be that these structures are layer structures. due to the compression used in DFTB, in this case the inter-layer interaction is not as high as it should be. The intra-layer interaction leads then to the transition into the other phase. For this phase also the layer-layer distance differs to the reference by 10%, while the intra-layer distances differ by only 2%. Also the electronic structures of periodic systems have been examined. While they show a reasonable agreement with the results from DFT calculations, it should be noted that due to the minimal basis deviations occur in the conduction band. Nevertheless, overall it can be concluded that the parametrization was successful.

For future work further parametrization for additional element combinations would enlarge the application range of the parameters even further. An extension of this work, boron-oxygen and boron-silicon parameters should be derived and could help to expand said application range. For the application of the presented parameters so far, there are cooperations with scientist from other universities, who look forward to use the parameters for boron nitride nanotubes (BNNT) and functionalized BNTs. Of course, additional parameters might be useful or needed depending of the functionalization considered. A possible next step is also the investigation of boron nitride layers in graphene bilayer systems or the examination of moiré supercells, which are formed from the lattice mismatch of graphene and hexagonal boron nitride.

9. Graphene with Adatoms

For the application of graphene in electronic devices and the usage of the high mobility of the charge carriers in graphene, it is a necessary goal to be able to control the opening of a band gap in the electronic structure of graphene. A means for this is the sublattice symmetry broken adsorption of covalent bonding partners like hydrogen.[185–187] But the (one-sided) adsorption of hydrogen does not lead to any kind of adsorption pattern in calculations or experiments until a concentration of 25% hydrogen. For this concentration emerges an ordered structure with benzene-like six-membered rings separated by hydrogens and an overall chemical formula of C_4H.[189] The hydrogens in this formation occupy both graphene sublattices equally in a para-type adsorption pattern and thus prevent the opening of a band gap.

In order to further the possibilities of a band gap opening in partially functionalized graphene as predicted by [185–187], DFTB calculations were preformed hydrogenated and fluorinated graphene. The applicability of the DFTB parameters of the *mio-* and *pbc-*SKF-sets[140], for the hydrogenated and fluorinated case, respectively, were confirmed by comparison to full DFT calculations (sections 7.1.1 and 7.2.1). The calculations showed very good agreement for the relative energies of closely adsorbed pairs of hydrogens. In case of fluorine, the agreement is not quite as good since the adsorption on the same sublattice is even less favorable in DFTB than it is in DFT already. While this result could prevent the observation of sublattice symmetry breaking, it could also mean, that with the occurrence of sublattice symmetry breaking, the extend of favoritism is higher than the results suggest. In other words, no sublattice symmetry breaking in the results does not mean, it does not occur, but if the results show sublattice symmetry breaking than it really should occur.

About 100 calculations have been performed for different adsorbate concentrations of hydrogen (in the range from 10 to 50% coverage) (see section 7.1.2). Within these, three adsorption pattern were tested: The one-sided, total symmetry broken "A only" or "A/B = 1/0", the one-sided, equal distribution between both sublattices "AB one-sided" or "A/B = 1/1" and the sublattice side determining adsorption "A top, B down" or "A/B = 1/-1". Of these three, the "A/B = 1/-1" is the most favorable since its leads to the formation of graphane and has the least hydrogen-hydrogen repulsion and the least formation of traps for unpaired electrons. The "A/B = 1/1" pattern has to cope with hydrogen-hydrogen repulsion while the formation of "radical traps" is still less of a problem. At about 25% adsorbate concentration the energy dependence flattens, which is a hint that here the hydrogen-hydrogen repulsion becomes dominant. For the "A/B = 1/0" the lack of possibility for the reformation of π-bond is the most important aspect. This results in an

increase of the energy with the concentration of adsorbates. Overall these results confirm the results from [185], [187] and [189] and show that adsorbate concentration modification is not enough in order to achieve sublattice symmetry breaking.

More than 2000 calculations, which were performed using the virtual crystal approach (VCA) [190, 191] in order to evaluate charge doping effects, revealed the possibility to break the sublattice symmetry when hydrogen or fluorine are adsorbed to graphene (sections 7.1.3 and 7.2.2, respectively). The concentration of the adsorbate was fixed to 10% for all these calculations as this concentration is sufficiently below the determined maximum 25% of Haberer et. al.[189] and high enough that the impurities could effect each other. For the adsorption three one-sided pattern were considered with different sublattice occupancies: A/B = 1/0, A/B = 3/1 and A/B = 1/1. Only the one-sided adsorption was allowed since the experimental set-up for the charge doping could be the intercalation of transition or alkali metals between graphene and the substrate. That would leave only one side of the graphene open for the adsorption of hydrogen or fluorine. Based on the polarization of the bond formed between the adatom and the graphene, the preferred type of doping changes: electron-doping for more electron-negative adsorbates (fluorine) and hole-doping for more electron-positive (hydrogen). From the contrasting juxtaposition of the results for the tested adatom concentration of 10%, it can be seen that fluorine and hydrogen are able to switch from an equal distributed adsorption pattern to a symmetry broken one, if the doping level surpasses +0.10 and -0.10 electrons, respectively. For these values the number of electrons in the systems resembles the one of pristine graphene with all hydrogens being H^+ or all fluorines being F^-, respectively. Since the ionic interaction of such charged species is neglected by using the VCA, the situation might be viewed as the adsorption of a noble gas on pristine graphene.

The results clearly show, that according to the preformed calculations the formation of sublattice symmetry broken adsorption patterns of hydrogen and fluorine on graphene should be possible if the graphene can be charge doped to a certain extend.

For the continuation of this work, the question if the realization of the sublattice symmetry breaking is possible at ambient condition, could be examined by molecular dynamic simulations. Also other adatom concentrations should be considered, since the necessary doping might not be the same, if the adsorbate concentration is varied. A lesser extend of doping might be easier to achieve by experimentalists, although the intercalation allows doping of graphene to a large extend. Even more complex adsorbates like OH or alkyl groups might be interesting. An adsorbate, which adsorbs at two sites at once and at the same time bridges the distance between two positions of one sublattice, could even make less doping necessary.

10. Thanks

... what else could I say? My deepest gratitude goes to

Thomas Frauenheim for giving me the chance to work at the BCCMS and being the first examiner of this thesis

Thomas Niehaus for giving me the chance to work at the BCCMS and all his invaluable advice

Tim Wehling for introducing me to the Graphene topic and being the second examiner of this thesis

Balint Aradi for all the scientific and technical support and the remarks on this work

Christof Köhler for all the scientific and technical support

Volker Weiß for all the scientific support and being the fellow you are

all members of the BCCMS - former and today - for the pleasant atmosphere, all the help you provided and the great time I had among you

my parents without your help, support and faith I would not be here

my dear Yvonne for always being at my side

Bibliography

[1] Jones, R. O.; Gunnarsson, O. *Rev. Mod. Phys.* **1989**, *64*, 689.

[2] Dreizler, R. M.; Gross, E. K. U. *Density Functional Theory*; Springer: Berlin and Heidelberg, 1990.

[3] Gross, E. K. U.; Dreizler, R. M. In *Density Functional Theory*; Fiolhais, C., Nogueira, F., Marques, M., Eds.; Plenum Press: New York and London, 1994.

[4] Kohn, W. In *Density Functional Theory*; Fiolhais, C., Nogueira, F., Marques, M., Eds.; Plenum Press: New York and London, 1994; Chapter Overview of Density Functional Theory, pp 3–10.

[5] Kohn, W. *Rev. Mod. Phys.* **1999**, *71*, 1253.

[6] Sternberg, M. The Atomic Structure of Diamond Surfaces and Interfaces. Ph.D. thesis, University Paderborn, 2001.

[7] Frauenheim, T.; Seifert, G.; Elsterner, M.; Hajnal, Z.; Jungnickel, G.; Porezag, D.; Suhai, S.; Scholz, R. *Physica Status Solidi (b)* **2000**, *217*, 41–62.

[8] Frauenheim, T.; Seifert, G.; Elstner, M.; Niehaus, T. A.; Koehler, C.; Amkreutz, M.; Sternberg, M.; Hajnal, Z.; Di Carlo, A.; Suhai, S. *J. Phys. Condens. Mater.* **2002**, *14*, 3015.

[9] Seifert, G. *J. Phys. Chem. A* **2007**, *111*, 5609.

[10] Seifert, G.; Eschrig, H.; Bieger, W. *Z. Phys. Chem.* **1986**, *267*, 529.

[11] Porezag, D.; Frauenheim, T.; Koehler, T.; Seifert, G.; Kaschner, R. *Phys. Rev. B* **1995**, *51*, 12947–12957.

[12] Porezag, D. Development of ab-initio and approximate density functional methods and their application to complex fullerene systems. Ph.D. thesis, Technische Universitaet Chemnitz-Zwickau, 1997.

[13] Elstner, M.; Porezag, D.; Jungnickel, G.; Elsner, J.; Haugk, M.; Frauenheim, T.; Suhai, S.; Seifert, G. *Phys. Rev. B* **1998**, *58*, 7260–7268.

[14] Elstner, M. Weiterentwicklung quantenmechanischer Rechenverfahren fuer organische Molekuele und Polymere. Ph.D. thesis, Universitaet Gesamthochschule Paderborn, 1998.

[15] Elstner, M.; Jalkanen, K. J.; Knapp-Mohammady, M.; Frauenheim, T.; Suhai, S. *Chemical Physics* **2001**, *263*, 203 – 219.

[16] Elstner, M.; Hobza, P.; Frauenheim, T.; Suhai, S.; Kaxiras, E. *The Journal of Chemical Physics* **2001**, *114*, 5149–5155.

[17] Niehaus, T. A.; Elstner, M.; Frauenheim, T.; Suhai, S. *Journal of Molecular Structure: THEOCHEM* **2001**, *541*, 185 – 194.

[18] Kruger, T.; Elstner, M.; Schiffels, P.; Frauenheim, T. *The Journal of Chemical Physics* **2005**, *122*, 114110.

[19] Koehler, C.; Seifert, G.; Frauenheim, T. *Chem. Phys.* **2005**, 309.

[20] Elstner, M. *The Journal of Physical Chemistry A* **2007**, *111*, 5614–5621.

[21] Knaup, J. M.; Hourahine, B.; Frauenheim, T. *The Journal of Physical Chemistry A* **2007**, *111*, 5637–5641, PMID: 17428042.

[22] Moreira, N. H.; Dolgonos, G.; Aradi, B.; da Rosa, A. L.; Frauenheim, T. *Journal of Chemical Theory and Computation* **2009**, *5*, 605–614.

[23] Dolgonos, G.; Aradi, B.; Moreira, N. H.; Frauenheim, T. *Journal of Chemical Theory and Computation* **2010**, *6*, 266–278.

[24] Moreira, N. H.; Aradi, B.; Rosa, A. L. d.; Frauenheim, T. *The Journal of Physical Chemistry C* **2010**, *114*, 18860–18865.

[25] Bodrog, Z.; Aradi, B.; Frauenheim, T. *Journal of Chemical Theory and Computation* **2011**, *7*, 2654–2664.

[26] Gaus, M.; Cui, Q.; Elstner, M. *Journal of Chemical Theory and Computation* **2011**, *7*, 931–948.

[27] Hehre, W. J.; Radom, L.; von Rague Schleyer, P.; Pople, J. A. *Ab Initio Molecular Orbital Theory*; John Wiley & Sons: New York, 1985.

[28] Schroedinger, E. *Ann. Phys. (Leipzig) (IV)* **1926**, *79*, 361.

[29] Hartree, D. R. *Proc. Cambr. Phil. Soc.* **1928**, *24*, 89.

[30] Fock, V. *Z. f. Physik* **1930**, *61*, 126.

[31] Roothaan, C. C. J. *Rev. Mod. Phys.* **1951**, *23*, 69.

[32] Hohenberg, P.; Kohn, W. *Phys. Rev.* **1964**, *136*, B864.

[33] Thomas, L. H. *Proc. Cambr. Phil. Soc.* **1927**, *23*, 542.

[34] Fermi, E. *Rend. Lincei* **1927**, *6*, 602.

[35] Lieb, E. H. *Rev. Mod. Phys.* **1981**, *53*, 603.

[36] Kohn, W. Highlights of condensed-matter theory. 1985.

[37] Davydov, A. S. *Quantum mechanics*; Pergamon Press: Oxford, 1976.

[38] Levy, M. *Phys. Rev. A* **1982**, *26*, 1200.

[39] Lieb, E. H. *Int. J. Quantum Chem.* **1983**, *24*, 243.

[40] Kohn, W.; Sham, L. J. *Phys. Rev.* **1965**, *140*, A1133.

[41] Janak, J. F. *Phys. Rev. B* **1978**, *18*, 7165.

[42] Perdew, J. P.; Kurth, S. In *Density Functionals: Theory and Applications*; Joubert, D., Ed.; Springer: Berlin, 1998; Chapter Density functionals for non-relativistic Coulomb systems, pp 8–59.

[43] Perdew, J. P.; Parr, R. G.; Levy, M.; Balduz, J. L. *Phys. Rev. Lett.* **1982**, *49*, 1691–1694.

[44] Perdew, J. P.; Levy, M. *Phys. Rev. B* **1997**, *56*, 16021–16028.

[45] Almbladh, C. O.; von Barth, U. *Phys. Rev. B* **1985**, *31*, 3231.

[46] Harris, J. *Phys. Rev. B* **1985**, *31*, 1770.

[47] Foulkes, W. M. C.; Haydock, R. *Phys. Rev. B* **1989**, *39*, 12520.

[48] Scholz, M.; Koehler, H.-J. *Quantenchemische Naeherungsverfahren und ihre Anwendung in der organischen Chemie*; Deutscher Verlag der Wissenschaften: Berlin, 1981.

[49] Ohno, K. *Theoret. chim. Acta (Berlin)* **1964**, *2*, 219.

[50] Klopman, G. *J. Am. Chem. Soc.* **1964**, *86*, 4550.

[51] Aradi, B.; Hourahine, B.; Frauenheim, T. *The Journal of Physical Chemistry A* **2007**, *111*, 5678–5684, PMID: 17567110.

[52] Holleman, A. F.; Wiberg, E. *Lehrbuch der Anorganischen Chemie*, 101st ed.; de Gruyter: Berlin, 1995.

[53] Smith, H. W.; Lipscomb, W. N. *The Journal of Chemical Physics* **1965**, *43*, 1060–1064.

[54] Nordman, C. E.; Lipscomb, W. N. *The Journal of Chemical Physics* **1953**, *21*, 1856–1864.

[55] Dulmage, W.; Lipscomb, W. *Acta Crystallogr.* **1952**, *5*, 260.

[56] Riedel, E.; Janiak, C. *Anorganische Chemie*, 5th ed.; Walter de Gruyter: Berlin, New York, 2002.

[57] Anane, H.; Boutalib, A.; Nebot-Gil, I.; Tomas, F. *The Journal of Physical Chemistry A* **1998**, *102*, 7070–7073.

[58] Loschen, C.; Voigt, K.; Frunzke, J.; Diefenbach, A.; Diedenhofen, M.; Frenking, G. *Z. Anorg. Allg. Chem.* **2002**, *628*, 1294.

[59] Foerster, D. Elektronendichteuntersuchengen an Boranen, Boraten und Boranaten zur Analyse von Zwei-Elektronen-Drei-Zentren-Bindungen und Lewis-Saeure-Basen-Wechselwirkungen. Ph.D. thesis, Freie UniversitÃt Berlin, 2008.

[60] Oganov, A. R.; Chen, J.; Gatti, C.; Ma, Y.; Ma, Y.; Glass, C. W.; Liu, Z.; Yu, T.; Kurakevych, O. O.; Solozhenko, V. L. *Nature* **2009**, *457*, 863.

[61] Douglas, B. E.; Ho, S.-M. *Structure and Chemistry of Crystalline Solids*; Springer: Heidelberg, 2006.

[62] Chase, M. W. J. *J. Phys. Chem. Ref. Data* **1998**, *9*.

[63] Will, G.; Kiefer, B. *ZAAC* **2001**, *627*, 2100–2104.

[64] Lee, S.; Bylander, D. M.; Kleinman, L. *Phys. Rev. B* **1990**, *42*, 1316–1320.

[65] Slack, G. A.; Hejna, C. I.; Garbauskas, M. F.; Kasper, J. S. *J. Solid State Chem.* **1988**, *76*, 52.

[66] Vlasse, M.; Naslain, R.; Kasper, J. S.; Ploog, K. *J. Solid State Chem.* **1979**, *28*, 289.

[67] Wentorf, R. H. *Science* **1965**, *147*, 49.

[68] Masago, S. K., A.; Katayama-Yoshida, H. *Phys. Rev. B* **2006**, *73*, 104102.

[69] van Setten, M. J.; Uijttewaal, M. A.; de Wijs, G. A.; de Groot, R. A. *J. Am. Chem. Soc.* **2007**, *129*, 2458–2465.

[70] Sanz, D. N.; Loubeyre, P.; Mezouar, M. *Phys. Rev. Lett.* **2002**, *89*, 245501.

[71] Haeussermann, U.; Simak, S. I.; Ahuja, R.; Johansson, B. *Phys. Rev. Lett.* **2003**, *90*, 065701.

[72] Eremets, M. I.; Struzhkin, V. W.; Mao, H. K.; Hemley, R. J. *Science* **2001**, *293*, 272–274.

[73] Boustani, I. *J. Solid State Chem.* **1997**, *133*, 182.

[74] Boustani, I.; Quandt, A. *Europhys. Lett.* **1997**, *39*, 527.

[75] Zhai, H.-J.; Kiran, B.; Li, J.; Wang, L.-S. *Nat. Mater.* **2003**, *2*, 827.

[76] Oger, E.; Crawford, N.; Kelting, R.; Weis, P.; Kappes, M.; R., A. *Angew. Chem. Int. Ed.* **2007**, *46*, 8503.

[77] Boustani, I. *Surf. Sci.* **1997**, *370*, 355.

[78] Szwacki, N. G.; Sadrzadeh, A.; Yakobson, B. I. *Phys. Rev. Lett.* **2007**, *98*, 166804.

[79] Boustani, I.; Quandt, A.; Hernadez, E.; Rubio, A. *J. Chem. Phys.* **1999**, *110*, 3176.

[80] Yang, X.; Ding, Y.; Ni, J. *Phys. Rev. B* **2008**, *77*, 041402(R)–1.

[81] Lau, K. C.; Pati, R.; Pandey, R.; Pineda, A. C. *Chem. Phys. Lett.* **2006**, *418*, 549.

[82] Tang, H.; Ismail-Beigi, S. *Phys. Rev. Lett.* **2007**, *99*, 115501–1.

[83] Singh, A.; Sadrzadeh, A.; Yakobson, B. *Nano. Lett.* **2008**, *8*, 1314.

[84] Kunstmann, J.; Quandt, A. *Phys. Rev. B* **2006**, *74*, 035413–1.

[85] Ciuparu, D.; Klie, R. F.; Zhu, Y.; Pfefferle, L. *J. Phys. Chem. B* **2004**, *108*, 3967.

[86] Liu, J.; Iqbal, Z. *MRS Online Proc. Lib.* **2011**, *1307*, mrsf10–1307–cc05–21.

[87] Liu, F.; Shen, C.; Su, Z.; Ding, X.; Deng, S.; Chen, J.; Xu, N.; Gao, H. *J. Mater. Chem.* **2010**, *20*, 2197.

[88] Bezugly, V.; Kunstmann, J.; Grundkoetter-Stock, B.; Frauenheim, T.; Niehaus, T.; Cuniberti, G. *ACS Nano* **2011**, *5*, 4997–5005.

[89] Lau, K. C.; Pandey, R. *J. Phys. Chem. B* **2008**, *112*, 10217–10220.

[90] Szwacki, N. G.; Tymczak, C. J. *Chem. Phys. Lett.* **2010**, *494*, 80–83.

[91] Tang, H.; Ismail-Beigi, S. *Phys. Rev. B* **2010**, *82*, 115412–1–20.

[92] He, H.; Pandey, R.; Boustani, I.; Karna, S. P. *J. Phys. Chem. C* **2010**, *114*, 4149–4152.

[93] Li, G. Q. *Appl. Phys. Lett.* **2009**, *94*, 193116–1–3.

[94] Li, G. Q. *Chin. Phys. B* **2010**, *19*, 017201–1–5.

[95] Lau, K. C.; Pandey, R.; Pati, R.; Karna, S. P. *Appl. Phys. Lett.* **2006**, *88*, 212111–1–3.

[96] Guo, W.; Hu, Y.-B.; Zhang, Y.-Y.; Du, S.-X.; Gao, H.-J. *Chin. Phys. B* **2009**, *18*, 2502–2506.

[97] Longuet-Higgins, H.; Bell, R. *Journal of the Chemical Society* **1943**, 250.

[98] Huebschle, C.; Messerschmidt, M.; Lentz, D.; Luger, P. *Z. Allg. Anorg. Chem.* **2004**, *630*, 1313.

[99] Laszlo, P. *Angew. Chem. Int. Ed.* **2000**, *39*, 2071.

[100] Casanova, J. *The Borane, Carborane, Carbocation Continuum*; Wiley: New York, 1998.

[101] Lipscomb, W. *Boron Hydrides*; W. A. Benjamin Inc.: New York, 1963.

[102] Wade, K. *Adv. Inorg. Radiochem.* **1971**, *18*, 1.

[103] Wade, K. *J. Chem. Soc., Chem. Comm.* **1971**, 792.

[104] Williams, R. E. *Chem. Rev.* **1992**, *92*, 177.

[105] Morrison, J. A. *Chem. Rev.* **1991**, *91*, 35.

[106] Stone, A. *J. Mol. Phys.* **1980**, *41*, 1339.

[107] Stone, A. *J. Inorg. Chem.* **1981**, *20*, 563.

[108] Jemmis, E. D. *J. Am. Chem. Soc.* **1982**, *104*, 7017.

[109] King, R. P.; Rouvray, D. H. *J. Am. Chem. Soc.* **1977**, *99*, 7834.

[110] King, B. *Chem. Rev.* **2001**, *101*, 1119.

[111] Chen, Z.; King, B. *Chem. Rev.* **2005**, *105*, 3613.

[112] Pauling, L. *Die Natur der chemischen Bindung*; Verlag der Chemie: Weinheim, 1976.

[113] Guryanova, E. N.; Goldstein, I. P.; Romm, I. P. *The Donor-Acceptor Bond*; Wiley: New York, 1975.

[114] Pearson, R. G., Ed. *Hard and Soft Acids and Bases*; Dowden, Hutchinson and Ross: Stroudsburg, PA, USA, 1973.

[115] Gutman, V. *The Donor-Acceptor Approach to Molecular Interactions*; Plenum: New York, 1978.

[116] Lewis, N. G. *Valence and Structure of Atoms and Molecules*; The Chemical Catalog Co., Inc.: New York, 1923.

[117] Pearson, R. G. *J. Am. Chem. Soc.* **1963**, *85*, 3533.

[118] Pearson, R. G.; Songstad, J. *J. Am. Chem. Soc.* **1967**, *89*, 1827.

[119] Jonas, V.; Frenking, G.; Reetz, M. T. *J. Am. Chem. Soc.* **1994**, *116*, 8741.

[120] Haaland, A. *Angew. Chem.* **1989**, *101*, 1017.

[121] Buhl, M.; Steinke, T.; Schleyer, P. V. R.; Boese, R. *Angew. Chem.* **1991**, *103*, 1179.

[122] Geller, S.; Hoard, J. *Acta Crystallogr.* **1951**, *4*, 399.

[123] Hoard, J.; Geller, S.; Owen, T. B. *Acta Crystallogr.* **1951**, *4*, 405.

[124] Hargittai, M.; Hargiitai, I. *J. Mol. Struc.* **1977**, *39*, 79.

[125] Clippard, P. H.; Hanson, J. C.; Taylor, R. C. *J. Cryst. Mol. Struc.* **1971**, *1*, 363.

[126] Hess, H. *Acta Crystallogr. B* **1969**, *25*, 2338.

[127] Burns, W. A.; Leopold, K. R. *J. Am. Chem. Soc.* **1993**, *115*, 11622.

[128] Martin, J. E. *Physics of Radiation Protection: A Handbook*; Wiley, 2008.

[129] May, G. S.; Spanos, C. J. *Fundamentals of semiconductor manufacturing and process control*; Wiley and Sons: New York, 2006.

[130] Gogotsi, Y. G.; Andrievski, R. A. *Materials Science of Carbides, Nitrides and Borides*; Springer: Berlin, 1999.

[131] Pfaender, H. G. *Schott guide to glass*; Springer: Berlin, 1996.

[132] Jacob III, P.; C., B. H. *J. Org. Chem.* **1977**, *42*, 579.

[133] Miyaura, N.; Yamada, K.; Suzuki, A. *Tetrahedron Letters* **1979**, *36*, 3437.

[134] Sutton, A. D.; Burrell, A. K.; Dixon, D. A.; Garner III, E. B.; Gordon, J. C.; Nakagawa, T.; Ott, K. C.; Robinson, J. P.; Vasiliu, M. *Science* **2011**, *331*, 1426.

[135] Moury, R.; Moussa, G.; Demirci, U. B.; Hannauer, J.; Bernard, S.; Petit, E.; Lee, A. v. d.; Miele, P. *Phys. Chem. Chem. Phys.* **2012**, *14*, 1768.

[136] Grundkoetter-Stock, B.; Bezugly, V.; Kunstmann, J.; Cuniberti, G.; Frauenheim, T.; Niehaus, T. A. *Journal of Chemical Theory and Computation* **2012**, *8*, 1153–1163.

[137] Becke, A. D. *J. Chem. Phys.* **1993**, *98*, 5648–5652.

[138] Stephens, P. J.; Devlin, F. J.; Chabalowski, C. F.; Frisch, M. J. *J. Phys. Chem.* **1994**, *98*, 11623–11627.

[139] Frisch, M. J. et al. Gaussian 03, Revision C.02. Gaussian, Inc., Wallingford, CT, 2004.

[140] dftb.org, (accessed Feb. 2012); http://www.dftb.org/parameters/download/mio.

[141] Perdew, J. P.; Burke, K.; Ernzerhof, M. *Phys. Rev. Lett.* **1996**, *77*, 3865–3868.

[142] Dewar, M. J. S.; Zoebisch, E. G.; Healy, E. F.; Stewart, J. J. P. *J. Am. Chem. Soc.* **1985**, *107*, 3902.

[143] Dewar, M.; Thiel, W. *J. Am. Chem. Soc.* **1977**, *99*, 4899.

[144] Frenzel, J.; Oliveira, A. F.; Jardillier, N.; Heine, T.; Seifert, G. Semi-relativistic, self-consistent charge Slater-Koster tables for densityfunctional based tight-binding (DFTB) for materials science simulations. TU-Dresden: Dresden, Germany, 2004.

[145] McKee, M. L.; Wang, Z.-X.; von Rague Schleyer, P. *J. Am. Chem. Soc.* **2000**, *122*, 4781.

[146] Kresse, G.; Joubert, D. *Phys. Rev. B* **1999**, *59*, 1758–1775.

[147] Kresse, G.; Furthmueller, J. *Phys. Rev. B* **1996**, *54*, 11169–11186.

[148] Paier, J.; Marsman, M.; Kresse, G. *J. Chem. Phys.* **2007**, *127*, 024103–1–0.

[149] Horn, F. H.; Taft, E. A.; Oliver, D. W. In *Boron*; Gaule, O. K., Ed.; Plenum Press: New York, 1965; Vol. 2; p 231.

[150] Golikova, O. A.; Solovev, N. E.; Ugai, Y.; Feigelman, V. A. *Sov. Phys. Semicond.* **1979**, *13*, 486, (English Transl.).

[151] Golikova, O. A.; Solovev, N. E.; Ugai, Y.; Feigelman, V. A. *Fiz. Tekh. Poluprovodn.* **1979**, *13*, 825.

[152] Werheit, H.; Kuhlmann, U.; Solovev, N. E.; Tsiskarishvili, G. P.; Tsagareishvili, G. 1991.

[153] Valiev, M.; Bylaska, E.; Govind, N.; Kowalski, K.; Straatsma, T.; Dam, H. V.; Wang, D.; Nieplocha, J.; Apra, E.; Windus, T.; de Jong, W. *Computer Physics Communications* **2010**, *181*, 1477 – 1489.

[154] Krishnan, R.; Binkley, J. S.; Seeger, R.; Pople, J. A. *J. Chem. Phys.* **1980**, *72*, 650.

[155] Clark, T.; Chandrasekhar, J.; Spitznagel, G. W.; Schleyer, P. V. R. *J. Comp. Chem.* **1983**, *4*, 294.

[156] bse.pnl.gov, (accessed Feb. 2013); https://bse.pnl.gov/bse.

[157] Park, K. T.; Terakura, K.; Hamada, N. *J. Phys. C: Solid State Phys.* **1987**, *20*, 1241–1251.

[158] Landolt, H. H.; Boernstein, R. In *Landolt-Boernstein New Series: Physics of Group IV Elements and III-V Compunds*; Madlung, O., Ed.; Springer: Berlin, 1982.

[159] elk.sourceforge.net, (accessed Mar. 2013); http://elk.sourceforge.net.

[160] Pauling, L. *The Nature of the Chemical Bond*; Cornell University Press: Ithaca, NY, 1960.

[161] Curl, R. F. *Rev. Mod. Phys.* **1997**, *69*, 691.

[162] Kroto, H. *Rev. Mod. Phys.* **1997**, *69*, 703.

[163] Smalley, R. E. *Rev. Mod. Phys.* **1997**, *69*, 723.

[164] Iijima, S. *Nature* **1991**, *354*, 56.

[165] Novoselov, K. S. *Nature* **2005**, *438*, 197.

[166] Zhang, Y. *Nature* **2005**, *438*, 201.

[167] Novoselov, K. S. *Science* **2004**, *306*, 666.

[168] Novoselov, K. S. *Proc. Natl. Acad. Sci. USA* **2005**, *102*, 10451.

[169] Katnelson, M. I. *materials today* **2007**, *10*, 20.

[170] Peierls, R. E. *Helv. Phys. Acta* **1934**, *7*, 81.

[171] Peierls, R. E. *Ann. Inst. H. Poincare* **1935**, *5*, 177.

[172] Landau, L. D. *Phys. Z. Sowjet Union* **1937**, *11*, 26.

[173] Landau, L. D.; Lifshitz, E. M. *Statistical Physics, Part 1*; Pergamon: Oxford, USA, 1980.

[174] Dresselhaus, M. S.; Dresselhaus, G. *Adv. Phys.* **2002**, *51*, 1.

[175] Shioyama, H. *J. Mater. Sci. Lett.* **2001**, *20*, 499.

[176] Viculis, L. M. *Science* **2003**, *299*, 1361.

[177] Horiuchi, S. *Appl. Phys. Lett.* **2004**, *84*, 2403.

[178] Stankovich, S. *J. Mater. Chem.* **2006**, *16*, 155.

[179] Berger, C. *J. Phys. Chem. B* **2004**, *108*, 19912.

[180] Wallace, P. R. *Phys. Rev.* **1947**, *71*, 622.

[181] Semenoff, G. W. *Phys. Rev. Lett.* **1984**, *53*, 2449.

[182] Haldane, F. D. M. *Phys. Rev. Lett.* **1988**, *61*, 2015.

[183] Katnelson, M. I. *Nat. Phys.* **2006**, *2*, 620.

[184] Schulz, a. Chemisch funktionalisiertes Graphen. M.Sc. thesis, Universitaet Bremen, 2012.

[185] Shytov, A. V.; Abanin, D. A.; Levitov, L. S. *Phys. Rev. Lett.* **2009**, *103*, 016806.

[186] Abanin, D. A.; Shytov, A. V.; Levitov, L. S. *Phys. Rev. Lett.* **2010**, *105*, 086802.

[187] Cheianov, V. V.; Syljuasen, O.; Altshuler, B. L.; Fal'ko, V. I. *EPL (Europhysics Letters)* **2010**, *89*, 56003.

[188] Boukhvalov, D. W.; Katnelson, M. I.; Lichtenstein, A. I. *Phys. Rev. B* **2008**, *77*, 035427.

[189] Haberer, D. et al. *Advanced Materials* **2011**, *23*, 4463–4463.

[190] Freysoldt, C.; Neugebauer, J.; Van de Walle, C. G. *Phys. Rev. Lett.* **2009**, *102*, 016402.

[191] Makov, G.; Payne, M. C. *Phys. Rev. B* **1995**, *51*, 4014–4022.

Part V.

Appendix

List of Figures

List of Tables

A. Example Input Files

A.1. Gaussian 2003

Input example for a DFT-B3LYP / 6-31G(d) calculation of B_2H_6 in xyz-format; for a PBE/LDA calculation "b3lyp" was replaced by "pbepbe"/"lsda"

%nproc=1

#P Opt b3lyp/6-31G(d) freq

diborane(6)

0 1

B 0.891419 0.000000 -0.000000

B -0.891419 0.000000 -0.000000

H -1.465290 -1.036950 0.000000

H -1.465290 1.036950 0.000000

H 1.465290 -1.036950 -0.000000

H 1.465290 1.036950 -0.000000

H 0.000000 -0.000000 0.977035

H 0.000000 -0.000000 -0.977035

A.2. MoPac 7.01 (AM1 and MNDO)

Input example for a MNDO calculation of B_2H_6 in xyz-format; for an AM1 calculation "MNDO" was replaced by "AM1"

MNDO VECTORS LOCAL PI force

B2H6

B -0.88521900 1 0.00000000 1 0.00000000 1

B 0.88521900 1 0.00000000 1 0.00000000 1

H 1.46217200 1 1.04183600 1 0.00000000 1

H 1.46217200 1 -1.04183600 1 0.00000000 1

H -1.46217200 1 1.04183600 1 0.00000000 1

H -1.46217200 1 -1.04183600 1 0.00000000 1

H 0.00000000 1 0.00000000 1 0.97569600 1

H 0.00000000 1 0.00000000 1 -0.97569600 1

A.3. DFTB+ 1.0 and 1.2

Input example from the dftb_pin.hsd for a geometry optimization of $B_{12}H_{12}^{2-}$

Geometry = GenFormat {

24 C

B H

1 1 0.00000000 0.89341100 1.44556900

2 1 -1.44556900 0.00000000 0.89341100

3 1 -1.44556900 0.00000000 -0.89341100

4 1 -0.89341100 -1.44556900 0.00000000

5 1 0.89341100 -1.44556900 0.00000000

6 1 1.44556900 0.00000000 -0.89341100

7 1 1.44556900 0.00000000 0.89341100

8 1 0.89341100 1.44556900 0.00000000

9 1 -0.89341100 1.44556900 0.00000000

10 1 0.00000000 0.89341100 -1.44556900

11 1 0.00000000 -0.89341100 -1.44556900

12 1 0.00000000 -0.89341100 1.44556900

13 2 -1.52826700 -2.47278800 0.00000000

14 2 1.52826700 2.47278800 0.00000000

15 2 -1.52826700 2.47278800 0.00000000

16 2 1.52826700 -2.47278800 0.00000000

17 2 -2.47278800 0.00000000 -1.52826700

18 2 2.47278800 0.00000000 1.52826700

19 2 0.00000000 -1.52826700 -2.47278800

20 2 0.00000000 1.52826700 2.47278800

21 2 2.47278800 0.00000000 -1.52826700

22 2 -2.47278800 0.00000000 1.52826700

```
23 2 0.00000000 -1.52826700 2.47278800
24 2 0.00000000 1.52826700 -2.47278800
}
Driver = ConjugateGradient {
MovedAtoms = Range { 1 -1 }
MaxForceComponent = 1.0e-4
MaxSteps = 100
OutputPrefix = "geom.out"
AppendGeometries = No
Constraints = {}
}
Hamiltonian = DFTB {
SCC = Yes
SCCTolerance = 1.0e-5
MaxSCCIterations = 1000
Mixer = Broyden {
MixingParameter = 0.2
CachedIterations = -1
InverseJacobiWeight = 1.000000000000000E-002
MinimalWeight = 1.00000000000000
MaximalWeight = 100000.000000000
WeightFactor = 1.000000000000000E-002
}
SlaterKosterFiles = {
H-H = "./H-H.skf"
B-H = "./B-H.skf"
H-B = "./H-B.skf"
B-B = "./B-B.skf"
}
MaxAngularMomentum = {
B = "p"
H = "s"
```

```
}
Charge = -2.0
SpinPolarisation = {}
Filling = Fermi {
Temperature = 1.000000000000000E-008
}
ElectricField = {}
OrbitalResolvedSCC = No
ReadInitialCharges = No
Eigensolver = DivideAndConquer {}
OldSKInterpolation = No
OrbitalPotential = {}
Dispersion = {}
}
Options = {
WriteEigenvectors = No
WriteAutotestTag = No
WriteDetailedXML = No
WriteResultsTag = No
WriteDetailedOut = Yes
WriteBandOut = Yes
AtomResolvedEnergies = No
RestartFrequency = 20
RandomSeed = 0
}
ParserOptions = {
ParserVersion = 3
WriteHSDInput = Yes
WriteXMLInput = No
StopAfterParsing = No
}
```

A.4. NWChem 5.1 and 6.1

Input example for a DFT-B3LYP / 6-311++G** calculation of $ortho - C_2B_{10}H_{12}$; for a PBE/LDA calculation "XC b3lyp" was replaced by "XC pbe0"/"XC slater vwn_5"

```
start C2B10H12o
title "C2B10H12o B3LYP geometry optimization"
geometry
C 0.000000 0.811566 1.313761
C -1.452297 -0.010390 0.881206
B -1.456228 -0.001871 -0.902741
B -0.900011 -1.457730 -0.002535
B 0.900011 -1.457730 -0.002535
B 1.456228 -0.001871 -0.902741
B 1.452297 -0.010390 0.881206
B 0.897565 1.442041 -0.017367
B -0.897565 1.442041 -0.017367
B 0.000000 0.898570 -1.458632
B 0.000000 -0.898293 -1.453329
B 0.000000 -0.907661 1.436558
H -1.532342 -2.466963 0.018998
H 1.482483 2.467757 0.112499
H -1.482483 2.467757 0.112499
H 1.532342 -2.466963 0.018998
H -2.478988 0.011894 -1.513172
H 2.398613 0.069507 1.594732
H 0.000000 -1.524847 -2.467159
H 0.000000 1.380533 2.233339
H 2.478988 0.011894 -1.513172
H -2.398613 0.069507 1.594732
H 0.000000 -1.413089 2.511521
H 0.000000 1.544730 -2.459301
end
BASIS "ao basis" PRINT
```

#BASIS SET: (6s,1p) -> [4s,1p]

H S

33.8650000 0.0254938

5.0947900 0.1903730

1.1587900 0.8521610

H S

0.3258400 1.0000000

H S

0.1027410 1.0000000

H S

0.0360000 1.0000000

H P

0.7500000 1.0000000

#BASIS SET: (12s,6p,1d) -> [5s,4p,1d]

B S

2858.8900000 0.00215375

428.1400000 0.0165823

97.5282000 0.0821870

27.9693000 0.2766180

8.2157700 0.6293160

1.1127800 0.1737700

B SP

13.2415000 0.1174430 0.0418100

3.0016600 0.9180020 0.2365750

0.9128560 -0.00265105 0.8162140

B SP

0.3154540 1.0000000 1.0000000

B SP

0.0988563 1.0000000 1.0000000

B SP

0.0315000 1.0000000 1.0000000

B D

0.4010000 1.0000000

#BASIS SET: (12s,6p,1d) -> [5s,4p,1d]

C S

4563.2400000 0.00196665

682.0240000 0.0152306

154.9730000 0.0761269

44.4553000 0.2608010

13.0290000 0.6164620

1.8277300 0.2210060

C SP

20.9642000 0.1146600 0.0402487

4.8033100 0.9199990 0.2375940

1.4593300 -0.00303068 0.8158540

C SP

0.4834560 1.0000000 1.0000000

C SP

0.1455850 1.0000000 1.0000000

C SP

0.0438000 1.0000000 1.0000000

C D

0.6260000 1.0000000

#BASIS SET: (12s,6p,1d) -> [5s,4p,1d]

N S

6293.4800000 0.00196979

949.0440000 0.0149613

218.7760000 0.0735006

63.6916000 0.2489370

18.8282000 0.6024600

2.7202300 0.2562020

N SP

30.6331000 0.1119060 0.0383119

7.0261400 0.9216660 0.2374030

```
2.1120500 -0.00256919 0.8175920
N SP
0.6840090 1.0000000 1.0000000
N SP
0.2008780 1.0000000 1.0000000
N SP
0.0639000 1.0000000 1.0000000
N D
0.9130000 1.0000000
END
dft
XC b3lyp
grid fine
mulliken
print "mulliken ao"
TOLERANCES tight
iterations 50
end
driver
maxiter 50
end
freq
animate
end
task dft optimize
```

A.5. Elk 1.4.18

Input example for the band structure calculation of $\alpha - \mathrm{BN}$ with DFT-PBE

```
! Ground state of alpha-boronnitrid.
tasks
0
```

```
20
! You can add notes to the INFO.OUT file using the "notes" block notes
Calculation of the ground state of alpha-boronnitrid and bandstructure
calculation using PBE.
xctype
20
avec
2.36593800 -4.09792500 0.00000000
2.36593800 4.09792500 0.00000000
0.00000000 0.00000000 12.58784900
! this is the relative path to the species files sppath
'~/Elk/elk-1.4.18/species/'
atoms
2 : nspecies
'B.in' : spfname
2 : natoms
0.33333333 0.66666667 0.25 0.0 0.0 0.0 : atposl, bfcmt
0.66666667 0.33333333 0.75 0.0 0.0 0.0
'N.in' : spfname
2 : natoms
0.33333333 0.66666667 0.75 0.0 0.0 0.0 : atposl, bfcmt
0.66666667 0.33333333 0.25 0.0 0.0 0.0
ngridk
4 4 4
vkloff
0.5 0.5 0.5
plot1d
7 601 : nvp1d, npp1d
0.00 0.50 0.00 : vlvp1d
0.00 0.00 0.00
-0.33333333 0.33333333 0.00
-0.33333333 0.33333333 0.50
```

0.00 0.00 0.50

0.00 0.50 0.50

0.00 0.50 0.00

B. SCC-DFTB Parametrization Structures

B.1. Boranes

B.1.1. Planar dodecaboron (B_{12})

Ball-stick model representation

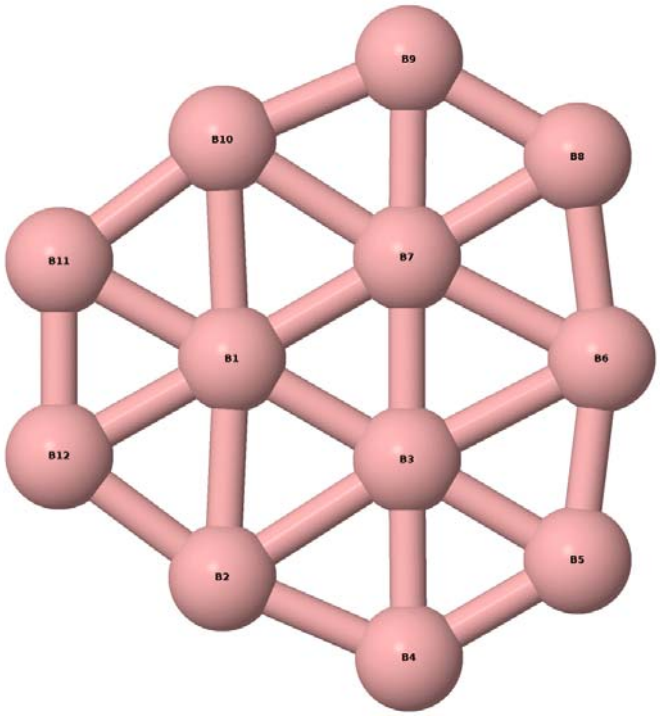

Table of optimized structure in angstrom at DFT-B3LYP / 6-31G(d) level in xyz-format

Atom Label	x	y	z
B1	0.216922	0.000000	0.000000
B2	0.138213	0.000000	1.779403
B3	1.639889	0.000000	0.821549
B4	1.656176	0.000000	2.431915
B5	3.026336	0.000000	1.640877
B6	3.220232	0.000000	0.000000
B7	1.639889	0.000000	−0.821549
B8	3.026336	0.000000	−1.640877

Atom Label	x	y	z
B9	1.656176	0.000000	−2.431915
B10	0.138213	0.000000	−1.779403
B11	−1.185864	0.000000	−0.791046
B12	−1.185864	0.000000	0.791046

B.1.2. Borane (3) (BH_3)

Ball-stick model representation

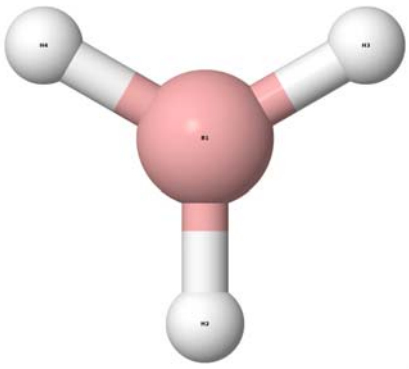

Table of optimized structure in angstrom at DFT-B3LYP / 6-31G(d) level in xyz-format

Atom Label	x	y	z
B1	0.000000	0.000000	0.000000
H2	0.000000	0.000000	1.193674
H3	1.033752	0.000000	−0.596837
H4	−1.033752	0.000000	−0.596837

B.1.3. Diborane (2) (B_2H_2)

Ball-stick model representation

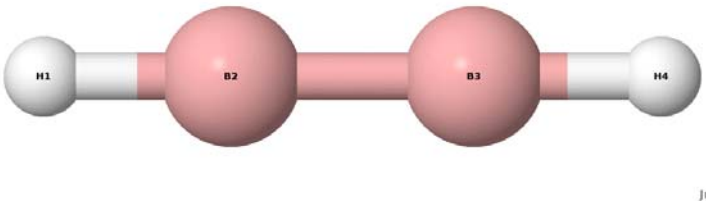

Table of optimized structure in angstrom at DFT-B3LYP / 6-31G(d) level in xyz-format

Atom Label	x	y	z
H1	0.000000	0.000000	0.120791
B2	0.000000	0.000000	1.297932
B3	0.000000	0.000000	2.822468
H4	0.000000	0.000000	3.999609

B.1.4. Diborane (4) (B_2H_4)

Ball-stick model representation

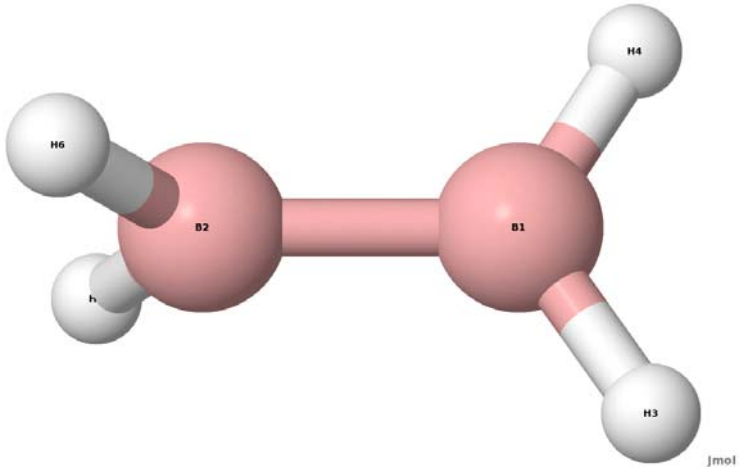

Table of optimized structure in angstrom at DFT-B3LYP / 6-31G(d) level in xyz-format

Atom Label	x	y	z
B1	0.820067	−0.000001	−0.000004
B2	−0.820323	0.000000	−0.000001
H3	1.461737	−0.934693	0.395737
H4	1.461738	0.934694	−0.395733
H5	−1.461611	−0.396056	−0.934541
H6	−1.461607	0.396055	0.934542

B.1.5. Diborane (6) (B_2H_6)

Ball-stick model representation

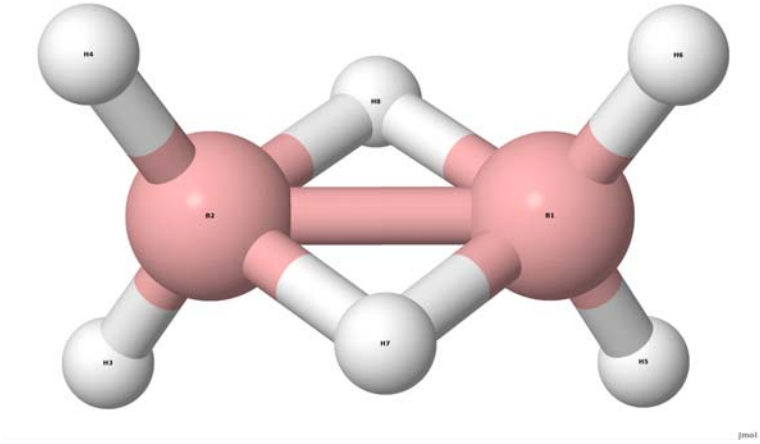

Table of optimized structure in angstrom at DFT-B3LYP / 6-31G(d) level in xyz-format

Atom Label	x	y	z
B1	0.885219	0.000000	0.000000

Atom Label	x	y	z
B2	−0.885219	0.000000	0.000000
H3	−1.462172	−1.041836	0.000000
H4	−1.462172	1.041836	0.000000
H5	1.462172	−1.041836	0.000000
H6	1.462172	1.041836	0.000000
H7	0.000000	0.000000	0.975696
H8	0.000000	0.000000	−0.975696

B.1.6. Triborane (5) (B_3H_5)

Ball-stick model representation

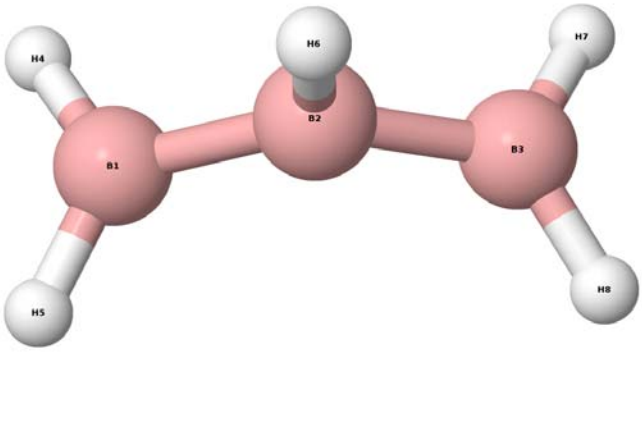

Table of optimized structure in angstrom at DFT-B3LYP / 6-31G(d) level in xyz-format

Atom Label	x	y	z
B1	0.400671	−0.345212	0.007994
B2	0.699579	−0.547985	1.605446
B3	1.647778	0.337401	2.605164
H4	−0.513715	0.324959	−0.384528
H5	1.077108	−0.870295	−0.832183
H6	0.140445	−1.487461	2.124064
H7	1.215822	1.271203	3.222058
H8	2.807284	0.078280	2.771308

B.1.7. Tetraborane (6) (B_4H_6)

Ball-stick model representation

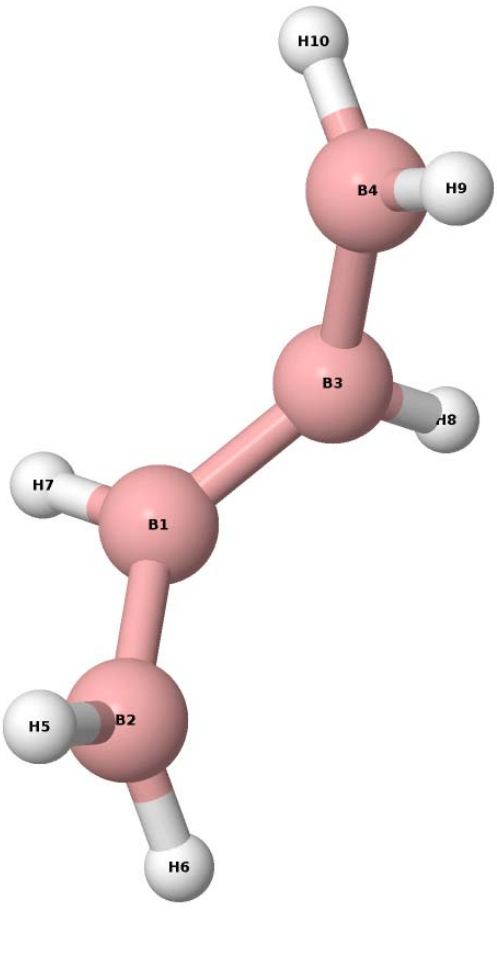

Table of optimized structure in angstrom at DFT-B3LYP / 6-31G(d) level in xyz-format

Atom Label	x	y	z
B1	0.447986	−0.535027	0.185202
B2	0.239675	0.363421	1.540296
B3	1.720037	−0.530856	−0.846537
B4	1.942740	0.398081	−2.178532
H5	−0.305963	1.432009	1.504914
H6	0.610776	−0.008700	2.618626
H7	−0.434898	−1.309618	−0.097309
H8	2.592002	−1.324535	−0.583452
H9	2.504085	1.457094	−2.115624
H10	1.568405	0.058129	−3.266190

B.1.8. Tetraborane (10) (B_4H_{10})

Ball-stick model representation

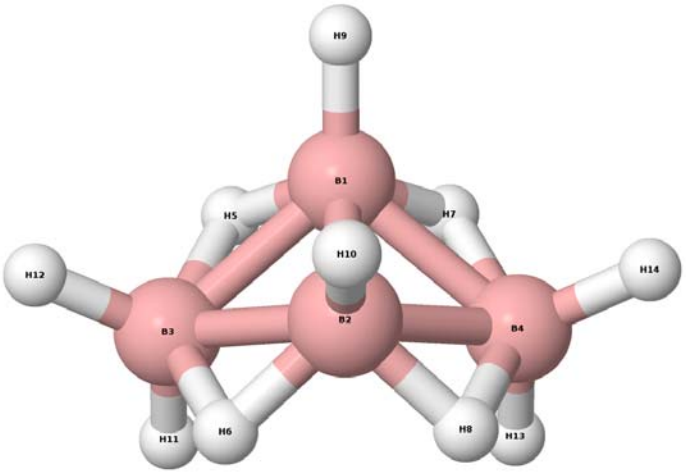

Table of optimized structure in angstrom at DFT-B3LYP / 6-31G(d) level in xyz-format

Atom Label	x	y	z
B1	−0.861927	0.000000	−0.463448
B2	0.861927	0.000000	−0.463448
B3	0.000000	1.411791	0.392181
B4	0.000000	−1.411791	0.392181
H5	−1.322452	0.920238	0.258933
H6	1.322452	0.920238	0.258933
H7	−1.322452	−0.920238	0.258933
H8	1.322452	−0.920238	0.258933
H9	−1.375430	0.000000	−1.532914
H10	1.375430	0.000000	−1.532914
H11	0.000000	1.447212	1.587548
H12	0.000000	2.435801	−0.216167
H13	0.000000	−1.447212	1.587548
H14	0.000000	−2.435801	−0.216167

B.1.9. Pentaborane (9) (B_5H_9)

Ball-stick model representation

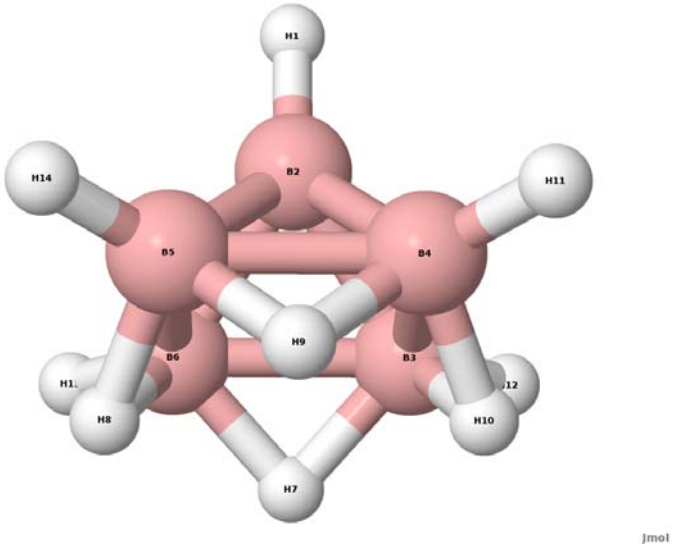

Table of optimized structure in angstrom at DFT-B3LYP / 6-31G(d) level in xyz-format

Atom Label	x	y	z
H1	0.000000	0.000000	0.600939
B2	0.000000	0.000000	1.785857
B3	1.141005	−0.562120	2.906154
B4	0.562120	1.141005	2.906154
B5	−1.141005	0.562120	2.906154
B6	−0.562120	−1.141005	2.906154
H7	0.436900	−1.285395	3.799531
H8	−1.285395	−0.436900	3.799531
H9	−0.436900	1.285395	3.799531
H10	1.285395	0.436900	3.799531
H11	1.082490	2.197263	2.767634
H12	2.197263	−1.082490	2.767634
H13	−1.082490	−2.197263	2.767634
H14	−2.197263	1.082490	2.767634

B.1.10. Borane (4) anion $\left(\mathbf{BH}_4^{1-}\right)$

Ball-stick model representation

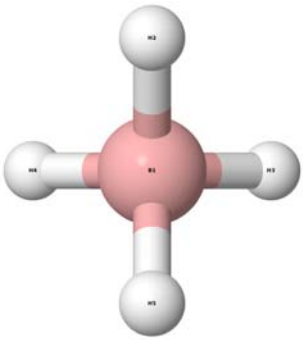

Table of optimized structure in angstrom at DFT-B3LYP / 6-31G(d) level in xyz-format

Atom Label	x	y	z
B1	0.000000	0.000000	0.000000
H2	0.000000	1.013405	0.716573
H3	1.013405	0.000000	−0.716573
H4	−1.013405	0.000000	−0.716573
H5	0.000000	−1.013405	0.716573

B.1.11. Pentaborane (5) dianion $\left(B_5H_5^{2-}\right)$

Ball-stick model representation

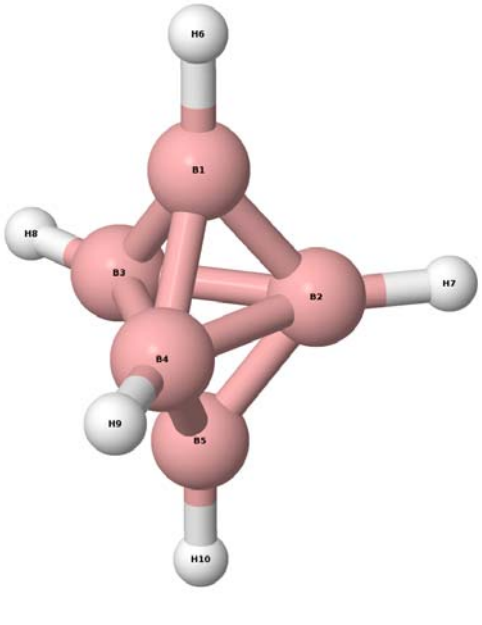

Table of optimized structure in angstrom at DFT-B3LYP / 6-31G(d) level in xyz-format

Atom Label	x	y	z
B1	0.000012	0.000000	1.300094
B2	1.058481	0.000000	0.000000
B3	−0.529190	0.916591	0.000000
B4	−0.529190	−0.916591	0.000000

Atom Label	x	y	z
B5	0.000012	0.000000	−1.300094
H6	0.000090	0.000000	2.520431
H7	2.288137	0.000000	0.000000
H8	−1.144221	1.981383	0.000000
H9	−1.144221	−1.981383	0.000000
H10	0.000090	0.000000	−2.520431

B.1.12. Hexaborane (6) dianion $\left(B_6H_6^{2-}\right)$

Ball-stick model representation

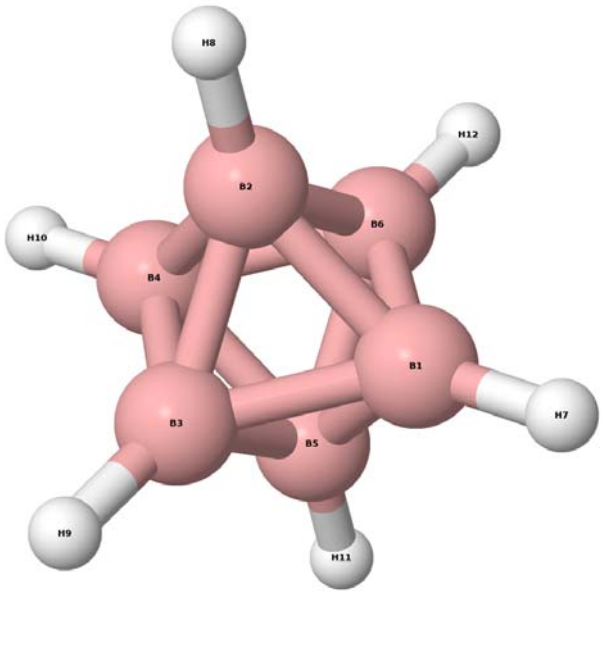

Table of optimized structure in angstrom at DFT-B3LYP / 6-31G(d) level in xyz-format

Atom Label	x	y	z
B1	1.227026	0.000000	0.000000
B2	0.000000	1.227026	0.000000
B3	0.000000	0.000000	1.227026
B4	−1.227026	0.000000	0.000000
B5	0.000000	−1.227026	0.000000
B6	0.000000	0.000000	−1.227026
H7	2.449583	0.000000	0.000000
H8	0.000000	2.449583	0.000000
H9	0.000000	0.000000	2.449583
H10	−2.449583	0.000000	0.000000
H11	0.000000	−2.449583	0.000000
H12	0.000000	0.000000	−2.449583

B.1.13. Heptaborane (7) dianion $\left(B_7H_7^{2-}\right)$

Ball-stick model representation

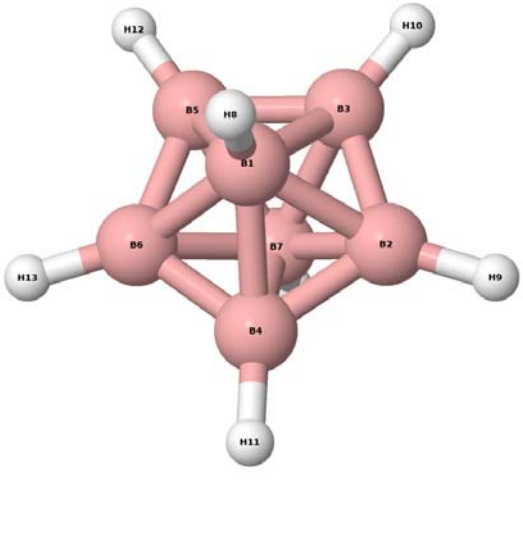

Table of optimized structure in angstrom at DFT-B3LYP / 6-31G(d) level in xyz-format

Atom Label	x	y	z
B1	−0.035115	0.000000	1.165458
B2	1.373440	0.000000	0.000000
B3	0.399927	1.340408	0.000000
B4	0.399927	−1.340408	0.000000
B5	−1.175172	0.828206	0.000000
B6	−1.175172	−0.828206	0.000000
B7	−0.035115	0.000000	−1.165458
H8	−0.035263	0.000000	2.387956
H9	2.594199	0.000000	0.000000
H10	0.777948	2.501131	0.000000
H11	0.777948	−2.501131	0.000000
H12	−2.163151	1.545340	0.000000
H13	−2.163151	−1.545340	0.000000
H14	−0.035263	0.000000	−2.387956

B.1.14. Octaborane (8) dianion $\left(B_8H_8^{2-}\right)$

Ball-stick model representation

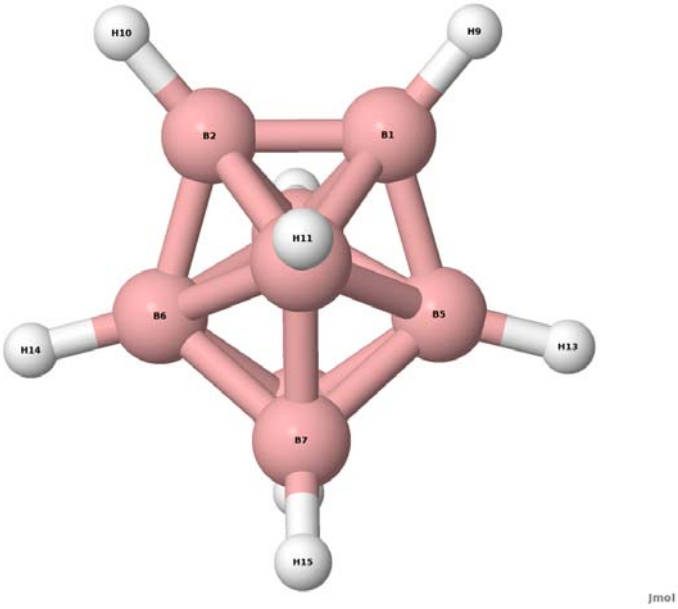

Table of optimized structure in angstrom at DFT-B3LYP / 6-31G(d) level in xyz-format

Atom Label	x	y	z
B1	0.808314	0.000010	−0.055330
B2	−0.808314	0.000010	−0.055330
B3	0.000000	1.275191	0.962870
B4	0.000000	−1.275094	0.962935
B5	1.274888	−0.000003	1.587420
B6	−1.274888	−0.000003	1.587420
B7	0.000000	0.808584	2.605147
B8	0.000000	−0.808681	2.605122
H9	1.591786	−0.000003	−0.985779
H10	−1.591786	−0.000003	−0.985779
H11	0.000000	2.456464	0.654664
H12	0.000000	−2.456390	0.654820
H13	2.456179	0.000006	1.894825
H14	−2.456179	0.000006	1.894825
H15	0.000000	1.591822	3.536092
H16	0.000000	−1.591916	3.536075

B.1.15. Nonaborane (9) dianion $\left(\mathbf{B_9H_9^{2-}}\right)$

Ball-stick model representation

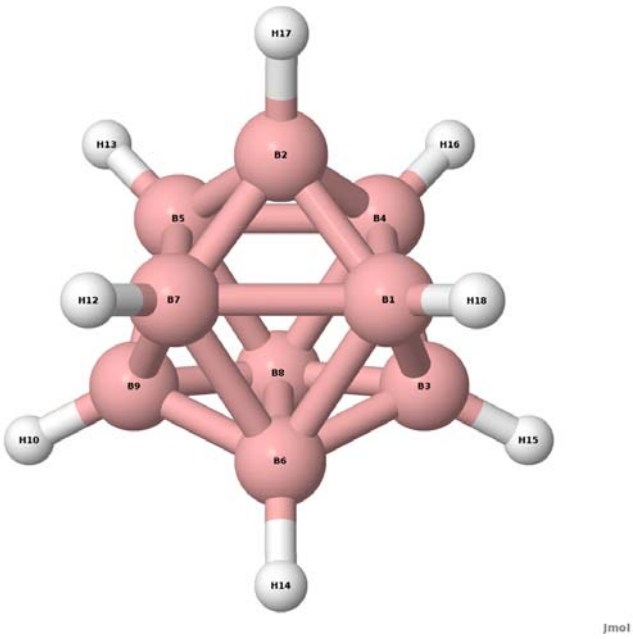

Table of optimized structure in angstrom at DFT-B3LYP / 6-31G(d) level in xyz-format

Atom Label	x	y	z
B1	0.541583	0.166415	0.627947
B2	0.293000	0.182010	2.321134
B3	2.192550	0.347654	0.212727
B4	1.849679	−0.268760	1.771563
B5	1.430299	1.341347	2.859614
B6	1.450181	1.889601	0.241789
B7	0.123053	1.773958	1.714481
B8	2.758718	1.457304	1.385911
B9	1.592653	2.649830	1.768107
H10	1.763804	3.822986	2.016315
H11	3.944646	1.700668	1.484763
H12	−0.943183	2.351107	1.789244
H13	1.635872	1.500683	4.046100
H14	1.365694	2.551485	−0.773254
H15	2.807214	−0.177526	−0.689289
H16	2.364619	−1.300162	2.154220
H17	−0.493824	−0.465804	2.975578
H18	−0.213818	−0.443470	−0.101912

B.1.16. Decaborane (10) dianion $\left(B_{10}H_{10}^{2-}\right)$

Ball-stick model representation

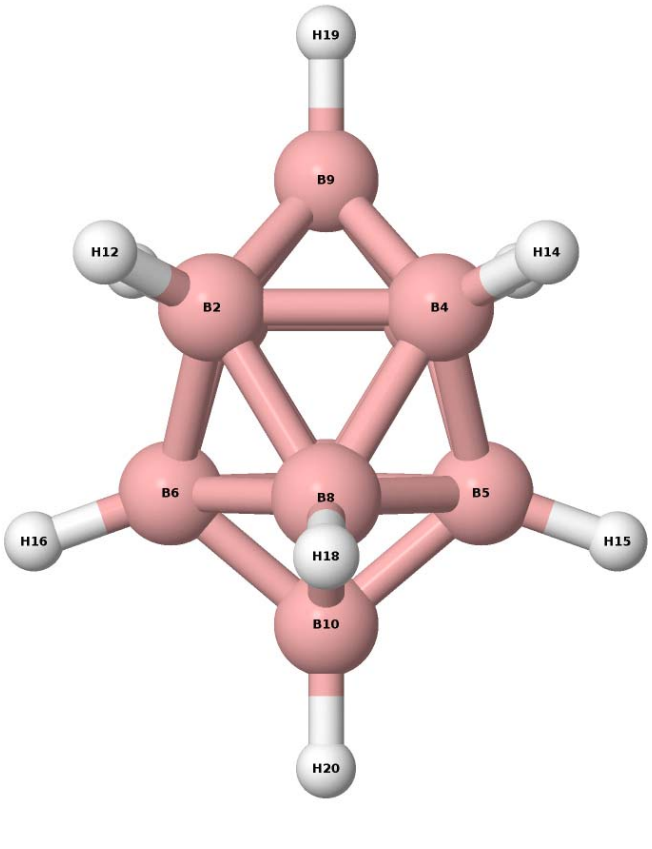

Table of optimized structure in angstrom at DFT-B3LYP / 6-31G(d) level in xyz-format

Atom Label	x	y	z
B1	0.920913	0.920913	0.761796
B2	−0.920913	−0.920913	0.761796
B3	−0.920913	0.920913	0.761796
B4	0.920913	−0.920913	0.761796
B5	1.301840	0.000000	−0.761722
B6	−1.301840	0.000000	−0.761722
B7	0.000000	1.301840	−0.761722
B8	0.000000	−1.301840	−0.761722
B9	0.000000	0.000000	1.858819
B10	0.000000	0.000000	−1.859471
H11	1.727434	1.727434	1.168932
H12	−1.727434	−1.727434	1.168932
H13	−1.727434	1.727434	1.168932
H14	1.727434	−1.727434	1.168932
H15	2.442872	0.000000	−1.168811
H16	−2.442872	0.000000	−1.168811
H17	0.000000	2.442872	−1.168811
H18	0.000000	−2.442872	−1.168811
H19	0.000000	0.000000	3.067398

Atom Label	x	y	z
H20	0.000000	0.000000	−3.067527

B.1.17. Undecaborane (11) dianion $(B_{11}H_{11}^{2-})$

Ball-stick model representation

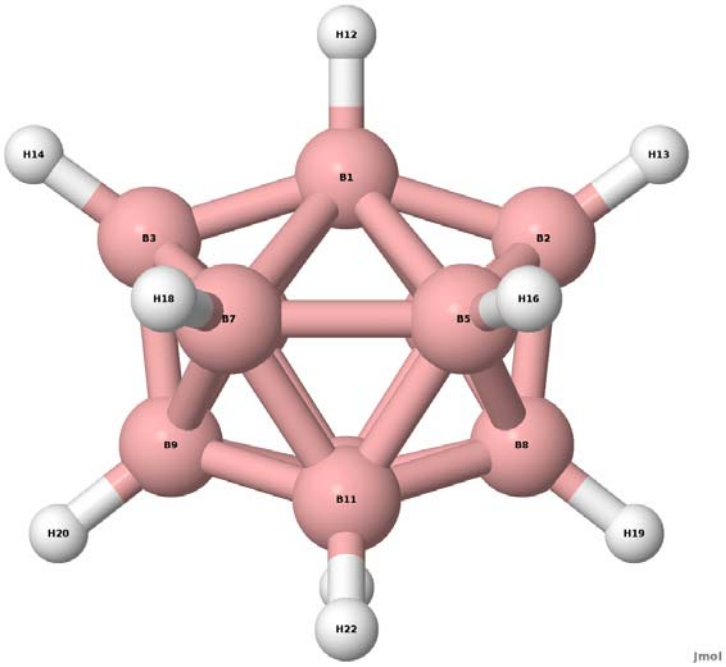

Table of optimized structure in angstrom at DFT-B3LYP / 6-31G(d) level in xyz-format

Atom Label	x	y	z
B1	0.000000	0.000000	−0.700729
B2	1.666698	0.000000	−1.216794
B3	−1.666698	0.000000	−1.216794
B4	0.934983	1.335981	−1.901971
B5	0.934983	−1.335981	−1.901971
B6	−0.934983	1.335981	−1.901971
B7	−0.934983	−1.335981	−1.901971
B8	1.485284	0.000000	−2.966606
B9	−1.485284	0.000000	−2.966606
B10	0.000000	0.915072	−3.363061
B11	0.000000	−0.915072	−3.363061
H12	0.000000	0.000000	0.509193
H13	2.642594	0.000000	−0.505960
H14	−2.642594	0.000000	−0.505960
H15	1.372762	2.454093	−1.748304
H16	1.372762	−2.454093	−1.748304
H17	−1.372762	2.454093	−1.748304

Atom Label	x	y	z
H18	−1.372762	−2.454093	−1.748304
H19	2.435813	0.000000	−3.714586
H20	−2.435813	0.000000	−3.714586
H21	0.000000	1.632271	−4.336676
H22	0.000000	−1.632271	−4.336676

B.1.18. Dodecaborane (12) dianion $\left(B_{12}H_{12}^{2-}\right)$

Ball-stick model representation

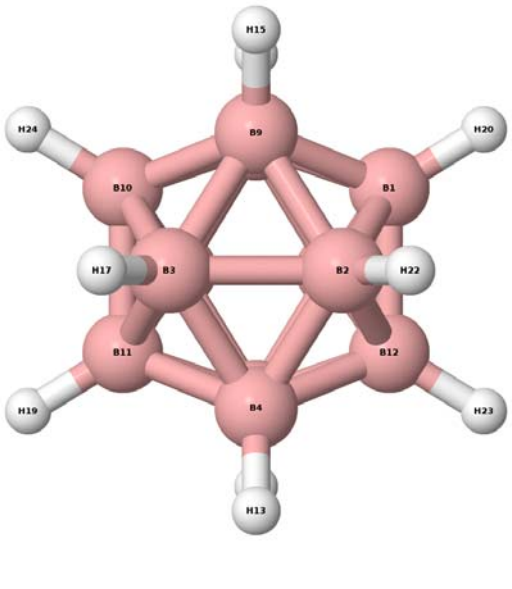

Table of optimized structure in angstrom at DFT-B3LYP / 6-31G(d) level in xyz-format

Atom Label	x	y	z
B1	0.000000	0.893411	1.445569
B2	−1.445569	0.000000	0.893411
B3	−1.445569	0.000000	−0.893411
B4	−0.893411	−1.445569	0.000000
B5	0.893411	−1.445569	0.000000
B6	1.445569	0.000000	−0.893411
B7	1.445569	0.000000	0.893411
B8	0.893411	1.445569	0.000000
B9	−0.893411	1.445569	0.000000
B10	0.000000	0.893411	−1.445569
B11	0.000000	−0.893411	−1.445569
B12	0.000000	−0.893411	1.445569
H13	−1.528267	−2.472788	0.000000
H14	1.528267	2.472788	0.000000
H15	−1.528267	2.472788	0.000000

Atom Label	x	y	z
H16	1.528267	−2.472788	0.000000
H17	−2.472788	0.000000	−1.528267
H18	2.472788	0.000000	1.528267
H19	0.000000	−1.528267	−2.472788
H20	0.000000	1.528267	2.472788
H21	2.472788	0.000000	−1.528267
H22	−2.472788	0.000000	1.528267
H23	0.000000	−1.528267	2.472788
H24	0.000000	1.528267	−2.472788

B.2. Carbaboranes

B.2.1. Boramethene ($CH_2 - BH$)

Ball-stick model representation

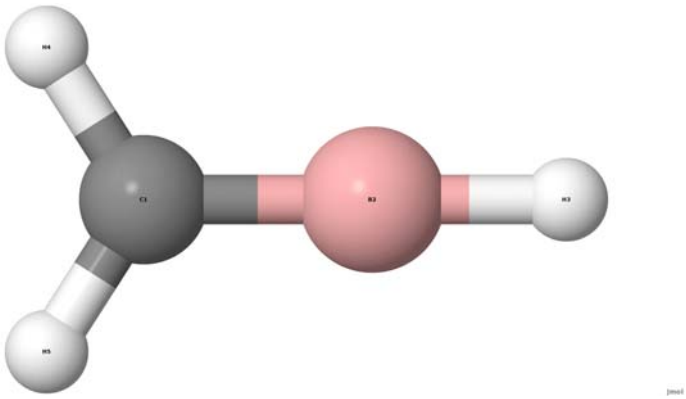

Table of optimized structure in angstrom at DFT-B3LYP / 6-311++G** level in xyz-format

Atom Label	x	y	z
C1	0.00000000	0.00000000	0.58954705
B2	0.00000000	0.00000000	−0.78607701
H3	0.00000000	0.00000000	−1.95603606
H4	0.00000000	0.91552514	1.17484158
H5	0.00000000	−0.91552514	1.17484158

B.2.2. Methylborane ($CH_3 - BH_2$)

Ball-stick model representation

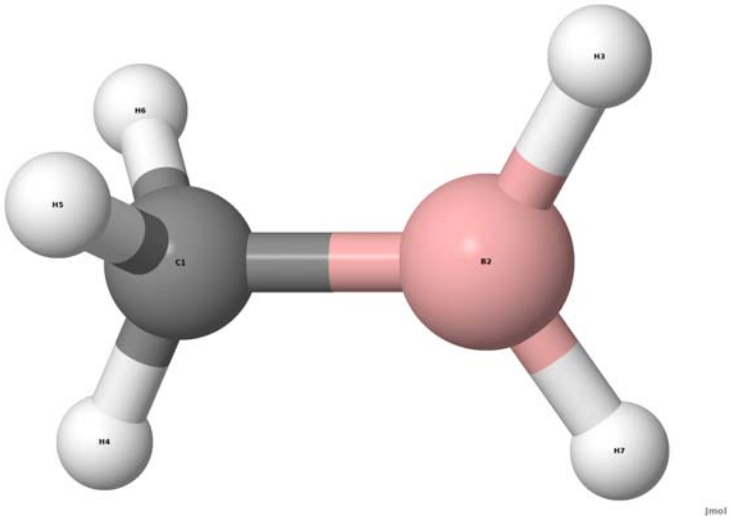

Table of optimized structure in angstrom at DFT-B3LYP / 6-311++G** level in xyz-format

Atom Label	x	y	z
C1	−0.03650335	0.69735625	0.00000000
B2	−0.01582732	−0.85903298	0.00000000
H3	1.03205892	−1.43351468	0.00000000
H4	−1.02344255	1.16284542	0.00000000
H5	0.52876070	1.07050376	0.86618223
H6	0.52876070	1.07050376	−0.86618223
H7	−1.01380569	−1.51443236	0.00000000

B.2.3. Ethylborane ($C_2H_5 - BH_2$)

Ball-stick model representation

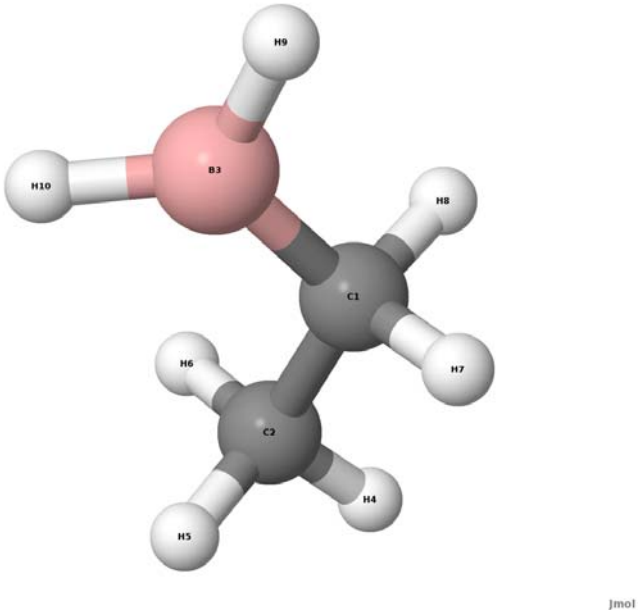

Table of optimized structure in angstrom at DFT-B3LYP / 6-311++G** level in xyz-format

Atom Label	x	y	z
C1	0.52073119	0.08719500	0.00000000
C2	−0.22830521	−1.25296140	0.00000000
B3	−0.31285335	1.40149470	0.00000000
H4	0.45585545	−2.10633580	0.00000000
H5	−0.87123177	−1.34478278	0.88004891
H6	−0.87123177	−1.34478278	−0.88004891
H7	1.21026669	0.14879501	0.85882490
H8	1.21026669	0.14879501	−0.85882490
H9	0.25021603	2.45548193	0.00000000
H10	−1.50850282	1.39874626	0.00000000

B.2.4. Dimethylborane $((CH_3)_2 - BH)$

Ball-stick model representation

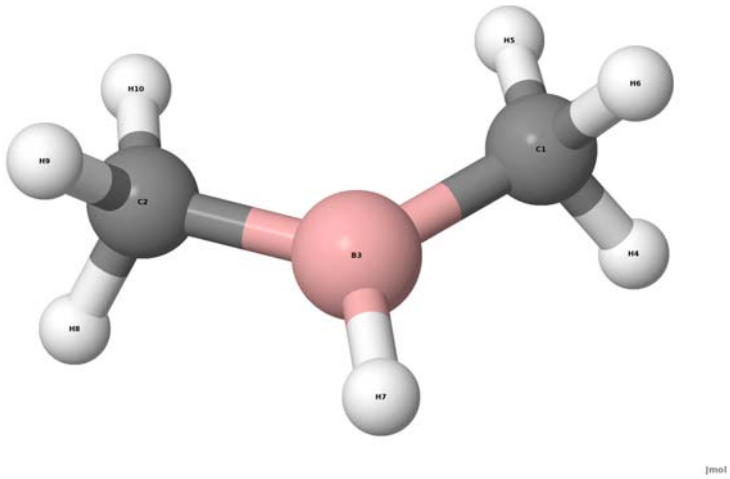

Table of optimized structure in angstrom at DFT-B3LYP / 6-311++G** level in xyz-format

Atom Label	x	y	z
C1	−0.19307536	0.00099433	1.38784570
C2	−0.19307536	0.00099433	−1.38784570
B3	0.52799708	0.00249868	0.00000000
H4	0.15489103	0.84944540	1.99283490
H5	−1.28523898	0.02339038	1.35097507
H6	0.11709204	−0.88481325	1.96016836
H7	1.72879154	−0.00273435	0.00000000
H8	0.15489103	0.84944540	−1.99283490
H9	0.11709204	−0.88481325	−1.96016836

Atom Label	x	y	z
H10	−1.28523898	0.02339038	−1.35097507

B.2.5. Diboramethane ($CH_2-(BH_2)_2$)

Ball-stick model representation

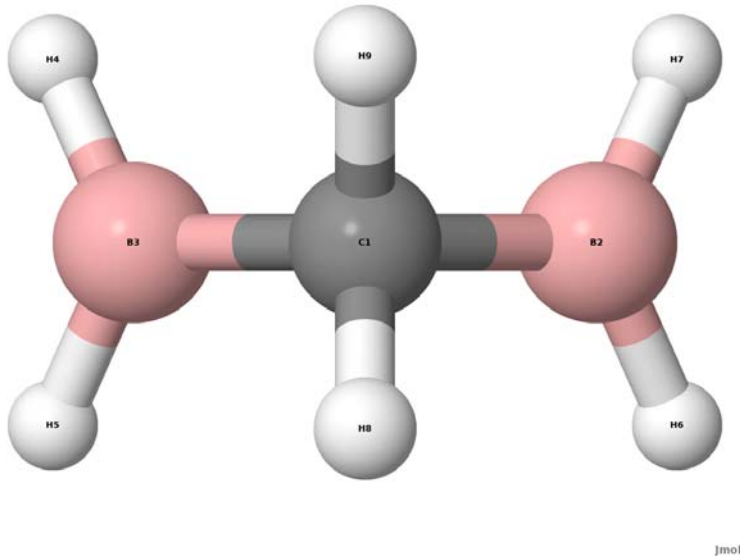

Table of optimized structure in angstrom at DFT-B3LYP / 6-311++G** level in xyz-format

Atom Label	x	y	z
C1	0.00000000	0.00000000	0.53216971
B2	1.26402989	0.00000000	−0.38590651
B3	−1.26402989	0.00000000	−0.38590651
H4	−1.74719771	1.02572881	−0.75387520
H5	−1.74719771	−1.02572881	−0.75387520
H6	1.74719771	−1.02572881	−0.75387520
H7	1.74719771	1.02572881	−0.75387520
H8	0.00000000	−0.91030381	1.14188873
H9	0.00000000	0.91030381	1.14188873

B.2.6. Methyldiborane (3) ($CH_3-B_2H_3$)

Ball-stick model representation

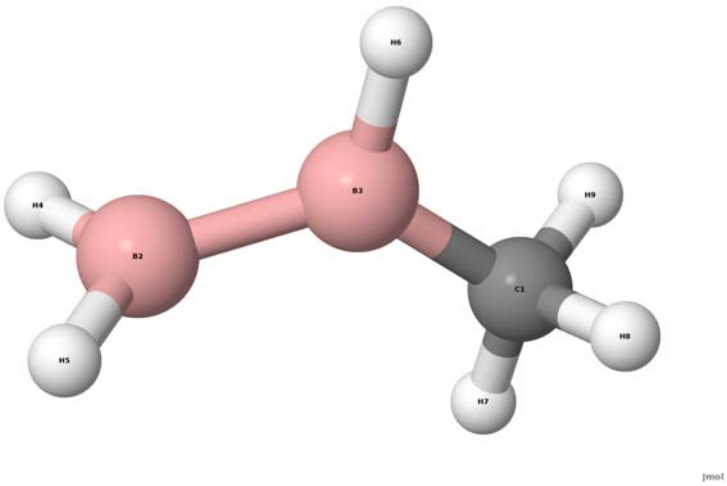

Table of optimized structure in angstrom at DFT-B3LYP / 6-311++G** level in xyz-format

Atom Label	x	y	z
C1	0.21533183	−1.30156928	0.00620557
B2	0.18837281	1.58911323	0.00246221
B3	−0.49593375	0.09836372	0.00352492
H4	0.41054180	2.18625935	1.01609466
H5	0.45888909	2.16954715	−1.00891300
H6	−1.70139917	0.07780958	−0.02011327
H7	1.30125353	−1.29431123	0.11733648
H8	−0.02354807	−1.79448952	−0.94807977
H9	−0.21643003	−1.95632122	0.77273658

B.2.7. 1,2-Dicarbahexaborane (6)$(1,2-\mathbf{C_2B_4H_6})$

Ball-stick model representation

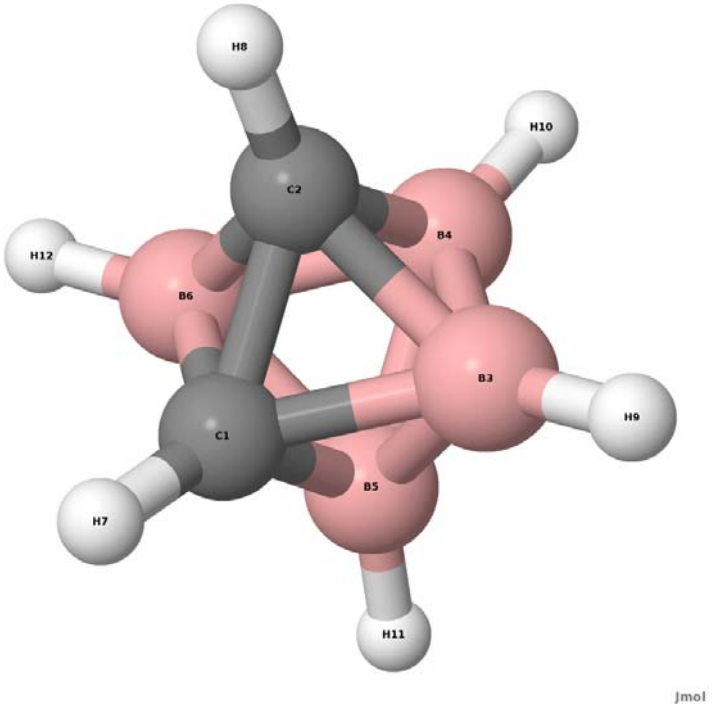

Table of optimized structure in angstrom at DFT-B3LYP / 6-311++G** level in xyz-format

Atom Label	x	y	z
C1	−0.68724373	−0.00000041	0.77236087
C2	−0.68724373	−0.00000041	−0.77236087
B3	0.04741248	1.21765534	0.00000000
B4	0.93839943	−0.00000002	−0.85409894
B5	0.93839943	−0.00000002	0.85409894
B6	0.04741373	−1.21765647	0.00000000
H7	−1.54352929	−0.00000067	1.42706545
H8	−1.54352929	−0.00000067	−1.42706545
H9	−0.14659945	2.37691317	0.00000000
H10	1.66555298	0.00000161	−1.77955146
H11	1.66555298	0.00000161	1.77955146
H12	−0.14660339	−2.37691304	0.00000000

B.2.8. 1,6-Dicarbahexaborane (6)$(1,6-\mathbf{C_2B_4H_6})$

Ball-stick model representation

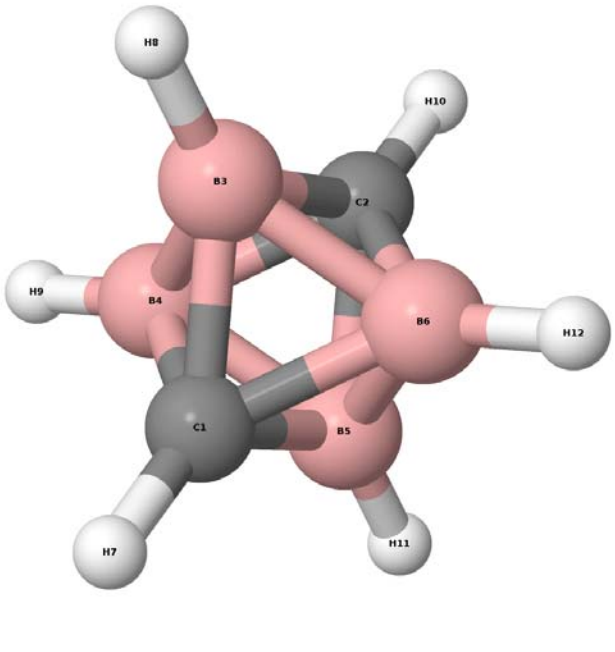

Table of optimized structure in angstrom at DFT-B3LYP / 6-311++G** level in xyz-format

Atom Label	x	y	z
C1	0.00000000	0.00000000	1.22702600
C2	0.00000000	0.00000000	−1.22702600
B3	0.00000000	1.22702600	0.00000000
B4	−1.22702600	0.00000000	0.00000000
B5	0.00000000	−1.22702600	0.00000000
B6	1.22702600	0.00000000	0.00000000
H7	0.00000000	0.00000000	2.44958300
H8	0.00000000	2.44958300	0.00000000
H9	−2.44958300	0.00000000	0.00000000
H10	0.00000000	0.00000000	−2.44958300
H11	0.00000000	−2.44958300	0.00000000
H12	2.44958300	0.00000000	0.00000000

B.2.9. 1,2-Dicarbaheptaborane (7)$(1,2-\mathbf{C_2B_5H_7})$

Ball-stick model representation

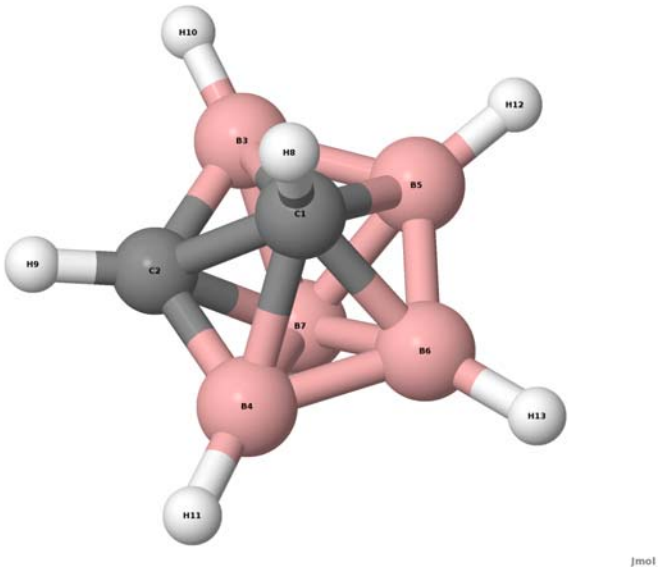

Table of optimized structure in angstrom at DFT-B3LYP / 6-311++G** level in xyz-format

Atom Label	x	y	z
C1	0.98375528	0.07398831	0.00000000
C2	−0.04600086	−1.20868361	0.00000000
B3	−0.06605647	−0.41433470	1.32215008
B4	−0.06605647	−0.41433470	−1.32215008
B5	−0.06310062	1.15446671	0.82683014
B6	−0.06310062	1.15446671	−0.82683014
B7	−1.24563206	0.09508601	0.00000000
H8	2.06066673	−0.02981464	0.00000000
H9	0.12517690	−2.27742877	0.00000000
H10	0.09747946	−0.89311090	2.38720914
H11	0.09747946	−0.89311090	−2.38720914
H12	0.11531338	2.07279236	1.54416076
H13	0.11531338	2.07279236	−1.54416076
H14	−2.41632973	−0.04505579	0.00000000

B.2.10. 1,7-Dicarbaheptaborane (7)$(1,7-\mathbf{C_2B_5H_7})$

Ball-stick model representation

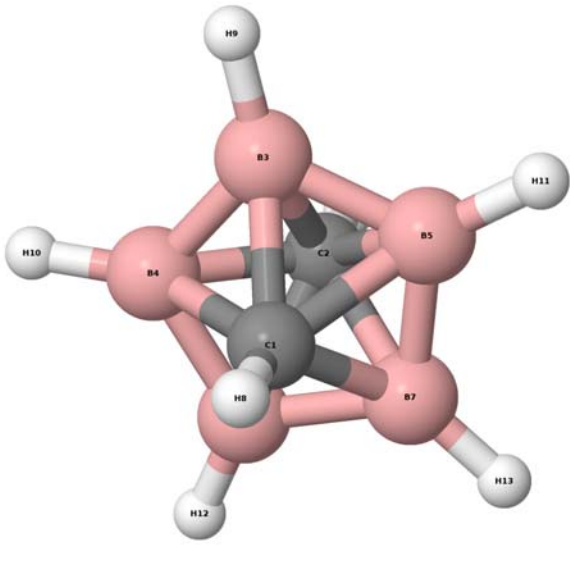

Table of optimized structure in angstrom at DFT-B3LYP / 6-311++G** level in xyz-format

Atom Label	x	y	z
C1	0.00000000	0.00000000	1.05333744
C2	0.00000000	0.00000000	−1.05333744
B3	0.00000000	1.38369478	0.00000000
B4	−1.31597193	0.42758520	0.00000000
B5	1.31597193	0.42758520	0.00000000
B6	−0.81331538	−1.11943259	0.00000000
B7	0.81331538	−1.11943259	0.00000000
H8	0.00000000	0.00000000	2.13618103
H9	0.00000000	2.56240057	0.00000000
H10	−2.43698776	0.79182532	0.00000000
H11	2.43698776	0.79182532	0.00000000
H12	−1.50614127	−2.07302561	0.00000000
H13	1.50614127	−2.07302561	0.00000000
H14	0.00000000	0.00000000	−2.13618103

B.2.11. 1,2-Dicarbadecaborane (10)$(1,2-\mathbf{C_2B_8H_{10}})$

Ball-stick model representation

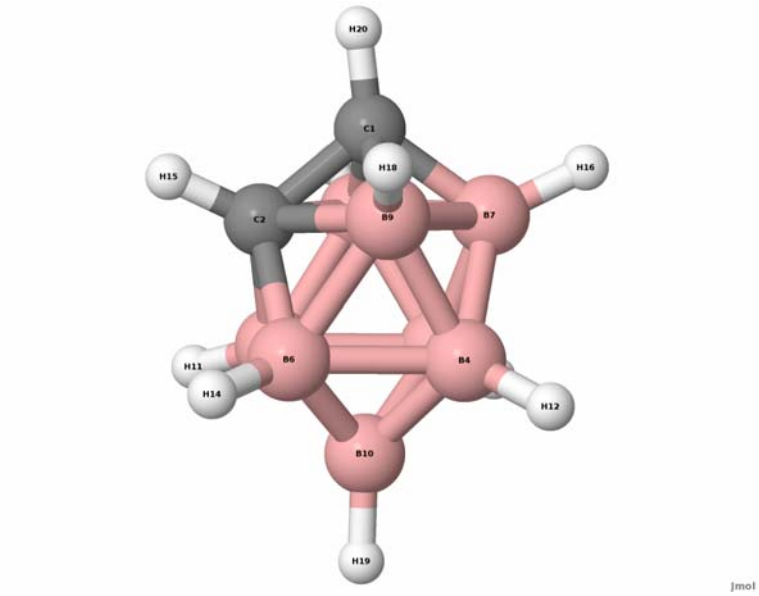

Table of optimized structure in angstrom at DFT-B3LYP / 6-311++G** level in xyz-format

Atom Label	x	y	z
C1	0.05194694	1.62293924	0.00000000
C2	−1.13692730	0.65225191	0.00000000
B3	−0.91212439	−0.77611859	−0.91607287
B4	0.93506277	−0.80683328	0.92735786
B5	0.93506277	−0.80683328	−0.92735786
B6	−0.91212439	−0.77611859	0.91607287
B7	1.35879152	0.68926553	0.00000000
B8	0.07630449	0.70498387	−1.31736448
B9	0.07630449	0.70498387	1.31736448
B10	−0.01042751	−1.88487890	0.00000000
H11	−1.76590111	−1.05877774	−1.68160108
H12	1.70171159	−1.22763283	1.72379311
H13	1.70171159	−1.22763283	−1.72379311
H14	−1.76590111	−1.05877774	1.68160108
H15	−2.11311606	1.11608010	0.00000000
H16	2.41971957	1.20253476	0.00000000
H17	−0.05658991	1.22357046	−2.36600180
H18	−0.05658991	1.22357046	2.36600180
H19	−0.05024294	−3.06211197	0.00000000
H20	−0.07006787	2.69303650	0.00000000

B.2.12. 1,6-Dicarbadecaborane (10)$(1,6-\mathbf{C_2B_8H_{10}})$

Ball-stick model representation

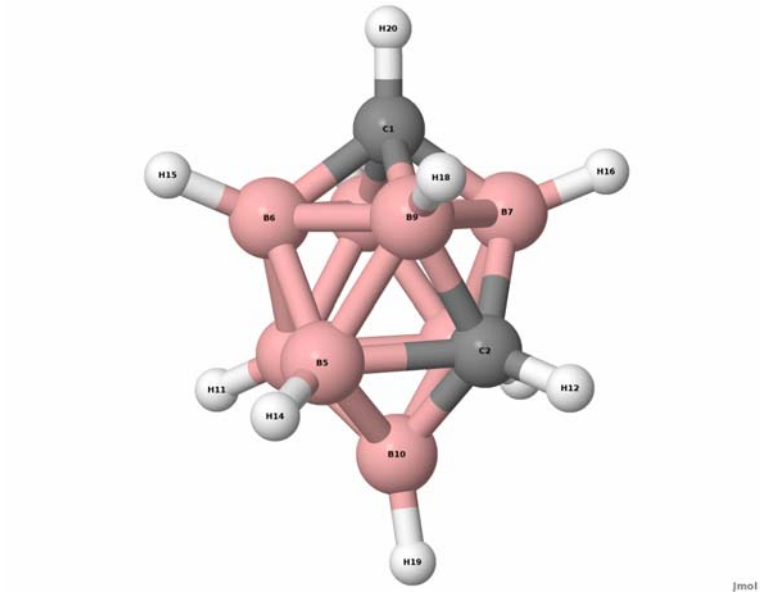

Table of optimized structure in angstrom at DFT-B3LYP / 6-311++G** level in xyz-format

Atom Label	x	y	z
C1	−0.02146931	1.66607276	0.00000000
C2	−1.11895508	−0.72295336	0.00000000
B3	1.35791361	−0.75118165	0.00000000
B4	0.06329688	−0.74774122	1.30399054
B5	0.06329688	−0.74774122	−1.30399054
B6	0.94274540	0.76790364	−0.92176481
B7	−0.89047811	0.71613992	0.93733497
B8	0.94274540	0.76790364	0.92176481
B9	−0.89047811	0.71613992	−0.93733497
B10	0.06210443	−1.83967198	0.00000000
H11	2.47063729	−1.14892524	0.00000000
H12	−2.12844745	−1.11262422	0.00000000
H13	−0.09308873	−1.20333026	2.38162094
H14	−0.09308873	−1.20333026	−2.38162094
H15	1.68419769	1.27216767	−1.68771496
H16	−1.72978697	1.10798018	1.66431950
H17	1.68419769	1.27216767	1.68771496
H18	−1.72978697	1.10798018	−1.66431950
H19	−0.08090541	−3.00696265	0.00000000
H20	−0.06879105	2.74237549	0.00000000

B.2.13. 1,10-Dicarbadecaborane (10)$(1,10-\mathbf{C_2B_8H_{10}})$

Ball-stick model representation

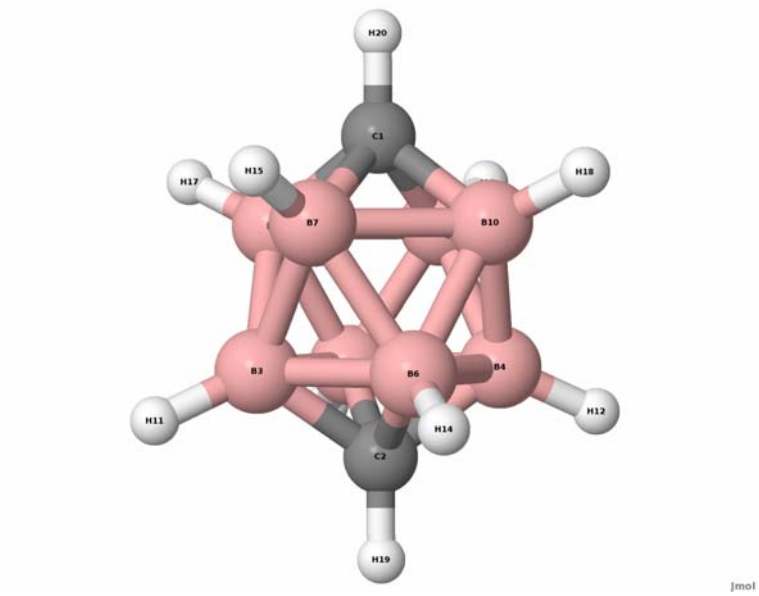

Table of optimized structure in angstrom at DFT-B3LYP / 6-311++G** level in xyz-format

Atom Label	x	y	z
C1	0.00000000	0.00000000	−1.67108604
C2	0.00000000	0.00000000	1.67108604
B3	−0.92753534	0.92753534	0.75474569
B4	0.92753534	−0.92753534	0.75474569
B5	−0.92753534	−0.92753534	0.75474569
B6	0.92753534	0.92753534	0.75474569
B7	0.00000000	1.31173305	−0.75474569
B8	0.00000000	−1.31173305	−0.75474569
B9	−1.31173305	0.00000000	−0.75474569
B10	1.31173305	0.00000000	−0.75474569
H11	−1.68651249	1.68651249	1.24561181
H12	1.68651249	−1.68651249	1.24561181
H13	−1.68651249	−1.68651249	1.24561181
H14	1.68651249	1.68651249	1.24561181
H15	0.00000000	2.38508883	−1.24561181
H16	0.00000000	−2.38508883	−1.24561181
H17	−2.38508883	0.00000000	−1.24561181
H18	2.38508883	0.00000000	−1.24561181
H19	0.00000000	0.00000000	2.74908290
H20	0.00000000	0.00000000	−2.74908290

B.2.14. 1,2-Dicarbadodecaborane (12)$(1,2-\mathbf{C_2B_{10}H_{12}})$

Ball-stick model representation

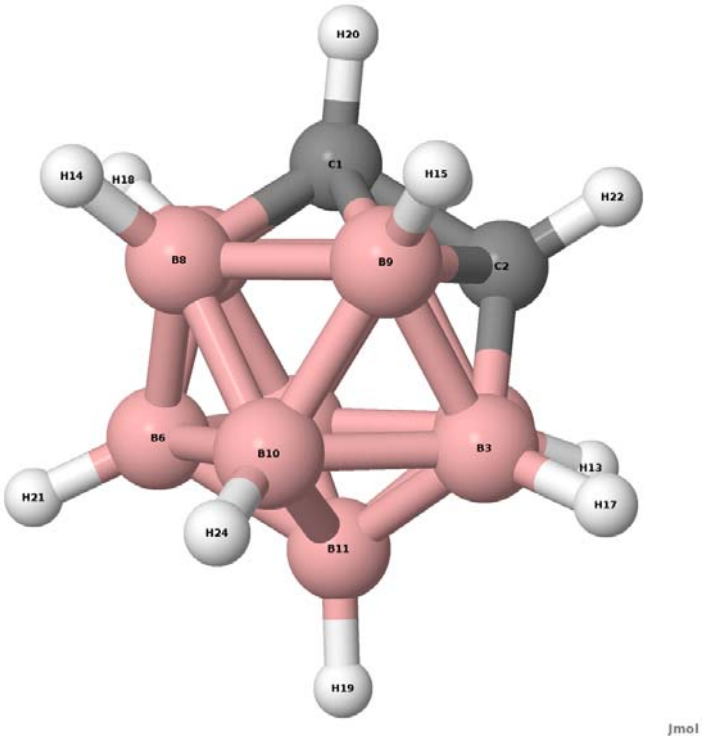

Table of optimized structure in angstrom at DFT-B3LYP / 6-311++G** level in xyz-format

Atom Label	x	y	z
C1	0.01052740	−0.21882347	1.48555235
C2	−0.00570380	−1.43455873	0.40607221
B3	−0.90684490	−1.03591463	−0.97423702
B4	0.87812003	−1.04696664	−0.98855002
B5	1.45177486	0.61354432	−0.69852804
B6	0.00617372	1.65762853	−0.50952029
B7	0.90643637	1.10776169	0.92295020
B8	−0.87767717	1.11886856	0.93730757
B9	−1.45388752	−0.53889331	0.64437188
B10	−1.45514666	0.63158515	−0.67518963
B11	−0.01164124	0.32277463	−1.69177847
B12	1.45711131	−0.55698658	0.62102873
H13	1.45509593	−1.91510189	−1.54023552
H14	−1.45446915	1.76461957	1.73759857
H15	−2.32804485	−1.05374312	1.24096418
H16	2.47602925	0.99422773	−1.14657789
H17	−1.50342061	−1.89669937	−1.51649610
H18	1.50398511	1.74619825	1.71382649
H19	−0.01990872	0.49596321	−2.86021262
H20	0.01709823	−0.50951658	2.52591647
H21	0.01074477	2.79680776	−0.82535027
H22	−0.00861019	−2.43381999	0.81559218

Atom Label	x	y	z
H23	2.33430262	−1.08272084	1.20353437
H24	−2.48165619	1.02506272	−1.10672299

B.2.15. 1,7-Dicarbadodecaborane (12)$(1,7-\mathbf{C_2B_{10}H_{12}})$

Ball-stick model representation

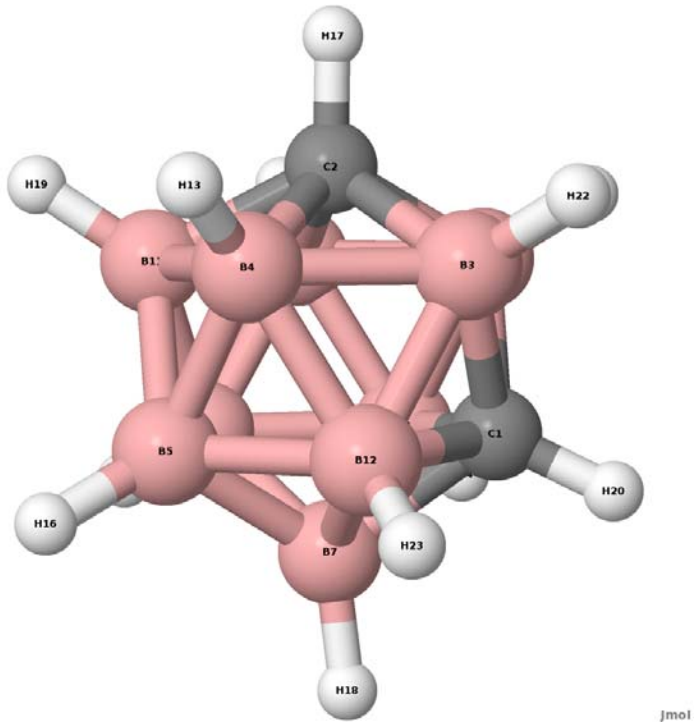

Table of optimized structure in angstrom at DFT-B3LYP / 6-311++G** level in xyz-format

Atom Label	x	y	z
C1	0.01031153	−0.28618841	−1.50816798
C2	0.00513938	1.44518895	0.43645256
B3	0.90805339	1.02887916	−0.93285776
B4	1.44412581	0.54742657	0.68000183
B5	0.88212948	−1.11582566	0.97371058
B6	−0.91101377	−1.10505795	0.95939185
B7	−0.00618299	−1.64876960	−0.47107578
B8	−1.44495506	−0.61157366	−0.66548041
B9	−0.88063806	1.03962154	−0.94721408
B10	−1.44821242	0.56484991	0.65683748
B11	−0.01183806	0.25498838	1.66590978
B12	1.44790671	−0.62896164	−0.64233554
H13	2.39149908	1.07555956	1.14108981
H14	−2.39178623	−0.98898671	−1.25778175

Atom Label	x	y	z
H15	−1.40270678	1.82588403	−1.64960571
H16	1.50792341	−1.85951498	1.64451623
H17	0.00908562	2.48520071	0.72905725
H18	−0.00889166	−2.73023611	−0.94258161
H19	−0.01879330	0.59551953	2.79506850
H20	0.01788525	−0.45209683	−2.57582681
H21	−1.55633635	−1.84112526	1.62002379
H22	1.45069402	1.80872018	−1.62675643
H23	2.39949601	−1.01776538	−1.21947620
H24	−2.39645952	1.10434937	1.10273704

B.2.16. 1,12-Dicarbadodecaborane (12)$(1,12-\mathbf{C_2B_{10}H_{12}})$

Ball-stick model representation

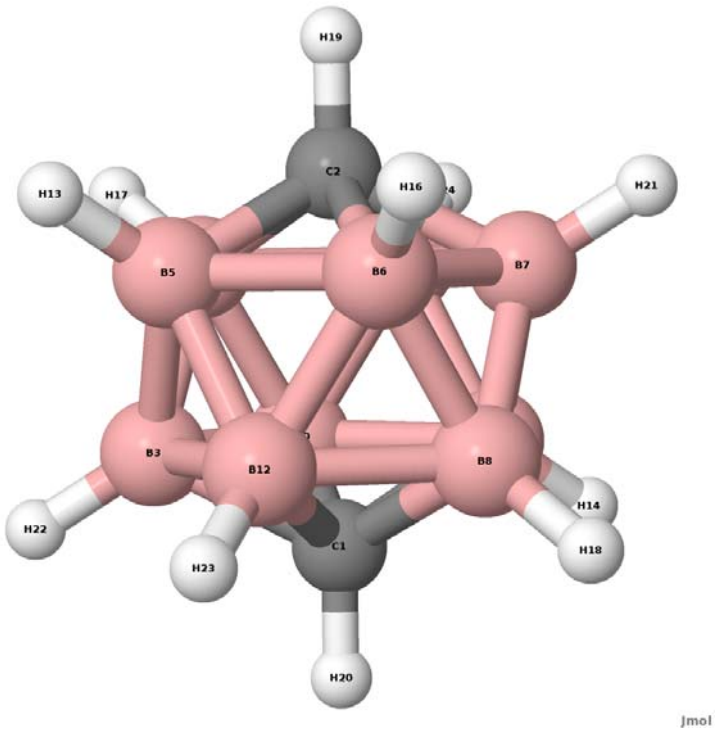

Table of optimized structure in angstrom at DFT-B3LYP / 6-311++G** level in xyz-format

Atom Label	x	y	z
C1	1.54398425	−0.03219781	0.00000000
C2	−1.50869483	0.03153690	0.00000000
B3	0.75607504	−0.48515744	−1.44430551
B4	−0.72023432	0.48452974	−1.44446031
B5	−0.75579896	−1.21319194	−0.89275232
B6	−0.75579896	−1.21319194	0.89275232

Atom Label	x	y	z
B7	−0.72023432	0.48452974	1.44446031
B8	0.75607504	−0.48515744	1.44430551
B9	0.79161821	1.21237864	0.89264944
B10	0.79161821	1.21237864	−0.89264944
B11	−0.69838495	1.53344522	0.00000000
B12	0.73422846	−1.53394981	0.00000000
H13	−1.39833469	−2.00757534	−1.47952999
H14	1.43371923	2.00694062	1.47957218
H15	1.43371923	2.00694062	−1.47957218
H16	−1.39833469	−2.00757534	1.47952999
H17	−1.33956954	0.80609222	−2.39380399
H18	1.37494227	−0.80678938	2.39388524
H19	−2.58953929	0.05413158	0.00000000
H20	2.62470221	−0.05479896	0.00000000
H21	−1.33956954	0.80609222	2.39380399
H22	1.37494227	−0.80678938	−2.39388524
H23	1.33859864	−2.54534558	0.00000000
H24	−1.30320332	2.54460789	0.00000000

B.2.17. 2-Carbapentaborane (5) anion $\left(2-\mathbf{CB_4H_5^{1-}}\right)$

Ball-stick model representation

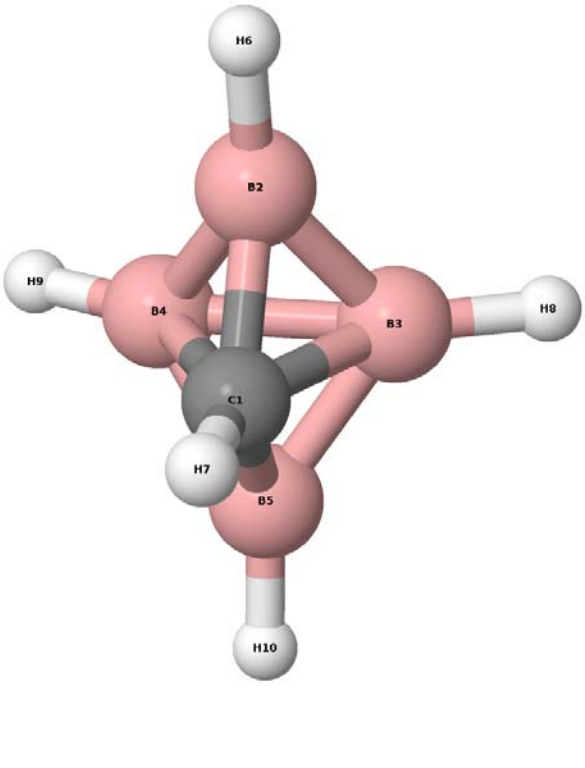

Table of optimized structure in angstrom at DFT-B3LYP / 6-311++G** level in xyz-

format

Atom Label	x	y	z
C1	0.00000000	0.00000000	0.84273469
B2	−1.27393272	0.00000000	−0.05065998
B3	0.00000000	0.90875474	−0.61343242
B4	0.00000000	−0.90875474	−0.61343242
B5	1.27393272	0.00000000	−0.05065998
H6	−2.44342922	0.00000000	0.15951689
H7	0.00000000	0.00000000	1.93124565
H8	0.00000000	2.01625047	−1.05321805
H9	0.00000000	−2.01625047	−1.05321805
H10	2.44342922	0.00000000	0.15951689

B.2.18. Carbahexaborane (6) anion $\left(CB_5H_6^{1-}\right)$

Ball-stick model representation

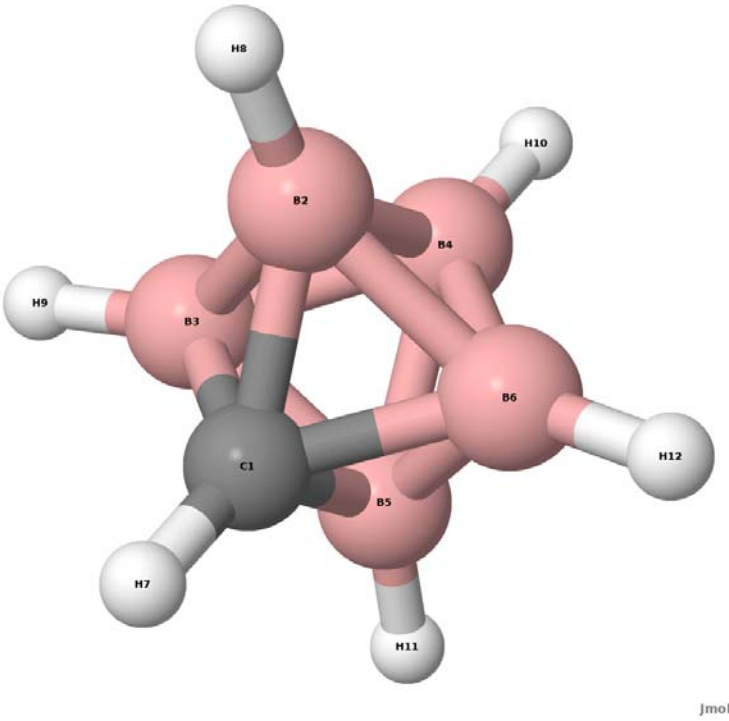

Table of optimized structure in angstrom at DFT-B3LYP / 6-311++G** level in xyz-format

Atom Label	x	y	z
C1	0.00000000	0.00000000	1.02812396
B2	0.00000000	1.21664343	−0.05270415
B3	−1.21664343	0.00000000	−0.05270415
B4	0.00000000	0.00000000	−1.28045353
B5	0.00000000	−1.21664343	−0.05270415

Atom Label	x	y	z
B6	1.21664343	0.00000000	−0.05270415
H7	0.00000000	0.00000000	2.11042634
H8	0.00000000	2.39672124	0.10709453
H9	−2.39672124	0.00000000	0.10709453
H10	0.00000000	0.00000000	−2.47361266
H11	0.00000000	−2.39672124	0.10709453
H12	2.39672124	0.00000000	0.10709453

B.2.19. 1-Carbaheptaborane (7) anion $\left(1-\mathrm{CB_6H_7^{1-}}\right)$

Ball-stick model representation

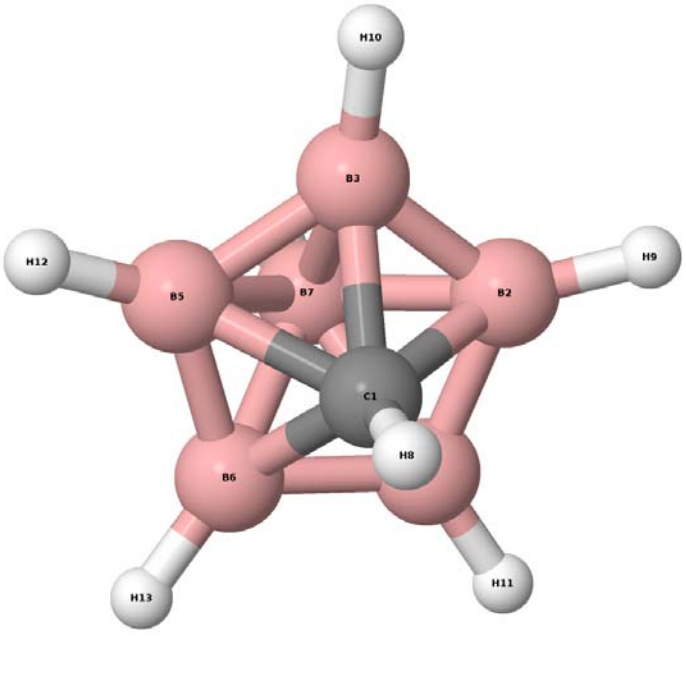

Table of optimized structure in angstrom at DFT-B3LYP / 6-311++G** level in xyz-format

Atom Label	x	y	z
C1	0.00000000	0.00000000	−0.97490286
B2	1.39431300	0.00000000	0.06515284
B3	0.43086641	−1.32607046	0.06515284
B4	0.43086641	1.32607046	0.06515284
B5	−1.12802291	−0.81955662	0.06515284
B6	−1.12802291	0.81955662	0.06515284
B7	0.00000000	0.00000000	1.24816223
H8	0.00000000	0.00000000	−2.06187072
H9	2.57284388	0.00000000	−0.12018396
H10	0.79505248	−2.44691993	−0.12018396

Atom Label	x	y	z
H11	0.79505248	2.44691993	−0.12018396
H12	−2.08147442	−1.51227969	−0.12018396
H13	−2.08147442	1.51227969	−0.12018396
H14	0.00000000	0.00000000	2.44321838

B.2.20. 2-Carbaheptaborane (7) anion $\left(2-\mathrm{CB_6H_7^{1-}}\right)$

Ball-stick model representation

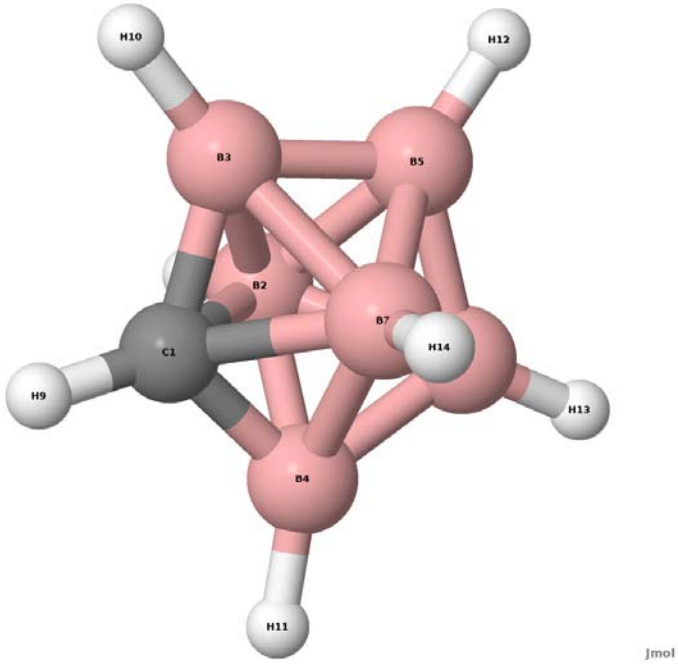

Table of optimized structure in angstrom at DFT-B3LYP / 6-311++G** level in xyz-format

Atom Label	x	y	z
C1	0.00000000	0.00000000	−1.21469547
B2	1.16746364	0.00000000	0.07617533
B3	0.00000000	1.31925032	−0.40401980
B4	0.00000000	−1.31925032	−0.40401980
B5	0.00000000	0.83013258	1.17202392
B6	0.00000000	−0.83013258	1.17202392
B7	−1.16746364	0.00000000	0.07617533
H8	2.35213833	0.00000000	−0.06352841
H9	0.00000000	0.00000000	−2.29891379
H10	0.00000000	2.40368125	−0.90115752
H11	0.00000000	−2.40368125	−0.90115752
H12	0.00000000	1.57244142	2.10646062
H13	0.00000000	−1.57244142	2.10646062

Atom Label	x	y	z
H14	−2.35213833	0.00000000	−0.06352841

B.2.21. 1-Carbaoctaborane (8) anion $\left(1-\mathrm{CB_7H_8^{1-}}\right)$

Ball-stick model representation

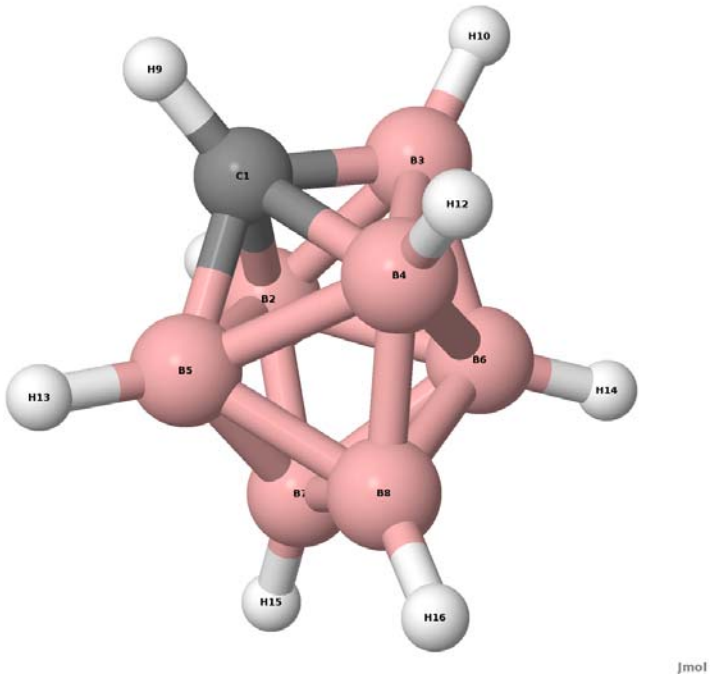

Table of optimized structure in angstrom at DFT-B3LYP / 6-311++G** level in xyz-format

Atom Label	x	y	z
C1	0.65361485	1.18075360	0.00000000
B2	−0.01443098	0.26798264	1.28392115
B3	−0.86512675	1.25476422	0.00000000
B4	−0.01443098	0.26798264	−1.28392115
B5	1.25610791	−0.30436844	0.00000000
B6	−1.28641370	−0.38300079	0.00000000
B7	0.03238494	−1.35680101	0.80816880
B8	0.03238494	−1.35680101	−0.80816880
H9	1.32008226	2.03355818	0.00000000
H10	−1.51324236	2.25305720	0.00000000
H11	0.02049335	0.69073541	2.39947846
H12	0.02049335	0.69073541	−2.39947846
H13	2.44307221	−0.43333017	0.00000000
H14	−2.43665619	−0.70965804	0.00000000
H15	0.04992542	−2.26840654	1.57731915
H16	0.04992542	−2.26840654	−1.57731915

B.2.22. 3-Carbaoctaborane (8) anion $(3 - CB_7H_8^{1-})$

Ball-stick model representation

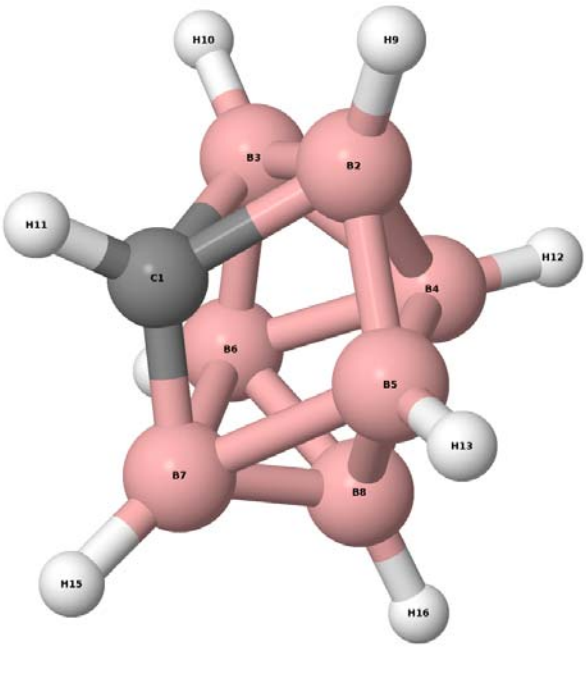

Table of optimized structure in angstrom at DFT-B3LYP / 6-311++G** level in xyz-format

Atom Label	x	y	z
C1	−1.16405563	−0.30098384	0.00000000
B2	0.01663868	−1.27017092	−0.81238912
B3	0.01663868	−1.27017092	0.81238912
B4	1.30668584	−0.31856151	0.00000000
B5	0.19371718	0.34045828	−1.30551656
B6	0.19371718	0.34045828	1.30551656
B7	−0.85506569	1.22282849	0.00000000
B8	0.77408432	1.34913547	0.00000000
H9	−0.15913154	−2.20770903	−1.52635651
H10	−0.15913154	−2.20770903	1.52635651
H11	−2.19638549	−0.65424515	0.00000000
H12	2.45943973	−0.62964459	0.00000000
H13	0.13229879	0.64967973	−2.45707949
H14	0.13229879	0.64967973	2.45707949
H15	−1.70103258	2.06616474	0.00000000
H16	1.42453538	2.34699937	0.00000000

B.2.23. 1-Carbanonaborane (9) anion $\left(1-\mathrm{CB_8H_9^{1-}}\right)$

Ball-stick model representation

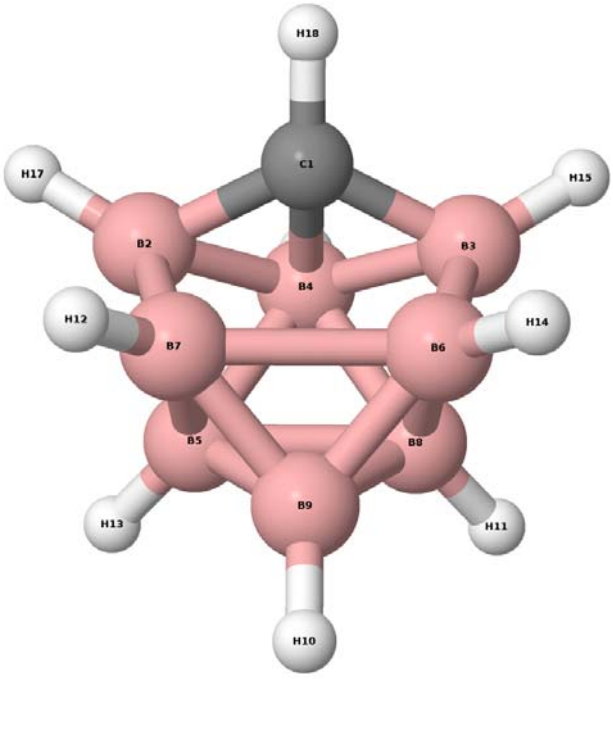

Table of optimized structure in angstrom at DFT-B3LYP / 6-311++G** level in xyz-format

Atom Label	x	y	z
C1	0.64480708	0.09635511	0.71450869
B2	0.25468015	0.21853543	2.23265423
B3	2.09841144	0.37901238	0.18628729
B4	1.90208980	−0.18459730	1.82527743
B5	1.46951917	1.31448864	2.82808861
B6	1.52570790	1.98196981	0.23440380
B7	0.11649575	1.85926927	1.79832142
B8	2.73329995	1.42447930	1.42550214
B9	1.56538684	2.68006977	1.74659240
H10	1.74195061	3.83007794	1.99589334
H11	3.90897559	1.61214411	1.49906232
H12	−0.97120338	2.34409970	1.80320321
H13	1.65343502	1.41583437	4.00229557
H14	1.37667825	2.54866408	−0.80230931
H15	2.61565539	−0.19808190	−0.71617862
H16	2.35342698	−1.23593869	2.14943887
H17	−0.53979471	−0.47264328	2.78594994
H18	0.01321817	−0.53441274	0.09604669

B.2.24. 4-Carbanonaborane (9) anion $\left(4-\mathrm{CB_8H_9^{1-}}\right)$

Ball-stick model representation

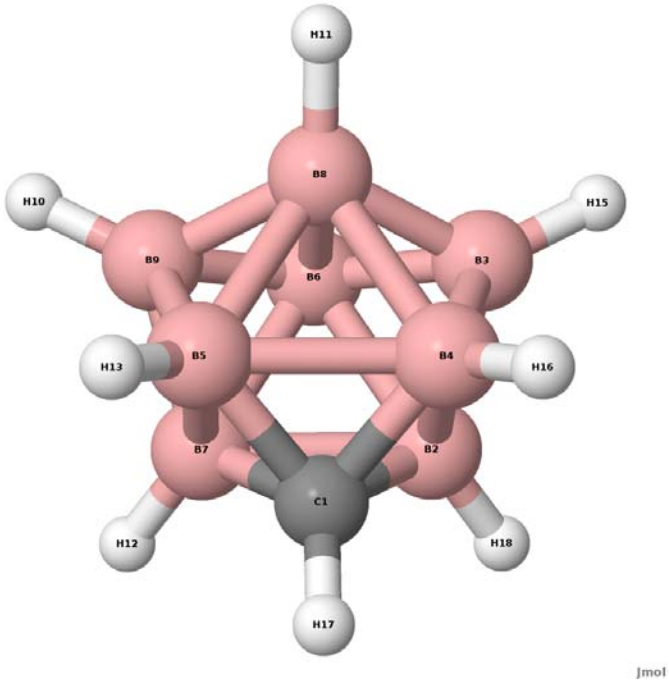

Table of optimized structure in angstrom at DFT-B3LYP / 6-311++G** level in xyz-format

Atom Label	x	y	z
C1	0.40938215	0.27795176	2.22411037
B2	0.55023925	0.16402374	0.62164774
B3	2.18995478	0.34415980	0.21425318
B4	1.85398352	−0.26878869	1.76243381
B5	1.43170159	1.35149529	2.85772023
B6	1.44832688	1.88700670	0.24460245
B7	0.12823393	1.78233549	1.71588874
B8	2.75506929	1.45533672	1.38727011
B9	1.58910291	2.64817252	1.77170682
H10	1.74740236	3.79946255	2.02625232
H11	3.92015886	1.68756150	1.49348193
H12	−0.96576035	2.23843612	1.82891636
H13	1.55988136	1.40393757	4.04028036
H14	1.35348281	2.53554487	−0.75190840
H15	2.78660321	−0.18579284	−0.66805486
H16	2.26170511	−1.28988620	2.21935495
H17	−0.29257008	−0.29955701	2.80764147
H18	−0.26415759	−0.45207389	0.00944043

B.2.25. 1-Carbadecaborane (10) anion $\left(1-\mathrm{CB_9H_{10}^{1-}}\right)$

Ball-stick model representation

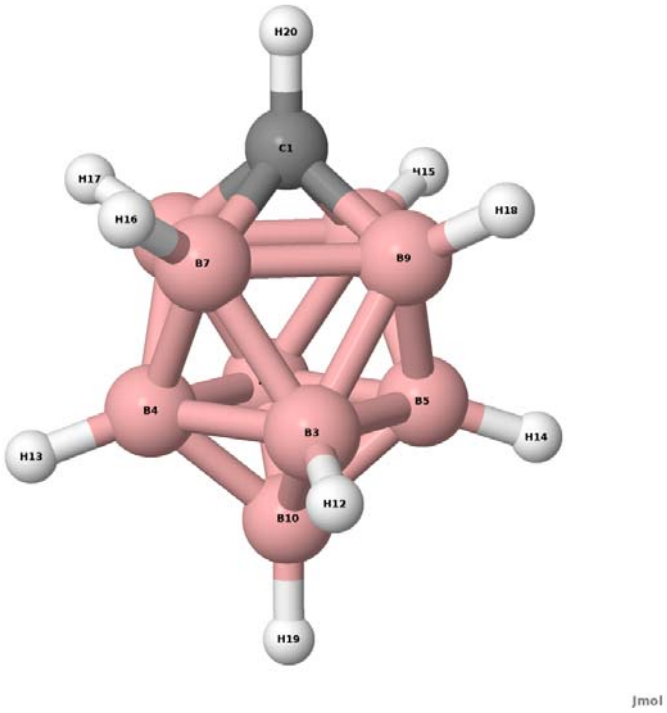

Table of optimized structure in angstrom at DFT-B3LYP / 6-311++G** level in xyz-format

Atom Label	x	y	z
C1	−0.00000002	−1.65494916	0.00000000
B2	−0.00000003	0.78410323	1.30450376
B3	−0.00000003	0.78410323	−1.30450376
B4	−1.30450379	0.78410331	0.00000000
B5	1.30450386	0.78410327	0.00000000
B6	0.92318539	−0.72335220	0.92318535
B7	−0.92318533	−0.72335218	−0.92318536
B8	−0.92318533	−0.72335218	0.92318536
B9	0.92318539	−0.72335220	−0.92318535
B10	0.00000007	1.87747920	0.00000000
H11	−0.00000009	1.18148694	2.42872953
H12	−0.00000009	1.18148694	−2.42872953
H13	−2.42872966	1.18148692	0.00000000
H14	2.42872957	1.18148715	0.00000000
H15	1.68404216	−1.22850475	1.68404190
H16	−1.68404211	−1.22850466	−1.68404192
H17	−1.68404211	−1.22850466	1.68404192
H18	1.68404216	−1.22850475	−1.68404190
H19	0.00000008	3.06613520	0.00000000

Atom Label	x	y	z
H20	−0.00000011	−2.73346980	0.00000000

B.2.26. 1-Carbaundecaborane (11) anion $\left(1-\mathbf{CB}_{10}\mathbf{H}_{11}^{1-}\right)$

Ball-stick model representation

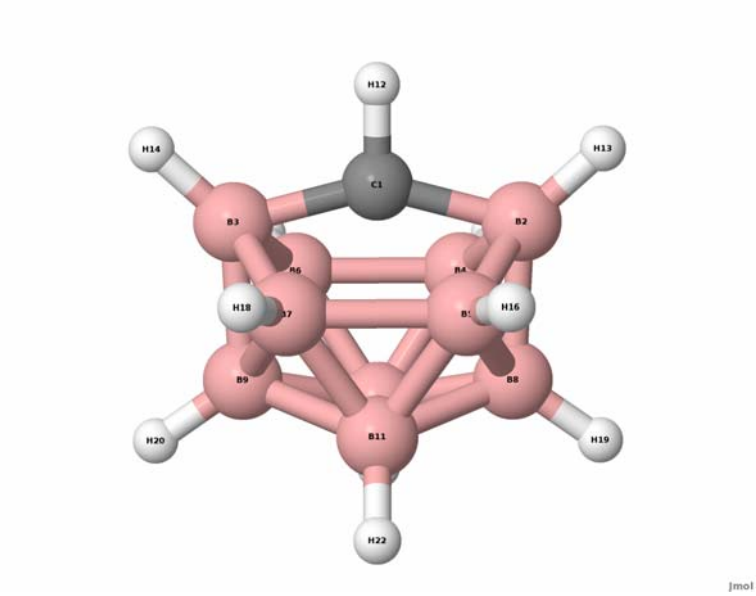

Table of optimized structure in angstrom at DFT-B3LYP / 6-311++G** level in xyz-format

Atom Label	x	y	z
C1	0.00000000	0.00000000	1.31570189
B2	0.00000000	−1.57323572	0.90712080
B3	0.00000000	1.57323572	0.90712080
B4	1.35803665	−0.94591018	0.14078376
B5	−1.35803665	−0.94591018	0.14078376
B6	1.35803665	0.94591018	0.14078376
B7	−1.35803665	0.94591018	0.14078376
B8	0.00000000	−1.48940136	−0.84362270
B9	0.00000000	1.48940136	−0.84362270
B10	0.91600737	0.00000000	−1.27458988
B11	−0.91600737	0.00000000	−1.27458988
H12	0.00000000	0.00000000	2.40457411
H13	0.00000000	−2.45074687	1.70908552
H14	0.00000000	2.45074687	1.70908552
H15	2.44458545	−1.34736736	0.40811067
H16	−2.44458545	−1.34736736	0.40811067
H17	2.44458545	1.34736736	0.40811067
H18	−2.44458545	1.34736736	0.40811067
H19	0.00000000	−2.46261081	−1.52859758

Atom Label	x	y	z
H20	0.00000000	2.46261081	−1.52859758
H21	1.63017639	0.00000000	−2.22768849
H22	−1.63017639	0.00000000	−2.22768849

B.2.27. Carbadodecaborane (12) anion$\left(CB_{11}H_{12}^{1-}\right)$

Ball-stick model representation

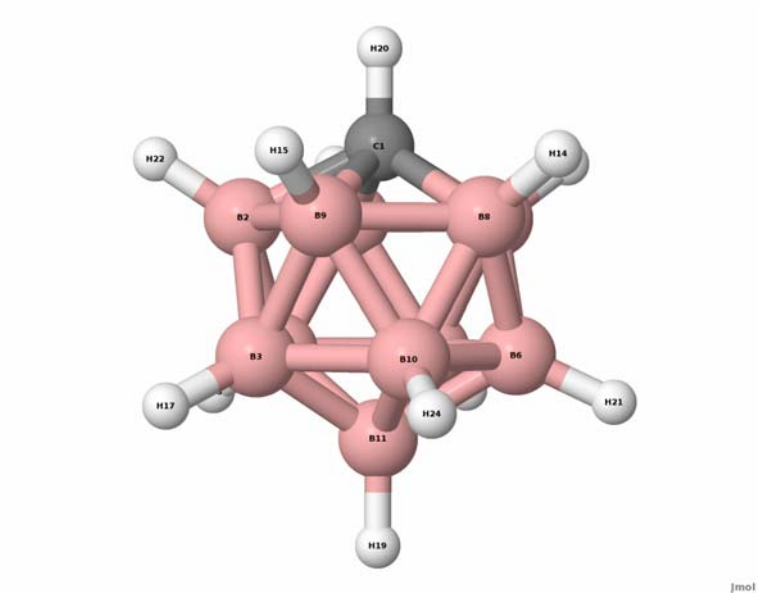

Table of optimized structure in angstrom at DFT-B3LYP / 6-311++G** level in xyz-format

Atom Label	x	y	z
C1	1.52221530	0.01252434	0.00000000
B2	0.73004895	0.47415633	1.44079830
B3	−0.76683796	−0.47644255	1.44684653
B4	−0.78065114	1.22448078	0.89426134
B5	−0.78065114	1.22448078	−0.89426134
B6	−0.76683796	−0.47644255	−1.44684653
B7	0.73004895	0.47415633	−1.44079830
B8	0.74420233	−1.21940391	−0.89041488
B9	0.74420233	−1.21940391	0.89041488
B10	−0.75786245	−1.52760842	0.00000000
B11	−1.70462560	−0.01401201	0.00000000
B12	0.72184694	1.52049665	0.00000000
H13	−1.29618949	2.08994078	1.52635548
H14	1.40088342	−2.01724603	−1.47414259
H15	1.40088342	−2.01724603	1.47414259
H16	−1.29618949	2.08994078	−1.52635548
H17	−1.27240929	−0.81292912	2.46935745

Atom Label	x	y	z
H18	1.37780209	0.78623787	−2.38501591
H19	−2.89467438	−0.02378219	0.00000000
H20	2.60343122	0.02123358	0.00000000
H21	−1.27240929	−0.81292912	−2.46935745
H22	1.37780209	0.78623787	2.38501591
H23	1.36367732	2.51881720	0.00000000
H24	−1.25695990	−2.60709861	0.00000000

B.3. Azaboranes

B.3.1. Ammonia borane (H_3B-NH_3)

Ball-stick model representation

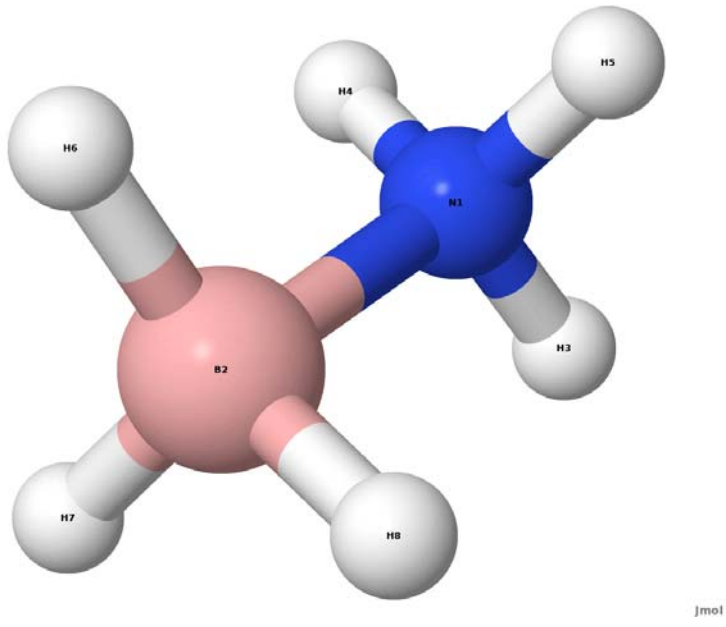

Table of optimized structure in angstrom at DFT-B3LYP / 6-311++G** level in xyz-format

Atom Label	x	y	z
N1	0.000000	0.726493	0.000000
B2	0.000000	−0.938673	0.000000
H3	0.949301	1.092662	0.000000
H4	−0.474650	1.092672	−0.822116
H5	−0.474650	1.092672	0.822116
H6	−1.167468	−1.248778	0.000000
H7	0.583734	−1.248769	−1.011062
H8	0.583734	−1.248769	1.011062

B.3.2. Aminoborane (H_2B-NH_2)

Ball-stick model representation

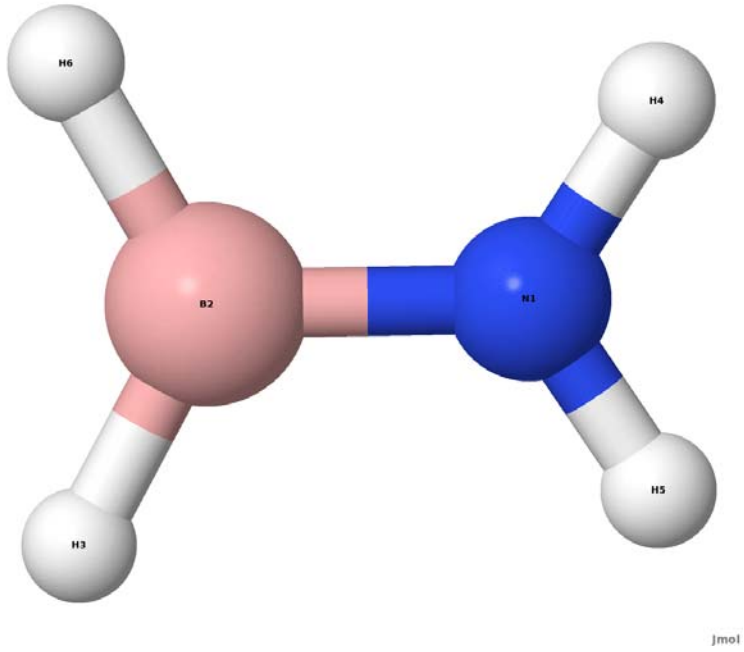

Table of optimized structure in angstrom at DFT-B3LYP / 6-311++G** level in xyz-format

Atom Label	x	y	z
N1	0.063388	0.561824	−0.181497
B2	0.027605	−0.819827	−0.027567
H3	−1.026378	−1.376382	−0.049251
H4	0.917920	1.097871	−0.174042
H5	−0.762870	1.125796	−0.312002
H6	1.051664	−1.411454	0.121813

B.3.3. Iminoborane (HB − NH)

Ball-stick model representation

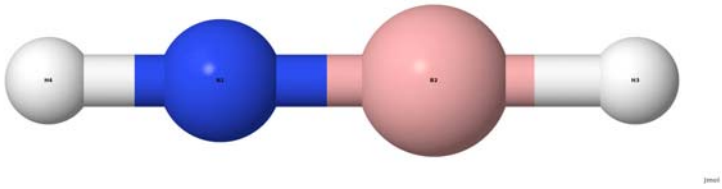

Table of optimized structure in angstrom at DFT-B3LYP / 6-311++G** level in xyz-format

Atom Label	x	y	z
N1	0.000000	0.000000	−0.574508

Atom Label	x	y	z
B2	0.000000	0.000000	0.661472
H3	0.000000	0.000000	1.827404
H4	0.000000	0.000000	−1.568373

B.3.4. Aminodiborane (3) ($H_2N - B_2H_3$)

Ball-stick model representation

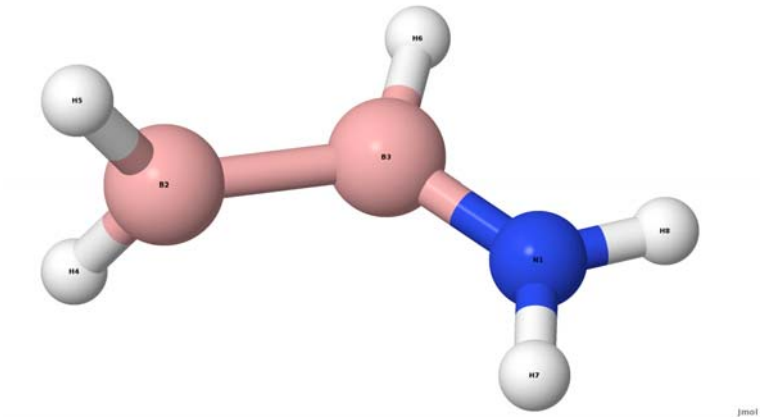

Table of optimized structure in angstrom at DFT-B3LYP / 6-311++G** level in xyz-format

Atom Label	x	y	z
N1	−0.039926	−1.282150	0.130907
B2	−0.262082	1.473068	0.043892
B3	0.511289	−0.002172	0.032771
H4	−0.601251	2.023235	−0.963763
H5	−0.421040	2.102114	1.049860
H6	1.711371	0.049884	−0.074898
H7	−1.026676	−1.467536	0.225451
H8	0.518736	−2.121793	0.114999

B.3.5. Diaminoborane ($(H_2N)_2 - BH$)

Ball-stick model representation

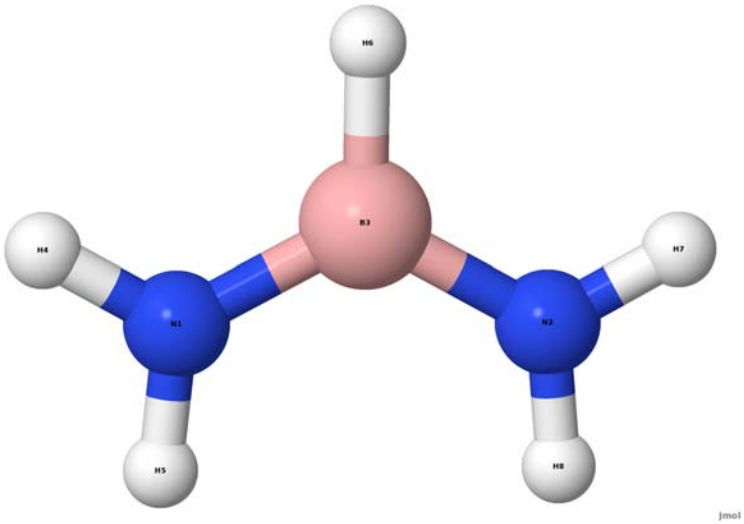

Table of optimized structure in angstrom at DFT-B3LYP / 6-311++G** level in xyz-format

Atom Label	x	y	z
N1	0.158280	0.144777	1.243261
N2	0.158280	0.144777	−1.243261
B3	−0.486677	−0.058311	0.000000
H4	−0.314003	−0.004044	2.118402
H5	1.114645	0.445693	1.347841
H6	−1.625774	−0.416777	0.000000
H7	−0.314003	−0.004044	−2.118402
H8	1.114645	0.445693	−1.347841

B.3.6. Diboranitride $((\mathbf{H_2B})_2 - \mathbf{NH})$

Ball-stick model representation

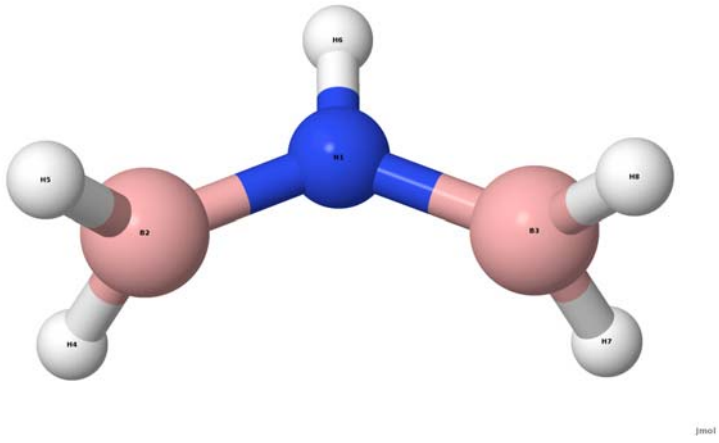

Table of optimized structure in angstrom at DFT-B3LYP / 6-311++G** level in xyz-format

Atom Label	x	y	z
N1	0.396626	−0.000330	0.000000
B2	−0.213869	1.321315	0.000000
B3	−0.214340	−1.321779	0.000000
H4	−0.479580	1.885922	−1.028875
H5	−0.479580	1.885922	1.028875
H6	1.412648	−0.000662	0.000000
H7	−0.480179	−1.886317	−1.028878
H8	−0.480179	−1.886317	1.028878

B.3.7. Borahydrazine ($H_2B - N_2H_3$)

Ball-stick model representation

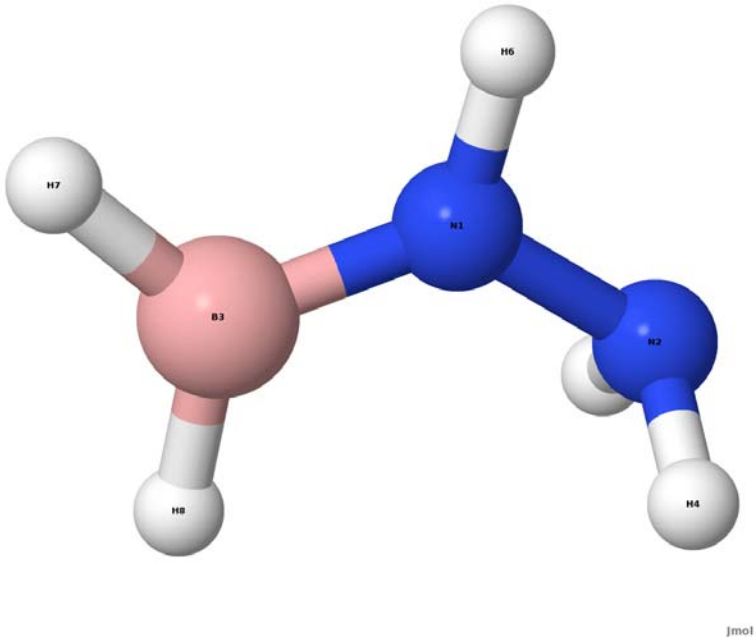

Table of optimized structure in angstrom at DFT-B3LYP / 6-311++G** level in xyz-format

Atom Label	x	y	z
N1	0.511480	0.077955	−0.258242
N2	0.030118	−1.258639	−0.093961
B3	−0.170668	1.258379	−0.006972
H4	−0.244292	−1.386783	0.875105
H5	−0.800186	−1.375998	−0.666351
H6	1.461957	0.066174	−0.599252
H7	0.400901	2.284479	−0.205898
H8	−1.292474	1.208975	0.394772

B.3.8. Borazine or 1,3,5-Triaza-2,4,6-triborinane ($B_3N_3H_6$)

Ball-stick model representation

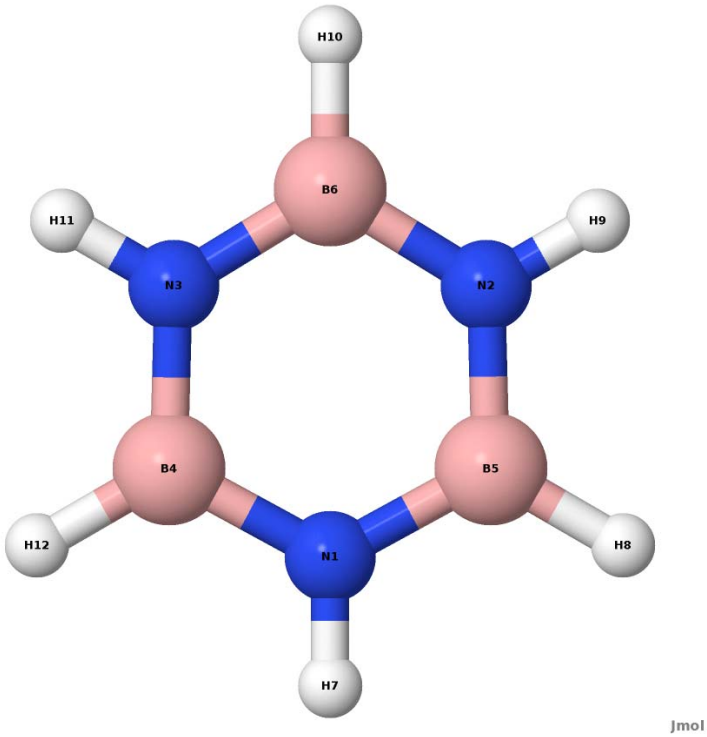

Table of optimized structure in angstrom at DFT-B3LYP / 6-311++G** level in xyz-format

Atom Label	x	y	z
N1	0.000000	0.000000	1.408965
N2	1.220210	0.000000	−0.704485
N3	−1.220210	0.000000	−0.704485
B4	−1.256833	0.000000	0.725631
B5	1.256833	0.000000	0.725631
B6	0.000000	0.000000	−1.451263
H7	0.000000	0.000000	2.417840
H8	2.288816	0.000000	1.321454
H9	2.093922	0.000000	−1.208923
H10	0.000000	0.000000	−2.642896
H11	−2.093922	0.000000	−1.208923
H12	−2.288816	0.000000	1.321454

B.3.9. 1,3,5,7,9-Pentaaza-2,4,6,8,10-pentabora-naphthalene ($B_5N_5H_8$)

Ball-stick model representation

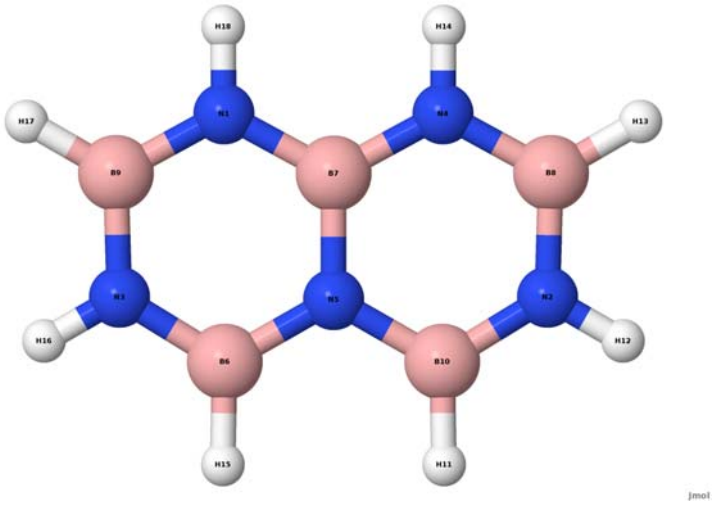

Table of optimized structure in angstrom at DFT-B3LYP / 6-311++G** level in xyz-format

Atom Label	x	y	z
N1	−1.264188	0.000000	−1.381282
N2	2.473323	0.000000	0.734450
N3	−2.473323	0.000000	0.734450
N4	1.264188	0.000000	−1.381282
N5	0.000000	0.000000	0.765468
B6	−1.256829	0.000000	1.480598
B7	0.000000	0.000000	−0.693496
B8	2.514499	0.000000	−0.697327
B9	−2.514499	0.000000	−0.697327
B10	1.256829	0.000000	1.480598
H11	1.277565	0.000000	2.670893
H12	3.344988	0.000000	1.242542
H13	3.547284	0.000000	−1.291928
H14	1.275641	0.000000	−2.390751
H15	−1.277565	0.000000	2.670893
H16	−3.344988	0.000000	1.242542
H17	−3.547284	0.000000	−1.291928
H18	−1.275641	0.000000	−2.390751

B.3.10. 2,4,6,8,10,12-Hexaaza-1,3,5,7,9,11,13-heptabora-phenalene ($B_7N_6H_9$)

Ball-stick model representation

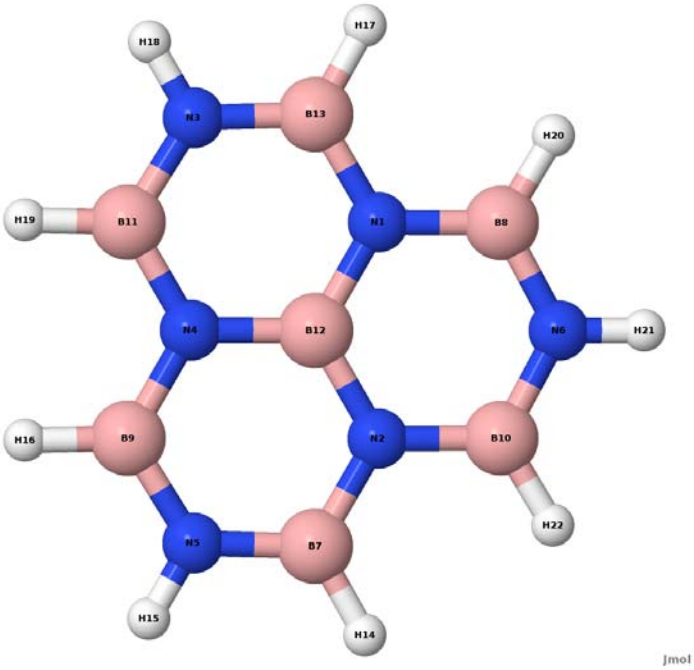

Table of optimized structure in angstrom at DFT-B3LYP / 6-311++G** level in xyz-format

Atom Label	x	y	z
N1	−0.947220	1.104930	0.000000
N2	1.430508	0.267852	0.000000
N3	−2.800228	−0.524355	0.000000
N4	−0.483287	−1.372782	0.000000
N5	1.854219	−2.162891	0.000000
N6	0.946009	2.687246	0.000000
B7	2.367938	−0.831924	0.000000
B8	−0.463502	2.466656	0.000000
B9	0.460378	−2.467262	0.000000
B10	1.906523	1.632330	0.000000
B11	−1.904436	−1.634733	0.000000
B12	0.000000	0.000000	0.000000
B13	−2.366901	0.834932	0.000000
H14	3.540901	−0.632874	0.000000
H15	2.511272	−2.929120	0.000000
H16	0.084346	−3.595998	0.000000
H17	−3.156399	1.724954	0.000000
H18	−3.792328	−0.710265	0.000000
H19	−2.318535	−2.750073	0.000000
H20	−1.222366	3.382947	0.000000
H21	1.281056	3.639385	0.000000
H22	3.072053	1.871045	0.000000

B.3.11. 1,3,5,7,9,11,13-Heptaaza-2,4,6,8,10,12,14-heptabora-anthracene ($B_7N_7H_{10}$)

Ball-stick model representation

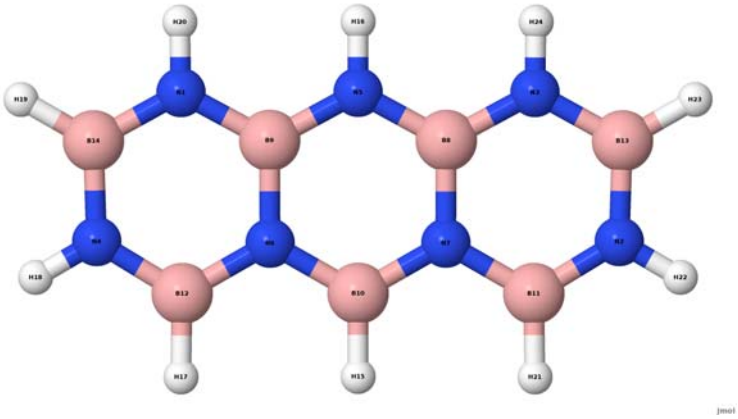

Table of optimized structure in angstrom at DFT-B3LYP / 6-311++G** level in xyz-format

Atom Label	x	y	z
N1	−2.525439	0.000000	−1.368274
N2	3.727946	0.000000	0.751921
N3	2.525439	0.000000	−1.368274
N4	−3.727946	0.000000	0.751921
N5	0.000000	0.000000	−1.372197
N6	−1.253730	0.000000	0.774368
N7	1.253730	0.000000	0.774368
B8	1.258373	0.000000	−0.685210
B9	−1.258373	0.000000	−0.685210
B10	0.000000	0.000000	1.488899
B11	2.508810	0.000000	1.494308
B12	−2.508810	0.000000	1.494308
B13	3.773340	0.000000	−0.679295
B14	−3.773340	0.000000	−0.679295
H15	0.000000	0.000000	2.677858
H16	0.000000	0.000000	−2.382248
H17	−2.525934	0.000000	2.684181
H18	−4.597852	0.000000	1.263002
H19	−4.807713	0.000000	−1.270827
H20	−2.541982	0.000000	−2.377574
H21	2.525934	0.000000	2.684181
H22	4.597852	0.000000	1.263002
H23	4.807713	0.000000	−1.270827
H24	2.541982	0.000000	−2.377574

B.3.12. 1,3,5,7,9,11,13,15-Octaaza-2,4,6,8,10,12,14,16-octabora-pyrene ($B_8N_8H_{10}$)

Ball-stick model representation

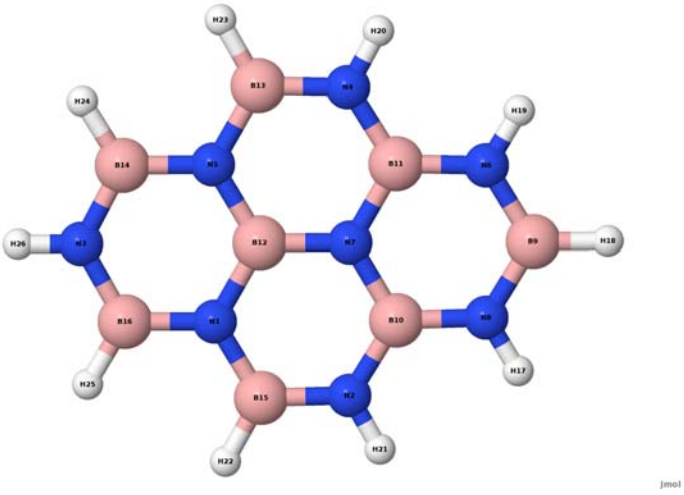

Table of optimized structure in angstrom at DFT-B3LYP / 6-311++G** level in xyz-format

Atom Label	x	y	z
N1	1.274821	−1.463796	0.000000
N2	2.473560	0.696067	0.000000
N3	0.032304	−3.595206	0.000000
N4	−2.485751	0.651425	0.000000
N5	−1.248364	−1.486524	0.000000
N6	−1.245862	2.857395	0.000000
N7	−0.006356	0.701674	0.000000
N8	1.194055	2.879376	0.000000
B9	−0.032618	3.609884	0.000000
B10	1.242196	1.442209	0.000000
B11	−1.268121	1.419613	0.000000
B12	0.006720	−0.746099	0.000000
B13	−2.505732	−0.769729	0.000000
B14	−1.230263	−2.929279	0.000000
B15	2.519213	−0.724454	0.000000
B16	1.282710	−2.906534	0.000000
H17	2.057490	3.401940	0.000000
H18	−0.043268	4.801687	0.000000
H19	−2.118626	3.364223	0.000000
H20	−3.372912	1.133332	0.000000
H21	3.351721	1.194223	0.000000
H22	3.564109	−1.294964	0.000000
H23	−3.540421	−1.358712	0.000000

Atom Label	x	y	z
H24	−2.244659	−3.552265	0.000000
H25	2.307953	−3.511445	0.000000
H26	0.041495	−4.604363	0.000000

B.3.13. 1,3,5,7,9,11,13,15,17-Nonaaza-2,4,6,8,10,12,14,16,18-nonaboratetracene ($B_9N_9H_{12}$)

Ball-stick model representation

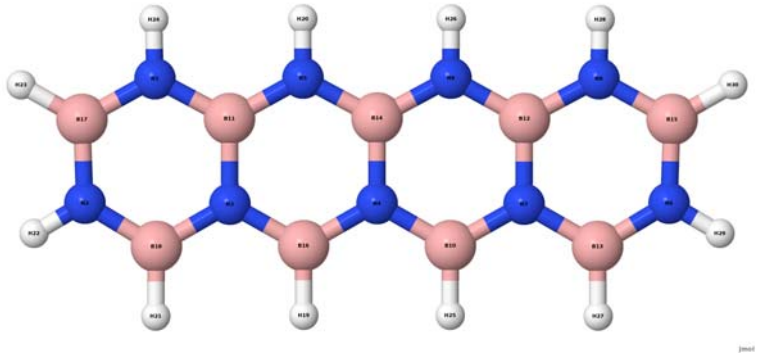

Table of optimized structure in angstrom at DFT-B3LYP / 6-311++G** level in xyz-format

Atom Label	x	y	z
N1	−3.786188	0.000000	−1.357097
N2	−4.982313	0.000000	0.766840
N3	−2.508234	0.000000	0.781483
N4	0.000000	0.000000	0.772858
N5	−1.261192	0.000000	−1.369525
N6	4.982313	0.000000	0.766840
N7	2.508234	0.000000	0.781483
N8	3.786188	0.000000	−1.357097
N9	1.261192	0.000000	−1.369525
B10	1.251968	0.000000	1.492092
B11	−2.517214	0.000000	−0.677749
B12	2.517214	0.000000	−0.677749
B13	3.760678	0.000000	1.505389
B14	0.000000	0.000000	−0.687209
B15	5.032034	0.000000	−0.664125
B16	−1.251968	0.000000	1.492092
B17	−5.032034	0.000000	−0.664125
B18	−3.760678	0.000000	1.505389
H19	−1.248512	0.000000	2.680520
H20	−1.266348	0.000000	−2.379646

Atom Label	x	y	z
H21	−3.773996	0.000000	2.695270
H22	−5.850673	0.000000	1.280468
H23	−6.068215	0.000000	−1.252811
H24	−3.806074	0.000000	−2.366359
H25	1.248512	0.000000	2.680520
H26	1.266348	0.000000	−2.379646
H27	3.773996	0.000000	2.695270
H28	3.806074	0.000000	−2.366359
H29	5.850673	0.000000	1.280468
H30	6.068215	0.000000	−1.252811

B.3.14. Boronnitride flake ($B_{11}N_{11}H_{12}$)

Ball-stick model representation

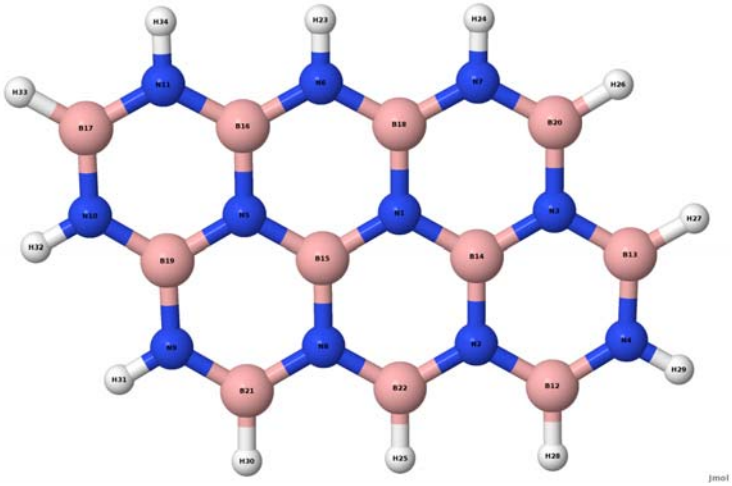

Table of optimized structure in angstrom at DFT-B3LYP / 6-311++G** level in xyz-format

Atom Label	x	y	z
N1	−0.473366	−0.558330	0.000000
N2	1.391482	−2.237517	0.000000
N3	−1.006741	−3.018598	0.000000
N4	0.848845	−4.644619	0.000000
N5	0.053893	1.897943	0.000000
N6	−2.302576	1.121422	0.000000
N7	−2.825738	−1.349130	0.000000
N8	1.918890	0.207766	0.000000
N9	2.424726	2.625609	0.000000
N10	0.557244	4.332981	0.000000
N11	−1.767666	3.591303	0.000000
B12	1.834491	−3.612790	0.000000

Atom Label	x	y	z
B13	−0.555829	−4.389000	0.000000
B14	−0.032717	−1.935621	0.000000
B15	0.495851	0.519489	0.000000
B16	−1.365727	2.209043	0.000000
B17	−0.830678	4.668077	0.000000
B18	−1.893252	−0.251211	0.000000
B19	1.027265	2.973896	0.000000
B 20	−2.421039	−2.711127	0.000000
B21	2.889790	1.282833	0.000000
B22	2.355730	−1.163610	0.000000
H23	−3.290115	1.332561	0.000000
H24	−3.816372	−1.154403	0.000000
H25	3.517771	−1.415446	0.000000
H26	−3.232212	−3.582513	0.000000
H27	−1.335866	−5.288235	0.000000
H28	2.993768	−3.880642	0.000000
H29	1.160920	−5.604412	0.000000
H30	4.056431	1.047712	0.000000
H31	3.115807	3.361582	0.000000
H32	1.227854	5.087097	0.000000
H33	−1.193352	5.803574	0.000000
H34	−2.750618	3.819794	0.000000

B.3.15. 1-Azapentaborane (5) $(1-\mathbf{NB_4H_5})$

Ball-stick model representation

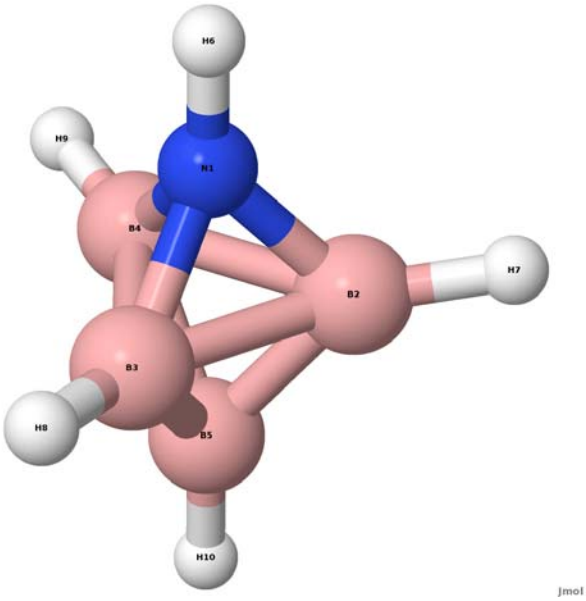

Table of optimized structure in angstrom at DFT-B3LYP / 6-311++G** level in xyz-format

Atom Label	x	y	z
N1	0.023865	0.985032	0.000000
B2	1.097110	−0.077159	0.000000
B3	−0.505480	−0.089811	0.925681
B4	−0.505480	−0.089811	−0.925681
B5	0.035882	−1.351120	0.000000
H6	0.021270	1.993284	0.000000
H7	2.257610	0.135992	0.000000
H8	−1.090718	0.116488	1.929733
H9	−1.090718	0.116488	−1.929733
H10	0.041022	−2.527967	0.000000

B.3.16. 2-Azapentaborane (5) $(2-\mathbf{NB_4H_5})$

Ball-stick model representation

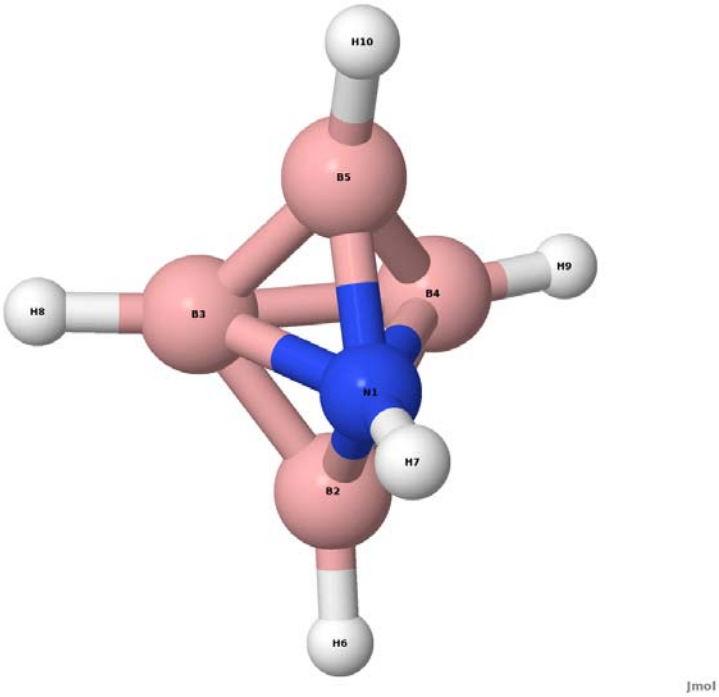

Table of optimized structure in angstrom at DFT-B3LYP / 6-311++G** level in xyz-format

Atom Label	x	y	z
N1	0.000000	0.000000	0.743910
B2	−1.264903	0.000000	−0.113460
B3	0.000000	0.897362	−0.710239
B4	0.000000	−0.897362	−0.710239
B5	1.264903	0.000000	−0.113460

Atom Label	x	y	z
H6	−2.388822	0.000000	0.225839
H7	0.000000	0.000000	1.762572
H8	0.000000	2.041184	−0.986235
H9	0.000000	−2.041184	−0.986235
H10	2.388822	0.000000	0.225839

B.3.17. Azahexaborane (6) (NB_5H_6)

Ball-stick model representation

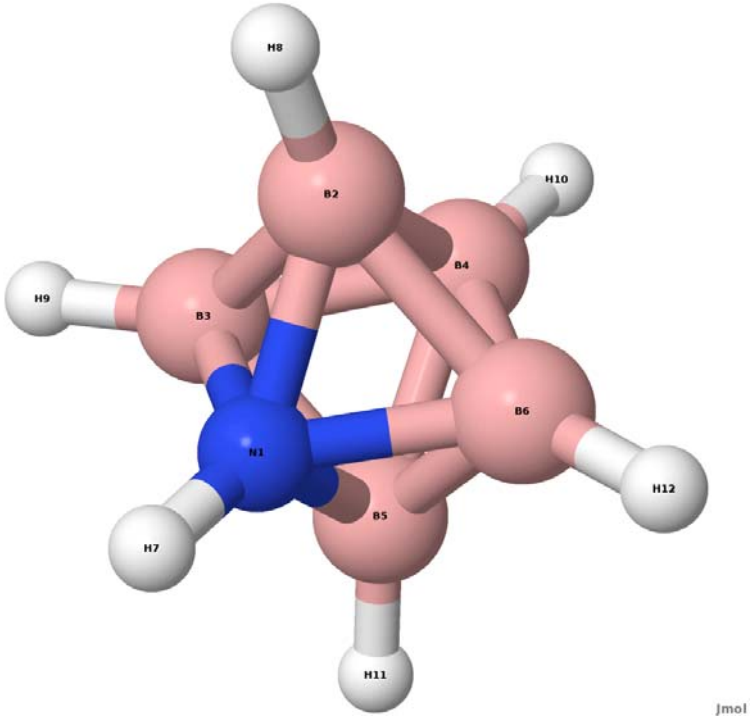

Table of optimized structure in angstrom at DFT-B3LYP / 6-311++G** level in xyz-format

Atom Label	x	y	z
N1	0.000000	0.000000	0.920987
B2	0.000000	1.223243	−0.122643
B3	−1.223243	0.000000	−0.122643
B4	0.000000	0.000000	−1.324133
B5	0.000000	−1.223243	−0.122643
B6	1.223243	0.000000	−0.122643
H7	0.000000	0.000000	1.934713
H8	0.000000	2.361739	0.171602
H9	−2.361739	0.000000	0.171602
H10	0.000000	0.000000	−2.502367
H11	0.000000	−2.361739	0.171602
H12	2.361739	0.000000	0.171602

B.3.18. 1-Azaheptaborane (7) $(1-NB_6H_7)$

Ball-stick model representation

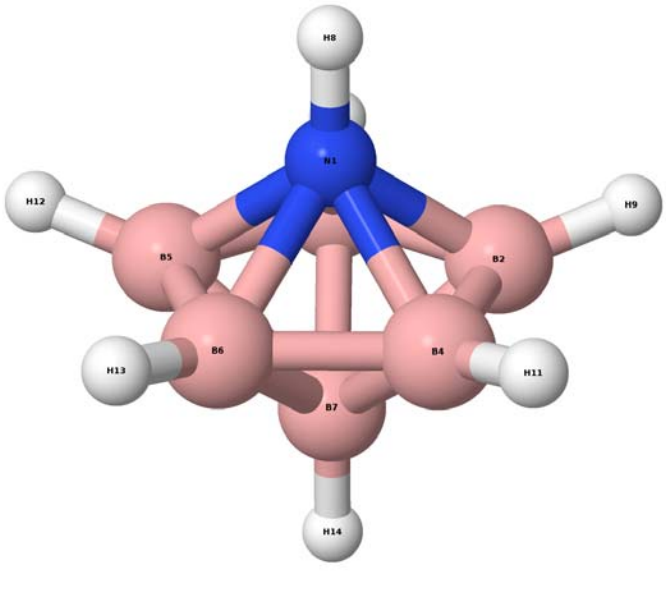

Table of optimized structure in angstrom at DFT-B3LYP / 6-311++G** level in xyz-format

Atom Label	x	y	z
N1	0.000000	0.000000	−0.906802
B2	1.408327	0.000000	0.145959
B3	0.435197	−1.339399	0.145959
B4	0.435197	1.339399	0.145959
B5	−1.139361	−0.827794	0.145959
B6	−1.139361	0.827794	0.145959
B7	0.000000	0.000000	1.277875
H8	0.000000	0.000000	−1.925684
H9	2.542795	0.000000	−0.178568
H10	0.785767	−2.418342	−0.178568
H11	0.785767	2.418342	−0.178568
H12	−2.057164	−1.494617	−0.178568
H13	−2.057164	1.494617	−0.178568
H14	0.000000	0.000000	2.459310

B.3.19. 2-Azaheptaborane (7) $(2-NB_6H_7)$

Ball-stick model representation

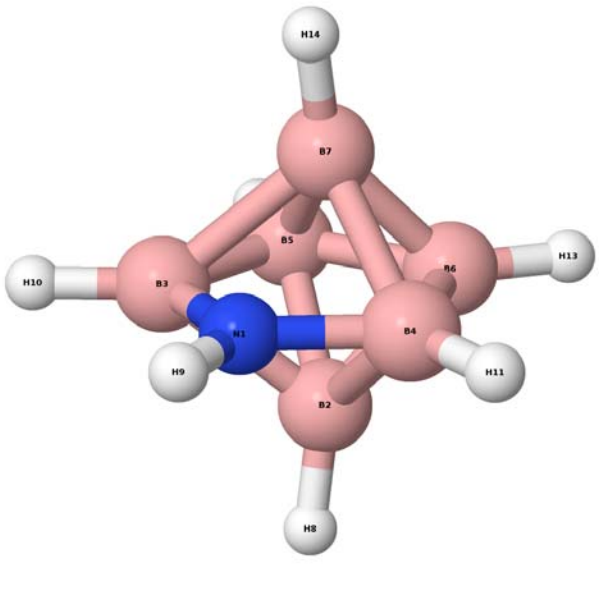

Table of optimized structure in angstrom at DFT-B3LYP / 6-311++G** level in xyz-format

Atom Label	x	y	z
N1	0.000000	0.000000	−1.216483
B2	1.227802	0.000000	0.341409
B3	0.000000	1.259315	−0.447512
B4	0.000000	−1.259315	−0.447512
B5	0.000000	0.859413	1.173018
B6	0.000000	−0.859413	1.173018
B7	−1.227802	0.000000	0.341409
H8	2.369922	0.000000	0.057436
H9	0.000000	0.000000	−2.234666
H10	0.000000	2.312301	−0.980879
H11	0.000000	−2.312301	−0.980879
H12	0.000000	1.671150	2.030160
H13	0.000000	−1.671150	2.030160
H14	−2.369922	0.000000	0.057436

B.3.20. 1-Azaoctaborane (8) $(1-\mathbf{NB_7H_8})$

Ball-stick model representation

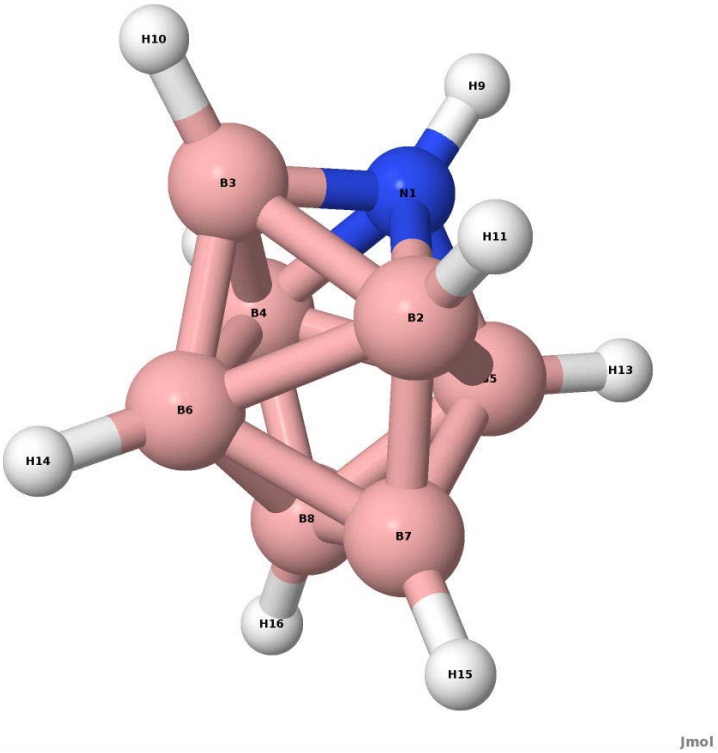

Table of optimized structure in angstrom at DFT-B3LYP / 6-311++G** level in xyz-format

Atom Label	x	y	z
N1	0.549426	1.114964	0.000000
B2	−0.078258	0.197018	1.322852
B3	−0.937317	1.164443	0.000000
B4	−0.078258	0.197018	−1.322852
B5	1.257142	−0.289597	0.000000
B6	−1.269522	−0.485910	0.000000
B7	0.101867	−1.387051	0.811384
B8	0.101867	−1.387051	−0.811384
H9	1.136697	1.942342	0.000000
H10	−1.523478	2.185872	0.000000
H11	−0.030155	0.753806	2.361969
H12	−0.030155	0.753806	−2.361969
H13	2.436158	−0.235187	0.000000
H14	−2.401446	−0.829352	0.000000
H15	0.157597	−2.291759	1.570118
H16	0.157597	−2.291759	−1.570118

B.3.21. 3-Azaoctaborane (8) $(3-NB_7H_8)$

Ball-stick model representation

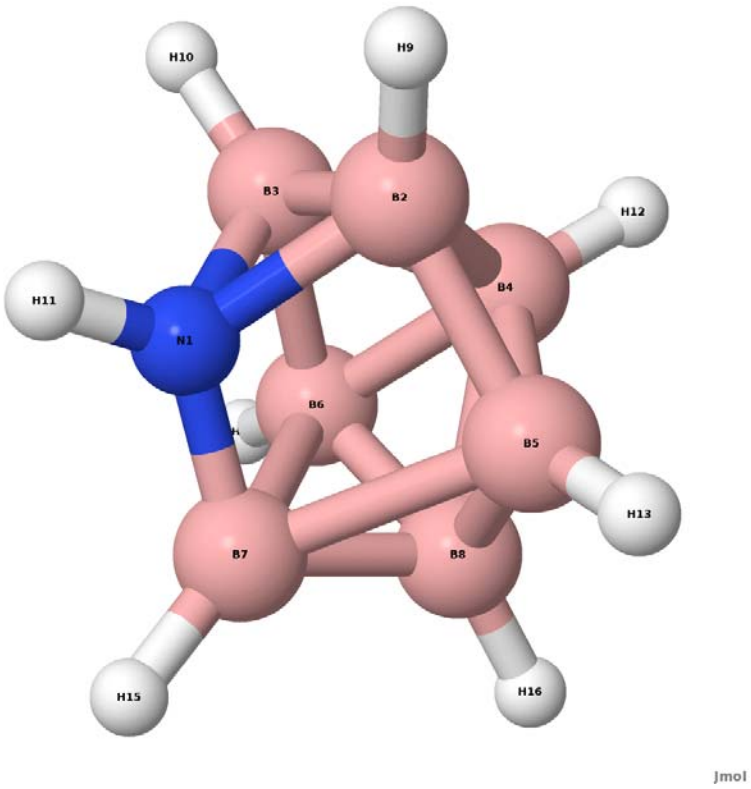

Table of optimized structure in angstrom at DFT-B3LYP / 6-311++G** level in xyz-format

Atom Label	x	y	z
N1	−1.188337	−0.394771	0.000000
B2	0.009386	−1.177502	−0.844442
B3	0.009386	−1.177502	0.844442
B4	1.284867	−0.363655	0.000000
B5	0.476007	0.439852	−1.376346
B6	0.476007	0.439852	1.376346
B7	−0.965091	1.059916	0.000000
B8	0.693479	1.399913	0.000000
H9	−0.232427	−2.132448	−1.491880
H10	−0.232427	−2.132448	1.491880
H11	−2.122912	−0.797916	0.000000
H12	2.410130	−0.731842	0.000000
H13	0.448100	0.748211	−2.516195
H14	0.448100	0.748211	2.516195
H15	−1.875156	1.816335	0.000000
H16	1.169402	2.484182	0.000000

B.3.22. 1-Azanonaborane (9) ($1-\mathbf{NB_8H_9}$)

Ball-stick model representation

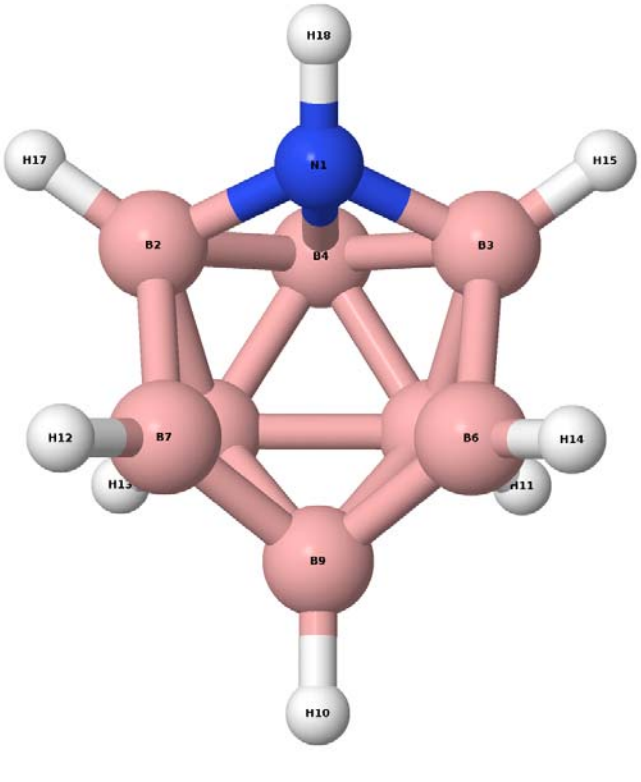

Table of optimized structure in angstrom at DFT-B3LYP / 6-311++G** level in xyz-format

Atom Label	x	y	z
N1	0.688076	−0.080495	0.739697
B2	0.210307	0.245015	2.128972
B3	1.988760	0.399855	0.155003
B4	1.932010	−0.168747	1.853498
B5	1.455540	1.286496	2.776168
B6	1.658533	2.180342	0.204886
B7	0.086026	2.043448	1.949968
B8	2.682527	1.393257	1.414431
B9	1.550397	2.744517	1.738128
H10	1.809374	3.858163	2.058917
H11	3.858083	1.544039	1.404755
H12	−1.036073	2.405468	1.899363
H13	1.559792	1.344086	3.955385
H14	1.460561	2.623122	−0.871001
H15	2.483061	−0.190358	−0.739565
H16	2.388618	−1.201662	2.183876
H17	−0.577726	−0.456733	2.657652
H18	0.264874	−0.890488	0.294906

B.3.23. 4-Azanonaborane (9) $(4-NB_8H_9)$

Ball-stick model representation

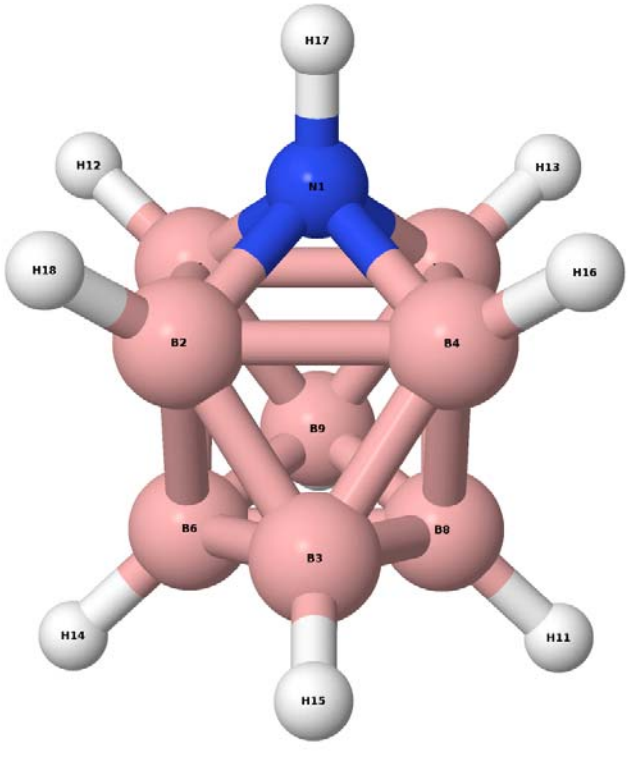

Table of optimized structure in angstrom at DFT-B3LYP / 6-311++G** level in xyz-format

Atom Label	x	y	z
N1	0.470588	0.327680	2.174031
B2	0.565019	0.161343	0.586954
B3	2.195823	0.344048	0.207940
B4	1.883751	−0.277606	1.740778
B5	1.450736	1.383690	2.863846
B6	1.432098	1.880466	0.247991
B7	0.132770	1.819041	1.707660
B8	2.750903	1.445256	1.400448
B9	1.592966	2.655795	1.770788
H10	1.752155	3.797059	2.020641
H11	3.905772	1.678619	1.500817
H12	−0.992426	2.140819	1.846254
H13	1.510147	1.314361	4.038786
H14	1.343612	2.524925	−0.739489
H15	2.788763	−0.178587	−0.667002
H16	2.185714	−1.277502	2.286648
H17	−0.187784	−0.213650	2.721004
H18	−0.317868	−0.446433	0.096943

B.3.24. 1-Azadecaborane (10) ($1-\mathbf{NB_9H_{10}}$)

Ball-stick model representation

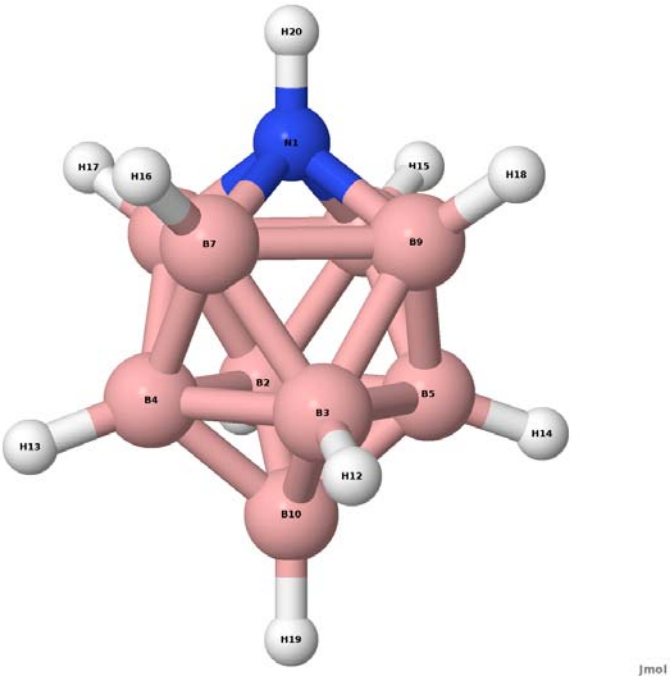

Table of optimized structure in angstrom at DFT-B3LYP / 6-311++G** level in xyz-format

Atom Label	x	y	z
N1	0.000000	−1.536128	0.000000
B2	0.000000	0.808287	1.311193
B3	0.000000	0.808287	−1.311193
B4	−1.311193	0.808286	0.000000
B5	1.311193	0.808286	0.000000
B6	0.938889	−0.665595	0.938889
B7	−0.938889	−0.665595	−0.938889
B8	−0.938889	−0.665595	0.938889
B9	0.938889	−0.665595	−0.938889
B10	0.000000	1.905468	0.000000
H11	0.000000	1.209402	2.424628
H12	0.000000	1.209402	−2.424628
H13	−2.424628	1.209402	0.000000
H14	2.424628	1.209402	0.000000
H15	1.649930	−1.277999	1.649930
H16	−1.649930	−1.277999	−1.649930
H17	−1.649930	−1.277999	1.649930
H18	1.649930	−1.277999	−1.649930
H19	0.000000	3.082900	0.000000
H20	0.000000	−2.548502	0.000000

B.3.25. 1-Azaundecaborane (11) ($1-\mathbf{NB_{10}H_{11}}$)

Ball-stick model representation

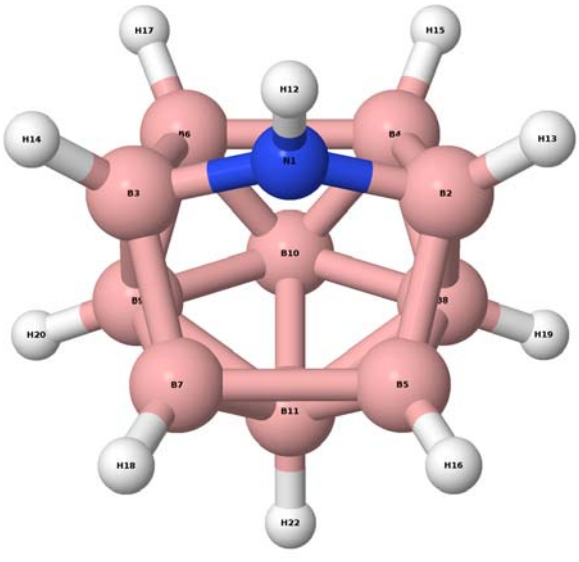

Table of optimized structure in angstrom at DFT-B3LYP / 6-311++G** level in xyz-format

Atom Label	x	y	z
N1	0.000000	0.000000	1.436772
B2	0.000000	−1.430814	0.949224
B3	0.000000	1.430814	0.949224
B4	1.454181	−1.029336	−0.026495
B5	−1.454181	−1.029336	−0.026495
B6	1.454181	1.029336	−0.026495
B7	−1.454181	1.029336	−0.026495
B8	0.000000	−1.475281	−0.781729
B9	0.000000	1.475281	−0.781729
B10	0.933379	0.000000	−1.300748
B11	−0.933379	0.000000	−1.300748
H12	0.000000	0.000000	2.457429
H13	0.000000	−2.296288	1.755986
H14	0.000000	2.296288	1.755986
H15	2.506922	−1.442902	0.300793
H16	−2.506922	−1.442902	0.300793
H17	2.506922	1.442902	0.300793
H18	−2.506922	1.442902	0.300793
H19	0.000000	−2.503868	−1.373142
H20	0.000000	2.503868	−1.373142
H21	1.614304	0.000000	−2.273471
H22	−1.614304	0.000000	−2.273471

B.3.26. Azadodecaborane (12) ($NB_{11}H_{12}$)

Ball-stick model representation

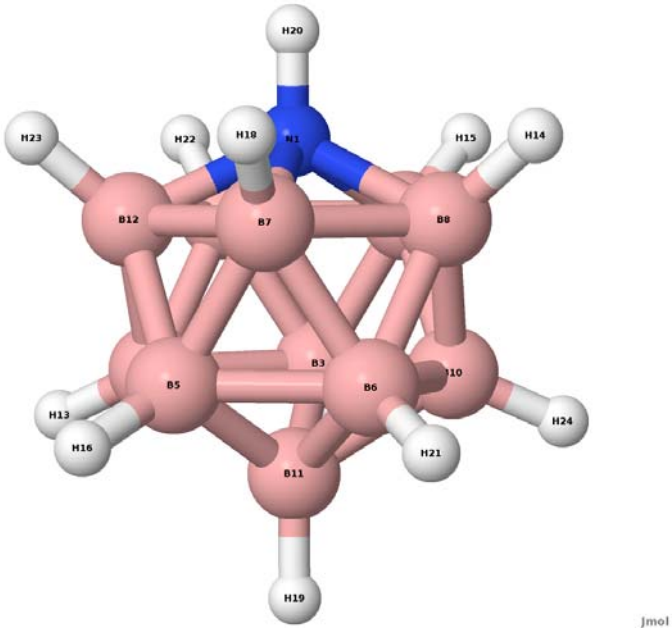

Table of optimized structure in angstrom at DFT-B3LYP / 6-311++G** level in xyz-format

Atom Label	x	y	z
N1	0.522352	−1.321842	0.000000
B2	−0.195432	−0.806193	1.471951
B3	0.144020	0.918897	1.451766
B4	−1.442921	0.291337	0.897043
B5	−1.442921	0.291337	−0.897043
B6	0.144020	0.918897	−1.451766
B7	−0.195432	−0.806193	−1.471951
B8	1.413559	−0.170476	−0.909546
B9	1.413559	−0.170476	0.909546
B10	1.125079	1.305968	0.000000
B11	−0.637310	1.612768	0.000000
B12	−1.189744	−1.199396	0.000000
H13	−2.431958	0.419515	1.531051
H14	2.368896	−0.612499	−1.437182
H15	2.368896	−0.612499	1.437182
H16	−2.431958	0.419515	−1.531051
H17	0.276832	1.490321	2.477714
H18	−0.173406	−1.616961	−2.325600
H19	−1.071842	2.712579	0.000000
H20	0.895489	−2.266461	0.000000

Atom Label	x	y	z
H21	0.276832	1.490321	−2.477714
H22	−0.173406	−1.616961	2.325600
H23	−1.744236	−2.238147	0.000000
H24	1.950911	2.151341	0.000000